

Investigating USP2 as a mediator of therapy resistance in lethal prostate cancer

PhD scholar

Fang Meiwen Danielle

B. of Science (Advanced) | B. of Science (1st class Honours)

Thesis submitted for the degree of Doctor of Philosophy (Medicine)



THE UNIVERSITY
of ADELAIDE

PhD Supervisors

Assoc. Prof. Luke Selth, Prof. Lisa Butler, Prof. Wayne Tilley

January 2023

Faculty of Health and Medical Sciences

School of Medicine

The University of Adelaide

TABLE OF CONTENTS

1	INVESTIGATING USP2 AS A MEDIATOR OF THERAPY RESISTANCE IN LETHAL PROSTATE CANCER	11
1.1	PROJECT DETAILS.....	11
1.1.1	<i>Abstract</i>	11
1.1.2	<i>Declaration</i>	14
1.2	ACKNOWLEDGEMENTS.....	15
1.3	THE PROSTATE IS AN ANDROGEN-REGULATED GLAND	17
1.4	ANDROGEN RECEPTOR (AR).....	20
1.4.1	<i>Gene, structure, and functions of Androgen Receptor (AR)</i>	20
1.5	EPIDEMIOLOGY OF PROSTATE CANCER.....	24
1.6	DIAGNOSIS OF PROSTATE CANCER	28
1.7	GRADING / STAGING OF PROSTATE CANCER	29
1.8	CURRENT MANAGEMENT OPTIONS FOR PROSTATE CANCER	33
1.8.1	<i>Treatment of localised prostate cancer</i>	33
1.8.2	<i>Treatment of metastatic prostate cancer</i>	34
1.8.3	<i>Treatment of castrate-resistant prostate cancer (CRPC)</i>	37
1.9	MECHANISMS OF RESISTANCE TO AR-TARGETED THERAPIES	39
1.9.1	<i>AR-dependent mechanisms of resistance in prostate cancer</i>	39
1.9.2	<i>AR-independent mechanisms of resistance in CRPC</i>	41
1.10	UBIQUITIN-PROTEASOME SYSTEM.....	45
1.11	THE IMPORTANCE OF THE UBIQUITIN PROTEASOME SYSTEM IN CANCER	48
1.12	INTERPLAY BETWEEN UBIQUITIN-SPECIFIC PROTEASES AND ANDROGEN RECEPTOR SIGNALLING....	50
1.13	USP2 IN PROSTATE CANCER	52
1.14	GENE, PROTEIN STRUCTURE AND FUNCTION OF USP2	53
1.15	USP2 (OR USP2A) FUNCTIONS AS AN ONCO-PROTEIN IN SEVERAL CANCERS	56
1.15.1	<i>High expression of USP2 or USP2 fusion proteins in tumours correlated with poor prognosis.</i>	56
1.15.2	<i>USP2 suppresses p53 signalling pathway through stabilisation of MDM2 and MDM4.</i>	57
1.15.3	<i>USP2 promotes metastasis and epithelial-to-mesenchymal transition (EMT).</i> 58	
1.15.4	<i>USP2 enhances growth of cancer cells.</i>	59
1.15.5	<i>USP2 is important in endocytosis and autophagy.</i>	60
1.15.6	<i>USP2 is important in metastasis.</i>	61
1.16	GAPS IN KNOWLEDGE RELATED TO MY PROJECT	64
1.17	RESEARCH HYPOTHESIS.....	64
1.18	AIMS OF THE PROJECT	64
2	MATERIALS AND METHODS	66
2.1	MAINTENANCE OF PROSTATE CANCER CELL LINES	70
2.2	GENERATION OF LNCAP CELLS OVER-EXPRESSING USP2	74
2.2.1	<i>Insertion of triple FLAG tagged USP2a gene block into pDONR221 vector.</i> __	74
2.2.2	<i>Insertion of TF-USP2 transgene from a Gateway entry clone into a destination vector</i>	76

2.3	LENTIVIRAL TRANSDUCTION OF LNCAP CELLS	79
2.4	PREPARATION OF PROTEIN SAMPLES FOR WESTERN BLOTTING	80
2.4.1	<i>Sodium Dodecyl Sulfate Polyacrylamide Gel Electrophoresis (SDS-PAGE)</i> _____	80
2.4.2	<i>Western blotting</i> _____	81
2.5	RNA EXTRACTION FROM PROSTATE CANCER CELL LINES	85
2.6	REVERSE TRANSCRIPTION OF MRNA TO GENERATE COMPLEMENTARY DNA (cDNA)	85
2.7	QUANTITATIVE REAL-TIME PCR.....	86
2.8	TRYPAN BLUE CELL VIABILITY ASSAYS FOR siRNA TRANSFECTIONS	86
3	USP2 IS A NOVEL DRIVER OF LETHAL PROSTATE CANCER AND MEDIATOR OF THERAPY RESISTANCE.	89
3.1	INTRODUCTION.....	89
3.2	MATERIALS AND METHODS.....	91
3.2.1	<i>Tissue collection from a matched normal to tumour cohort</i> _____	91
3.2.2	<i>Ex vivo culture of human prostate tumours</i> _____	92
3.2.3	<i>Androgen and AR-antagonist treatment of androgen responsive cell lines</i> _____	93
3.2.4	<i>Measurements of neurite lengths</i> _____	93
3.2.5	<i>Chromatin immunoprecipitation qPCR (ChIP-qPCR)</i> _____	94
3.2.6	<i>Single-sample Gene Set Enrichment Analysis (ssGSEA)</i> _____	94
3.3	RESULTS.....	97
3.3.1	<i>USP2 is upregulated in response to AR-targeted therapy.</i> _____	97
3.3.2	<i>USP2 is associated with neuroendocrine PCa.</i> _____	111
3.3.3	<i>USP2 is upregulated during the evolution to neuroendocrine prostate cancer.</i> 117	
3.3.4	<i>Overexpressing USP2 induces a neuroendocrine phenotype.</i> _____	119
3.3.5	<i>Elevated levels of USP2 in adenocarcinoma LNCaP mediates resistance to AR-targeted therapy and chemotherapy.</i> _____	125
3.3.6	<i>Aurora kinase A, Cyclin D1 and FAS appears to be stabilised by USP2 in adenocarcinoma LNCaP cells overexpressing USP2.</i> _____	131
3.3.7	<i>USP2 expression is elevated in tumours with loss of PTEN, RB1 and P53</i> _____	134
3.3.8	<i>Lack of a suitable USP2 antibody hinders research on this factor</i> _____	136
3.4	DISCUSSION.....	140
4	TARGETING USP2 IN ADVANCED PROSTATE CANCER SUPPRESSES TUMOUR GROWTH AND DESTABILISES ITS ONCO-SUBSTRATES.....	146
4.1	INTRODUCTION.....	146
4.2	MATERIALS AND METHODS.....	148
4.2.1	<i>Transient RNA interference</i> _____	148
4.2.2	<i>Trypan blue cell viability assays</i> _____	148
4.2.3	<i>Cell viability assays using an Incucyte</i> _____	149
4.2.4	<i>AnnexinV-PE and 7AAD flow cytometry</i> _____	149
4.2.5	<i>Orthotopic xenograft model</i> _____	149
4.3	RESULTS.....	151
4.3.1	<i>Pharmacological inhibition of USP2 reduced cell viability and increased cell apoptosis of neuroendocrine-like prostate cancer cells</i> _____	151
4.3.2	<i>Knockdown of USP2 inhibits growth and induced death of PCa cells.</i> _____	158

4.3.3	<i>In vivo activity of a small molecule inhibitor of USP2, ML364</i>	160
4.3.4	<i>Aurora kinase A, Cyclin D1 and FAS may be putative substrates of USP2 in prostate cancer.</i>	163
4.3.5	<i>LNCaP cells expressing elevated levels of USP2 were more sensitive to Aurora A inhibition.</i>	168
4.4	DISCUSSION	171
5	INTEGRATIVE OMICS TO DEFINE USP2 FUNCTION IN PROSTATE CANCER	177
5.1	INTRODUCTION	177
5.2	METHODS	179
5.2.1	<i>Proteomics</i>	179
5.2.2	<i>RNA sequencing</i>	181
5.3	RESULTS	184
5.3.3	<i>Overview of experimental strategy to identify USP2 substrates</i>	184
5.3.4	<i>Analyses of the global proteome in MR42D cells treated with the USP2 inhibitor, called ML364.</i>	186
5.3.5	<i>Analyses of the global proteome when LNCaP cells overexpressed USP2</i>	198
5.3.6	<i>Analyses of the global transcriptome when LNCaP cells overexpress USP2</i>	210
5.3.7	<i>Integration of the three sets of proteomics and transcriptomics expression data</i>	221
5.4	DISCUSSION	227
6	DISCUSSION	236
6.1	USP2 CAN DRIVE THE DEVELOPMENT OF TREATMENT-EMERGENT NEUROENDOCRINE PHENOTYPE AND CONFERS THERAPY RESISTANCE.	239
6.2	USP2 IS A BONA FIDE THERAPEUTIC TARGET IN PROSTATE CANCER.	242
6.3	INTEGRATIVE OMICS REVEALS NEW FUNCTIONS OF USP2	244
6.4	OVERALL CONCLUSION	246
7	APPENDICES	248
7.1	PROTEOMICS DATA FROM MR42D CELLS TREATED WITH ML364	248
7.2	PROTEOMICS DATA FROM LNCAP CELLS OVEREXPRESSIONG USP2	261
7.3	TRANSCRIPTOMICS DATA FROM LNCAP CELLS OVEREXPRESSIONG USP2	276
7.4	CONFERENCE PRESENTATIONS (2019 TO 2022)	295
	REFERENCES	296

List of Figures

FIGURE 1.1. DIAGRAM DESCRIBING THE ANATOMY SURROUNDING THE MALE REPRODUCTION SYSTEM.....	18
FIGURE 1.2. THIS IS THE FEEDBACK LOOP OF THE HYPOTHALAMIC-PITUITARY-TESTICULAR AXIS IN MALES AND ITS OUTCOMES ARE ANDROGEN PRODUCTION AND SPERMATOGENESIS.	19
FIGURE 1.3. THE AR COMPRISES OF 4 DOMAINS: N-TERMINAL DOMAIN (NTD), DNA-BINDING DOMAIN (DBD), HINGE DOMAIN AND LIGAND-BINDING DOMAIN (LBD).	22
FIGURE 1.4. A SUMMARY OF HOW AR CAN FUNCTION AS A TRANSCRIPTION FACTOR WHEN BOUND TO DHT.	23
FIGURE 1.5. THE AGE-STANDARDISED INCIDENCE RATES OF PROSTATE CANCER IN MALES OF ALL AGES WORLDWIDE WHO WERE DIAGNOSED IN 2018.	25
FIGURE 1.6. A COMPARISON OF THE NUMBER OF NEW CANCER CASES AND DEATHS ACROSS THE DIFFERENT TYPES OF CANCERS THAT OCCURRED IN 2018 AND IN BOTH SEXES OF ALL AGES.	26
FIGURE 1.7. A COMPARISON OF AGE-STANDARDISED INCIDENCES AND MORTALITY RATES FOR PROSTATE CANCER BETWEEN COUNTRIES IN 2018.	27
FIGURE 1.8. TYPICAL PICTURES OF PROSTATE TUMOUR ASSOCIATED WITH THE CORRESPONDING GLEASON GRADES/PATTERNS (RANGING FROM 1 TO 5) AND GROUPED INTO VARIOUS GLEASON GRADE GROUPS (I TO V) USING THEIR GLEASON SCORES (CHEN AND ZHOU, 2016).	31
FIGURE 1.9. VARIOUS GLEASON SCORES CAN BE GROUPED INTO 5 DIFFERENT GLEASON GRADE GROUPS IN ACCORDANCE TO THE INTERNATIONAL SOCIETY OF UROLOGICAL PATHOLOGY 2014 (MOTTET ET AL., 2017).	32
FIGURE 1.10. THE TNM STAGING FOR PROSTATE CANCER, WHICH STANDS FOR TUMOUR (T), REGIONAL LYMPH NODE STATUS (N); AND PRESENCE OF DISTANT METASTASES (M) (STEPHENS ET AL., 2008).	32
FIGURE 1.11. THE UBIQUITINATION/ DE-UBIQUITINATION PROCESS REGULATES SEVERAL INTRACELLULAR PROCESS AND SIGNALLING.	47
FIGURE 1.12. SCHEMATIC DIAGRAM OF USP2 GENE AND ITS ENCODED MRNA VARIANTS AND PROTEIN VARIANTS USP2A, USP2B AND USP2C.	55
FIGURE 1.13. SUMMARY OF USP2 AND THE SUBSTRATES THAT USP2 STABILISES TO CARRY OUT ITS FUNCTIONS AS AN ONCOPROTEIN IN VARIOUS CANCER TYPES.	63
FIGURE 2.1. THE PENTR-TF-USP2A CONTAINS THE G-BLOCK INSERTED INTO THE PDONR221 VECTOR THROUGH RECOMBINATION AT THE ATTB SITES PRESENT IN THE G-BLOCK AND AATP SITES PRESENT IN THE PDONR221 VECTOR USING BP CLONASE ENZYME (INVITROGEN GATEWAY BP CLONASE II ENZYME MIX).	75
FIGURE 2.2. THE INSERTION OF THE TRIPLE FLAG TAGGED USP2 FUSION GENE (TF-USP2) FROM THE ENTRY CLONE INTO THE DESTINATION VECTOR HAPPENS THROUGH THE RECOMBINATION AT THE ATTL AND ATTR SITES ON THE ENTRY CLONE AND DESTINATION VECTOR RESPECTIVELY.	77
FIGURE 2.3. THE DIAGRAM DEPICTS THE FLAG-USP2 EXPRESSION VECTOR GENERATED FROM THE LR REACTION BETWEEN THE PENTR-TF-USP2A ENTRY CLONE AND THE DESTINATION VECTOR, MND-DEST MPGK-HYGRO.	78
FIGURE 3.1. USP2 EXPRESSION INCREASED IN PATIENT-DERIVED EXPLANTS PDES AFTER 48 HOURS OF ENZALUTAMIDE TREATMENT.	99
FIGURE 3.2. USP2 EXPRESSION IS UPREGULATED IN RESPONSE TO AR-TARGETED THERAPY.	102
FIGURE 3.3. USP2 EXPRESSION IS THE HIGHEST IN CASTRATE RESISTANT PCA (CRPC) CELL LINES.	105
FIGURE 3.4. USP2 EXPRESSION IS UPREGULATED BY ANTI-ANDROGEN AND REPRESSED WITH ANDROGEN.	106
FIGURE 3.5. THE USP2 GENE MAY BE DIRECTLY REPRESSED BY THE AR.	109
FIGURE 3.6. USP2 EXPRESSION IS ELEVATED IN NEUROENDOCRINE PROSTATE CANCER (PCA).	112
FIGURE 3.7. INCREASING USP2 EXPRESSION DIRECTLY CORRELATED WITH INCREASING NEPC SCORE AND INVERSELY CORRELATED WITH INCREASING AR ACTIVITY.	115
FIGURE 3.8. INCREASED USP2A EXPRESSION IS ASSOCIATED WITH NEUROENDOCRINE PROSTATE CANCER PHENOTYPE.	118
FIGURE 3.9. USP2 DRIVES THE DEVELOPMENT OF THE NEUROENDOCRINE-LIKE PHENOTYPE.	121
FIGURE 3.10. ELEVATED LEVELS OF USP2 EXPRESSION IN ADENOCARCINOMA LNCAP INDUCED LINEAGE PLASTICITY AND INDUCED THE EMT PATHWAY.	123

FIGURE 3.11. OVEREXPRESSION OF USP2 IN LNCAP CELLS CONFERRED GROWTH ADVANTAGE IN ANDROGEN-DEPLETED CONDITIONS AND WITH ENZALUTAMIDE TREATMENT.	127
FIGURE 3.12. ELEVATED LEVELS OF USP2 IN LNCAP CELLS CONFERS SURVIVAL ADVANTAGE WHEN TREATED WITH OF THE CHEMOTHERAPEUTIC DRUG, DOCETAXEL.	129
FIGURE 3.13. OVEREXPRESSION OF USP2 IN LNCAP CELLS RESULTED IN INCREASED LEVELS AND STABILITY OF PUTATIVE USP2 SUBSTRATES IN LNCAP CELLS, SUCH AS CYCLIN D1 AND AURORA A.	132
FIGURE 3.14. CONSTITUTIVE OVEREXPRESSION OF USP2 IN LNCAP CELLS RESULTED IN INCREASED LEVELS OF PUTATIVE SUBSTRATE FAS, YET AR AND FKBP5 LEVELS REMAIN UNCHANGED.	133
FIGURE 3.15. USP2 EXPRESSION IS THE HIGHEST IN PROSTATE TUMOUR MODELS REPRESENTING EPITHELIAL-NEUROENDOCRINE PLASTICITY.	135
FIGURE 3.16. THE USP2 N-TERM PRIMARY RABBIT ANTIBODY (ABCEPTA) IS NOT DETECTING USP2A. EACH LANE CONTAINED 40µG OF PROTEIN.	138
FIGURE 3.17. THE USP2 (PROTEINTECH 10392-1-AP) PRIMARY RABBIT ANTIBODY (ABCEPTA) IS NOT DETECTING USP2A.	139
FIGURE 4.1. PHARMACOLOGICAL INHIBITION OF USP2 WITH ML364 AS A POTENTIAL TREATMENT FOR AGGRESSIVE PROSTATE CANCER.	153
FIGURE 4.2. THE USP2 INHIBITOR, ML364, REDUCED CELL VIABILITY AND INDUCED CELL DEATH IN SEVERAL PROSTATE CANCER CELL LINES IN A DOSE DEPENDENT MANNER.	155
FIGURE 4.3. THE USP2 INHIBITOR, ML364, INDUCES CELL APOPTOSIS WHEN NEUROENDOCRINE-LIKE MR42D CELLS WERE TREATED WITH INCREASING CONCENTRATIONS OF ML364.	156
FIGURE 4.4. GENETIC MANIPULATION OF USP2A RESULTED IN REDUCED CELL VIABILITY AND INCREASED CELL DEATH OF NEUROENDOCRINE-LIKE PROSTATE CANCER CELLS.	159
FIGURE 4.5. A SMALL MOLECULE INHIBITOR OF USP2, ML364, SIGNIFICANTLY REDUCED GROWTH OF NEUROENDOCRINE-LIKE TUMOURS IN AN ORTHOTOPIC PC3-LUCIFERASE XENOGRAFT MODEL.	161
FIGURE 4.6. KNOCKING DOWN OF USP2 RESULTED IN DECREASED PROTEIN LEVELS OF AURORA KINASE A IN THE ANDROGEN-INSENSITIVE MR42D AND AR-NULL PC3 CELLS.	164
FIGURE 4.7. INHIBITION OF USP2 REDUCED THE PROTEIN LEVELS OF FAS, AURORA KINASE A AND CYCLIN D1.	166
FIGURE 4.8. OVEREXPRESSION OF USP2 IN LNCAP SENSITISES CELLS TO AURORA KINASE A INHIBITION BY THE SMALL MOLECULE INHIBITOR, CALLED ALISERTIB.	169
FIGURE 5.1. SCHEMATIC DIAGRAM DEPICTING THE OVERALL EXPERIMENTAL APPROACH FOR QUANTITATIVE PROTEOMICS AND TRANSCRIPTOMICS IN THIS STUDY.	185
FIGURE 5.2. PRINCIPAL COMPONENT ANALYSIS OF THE GLOBAL PROTEOMES FROM MR42D CELLS TREATED WITH VEHICLE (CONTROL) VERSUS 5µM ML364.	187
FIGURE 5.3. VOLCANO PLOT OF THE PROTEINS AT DIFFERENT ABUNDANCE LEVELS WERE IDENTIFIED BETWEEN THE MR42D CELLS TREATED WITH 24 HOURS OF 5µM ML364 AND THE CONTROL GROUP.	190
FIGURE 5.4. GSEA ANALYSIS OF PROTEOMICS DATA FROM MR42D CELLS EXPOSED TO 5µM ML364 REVEALED INHIBITION OF CELL CYCLE PATHWAYS.	194
FIGURE 5.5. INHIBITION OF USP2 IN NEUROENDOCRINE-LIKE PCA CELLS IS ASSOCIATED WITH AN INHIBITION OF GLYCOLYSIS, CELL CYCLE AND FATTY ACID METABOLISM.	195
FIGURE 5.6. INHIBITION OF USP2 IN NEUROENDOCRINE-LIKE PCA CELLS IS ASSOCIATED WITH AN ACTIVATION OF CELLULAR POLYSACCHARIDE CATABOLIC PROCESS.	196
FIGURE 5.7. PRINCIPAL COMPONENT ANALYSIS OF THE GLOBAL PROTEOME DIFFERENTIATED THE GLOBAL PROTEOME PROFILES OF THE LNCAP CELLS OVEREXPRESSION USP2 (USP2-OE) VERSUS CONTROL CELLS OVEREXPRESSION THE NEON TRANSGENE.	199
FIGURE 5.8. VOLCANO PLOT OF PROTEINS AT DIFFERENT ABUNDANCE LEVELS WERE IDENTIFIED BETWEEN THE USP2-OE LNCAP CELLS AND THE CONTROL GROUP.	202
FIGURE 5.9. GSEA PATHWAY ANALYSIS OF THE ALTERED PROTEOME IN RESPONSE TO USP2 OVEREXPRESSION IN LNCAP CELLS REVEALED NOVEL ASSOCIATIONS WITH UPREGULATION OF CCDN1 SIGNALLING AND FATTY ACID METABOLISM.	206
FIGURE 5.10. ELEVATED USP2 EXPRESSION IN LNCAP CELLS IS ASSOCIATED WITH ACTIVATION OF NEUROENDOCRINE-ASSOCIATED SIGNALLING AND LIPID METABOLISM.	207
FIGURE 5.11. ELEVATED USP2 EXPRESSION IN LNCAP CELLS IS ASSOCIATED WITH INHIBITION OF PROTEIN UBIQUITINATION, APOPTOSIS, AND INTERFERON SIGNALLING.	209

FIGURE 5.12. PRINCIPAL COMPONENT ANALYSIS OF THE GLOBAL TRANSCRIPTOME GROUPED THE TRANSCRIPTOMES OF THE LNCAP CELLS OVEREXPRESSIONING USP2 (USP2-OE) AND LNCAP CELLS OVEREXPRESSIONING THE NEON TRANSGENE (CONTROL) INTO TWO CLEAR CLUSTERS. 212

FIGURE 5.13. VOLCANO PLOT OF TRANSCRIPTS AT DIFFERENT ABUNDANCE LEVELS BETWEEN THE USP2-OE LNCAP CELLS AND THE CONTROL LNCAP CELLS. 214

FIGURE 5.14. GSEA ANALYSIS OF TRANSCRIPTOMIC DATA CONDUCTED ON LNCAP CELLS OVEREXPRESSIONING USP2 (USP2-OE) VERSUS LNCAP CELLS OVEREXPRESSIONING THE NEON TRANSGENE (CONTROL) REVEALED ASSOCIATIONS OF USP2 WITH INHIBITION OF INTERFERON SIGNALLING AND ACTIVATION OF HYPOXIA AND MITOTIC SPINDLE PATHWAYS. 216

FIGURE 5.15. ELEVATED USP2 EXPRESSION IN LNCAP CELLS IS ASSOCIATED WITH ACTIVATION OF NEUROENDOCRINE-ASSOCIATED SIGNALLING AND FATTY ACID METABOLISM. 218

FIGURE 5.16. ELEVATED USP2 EXPRESSION IN LNCAP CELLS IS ASSOCIATED WITH INHIBITION OF INTERFERON SIGNALLING AND EXPRESSION OF INTERFERON-INDUCED GENES. 220

FIGURE 5.17. THIRTEEN PROTEINS WERE IDENTIFIED AS POTENTIAL NOVEL USP2 SUBSTRATES. 222

FIGURE 5.18. SEVERAL OF THESE THIRTEEN HIGH-PRIORITY CANDIDATES AS USP2 SUBSTRATES WERE ASSOCIATED WITH NEUROENDOCRINE TUMOURS AND RESISTANCE TO CHEMOTHERAPY AND IMMUNOTHERAPY. 225

FIGURE 5.19. NEUROENDOCRINE- AND MESENCHYMAL-RELATED FACTORS THAT ARE INCREASED WITH UPREGULATION OF USP2 EXPRESSION IN LNCAP CELLS. 229

FIGURE 6.1. DIAGRAM SUMMARISING THE KEY FINDINGS IN MY PHD DISSERTATION. 238

Abbreviations

Androgen deprivation therapy	ADT
Apoptosis inducing factor	AIF
Active surveillance	AS
Androgen receptor	AR
Androgen response element	ARE
AR-Chromatin Immunoprecipitation	AR-ChIP
AR-variants	AR-Vs
Australia and New Zealand	ANZ
Brachytherapy	BT
Breast cancer	BCa
Benign prostatic hyperplasia	BPH
Breast cancer 1/2, early onset	BRCA1/2
Castrate-resistant prostate cancer	CRPC
NEPC that arose from CRPC	CRPC-NEPC
DNA-binding domain	DBD
5 α -dihydrotestosterone	DHT
Digital rectal examination	DRE
Deubiquitinating enzymes	DUBs
DNA damage repair	DDR
European Association of Urology	EAU
Epithelial to mesenchymal transition	EMT
External beam radiotherapy	ERBT

Fatty acid synthase	FASN
Follicle-stimulating hormone	FSH
Glutathione	GSH
Gonadotropin-releasing hormone	GnRH
Kallikrein-related peptidase-3 gene	KLK3
Luteinizing hormone	LH
Ligand-binding domain	LBD
Magnetic resonance imaging	MRI
Metastatic prostate cancer	mPCa
Mouse double minute 2 homolog	MDM2
Small molecule inhibitor of USP2	ML364
Multi-parametric MRI	mpMRI
Multiple myeloma	MM
N'-nitro-N'-nitrosoguanidine	MNNG
Neuroendocrine prostate cancer	NEPC
N-terminal domain	NTD
Non-small cell lung cancer	NSCLC
Nuclear co-activators 1 and 2	NCOA1 and NCOA2
Nuclear co-repressors 1 and 2	NCOR1 and NCOR2
Nuclear localisation signal	NLS
Prostate cancer	PCa
Patient-derived explants	PDE
Poly-adenosine diphosphate-ribose polymerase	PARP

Progression free survival	PFS
Prostate specific antigen	PSA
Radical prostatectomy	RP
Real-time-quantitative polymerase chain reaction	RT-qPCR
RNA-sequencing	RNA-seq
National Surveillance, Epidemiology and End Results	SEER
Single-cell RNA sequencing	scRNA-seq
Transcriptional factor	TF
Transrectal Ultrasound	TRUS
Extent of local tumour (T), regional lymph node status (N), presence of distant metastases (M)	TNM
Ubiquitin-activating enzyme	E1
Ubiquitin-conjugating enzyme	E2
Ubiquitin ligase	E3
Ubiquitin proteasome system	UPS
Ubiquitin-specific proteases	USPs
Ubiquitin-specific protease 2a	USP2a
LNCaP cells overexpressing USP2	USP2-OE
<i>3β-hydroxysteroid dehydrogenase type 1 gene</i>	<i>HSD3B1 gene</i>

1 Investigating USP2 as a mediator of therapy resistance in lethal prostate cancer

1.1 Project Details

1.1.1 Abstract

The growth of prostate cancer (PCa) is dependent on male sex hormones, termed androgens, and the androgen receptor (AR). Therefore, implementing strategies to inhibit AR activity, collectively referred to as androgen deprivation therapy (ADT), is the key therapeutic strategy for metastatic prostate cancer. Unfortunately, ADT is never curative, and patients eventually develop a lethal therapy resistant form of the disease termed castration-resistant prostate cancer (CRPC). The AR signalling pathway is altered in CRPC and a subset of CRPC tumours may evade inhibition by ADT by progressing to a state in which tumour growth is independent of this pathway. One such AR-independent CRPC subtype is termed neuroendocrine PCa (NEPC). Understanding how tumours transition to therapy-resistant, AR-independent states is crucial for the development of new and more effective therapies.

We recently undertook transcriptomic profiling of patient tumours treated *ex vivo* with a clinical AR antagonist, enzalutamide, as a strategy to identify therapy-mediated adaptive changes. This study identified *Ubiquitin specific protease 2 (USP2)* as being increased in response to enzalutamide. The role of USP2 is to remove ubiquitin groups from proteins that causes therapy resistance and cancer progression, thereby preventing these proteins from degradation and increasing their stability in cancer cells. Thus, we hypothesised that

USP2 can mediate resistance to ADT by stabilising key oncoproteins, a concept that was tested in my PhD project.

Increased USP2 expression in response to ADT and in therapy-resistant states was validated in multiple prostate cancer cell line models, clinical transcriptomic cohorts, and additional patient tumours. Growing androgen-dependent cell lines in the presence of enzalutamide resulted in increased USP2 expression; conversely, androgen treatment resulted in the repression of USP2 expression. Clinical datasets also revealed that USP2 expression is elevated in AR-low/negative CRPC tumours, particularly those classified as neuroendocrine PCa.

These observations suggest that USP2 is consistently upregulated in response to AR-targeted therapies and may represent a previously unknown resistance factor. Supporting this, targeting USP2 in multiple castrate-resistant prostate cancer models, either pharmacologically with a USP2-specific inhibitor (ML364) or by genetic knockdown, resulted in reduced cell viability and increased cell death. In contrast, overexpression of USP2 drove the development of an aggressive, therapy-resistant neuroendocrine phenotype and conferred partial resistance to enzalutamide and a growth advantage in androgen-depleted growth conditions. Importantly, ML364 was also potently active in an *in vivo* model of aggressive, AR-negative prostate cancer.

Mechanistically, we found that USP2 stabilises the levels of oncogenic proteins including Aurora kinase A (AURKA), Cyclin D1 and Fatty acid synthase (FAS). Interrogation of

the proteome and transcriptome of PCa cells overexpressing USP2 revealed positive enrichment of neuroendocrine-associated signalling, lipid metabolism and cell cycle, and negative enrichment of interferon signalling. All these enriched pathways are important in driving growth, survival, and progression of cancer.

Overall, the findings herein revealed that USP2 can promote the development of neuroendocrine prostate cancer and acts to confer resistance to standard-of-care therapies, revealing it as a bona fide therapeutic target.

1.1.2 Declaration

I certify that this work contains no material which has been accepted for the award of any other degree or diploma in my name in any university or other tertiary institution and, to the best of my knowledge and belief, contains no material previously published or written by another person, except where due reference has been made in the text. In addition, I certify that no part of this work will, in the future, be used in a submission in my name for any other degree or diploma in any university or other tertiary institution without the prior approval of the University of Adelaide and where applicable, any partner institution responsible for the joint award of this degree.

I give permission for the digital version of my thesis to be made available on the web, via the University's digital research repository, the Library Search and also through web search engines, unless permission has been granted by the University to restrict access for a period of time.

Name: Fang Meiwen Danielle

Date: January 2023

1.2 Acknowledgements

I would like to express my deepest gratitude to my parents and family for their endless support and encouragement. Additionally, I would like to thank the University of Adelaide for granting me the University of Adelaide PhD scholarship.

In addition, this endeavour would not have been possible without my supervisors A/Prof. Luke Selth, Prof. Lisa Butler and Prof. Wayne Tilley. Their words of wisdom and invaluable guidance have helped to shape my PhD project.

Additionally, I would like to extend my thanks to my PhD host labs for their support: Prostate Cancer Research Group (FCIC) (Selth lab), Dame Roma Mitchell Cancer Research Lab (University of Adelaide) (Tilley lab) and Prostate Cancer Research Group (SAHMRI) (Butler Lab). Many thanks to Dr. Jianling Xie, Scott Townley and Adrienne Hanson from the Prostate Cancer Research Group at the Flinders Centre for Innovation in Cancer (FCIC) (Selth Lab) for training me in various techniques and supporting my PhD project. In addition, a huge thank you to the SAHMRI mice, Flinders Omics and South Australian Genomic Centre (SAGC) facilities for their support in this project.

Lastly, I would like to thank my friends for being supportive, encouraging and understanding towards me. Thank you to my family, host labs and friends for making my life full of laughter and happiness.

Table 1.1. List of contributions

Name	Contribution to the specific activity	Percentage of contribution (%)
Scott Townley	Technical assistance with qRT-PCR in Figure 3.5D , Western blot in Figure 3.14 and growth assay in Figure 4.8 .	15
Jianling Xie	Assisted with the design of the mice experiment	10
Adrienne Hanson	Assisted with lentiviral cell line work	5
Richard Iggo	Assisted in the design of the lentiviral vector overexpressing USP2	10
Zeyad Nassar	Assisted with the design of the mice experiment	10
Madison Helm	Mice surgery and dissection	50
Tim Chataway	Proteomics data analysis	10
Alex Colella	Proteomics data analysis	10
Shashikanth Marri	Transcriptomics data analysis	20
Giles Best	Assisted with AnnexinV-PE and 7AAD flow cytometry (Figure 4.3)	10
Margaret Centenera	Undertook the patient-derived explant RNA-seq experiment (Figure 3.1A)	50

1.3 The prostate is an androgen-regulated gland

The main function of the prostate gland is to secrete a fluid containing zinc, phosphatases and proteases, blood coagulases, profibrinolysin and albumin (Dow and Bavister, 1989, Kumar and Majumder, 1995, Hall and Guyton, 2011). This fluid, which forms part of the semen, enhances sperm motility and fertility and is slightly alkaline to counteract the relatively acidic fluid from the vas deferens (**Figure 1.1**) (Kumar and Majumder, 1995, Hall and Guyton, 2011). Another prostate function is controlling urine flow from the bladder (Kumar and Majumder, 1995).

Growth and homeostasis of the prostate gland are controlled by androgens, which signal through the androgen receptor (AR) (Carson and Rittmaster, 2003). The brain hypothalamus secretes Gonadotropin-releasing hormone (GnRH) into the anterior pituitary and stimulates it to secrete the follicle-stimulating hormone (FSH) and luteinizing hormone (LH) (**Figure 1.2**) (Hall and Guyton, 2011). The LH then stimulates the Leydig cells within the testis to release testosterone, while FSH stimulates spermatogenesis (**Figure 1.2**). Within the prostate, testosterone is converted by 5α -reductase into 5α -dihydrotestosterone (DHT), which is a more potent androgen that has higher affinity for AR (**Figure 1.4**) (Wright et al., 1996). DHT is important for foetal prostate differentiation and development of the male external genitalia that occurs during normal early development (Carson and Rittmaster, 2003). In adults, DHT and other androgens may be important in maintaining the balance between cell proliferation and apoptosis in prostate (Carson and Rittmaster, 2003).

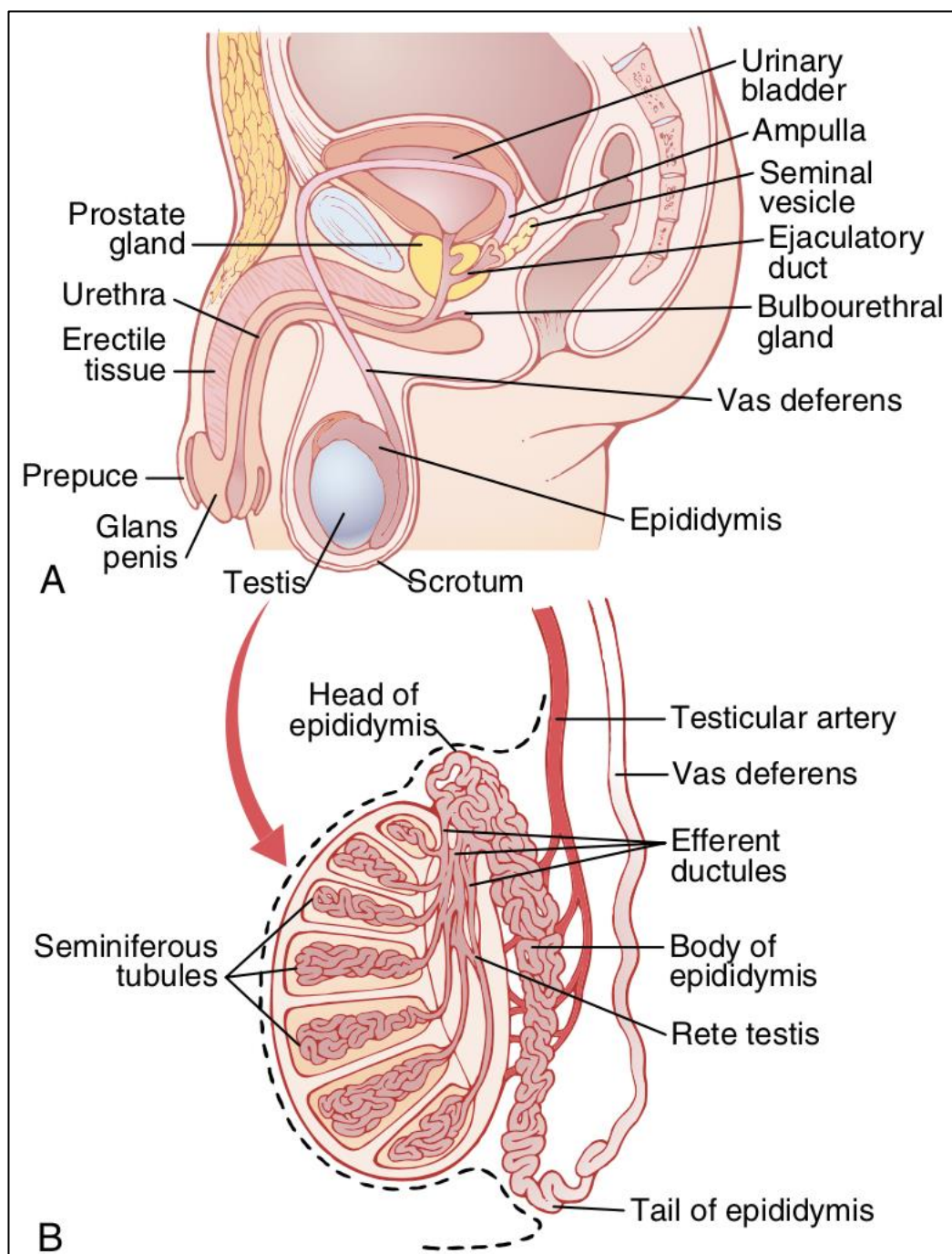


Figure 1.1. Diagram describing the anatomy surrounding the male reproduction system. A) The side-view of the male reproduction system is shown. **B)** The internal structure of the testis is shown. Figure (A) and (B) were taken directly from (Hall and Guyton, 2011).

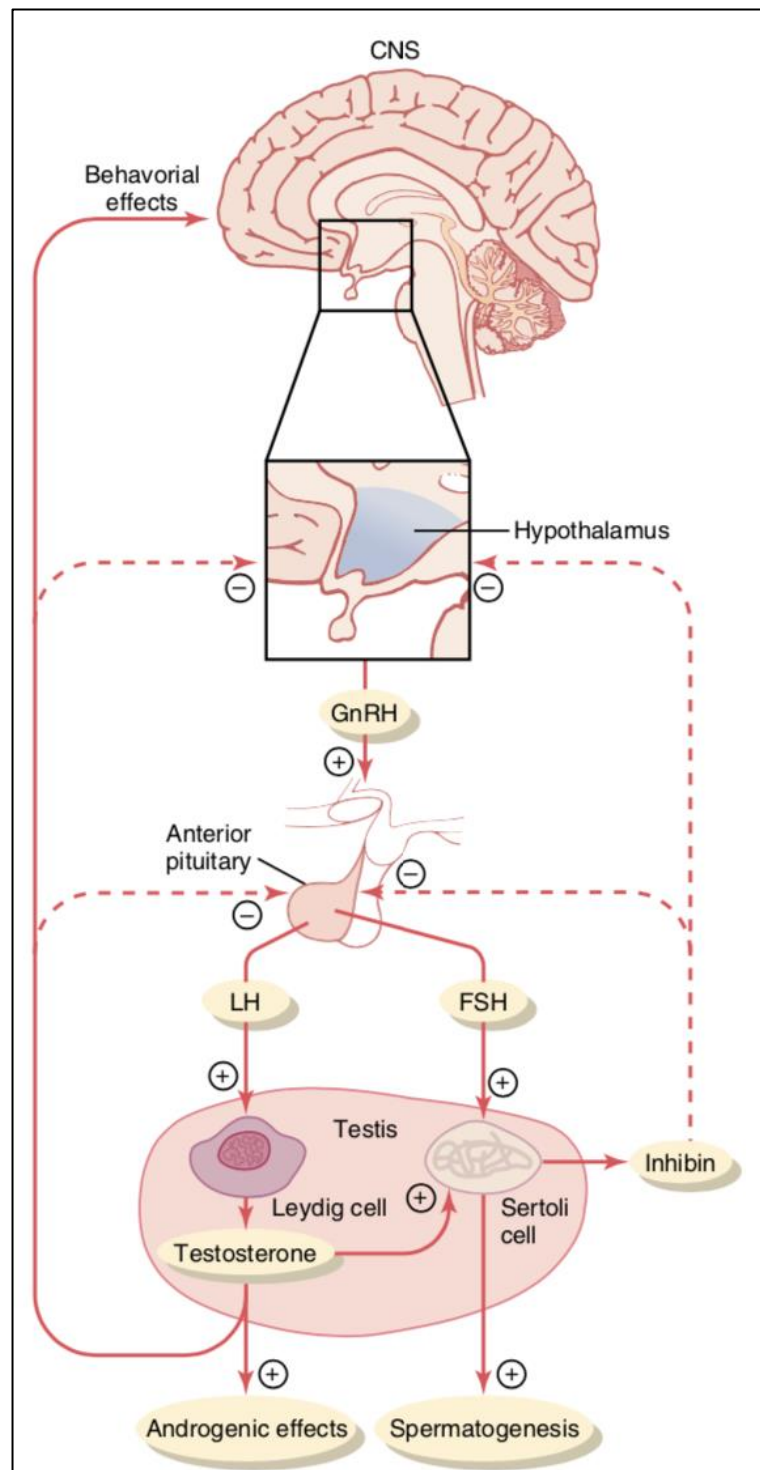


Figure 1.2. This is the feedback loop of the hypothalamic-pituitary-testicular axis in males and its outcomes are androgen production and spermatogenesis. (+) indicates stimulation, while (-) indicates inhibition through negative feedback (Hall and Guyton, 2011).

1.4 Androgen Receptor (AR)

1.4.1 Gene, structure, and functions of Androgen Receptor (AR)

The AR is part of the steroid and nuclear receptor superfamily and is encoded by the *AR* gene that is localised to the q11-12 region of the human X chromosome (**Figure 1.3**) (Lubahn et al., 1988, Brown et al., 1989). The gene has 8 exons and encodes for a 110kDa protein that is 919 amino acids long (**Figure 1.3**) (Lubahn et al., 1988, Brown et al., 1989). The AR is a modular protein with four distinct domains: the ligand-binding domain (LBD), which is where androgens bind and activate AR; the hinge domain, which contains the putative conserved bipartite nuclear localisation signal (NLS) and is important for binding to importin- α so that AR can be transported into nucleus; the DNA-binding domain (DBD), which can mediate AR homodimerization and subsequent binding to specific DNA regions named androgen response elements (ARE); and the N-terminal domain (NTD), which contains the transactivation domain (**Figure 1.3**) (He et al., 2000, He and Wilson, 2003, He et al., 1999, Tremblay et al., 1999, Langley et al., 1998, Coutinho et al., 2016).

AR can function as a transcription factor (TF) (**Figure 1.3**) and have different roles in normal development and prostate cancer (PCa) development (Notini et al., 2005, Shiota et al., 2011). In normal development, AR is important in the development of the prostate gland (Notini et al., 2005). However, during carcinogenesis, AR's signalling outputs change from being anti-proliferative and pro-differentiative to pro-proliferative and anti-differentiative (Notini et al., 2005). In carcinogenesis, the androgen-AR signalling pathway is the key driver for PCa growth and progression (Shiota et al., 2011). For example, AR can increase expression

of oncoproteins like MYC, which is a transcription factor that can regulate cell cycle progression, and decrease expression of tumour suppressors like P53, which is a transcription factor involved in DNA repair and cell cycle arrest (Shiota et al., 2011).

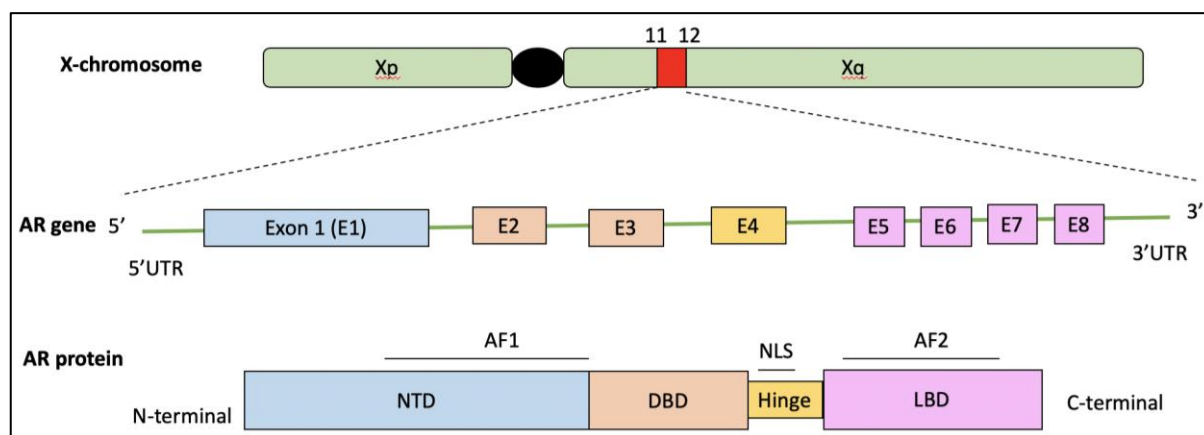


Figure 1.3. The AR comprises of 4 domains: N-terminal domain (NTD), DNA-binding domain (DBD), hinge domain and ligand-binding domain (LBD).

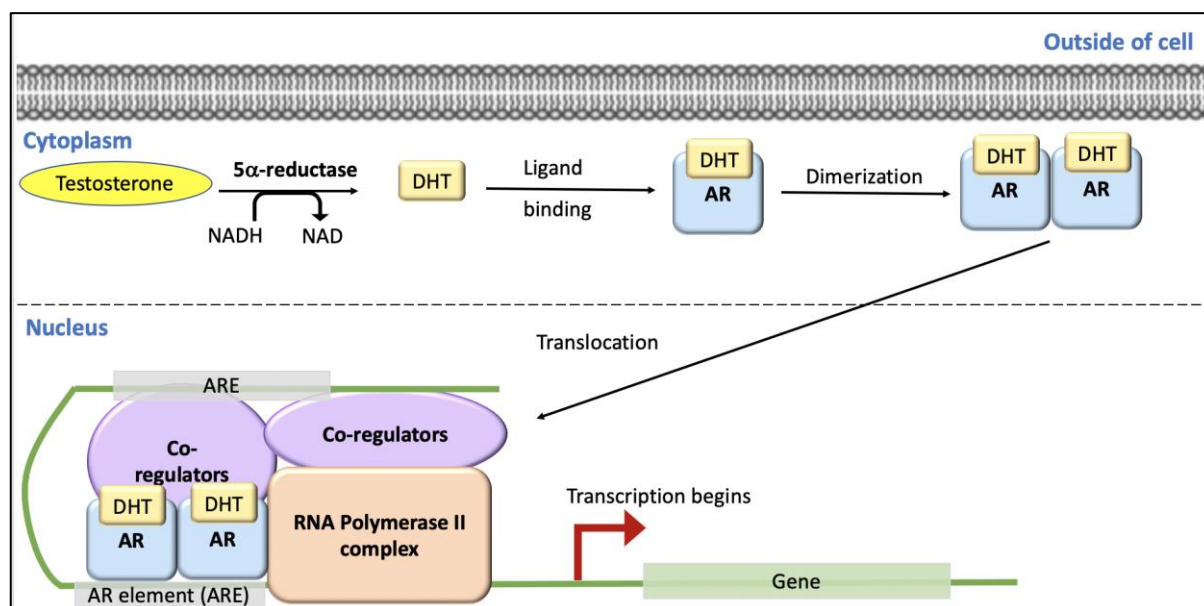


Figure 1.4. A summary of how AR can function as a transcription factor when bound to DHT.

Testosterone enters the prostate epithelial cell and is converted to DHT by 5 α -reductase, while oxidising NADH. AR binds to DHT and form homodimers. AR homodimers then translocates into the nucleus and binds to AREs within the DNA and recruits co-regulators. If the co-regulators are co-activators of AR, then RNA polymerase II complex will be recruited, and transcription of a gene can begin. If the co-regulators are co-repressors of AR, then DNA methylases and histone deacetylases will be recruited to methylate and deacetylate the DNA to reduce transcription of the gene.

1.5 Epidemiology of Prostate Cancer

Prostate cancer is very prevalent worldwide (**Figure 1.5**). In 2018, 1.28 million cases of prostate cancer were reported, making it the fourth most diagnosed cancer in 2018 worldwide (**Figure 1.6**). Additionally, approximately 360,000 patients died from prostate cancer in that year worldwide (**Figure 1.6**). Australia and New Zealand (ANZ) have the highest age-standardised prostate cancer incidence worldwide (**Figure 1.5**) and a combined age-standardised prostate cancer mortality rate of 10.2 per 100,000 (**Figure 1.7**).

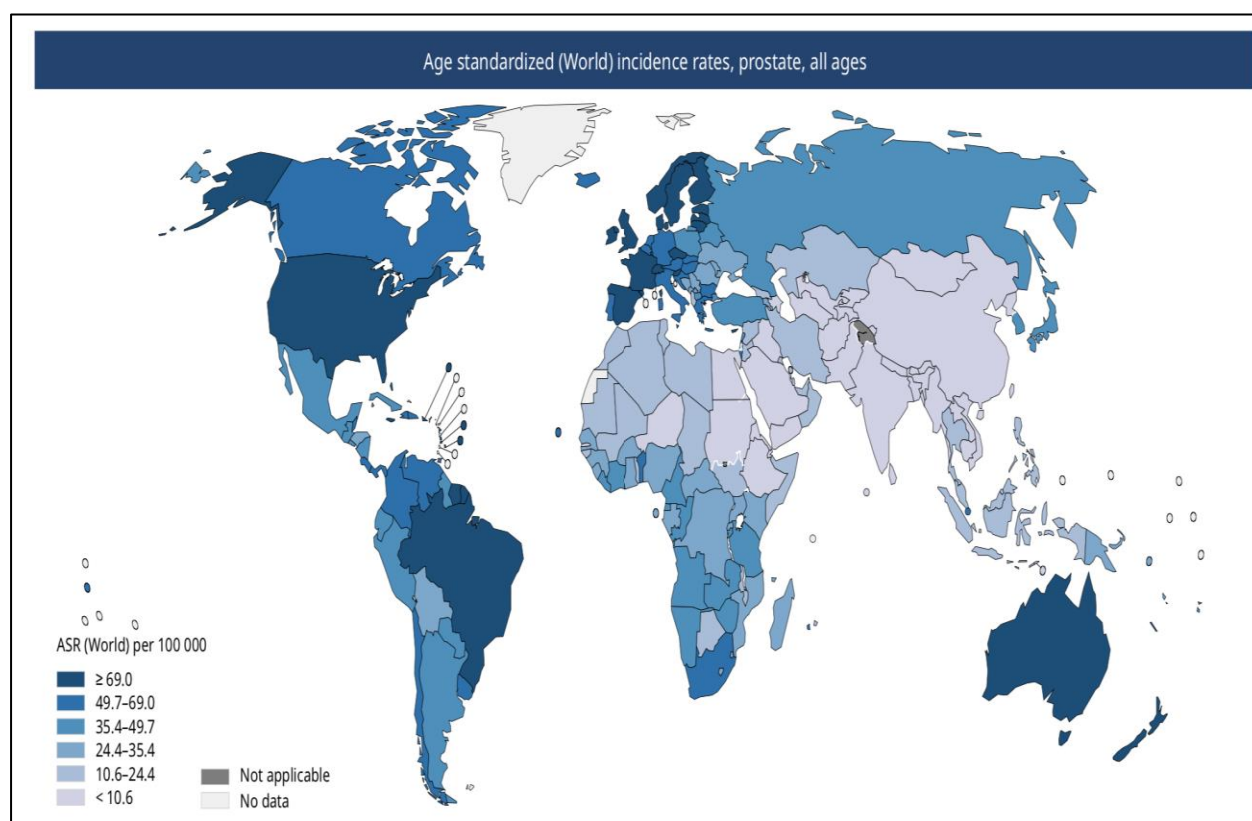


Figure 1.5. The age-standardised incidence rates of prostate cancer in males of all ages worldwide who were diagnosed in 2018. The higher the age-standardised incidence rate, the more intense the blue highlighting is. Australia and New Zealand has one of the highest age-standardised incidence rates in 2018. Statistics were provided by the World Health Organisation (Wang et al., 2022).

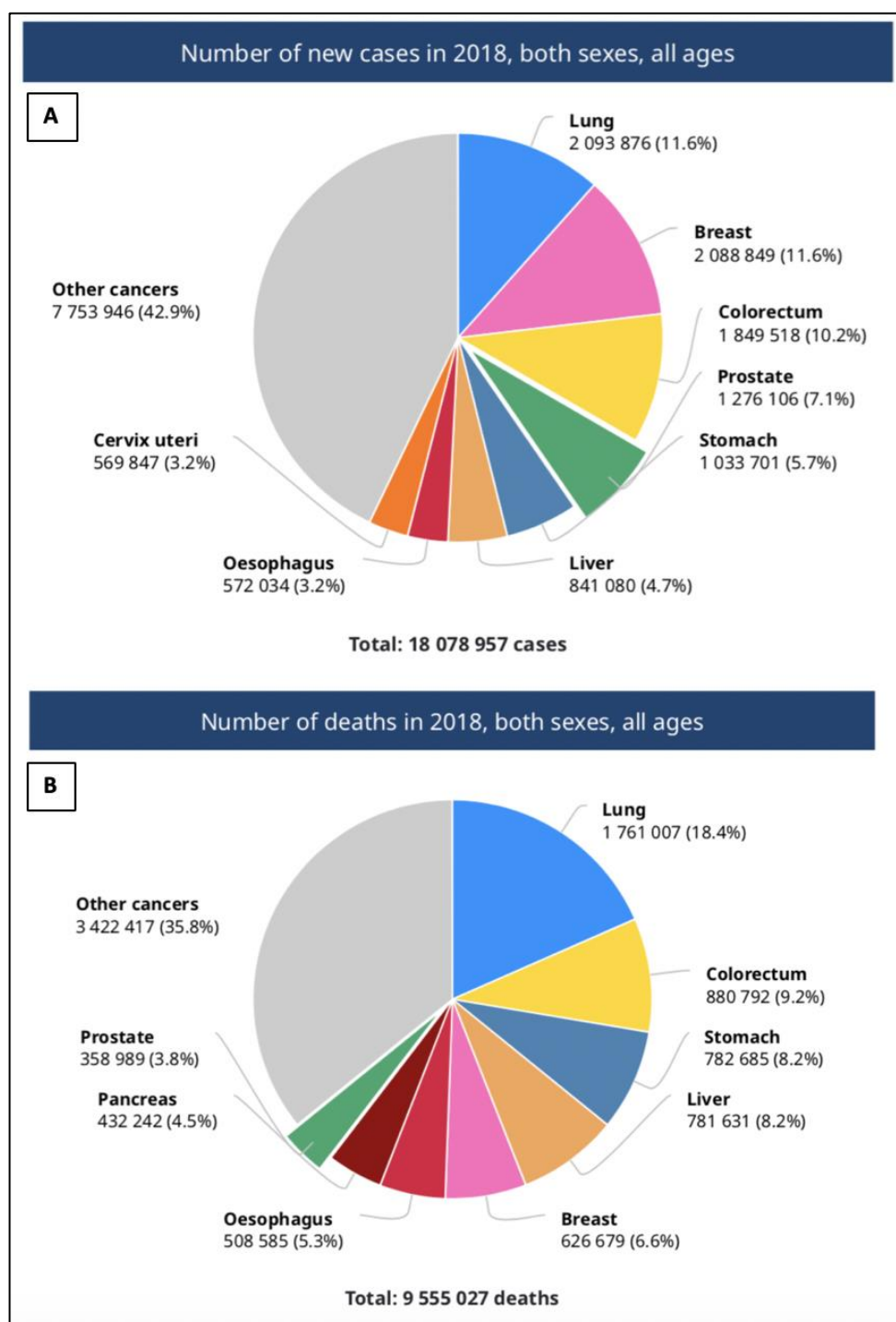


Figure 1.6. A comparison of the number of new cancer cases and deaths across the different types of cancers that occurred in 2018 and in both sexes of all ages. A) The number of new cancer cases diagnosed worldwide. B) The number of deaths that occurred worldwide. Statistics were provided by the World Health Organisation (Wang et al., 2022).

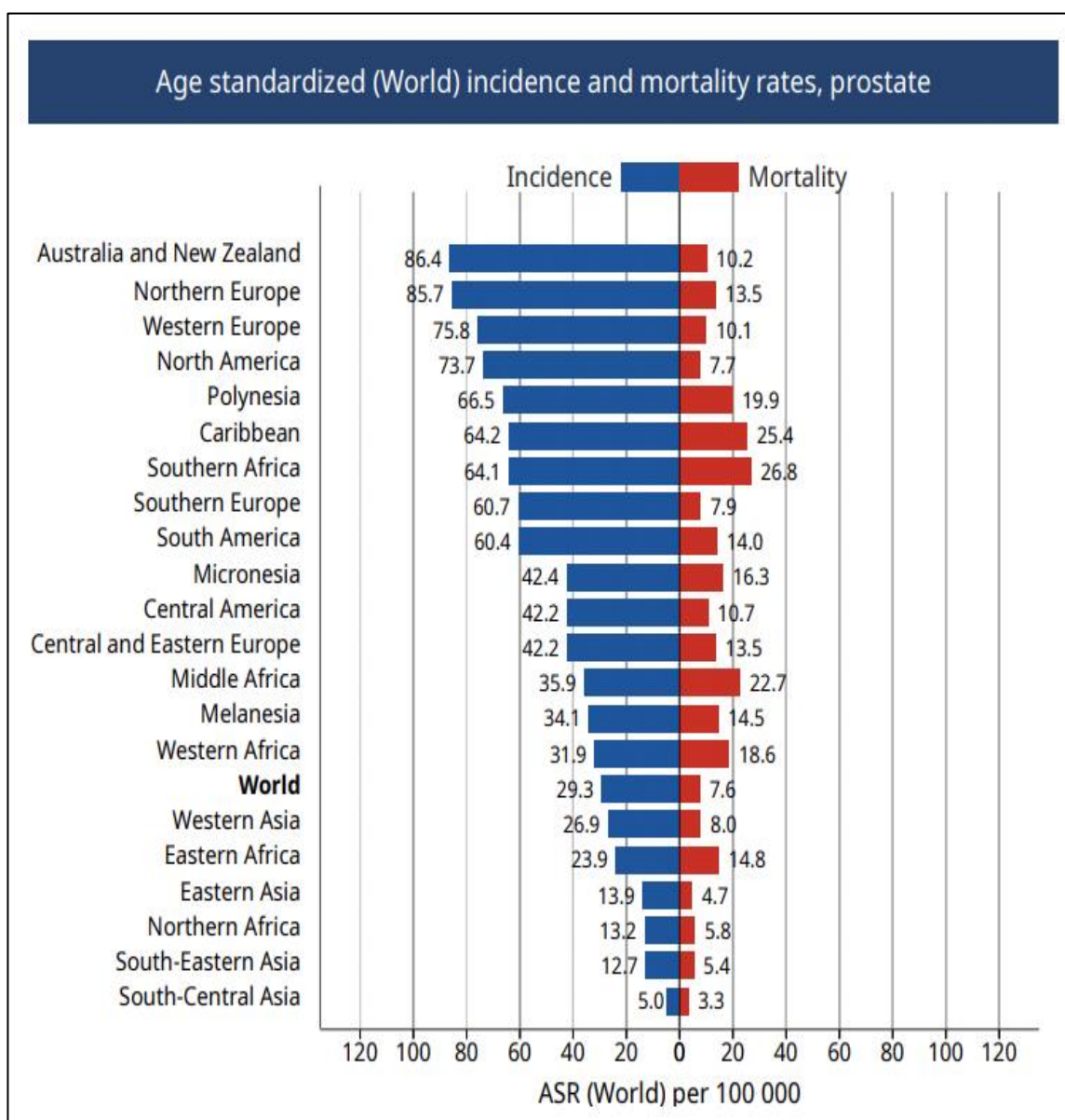


Figure 1.7. A comparison of age-standardised incidences and mortality rates for prostate cancer between countries in 2018. Statistics were provided by the World Health Organisation (Wang et al., 2022).

1.6 Diagnosis of prostate cancer

Testing for prostatic specific antigen (PSA) levels and conducting digital rectal examinations (DREs), which detects distended prostate glands, are the standard initial procedures to diagnose patients with prostate cancer (Catalona et al., 1993). PSA is encoded by the *KLK3* gene, which is AR-regulated, and becomes elevated in the patient's bloodstream when they have prostate cancer (Catalona et al., 1993). However, PSA can also increase in the bloodstream with increasing age, inflammation of prostate and benign prostatic hyperplasia (BPH), which is not cancerous (Haythorn and Ablin, 2011). Thus, PSA is not a specific marker for Pca.

In addition to PSA and DRE tests, magnetic resonance imaging (MRI) can be used to assist in Pca diagnosis (Barrett, 2015, Parker et al., 2020, Ahmed et al., 2017). MRI utilises radio-waves and a magnetic field to image an individual's interior body. It allows for earlier identification of abnormal growth in the prostate (Barrett, 2015).

When the results of the PSA (> 4 ng/mL), DRE and MRI tests are abnormal, a biopsy will be conducted. A biopsy is the definitive tool for diagnosis of Pca (Gordetsky and Epstein, 2016). Biopsies can be guided by either Transrectal Ultrasound (TRUS) or MRI scans (Mottet et al., 2017, Schoots et al., 2014). Normally, 12 separate samples are typically taken during biopsy, with additional samples taken from areas in the prostate that are suspected to have abnormal growth from the DRE/TRUS or MRI imaging (Mottet et al., 2017).

1.7 Grading / staging of prostate cancer

The Gleason grading system is used as a measure of the aggressiveness of a prostate tumour, which is how likely it will be to spread (Gordetsky and Epstein, 2016). There are 5 Gleason grades with Gleason grade/pattern 1 being well differentiated and correlated with favourable prognosis, while Gleason grade 5 is the most poorly differentiated and correlated with unfavourable prognosis (Chen and Zhou, 2016). Gleason grade 3 comprises of well-formed, discrete individual glands (**Figure 1.8**) (Gordetsky and Epstein, 2016). Gleason grade 4 consists of poorly-formed, fused and cribriform glands (**Figure 1.8**) (Gordetsky and Epstein, 2016). Gleason grade 5 comprises of sheets of tumour, cords of cells and individual cells (**Figure 1.8**) (Gordetsky and Epstein, 2016). Gleason grade 5 can also comprise of solid nests of cells with the occasional formation of gland space or vague micro-acinar (**Figure 1.8**) (Gordetsky and Epstein, 2016).

Gleason scores are calculated by the summation of the primary and secondary Gleason grades, which are the most extensive pattern observed in the tumour and the highest pattern (regardless of extent) respectively. These Gleason scores can be grouped into 5 different Gleason Grade Groups (**Figure 1.9**) (Mottet et al., 2017). The higher the Gleason Grade Group, the more likely it is that a tumour will grow quickly and metastasize (Chen and Zhou, 2016, Epstein et al., 2016).

In addition to Gleason scores, staging of prostate cancer can be conducted to assess how large the cancer is and whether spreading to other parts of the body has occurred (Mottet et al., 2017). Staging of prostate cancer is evaluated through three factors: extent of

local tumour (T); regional lymph node status (N); and presence of distant metastases (M) (Stephens et al., 2008). The TNM staging classification for Pca can be summarised in **Figure 1.10** (Stephens et al., 2008). Grading or staging of prostate cancer is a critical step in determining the most appropriate course of treatment, as described in the following section.

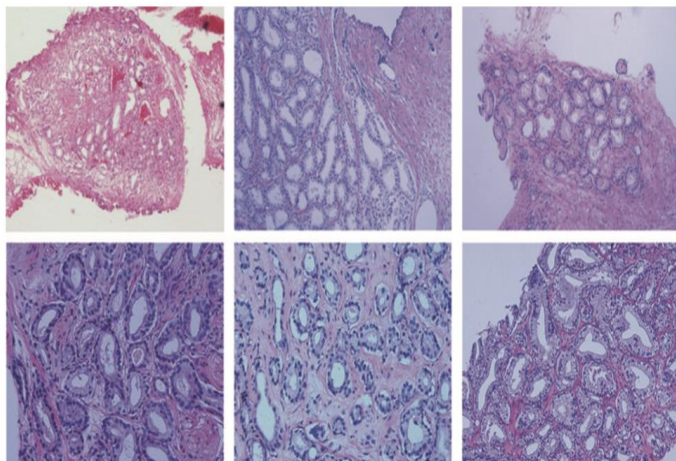
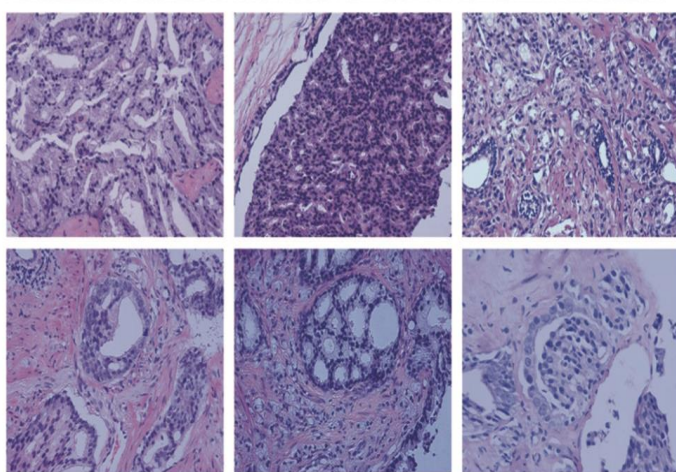
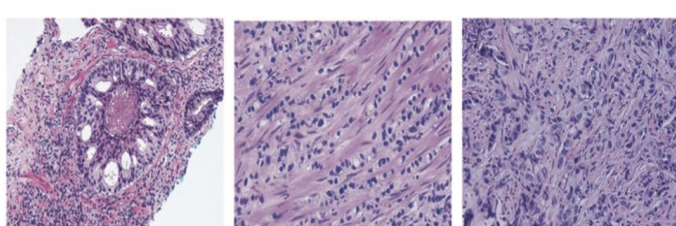
	Gleason patterns 1-3 distinct, discrete, individual glands	Gleason score ≤ 6	Grade group I	
		Gleason pattern 4 fused, cribriform, or poorly-formed glands, or glomerularion	Gleason score $3+4=7$	Grade group II
			Gleason score $4+3=7$	Grade group III
			Gleason score $4+4=8$ $3+5=8$ $5+3=8$	Grade group IV
		Gleason pattern 5 comedo necrosis, cords, sheets, solid nests, single cells	Gleason score $4+5=9$ $5+4=9$ $5+5=10$	Grade group V

Figure 1.8. Typical pictures of prostate tumour associated with the corresponding Gleason grades/patterns (ranging from 1 to 5) and grouped into various Gleason grade groups (I to V) using their Gleason scores (Chen and Zhou, 2016).

Gleason score	Grade group
≤6 (3+3 or 3+2 or 2+3 or 2+2)	1
7 (3 + 4)	2
7 (4 + 3)	3
8 (4+4 or 3+5 or 5+3)	4
9–10	5

Figure 1.9. Various Gleason scores can be grouped into 5 different Gleason grade groups in accordance to the International Society of Urological Pathology 2014 (Mottet et al., 2017).

Stage	Characteristic
Tx	Primary tumour cannot be assessed
T0	No evidence of primary tumour
T1	Clinically inapparent tumour neither palpable nor visible by imaging
T1a	Tumour incidental histological finding in ≤5% of tissue resected
T1b	Tumour incidental finding in >5% of tissue resected
T1c	Tumour identified by needle biopsy
T2	Tumour confined within prostate
T2a	Tumour involves one half of one lobe or less
T2b	Tumour involves more than one half of one lobe but not both lobes
T2c	Tumour involves both lobes
T3	Tumour extends through the prostate capsule
T3a	Extracapsular invasion (uni- or bilateral)
T3b	Tumour invades seminal vesicle(s)
T4	Tumour is fixed or invades adjacent structures other than seminal vesicles (bladder neck, external sphincter, rectum, levator muscles and/or pelvic sidewall)
Nx	Regional nodes not assessed
N0	No regional nodal metastasis
N1	Metastasis in regional node(s)
Mx	Distant metastasis not evaluated by any modality
M0	No distant metastasis
M1a	Non-regional lymph node(s)
M1b	Bone(s)
M1c	Other sites with or without bone disease

Figure 1.10. The TNM staging for prostate cancer, which stands for Tumour (T), regional lymph node status (N); and presence of distant metastases (M) (Stephens et al., 2008).

1.8 Current management options for prostate cancer

The treatment recommended for patients with prostate cancer is dependent on the tumour grade during diagnosis. The 5-year relative survival rate for patients with localised prostate cancer is approximately 99% in Australia (Siegel et al., 2016). However, approximately 30% of patients will subsequently experience disease recurrence (Singh et al., 2002). Additionally, the 5-year relative survival rate for patients with metastatic prostate cancer is approximately 30% (Siegel et al., 2023). Therefore, this highlights the need to recommend treatments based on the grade and type (i.e. localised versus metastatic) of prostate cancer in accordance with European Association of Urology (EAU) Guidelines (Heidenreich et al., 2015, Mottet et al., 2017, Cornford et al., 2017).

1.8.1 Treatment of localised prostate cancer

Active surveillance (AS) is a recommended observational strategy for patients with low-risk prostate cancer, which has a Gleason score of 6 or less (Mottet et al., 2017). AS aims to reduce overtreatment and minimise toxicity from treatments (Thomsen et al., 2014). During AS, patient may undergo several PSA, DRE, MRI and re-biopsy tests to check for abnormal tumour growth (Mottet et al., 2017).

For patients with Gleason score 7 and above or with a PSA > 10 ng/ml, the two main curative-intended treatments are radiotherapy (RT) and radical prostatectomy (RP) (Thomsen et al., 2014, Mottet et al., 2017). Radiotherapy is the use of radiation to kill cancer cells and may be given either externally through External Beam radiotherapy (ERBT) or internally

through Brachytherapy (BT) (Mottet et al., 2017). RP is the removal of prostate gland that contains the tumour (Mottet et al., 2017).

Patients with high-risk locally advanced prostate cancer (with Gleason score 9 to 10) often experience failure of mono-treatments (either radiotherapy or radical prostatectomy) and consequently relapse of prostate cancer (Hegemann et al., 2016, Kishan et al., 2018, Terlizzi and Bossi, 2022). For these patients, combinatorial treatments of radiotherapy (ERBT and BT) and androgen deprivation therapy (ADT) with radical prostatectomy improved overall survival and biochemical progression-free survival (Kishan et al., 2018, Terlizzi and Bossi, 2022).

1.8.2 Treatment of metastatic prostate cancer

The European Association of Urology (EAU) Guidelines on PCa defines recurrent PCa in patients as when there has been two consecutive increases in PSA value >0.2 ng/ml following radical prostatectomy (RP) and a PSA value of 2 ng/ml above the nadir following radiotherapy (Heidenreich et al., 2015). In addition to patients that experience recurrence after therapy, some patients are diagnosed with metastatic PCa (mPCa) – cancer that has spread beyond the prostate – during initial diagnosis (Aus et al., 2005, Cornford et al., 2017). Methods for detecting mPCa abnormalities include multi-parametric MRI (mpMRI), which is reported to be accurate at detecting local PCa recurrence and pelvic bone metastasis, and PET/CT scan, which is reported to be accurate at detecting pelvic bone and lymph-nodes metastasis (Kitajima et al., 2014, Draulans et al., 2019).

As described above, the androgen-AR signalling axis is the primary driver of PCa growth, therefore patients with mPCa are treated with ADT, which aims to block AR activity

(Cornford et al., 2017, Huggins et al., 1941). ADT is achieved through pharmacological castration (Kyriakopoulos et al., 2018). Pharmacological castration is generally achieved through the use of Luteinising hormone-releasing hormone (LHRH) agonist (Seidenfeld et al., 2000). LHRH agonists compete for the binding to pituitary LHRH receptors and desensitise them, resulting in a downregulation of LHRH receptors and consequently reduced production of LH and FSH in the anterior pituitary (**Figure 1.2**). Therefore, testosterone production levels will drop to 'castrate' levels (Brawer, 2004). Another pharmacological castration method is the use of a LHRH antagonist (Lin et al., 2011). LHRH antagonists inhibit the LHRH receptor, therefore resulting in a reduction of LH being released and testosterone levels drop (Lin et al., 2011). Another newer strategy to inhibit androgen biosynthesis is the use of abiraterone acetate (Kim and Kim, 2011). Abiraterone Acetate is a potent, specific, irreversible inhibitor of CYP17, which is important for androgen biosynthesis (Kim and Kim, 2011).

In addition to castration, another strategy to inhibit AR as a treatment for men with mPCa is the use of anti-androgens, also known as AR antagonists (Thomas and Neal, 2013, Siemens et al., 2018, Ammannagari and George, 2015). The first generation of AR antagonists include flutamide, nilutamide and bicalutamide (Siemens et al., 2018, Ammannagari and George, 2015), whereas newer "second-generation" AR antagonists include enzalutamide, apalutamide and darolutamide. AR antagonists bind directly to the AR LBD, thereby blocking androgen action and inhibiting AR activity (Thomas and Neal, 2013). Enzalutamide and apalutamide bind to the AR's LBD with higher affinity than their 1st generation counterpart bicalutamide (Tran et al., 2009, Smith et al., 2018b).

Historically, ADT, sometimes in combination with first-generation AR antagonists, was the primary treatment for men with metastatic PCa or PCa that had relapsed after surgery/radiation. More recently, clinical trials have demonstrated a significant overall survival benefit of ADT with chemotherapy and abiraterone acetate for patients with metastatic hormone naïve PCa, especially those with high-volume mPCa, as compared to patients who only had ADT (de Bono et al., 2011, Feyerabend et al., 2018, Sun et al., 2019, Kyriakopoulos et al., 2018). Additionally, three phase III clinical trials that are near completion are currently investigating the benefit of docetaxel in conjunction with ADT (NCT02446405; NCT01957436; NCT02489318). In those clinical trials, the drug used in ADT were either enzalutamide (NCT02446405) or abiraterone acetate (NCT01957436) or apalutamide (NCT02489318). Both cabazitazell and docetaxel are potent inhibitors of microtubule depolymerisation (Shapiro and Tareen, 2012). Notably, only patients who received docetaxel-based chemotherapy and ADT had improved overall survival benefit (STAMPEDE and CHAARTED trials) (James et al., 2016, Kyriakopoulos et al., 2018, Sun et al., 2019), while there was no additional survival benefit for patients who had estramustine-based chemotherapy and ADT (Sun et al., 2019, Noguchi et al., 2004).

There are a number of significant side-effects of ADT, including erectile dysfunction and compromised libido, reduced muscle mass with subsequent increase in body fat mass, increased risk of cardiovascular disease and osteoporosis (Thomas and Neal, 2013, Siemens et al., 2018). An acute side-effect when using LHRH agonists without anti-androgens is the initial testosterone surge that can lead to a hypercoagulation state and result in bladder outlet obstruction, renal failure and spinal cord compression (Thomas and Neal, 2013).

Notably, while ADT and chemotherapies are initially effective for most patients with mPCa, these therapeutic strategies will never cure a patient. ADT remains effective for an average duration of approximately 18 to 24 months, after which men relapse into a more aggressive PCa state termed castration-resistant prostate cancer (CRPC) (Shapiro and Tareen, 2012, Cornford et al., 2017, Saad and Hotte, 2010). CRPC is defined by a continuous increase in PSA levels when testosterone levels are at castrate levels in serum (<1.7nmol/l) and/or formation of new metastases or lesions (Saad and Hotte, 2010, Heidenreich et al., 2015).

1.8.3 Treatment of castrate-resistant prostate cancer (CRPC)

As described above, the androgen-AR signalling pathway is the key driver for PCa growth and progression (Shiota et al., 2011). Interestingly, most cases of CRPC remain driven by the AR despite patients having castrate levels of testosterone (Nuhn et al., 2019). Mechanisms by which AR continues to be active in CRPC tumours are described below (**Chapter 1 Section 1.9**). The key treatments for CRPC are second-generation AR antagonists – enzalutamide, apalutamide or darolutamide - or abiraterone acetate, all of which can prolong survival of some CRPC patients (Thomas and Neal, 2013, Smith et al., 2018b, Hussain et al., 2018).

When 2nd-generation ADT agents fail, CRPC is then treated with chemotherapy, such as Docetaxel and Cabazitaxel, which prolongs survival of some CRPC patients (Tannock et al., 2004). (de Bono et al., 2010). Other emerging therapies like poly-adenosine diphosphate-ribose polymerase (PARP) inhibitors or Radium-223 can be used to treat CRPC patients who no longer responded to 2nd-generation ADT or chemotherapy (Nuhn et al., 2019). The function

of PARP is to repair single-stranded breaks (Mateo et al., 2015, Teply and Antonarakis, 2017). CRPC tumours with mutations in DNA repair genes, such as BRCA1/2, are more likely to respond to the PARP inhibitor Olaparib (Mateo et al., 2015, Teply and Antonarakis, 2017). Radium-223 is a radioisotope drug that significantly improved overall survival of patients with CRPC and bone metastases (Shapiro and Tareen, 2012, Parker et al., 2012)

Although all of these treatments are capable of prolonging survival, the benefits are normally modest and patients will normally die from CRPC within a few years (Shapiro and Tareen, 2012). Therefore, this drives the need to understand the resistance mechanisms in PCa to improve develop new therapies.

1.9 Mechanisms of resistance to AR-targeted therapies

1.9.1 AR-dependent mechanisms of resistance in prostate cancer

Due to ADT exerting a selective pressure on the AR-related pathways in PCa cells, CRPC often arises as a result of alterations to the AR pathway and these alterations can allow PCa cells to adapt to the low androgen conditions. These alterations include AR overexpression, which is often due to amplification of the *AR* gene itself or to an upstream enhancer that promotes *AR* expression (Grasso et al., 2012, Coutinho et al., 2016, Takeda et al., 2018). AR overexpression can enable continued AR signalling even in the face of castrate levels of androgen (Coutinho et al., 2016, Grasso et al., 2012, Kawata et al., 2010, Chen et al., 2004).

Point mutations in AR can enable it to be activated by alternative ligands or even mediate antagonist-to-agonist switching (Coutinho et al., 2016, Lallous et al., 2016). For example, the recurrently occurring T878A and H875Y point mutations in the AR LBD allows AR to be a promiscuous receptor that can be activated by progesterone, estrogen and glucocorticoid (Lallous et al., 2016, Coutinho et al., 2016). The less common F877L and H875L mutations enable AR to be activated, rather than repressed, by enzalutamide (Lallous et al., 2016, Coutinho et al., 2016).

Another alteration to the AR signalling axis that is thought to enable resistance to therapies is elevated expression of AR-variants (AR-Vs), which lack all or part of the transcript encoding the AR-LBD. This occurs either via alternative splicing or by genomic rearrangements of the *AR* gene that result in deletion of exons encoding the LBD (Nyquist et al., 2013, Coutinho et al., 2016). AR-Vs are active in the absence of androgen and have been correlated

with therapy resistance and poor overall survival (Hu et al., 2009, Hörnberg et al., 2011, Guo et al., 2009, Welte et al., 2016, Efstathiou et al., 2015, Coutinho et al., 2016).

Another alteration to the AR signalling axis that is frequently observed in CRPC is the gain or loss in expression and activity of AR co-regulators (**Figure 1.4**) (Coutinho et al., 2016). Co-regulators of AR that enhance its activity are called co-activators and include factors such as nuclear co-activators 1 and 2 (NCOA1 and NCOA2); their expression and activity are often gained in CRPC (Grasso et al., 2012, TCGA, 2015, Robinson et al., 2015, Kumar et al., 2016). Examples of key NCOAs are SRC1 and TIF2, which are often overexpressed in recurrent PCa (Culig et al., 2004, Gregory et al., 2001). In contrast, co-repressors of AR such as nuclear co-repressors 1 and 2 (NCOR1 and NCOR2) inhibit its activity and their expression and activity are often decreased in CRPC (Grasso et al., 2012, TCGA, 2015, Robinson et al., 2015, Kumar et al., 2016).

Another mechanism of AR-dependent resistance in CRPC is alterations to the androgen biosynthetic pathways to enable tumours to make additional androgen. For example, androgen biosynthesis in CRPC tumours can be enhanced by a gain of function mutation within the *3 β -hydroxysteroid dehydrogenase type 1 (HSD3B1)* gene, which encodes an enzyme called 3 β -HSD1 that is important for the conversion of adrenal-derived steroids to DHT (Chang et al., 2013). In a multi-cohort of 443 patients, a homozygous gain of function mutation in *HSD3B1* gene correlated with reduced metastasis-free survival and overall survival of patients after radical prostatectomy and reduced progression-free survival (PFS) in patients treated with ADT (Hearn et al., 2016). The results suggest that identification of

mutations in *HSD3B1* gene can be a useful biomarker to identify patients that can eventually be more resistant to ADT (Hettel and Sharifi, 2018).

1.9.2 AR-independent mechanisms of resistance in CRPC

A smaller proportion of CRPC tumours develop a phenotype that is not dependent on AR signalling (Davies et al., 2021). A major class of AR-independent CRPC is treatment-emergent neuroendocrine prostate cancer (NEPC) (Davies et al., 2020), which is characterised by low or absent expression of AR and/or AR target genes and gain of a neuroendocrine phenotype (Davies et al., 2021, Beltran et al., 2016, Wang and Epstein, 2008, Aggarwal et al., 2018). Neuroendocrine markers such as Synaptophysin (SYP), neural cell adhesion molecule 1 (CD56), gamma-enolase (ENO2), chromogranin A (CHGA) and chromogranin B (CHGB) are typically expressed in neuroendocrine prostate tumours (Beltran et al., 2011).

Neuroendocrine PCa can occur *de novo* (Garabedian et al., 1998) or as a result from lineage trans-differentiation induced by long term ADT (Bluemn et al., 2017, Aggarwal et al., 2018, Abida et al., 2019). *De novo* NEPC is extremely rare and accounts for approximately 2% of all prostate cancers at time of diagnosis (Zaffuto et al., 2017, Yashi et al., 2006), with the majority of cases being diagnosed as metastatic (Zaffuto et al., 2017, Cattrini et al., 2020). *De novo* NEPC is proposed to originate from neuroendocrine prostatic cells that underwent malignant transformation (Garabedian et al., 1998).

The second and more common type of NEPC is that which arises as a mechanism of resistance to long-term treatment with inhibitors of the AR pathway (such as enzalutamide, darolutamide, apalutamide) (Bluemn et al., 2017, Aggarwal et al., 2018, Abida et al., 2019). Lineage plasticity of a cancer cell is defined as the ability to revert from a luminal

adenocarcinoma cell to a neuroendocrine cell (Davies et al., 2020, Quintanal-Villalonga et al., 2020, Beltran et al., 2016, Aggarwal et al., 2018, Zou et al., 2017). Importantly, androgen deprivation can activate such lineage plasticity, reprogramming androgen-sensitive PCa cells to differentiate into an aggressive androgen-insensitive neuroendocrine phenotype (Shen et al., 1997, Sánchez et al., 2020).

Treatment-emergent NEPC is observed in approximately 15 to 20% of patients with CRPC (Bluemn et al., 2017, Aggarwal et al., 2018, Abida et al., 2019, Beltran and Demichelis, 2021, Wang et al., 2021b, Zhang et al., 2020c, Yao et al., 2021). Treatment-emergent NEPC typically resembles the small cell neuroendocrine prostate carcinoma and it has a similar histology, morphology, disease progression and treatment response as small cell lung carcinoma (SCLC) and other small cell carcinomas that had metastasised (Têtu et al., 1987, Ro et al., 1987, Yao et al., 2006, Wang and Epstein, 2008). Patients with small cell NEPC have the worst outcomes (Deorah et al., 2012, Papandreou et al., 2002); indeed, it is associated with a median survival rate of 1 to 2 years (Deorah et al., 2012, Papandreou et al., 2002).

Lineage plasticity primarily occurs because of changes in the epigenome and transcriptome (Davies et al., 2020, Davies et al., 2021). For example, EZH2 has been reported as an epigenetic mediator of lineage plasticity in prostate cancer (Davies et al., 2021). EZH2 is a histone methyltransferase that mediates tri-methylation of histone 3 at Lysine 27 (H3K27me3) and represses transcription of target genes (Davies et al., 2021). Another example of an epigenetic factor is DNMT. Increased DNMT stability resulted in abnormal patterning of DNA methylation including at genes associated with neuroendocrine differentiation, such as FOXA1 and LHX2 (Shamma et al., 2013, Davies et al., 2020). Another example is LSD1. The phosphorylated form of LSD1 can target the promoter of the *CDH1* gene

and repress its transcription, thereby inducing the epithelial-mesenchymal plasticity (Feng et al., 2016, Davies et al., 2020). Collectively, changes in the cellular epigenome resulted in induction of lineage plasticity.

Additionally, several neuronal transcription factors have also been implicated as drivers of lineage plasticity. For example, N-MYC had been demonstrated to drive progression to NEPC by induction of an EZH2-mediated signalling (Dardenne et al., 2016, Berger et al., 2019). Another example is BRN2, which can mediate neuronal differentiation of PCa cells through interacting with SOX2 (Bishop et al., 2017, Lodato et al., 2013). SOX2 is a transcription factor required for pluripotency and neuronal differentiation into NEPC (Yu et al., 2014, Mu et al., 2017). Another example is FOXA2, which can mediate the adeno-to-neuroendocrine lineage transition in prostate cancer through the regulation of KIT pathway (Han et al., 2022). Therefore, these studies demonstrate that there are important transcriptional mediators of lineage plasticity in prostate cancer.

In terms of genomic alterations associated with NEPC, amplification of the *AURKA* and *MYCN* genes is frequently observed in these tumours, enabling higher expression of these genes (Beltran et al., 2011, Mosquera et al., 2013). More specifically, amplification of the *AURKA* gene was present in 65% of primary prostate tumours from patients who later developed treatment emergent NEPC and in 86% of metastases (Mosquera et al., 2013). Within those tumours, concurrent amplification of *MYCN* was identified in most cases (Mosquera et al., 2013). Notably, there was significantly higher frequency of concurrent overexpression and gene amplification of *AURKA* and *MYCN* in neuroendocrine prostate tumours (40% of the 37 cases) than in primary tumours (5% of the 169 cases) (Beltran et al.,

2011). Mechanistically, N-MYC interacts with AURKA to form a complex that results in stabilisation of both oncoproteins (Beltran et al., 2011, Dardenne et al., 2016).

Epithelial-neuroendocrine lineage plasticity resembles another type of lineage plasticity frequently observed in cancer, which is the epithelial-mesenchymal transition (EMT) (Uysal-Onganer et al., 2010). Indeed, the EMT-associated transcription factors, such as ZEB1 (Viswanathan et al., 2017), SNAIL (McKeithen et al., 2010), Slug (Esposito et al., 2015), FOXC2 (Paranjape et al., 2016) and TWIST (Shiota et al., 2013) have been implicated in NEPC. Mechanistically, the chemokine IL-6 acts as an activator of the STAT3 signalling pathway that correlated with increased expression of the transcription factor TWIST-related protein 1 (TWIST) and SOX2 in human prostate tumours and this in turn induces neuroendocrine differentiation (Schroeder et al., 2014, Rojas et al., 2011, Uysal-Onganer et al., 2010, Chang et al., 2014, Davies et al., 2020, Davies et al., 2018). Overall, these studies emphasized the similarities between the transcriptional networks involved in EMT and development of the neuroendocrine phenotype (Davies et al., 2018, Davies et al., 2020).

1.10 Ubiquitin-proteasome system

The ubiquitin-proteasome system (UPS) encompasses a large pathway and many proteins/enzymes that catalyse the addition of ubiquitin to target proteins, which marks them for degradation by the proteasome (Yuan et al., 2018, Rajkumar et al., 2005, Borg and Dixit, 2017). Ubiquitin is a highly conserved, 8.6kDa protein (Rajkumar et al., 2005). Ubiquitination of proteins is mediated by an ubiquitin-activating enzyme (E1), an ubiquitin-conjugating enzyme (E2) and an ubiquitin ligase (E3) (Rajkumar et al., 2005). The process results in the formation of a peptide bond between the amino group present in the side chain of a lysine in the target protein and the C-terminal carboxyl group of ubiquitin (Ronau et al., 2016, Passmore and Barford, 2004).

There are seven lysine residues present in Ubiquitin (Lys6, 11, 27, 29, 33, 48 and 63), thereby enabling formation of ubiquitin polymers (Ikeda and Dikic, 2008). Different types of ubiquitin linkages signal different functional outcomes for the targeted proteins (Haglund and Dikic, 2005, Cunningham et al., 2015, Durcan et al., 2014, Birsa et al., 2014, Ohtake et al., 2018, Locke et al., 2014, Farooq et al., 2022, Lin et al., 2016, Liu et al., 2018b). The outcomes of the various ubiquitin linkages is summarised (**Figure 1.11**). However, polyubiquitination of proteins formed via Lys48 is the primary signal for proteasomal degradation (Ikeda and Dikic, 2008, Haglund and Dikic, 2005).

Once a target protein is conjugated to ubiquitin chains formed via Lys48, it will be degraded in the 26S proteasome (Haglund and Dikic, 2005, Ikeda and Dikic, 2008). The 26S proteasome is an ATP-dependent multi-subunit proteolytic complex that comprises two 19S

regulatory complexes, which selects ubiquitinated-proteins and transfer them to the 20S core complex, and a catalytic 20S core complex, which is the protease's active site (Rajkumar et al., 2005, Yuan et al., 2018). The main functions of the UPS are to maintain signal transduction and cell survival pathways, response to stress and control cell cycle progression (Yuan et al., 2018, Rajkumar et al., 2005, Borg and Dixit, 2017). UPS carries out its role by degrading ubiquitinated proteins that regulate the aforementioned pathways (Harrigan et al., 2018).

The ubiquitination state of proteins in cells is a balance between adding and removing ubiquitin groups on protein (Harrigan et al., 2018, Komander et al., 2009, Rajkumar et al., 2005). The ubiquitination process can be reversed by deubiquitinating enzymes (DUBs) (Harrigan et al., 2018, Komander et al., 2009, Rajkumar et al., 2005). DUBs catalyse the removal of ubiquitin molecules from their target proteins (Komander et al., 2009). The human genome encodes for approximately 79 putative DUBs that are predicted to be functional (Nijman et al., 2005, Komander et al., 2009). Within the DUB family, there are 55 members in the ubiquitin-specific proteases (USP) class (Pal et al., 2014, Harrigan et al., 2018). Therefore, the USPs are the largest subfamily of DUBs (Pal et al., 2014, Harrigan et al., 2018).

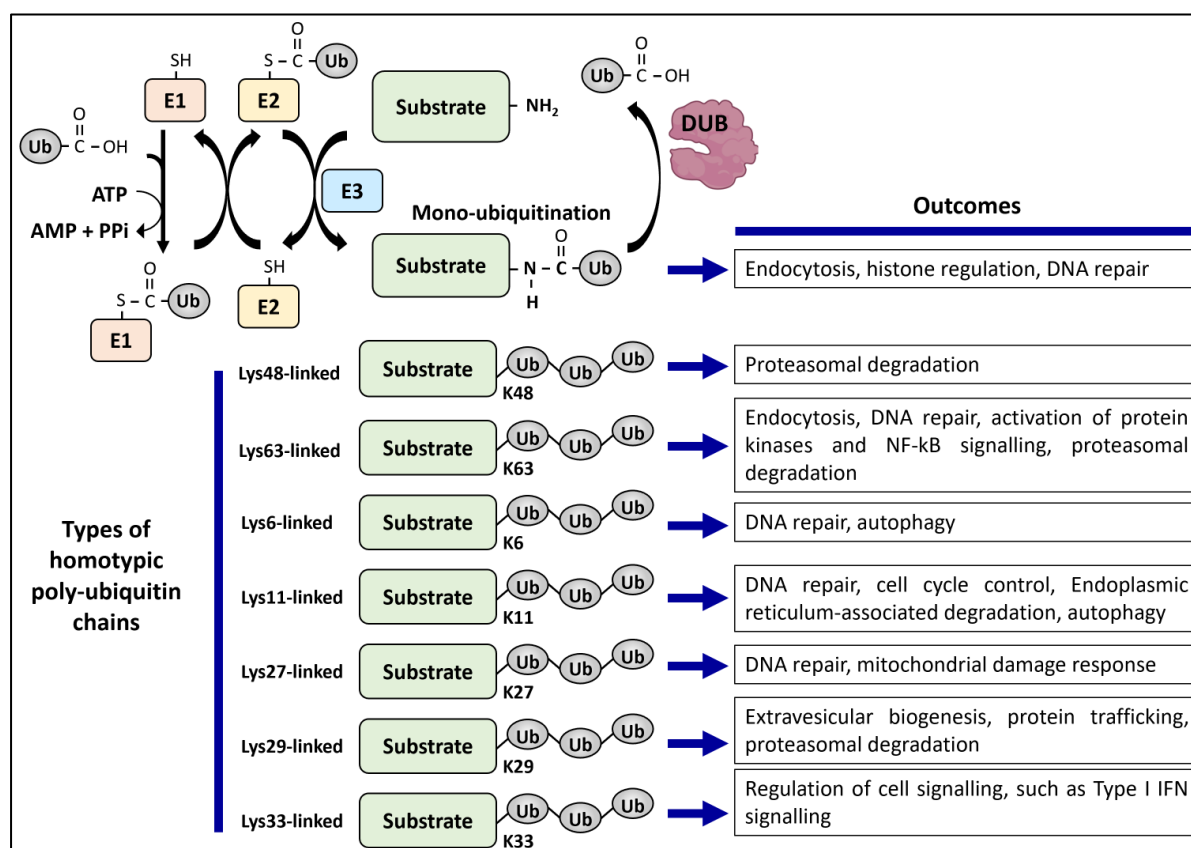


Figure 1.11. The ubiquitination/ de-ubiquitination process regulates several intracellular process and signalling. Ubiquitination is a three-step enzymatic reaction, which results in mono- or poly-ubiquitin molecules being covalently attached to target proteins. Different types of ubiquitin linkages signal different functional roles as outlined. Ubiquitination of a protein can be reversed by de-ubiquitinating enzymes that remove ubiquitin molecules.

1.11 The importance of the Ubiquitin Proteasome System in cancer

Dysregulation of the UPS may contribute to initiation and/or progression of cancer (Rajkumar et al., 2005, Harrigan et al., 2018). For example, USP15 is often amplified in cancer, and can deubiquitinate TGF- β receptor I and promote oncogenesis through the TGF- β pathway (Eichhorn et al., 2012). Another example is USP14, which is upregulated in the adhesive model of multiple myeloma (MM) (Xu et al., 2015). The last example is USP22, whose expression is higher in matched renal cell carcinoma (RCC) tissues compared to normal tissues (Lin et al., 2020). Given the importance of the UPS and how its dysregulation can promote carcinogenesis of different cancer types, it can therefore be postulated that the dysregulation of the UPS, particularly via upregulation of ubiquitin-specific proteases (USPs), can occur in prostate cancer.

In the context of prostate cancer, several USPs have elevated levels in prostate cancer compared to non-malignant prostate cells. The first example is USP10, which was found to be more highly expressed in prostate tumour tissues compared to matched benign tissues, as determined by immunohistochemistry (Takayama et al., 2018). The second example is USP17, whose mRNA and protein expression are higher in prostate tumours than in matched normal samples (Baohai et al., 2019). USP17 expression is also higher in the androgen-dependent PCa cell lines, such as LNCaP and VCaP, and androgen-insensitive PCa cell lines, such as DU145 and PC3, than in the non-malignant epithelial cell line of the prostate, such as RWPE-1 (Baohai et al., 2019). The third example is USP33, which is more highly expressed in the CRPC cell lines (C4-2B and PC3) than in LNCaP or RWPE-1 cells (Guo et al., 2020). The fourth example is

USP44, which is more highly expressed in PC3 and DU145 cells than in LNCaP or the non-malignant epithelial prostate cell line, such as RWPE-1 and RWPE-2 (Park et al., 2019). The last example is USP22, whose expression is higher in castrate resistant prostate tumours and primary prostate tumours with Gleason scores (7 to 9) than in tumours with Gleason scores (5 and 6) (Schrecengost et al., 2014). Collectively, this indicates that upregulation of USPs may have clinical significance in prostate carcinogenesis. It is hypothesised that these USPs stabilise oncoproteins, thereby contributing to the development and progression of cancer.

1.12 Interplay between ubiquitin-specific proteases and androgen receptor signalling

Given that the prostate cancer is highly dependent on androgens, the relationship between the AR and USPs has been investigated. For example, the *USP10* gene had been identified as an AR-regulated target gene (Takayama et al., 2018). Short-term treatment with androgens (DHT) resulted in enhanced *USP10* mRNA and protein levels, while bicalutamide reduced *USP10* mRNA levels (Takayama et al., 2018). Furthermore, *USP10* could indirectly activate AR activity to potentiate AR regulation of its target genes (Draker et al., 2011). This example demonstrates that AR can directly increase the levels of oncogenic USPs.

Several USPs, such as *USP12*, *USP22*, and *USP26*, were found to be important for the stability and thus activity of the androgen receptor (Burska et al., 2013, McClurg et al., 2015, Schrecengost et al., 2014, Dirac and Bernards, 2010). *USP12* interacts with co-factors *USP1-associated factor 1* (*Uaf-1*) and *WD20 repeats* (*WDR20*) and forms a complex that co-immunoprecipitated with full length AR and AR variants in androgen-dependent VCaP cells (Burska et al., 2013). The *USP12/Uaf-1/WDR20* complex is important for the stabilisation of AR, thereby increasing AR activity (Burska et al., 2013). Elevated expression of *USP22* in LNCaP cells resulted in increased levels and activity of AR and AR variants (Schrecengost et al., 2014). (Schrecengost et al., 2014). Likewise, *USP26* directly removed the ubiquitin groups from AR when HEK293 cells were exogenously overexpressing AR, and this effect was further augmented when these cells were treated with DHT (Dirac and Bernards, 2010). Knockdown of *USP26* reduced the transcription of canonical AR-targeted genes in LNCaP cells (Dirac and

Bernards, 2010). Conversely, overexpression of USP26 increased the activity of AR activated by androgens in HEK293 cells overexpressing AR and a luciferase reporter tagged with an AR enhancer region (Dirac and Bernards, 2010). Collectively, these studies demonstrate that USPs can suppress AR turnover by the proteasome, which results in enhanced AR signalling in PCa.

There have been several inhibitors that target the USP family evaluated in cancer/oncology research, with majority of the inhibitors being at the pre-clinical stage (Antao et al., 2020, Li et al., 2022) . An example of an inhibitor that has transitioned to clinical trials is the drug VLX1570, which inhibits USP14 and induces apoptosis of multiple myeloma (MM) cells (Wang et al., 2016). However, the clinical trial involving VLX1570 was recently suspended due to pulmonary toxicity observed in two patients (Rowinsky et al., 2020). The toxicity effects of VLX1570 observed were similar to the rare deaths noted with inhibitors of the 20S proteasome, such as bortezomib (Rowinsky et al., 2020, Kharel et al., 2018, Li et al., 2016). Nevertheless, VLX1570 successfully exerted anti-myeloma effects in some patients (Rowinsky et al., 2020), thereby providing rationale for identifying other DUB inhibitors with greater therapeutic indices as a result of the unique mechanism of action and robust activity of DUB inhibitors in tumours *in vivo*.

1.13 USP2 in prostate cancer

USP2 had been reported to be overexpressed in a subset of primary prostate tumours (Graner et al., 2004, Priolo et al., 2006). Similar to other USPs, the function of USP2 is to interact with and stabilise oncogenic proteins (Graner et al., 2004, Yuan et al., 2018, Priolo et al., 2006, Benassi et al., 2012, Benassi et al., 2013). For example, USP2 deubiquitinates fatty acid synthase (FAS) (Graner et al., 2004, Priolo et al., 2006), which adds acetyl and malonyl groups onto Malonyl-CoA to form long chains of saturated fatty acids during *de novo* lipogenesis (Butler et al., 2016). Additionally, USP2 overexpression in PCa cells can result in the increase in an oncoprotein called mouse double minute 2 homolog (MDM2) (Stevenson et al., 2007), which plays a major role in suppressing the tumour suppressors P53 and mir-34b/c (Benassi et al., 2012, Benassi et al., 2013). MDM2 is a E3 ubiquitin ligase and acts as a negative regulator of tumour-suppressor P53 (Huun et al., 2017). By stabilising MDM2 and decreasing p53 and mir-34b/c in immortalised non-transformed prostate epithelial cells, USP2 causes an increase in the oncoprotein c-Myc, which drives cellular growth (Benassi et al., 2013, Benassi et al., 2012). Collectively, these studies implicate USP2 as an oncogenic factor in prostate cancer.

1.14 Gene, protein structure and function of USP2

The *USP2* gene is found on the long arm of chromosome number 11, specifically on 11q23.3 (Graner et al., 2004, NCBI, 2016) and contains 13 exons (**Figure 1.12**) (NCBI, 2016). The *USP2* transcript is alternatively spliced to give the canonical mature mRNA, *USP2a*, and its alternative transcripts, *USP2b* and *USP2c* respectively (**Figure 1.12**). The coding sequences of the *USP2a*, *USP2b* and *USP2c* mRNA transcripts are 1818, 1191 and 1089 nucleotides (nt) respectively (**Figure 1.12**) (NCBI, 2016). These *USP2* transcripts are translated into their corresponding USP2a, USP2b and USP2c proteins, which have various lengths of 605, 396 and 362 amino acids respectively (Graner et al., 2004, Mahul-Mellier et al., 2012, NCBI, 2016), corresponding to the molecular weights of 68, 45.13 and 41.69kDa respectively (Stothard, 2000).

The USP2 isoforms comprise of an N-terminal region of varied lengths and a common C-terminal domain of 347 amino acids (**Figure 1.12**) (Renatus et al., 2006). The C-terminal domain is also the USP catalytic domain, which contains the active-site residues and Zinc-binding sites (Renatus et al., 2006, Apweiler et al., 2001).

As USP2 is a de-ubiquitinating enzyme and a cysteine isopeptidase, it contains a Zinc-binding site, and this site is defined as the CXXC-Xn-CXXC motif, whereby four cysteine residues bind to one Zinc molecule (Renatus et al., 2006, Krishna and Grishin, 2004, Tencer et al., 2016). This zinc “ribbon”, which is conserved among USPs, is located at the “tip” of the finger subdomain and the conserved cysteine residues in USP2a are: Cys428, Cys431, Cys476 and Cys479 (**Figure 1.12**) (Renatus et al., 2006, Krishna and Grishin, 2004, Tencer et al., 2016).

The ability to bind to Zinc is required for the activity of USP2 as a deubiquitinating enzyme (Tencer et al., 2016, Krishna and Grishin, 2004). Furthermore, this zinc ribbon domain can function as a scaffold for ubiquitin recognition (Krishna and Grishin, 2004, Tencer et al., 2016).

Additionally, USP2 contains a catalytic triad, which comprises of a Cysteine (Cys276), Histidine (His557) and Asparagine (Asn574) residue, within its active site (Renatus et al., 2006, Verma et al., 2016, Coulombe et al., 1996, NCBI, 2016, Yang and Wong, 2013, Tencer et al., 2016). Within the catalytic triad, the Cys276 residue functions as a nucleophile and the His557 residue function as a proton donor that increases the nucleophilicity of the cysteine residue (Renatus et al., 2006, Coulombe et al., 1996, Verma et al., 2016). The Asn574 residue functions as the oxyanion hole, which is important in the stabilisation of the protease's transition states (**Figure 1.12**) (Renatus et al., 2006, NCBI, 2016, Yang and Wong, 2013).

USP2 functions to remove ubiquitin groups from its substrates by interacting with Lys6 and Leu73 of the K48-linked ubiquitin molecules, (Tencer et al., 2016, Renatus et al., 2006, Bozza et al., 2012). USP2 can remove ubiquitin groups from its substrates as mono-ubiquitin or di-ubiquitin in a one-step binding or biphasic binding respectively (Bozza et al., 2012). USP2 can also directly cleave Lys27-linked poly-ubiquitin chains of certain proteins, such as SMAD7 (Tu et al., 2022).

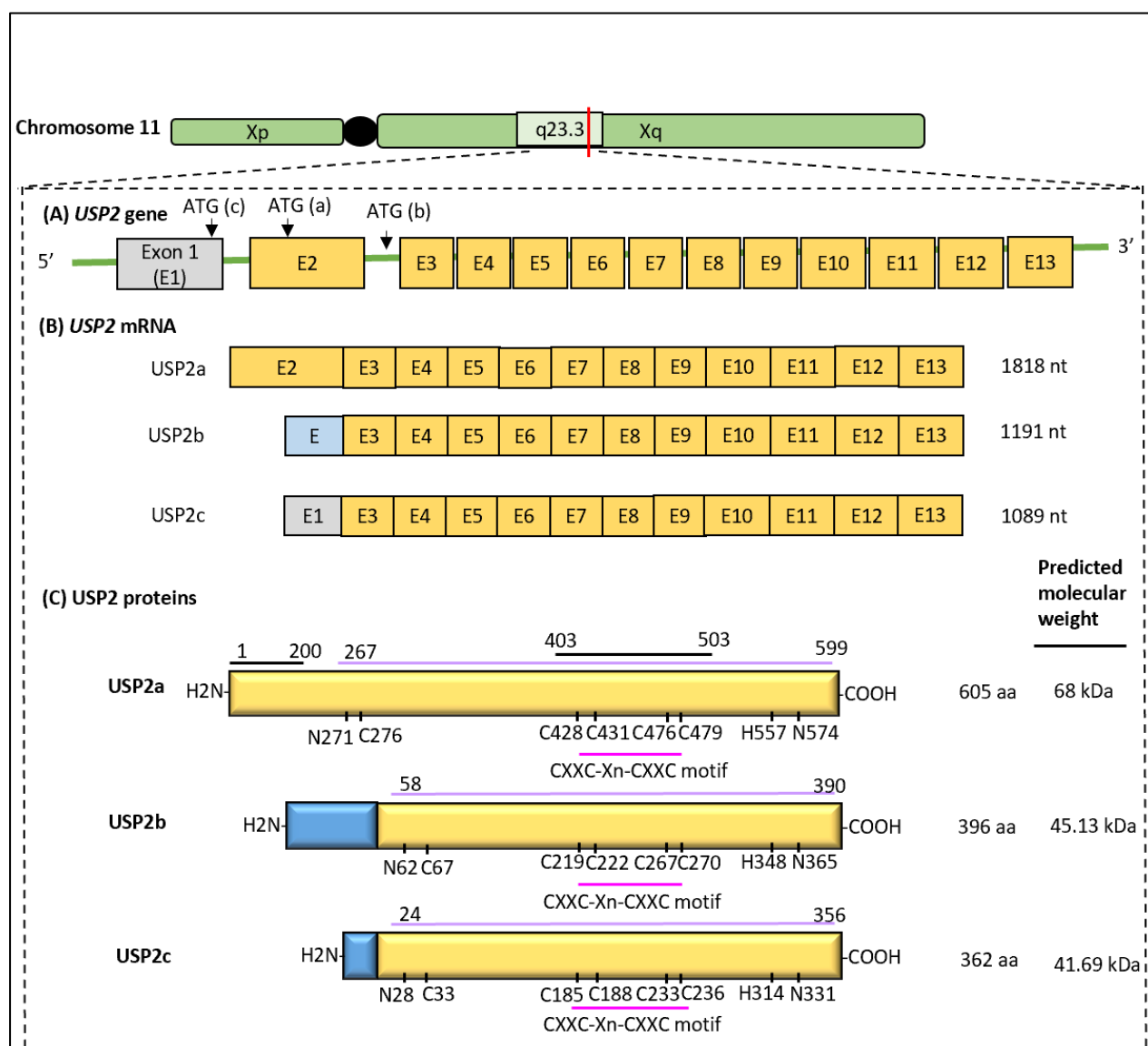


Figure 1.12. Schematic diagram of USP2 gene and its encoded mRNA variants and protein variants USP2a, USP2b and USP2c. (A) The *USP2* gene is found on chromosome number 11 region q23.3 and has 13 exons (E1 to E13). (B) The *USP2* gene is transcribed, and the resulting RNA transcript is alternatively spliced into three different mRNA variants. (C) Each of the mRNA variant gets translated into the corresponding USP2 variant protein.

1.15 USP2 (or USP2a) functions as an onco-protein in several cancers

Out of the three USP2 isoforms, the USP2a is the predominant isoform and has been implicated in cancer (Graner et al., 2004, Priolo et al., 2006). For example, overexpressing USP2a in mouse embryonic fibroblasts (MEF) cells could transform these cells to quickly form tumours in mice models (Priolo et al., 2006). Additionally, overexpressing USP2a in MEF cells resulted in the development of a sarcomatous phenotype (Priolo et al., 2006).

1.15.1 High expression of USP2 or USP2 fusion proteins in tumours correlated with poor prognosis.

High expression of USP2 or USP2 fusion proteins has been associated with poor prognosis in multiple cancer types. USP2a had been reported to be overexpressed in a subset of primary prostate tumours (Graner et al., 2004, Priolo et al., 2006). Patients with high expression of USP2 in upper tract urothelial tumours (Ke et al., 2022) or gastric tumours (Xiao et al., 2022) or hepatic tumours (Xiong et al., 2021) had a significantly lower percentage of overall survival and significantly shorter disease-free survival. Moreover, a *KMT2A-USP2* fusion gene in paediatric B-cell acute lymphoblastic leukemia (B-ALL), which results in high levels of *USP2* expression, is associated with poor outcome (Wang et al., 2021a). In short, these studies suggest that high expression of USP2 in different cancers is associated with

more aggressive disease. Mechanisms by which USP2 causes cancers to grow more aggressively and metastasise are described below.

1.15.2 USP2 suppresses p53 signalling pathway through stabilisation of MDM2 and MDM4.

One key oncoprotein that is stabilised by USP2 is MDM2. This has been observed in multiple tumour types, such as prostate cancer (Stevenson et al., 2007, Benassi et al., 2012, Benassi et al., 2013), non-small cell lung carcinoma (H1299) (Stevenson et al., 2007), human embryonal carcinoma (NTERA-2) (Stevenson et al., 2007) and cutaneous T-cell lymphocytes (CTCL) (Wei et al., 2016). A key function of MDM2 is to inhibit the function of the key tumour suppressor P53, which it does by adding ubiquitin groups onto P53 (Stevenson et al., 2007). By stabilising MDM2, USP2 causes inhibition of p53 signalling (Huun et al., 2017, Kim et al., 2017), which leads to USP2 functioning as a survival stress response to protect cancer cells from apoptosis induced by p53 and p53 signalling pathway (Benassi et al., 2012, Benassi et al., 2013, Wei et al., 2016). When P53 is activated by stress signals, such as DNA damage, transcription factor P53 upregulates genes involved in DNA repair, cell cycle arrest or apoptosis (Hientz et al., 2017). Additionally, USP2 can stabilise MDM2 in breast and ovarian cancers to promote cell migration, invasion, and epithelial mesenchymal transition (EMT) through activation of the TGF β -SMAD pathway (Chen et al., 2017a, Yang et al., 2006). Collectively, USP2 can contribute to therapeutic resistance in cancer cells through the removal of ubiquitin groups from MDM2, which will then stabilise MDM2 and therefore

enable MDM2 to antagonise the pro-apoptotic activity of P53 (Stevenson et al., 2007, Benassi et al., 2012, Benassi et al., 2013, Wei et al., 2016).

1.15.3 USP2 promotes metastasis and epithelial-to-mesenchymal transition (EMT).

Additionally, USP2 regulates the stability of key proteins in EMT, a process whereby epithelial cells trans-differentiate to a mesenchymal-like phenotype (Davies et al., 2020). EMT plays a major role in cancer metastasis because mesenchymal cells are more migratory and invasive (Davies et al., 2020, Davies et al., 2018). When exogenously expressed in HEK293T cells, USP2 removed ubiquitin groups from the EMT transcription factor TWIST, while a catalytically inactive USP2 mutant (C276A) was not able to induce TWIST deubiquitination (He et al., 2019). USP2 can also enhance EMT in NTERA-2 cells by stabilising the pro-EMT factor Aurora kinase A (Shi et al., 2011, Beltran et al., 2019, Wan et al., 2008, D'Assoro et al., 2014, Willems et al., 2018) .

Knockdown of USP2 in triple-negative breast cancer (MDA-MB-157 and BT549), which is an invasive and aggressive breast cancer type with poor prognosis outcome, led to reduced expression of mesenchymal drivers and markers such as TWIST, N-Cadherin (N-CAD), Fibronectin and BMI1 (He et al., 2019, Wahba and El-Hadaad, 2015). Additionally, in bladder cancer, USP2 can interact with the scaffolding protein Tight Junction Protein 1 (TJP1) and TWIST1 to upregulate expression of chemokine ligand 2 (CCL2), thereby promoting the EMT pathway (Liu et al., 2022). USP2 activation of the EMT pathway resulted in infiltration of

tumour-associated macrophage and tumour angiogenesis that promotes bladder cancer progression (Liu et al., 2022).

1.15.4 USP2 enhances growth of cancer cells.

Another key oncogenic role of USP2 appears to be in stabilising proteins involved in cell proliferation and mitosis. USP2 can regulate proliferation and the mitotic cycle through stabilisation of Aurora kinase A (AURK A), epidermal growth factor receptor (EGFR), Cyclin A1, Cyclin D1 and human epidermal growth factor receptor 2 (HER2) in NTERA-2, non-small cell lung cancer (NSCLC), T24 bladder cancer, colorectal cancer (HCT116), lymphoblasts (Mino) and HER2-overexpressing breast cancer (HCC1954 and SKBR3), respectively (Shi et al., 2011, Liu et al., 2013, Kim et al., 2012, Davis et al., 2016, Zhang et al., 2020a). Cyclin D1 and Cyclin A1 are oncoproteins that regulates cell cycle progression, proliferation and growth and induction of chemoresistance in cancer cells (Liao et al., 2007, Ramos-García et al., 2017, Moradi Binabaj et al., 2020, Huang et al., 2016, Miftakhova et al., 2016). Their results corroborated the findings in Davis et. al. (2016), which showed that Cyclin D1 decreased in prostate cancer cells (LNCaP) after 24 hours of pharmacological inhibition of USP2. Similarly, HER2 appears to be a unique substrate of USP2 (when investigated alongside with other DUBs such as AMSH and AMSHLP) in breast cancer cells (Zhang et al., 2020a). Overall, USP2 is an important de-ubiquitylating enzyme for pro-growth oncoproteins.

1.15.5 USP2 is important in endocytosis and autophagy.

USP2 can also regulate endocytosis in cancer cells. USP2 was found to localise to early endosomes in HeLa cells and non-small cell lung cancer (NSCLC), along with early endosomal markers such as early endosome antigen I (EEA1) and RAB5 (Liu et al., 2013). This observation was supported by Priolo *et al.* (2006), who demonstrated that prostate tumours with high USP2 expression was associated with upregulation of endocytic pathways, such as EEA1 and ERBB3 and RAB pathways. RAB5 can act via its main effector EEA1 to form early endosomes and fusions of early endosomes (Wandinger-Ness and Zerial, 2014, Bucci et al., 1992, Gorvel et al., 1991). Consequently, when USP2 stabilised EGFR and prevented lysosomal degradation of EGFR, there was increase in the amount of EGFR being recycled back to the cellular surface membrane (Liu et al., 2013). Collectively, these results suggest that USP2 is important in promoting recycling of oncoproteins back to the cell surface membrane and thereby driving tumorigenicity.

USP2 can regulate the stability of proteins important in autophagy. USP2 can directly remove the K48-ubiquitination of RAB1, thereby stabilising RAB1 and promoting the accumulation of RAB1a in hepatocarcinoma (HCC) cells (Xiong et al., 2021). RAB1 is a GTPase that is required for initiation of autophagosome formation (Carlos Martín Zoppino et al., 2010, Webster et al., 2016). Elevated expression of RAB1 also drives mTORC1-dependent growth in tumours and mTORC1 signalling, which can regulate autophagy (Wang et al., 2017), by regulating the interaction between mTORC1 and RHEB (Thomas et al., 2014, Lu et al., 2021). Additionally, USP2 can also de-ubiquitinate E2F4 in gastric cancer cells (Xiao et al., 2022). E2F4 was identified as a novel transcriptional activator for the expression of genes involved in autophagy, such as ULK2 and ATG2 (Xiao et al., 2022). ULK2 is important for initiation of

autophagy (Kim et al., 2016), while ATG2 is important for the formation of autophagosomes at a late-stage (Velikkakath et al., 2012). Importantly, inhibiting USP2 in a mice model of poorly differentiated gastric adenocarcinoma resulted in drastically reduced growth of those subcutaneous xenograft tumours (Xiao et al., 2022). Overall, these results suggest that the USP2-RAB1-autophagy or the USP2-E2F4-autophagy axes can be potential therapeutic targets in cancer.

1.15.6 USP2 is important in metastasis.

USP2 can promote migration and invasion of hepatocarcinoma (Xiong et al., 2021) and gastric adenocarcinoma cell lines (Xiao et al., 2022). Genetic silencing of USP2 significantly reduced the migratory and invasive abilities of hepatocarcinoma cells (Xiong et al., 2021). Conversely, overexpressing USP2 in hepatocarcinoma cells increased the number of cells that migrated or invaded through Matrigel (Xiong et al., 2021). Mechanistically, Xiong *et. al.* (2021) demonstrated that the ability of USP2 to promote migration and invasion of hepatocarcinoma cells is partly mediated through RAB1, which was identified to be a putative substrate in hepatocarcinoma. Similarly, through USP2 stabilisation of E2F4 in gastric cancer, the migratory and invasive abilities of gastric adenocarcinoma was promoted (Xiao et al., 2022). Xiao *et. al.* (2022) had attributed this phenomenon to the ability of USP2 to promote the accumulation of E2F4 in gastric cancer that then enabled E2F4 to upregulate expression of the *ULK2* gene, which encodes for ULK2 that is important in promoting EMT and thus invasiveness of cancer cells (Xiao et al., 2022, Kim et al., 2016). Therefore, these results strongly suggest that inhibiting USP2 in prostate cancer cells can also reduce their migratory

and invasive abilities. The importance of USP2 as an oncoprotein in various cancer types has been summarised in **Figure 1.13**.

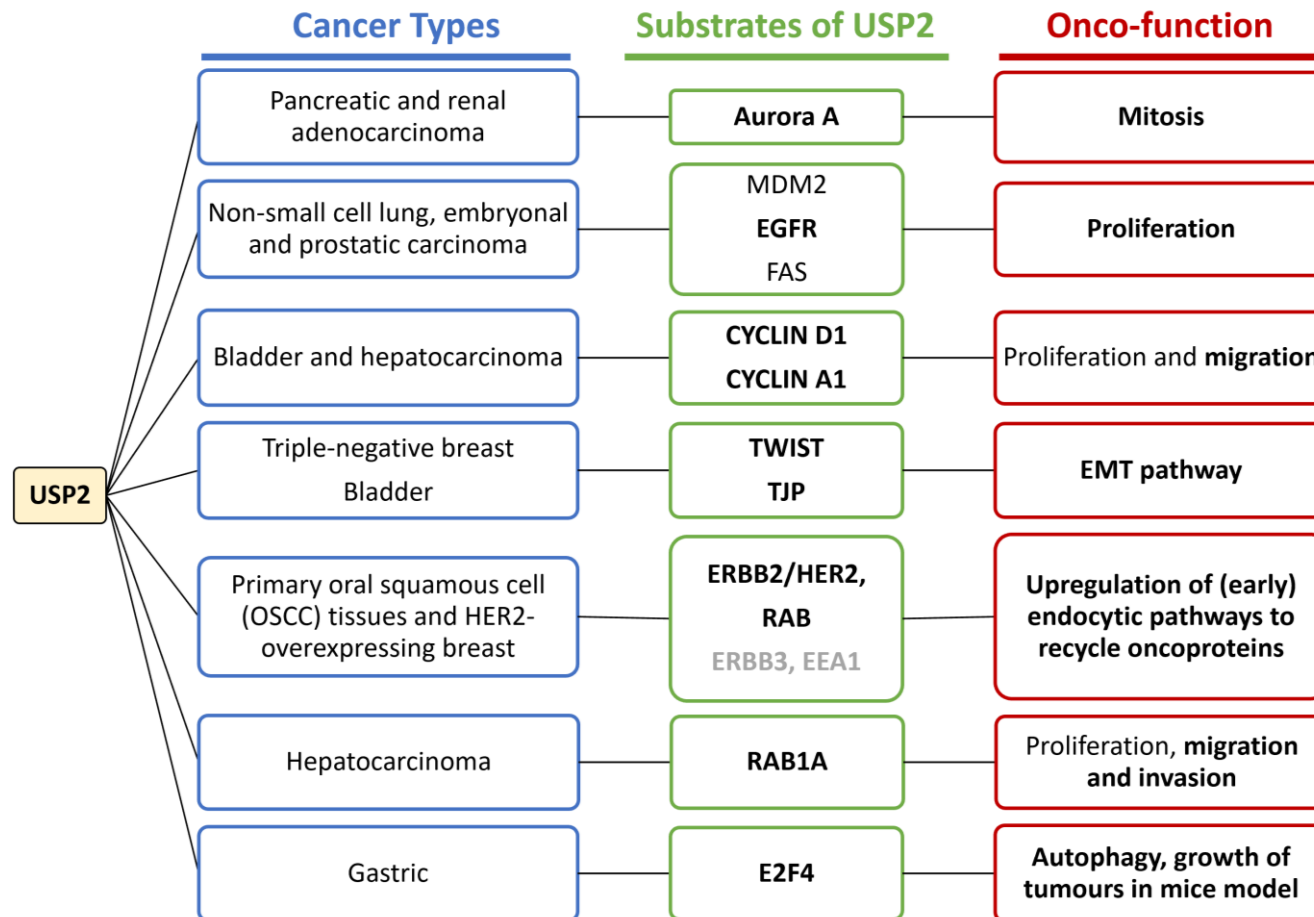


Figure 1.13. Summary of USP2 and the substrates that USP2 stabilises to carry out its functions as an oncoprotein in various cancer types. Highlighted in bold are substrates of USP2 and the functions of USP2 that have not been investigated in prostate cancer. Grey text indicates that these proteins co-localised with USP2.

1.16 Gaps in knowledge related to my project

Although the field has identified many mechanisms of therapy resistance, treating patients with CRPC remains a major challenge. Thus, there are clearly major mechanisms of resistance that remain to be identified, and some of these will represent therapeutic vulnerabilities in CRPC tumours. One common alteration that is observed in CRPC is changes to the ubiquitin proteasome system (UPS), but the relevance of this is largely unknown. In particular, whether USP2 has a role in mediating growth, survival and therapy resistance in prostate cancer has not been investigated, a gap that forms the basis of this project.

1.17 Research Hypothesis

USP2 is important for the growth and survival of prostate cancer and can mediate resistance to AR-targeted therapies and chemotherapy.

1.18 Aims of the project

Aim 1: Determine if USP2 can promote survival of prostate cancer cells against AR-targeted therapy and chemotherapy and drive the acquisition of the treatment-emergent neuroendocrine phenotype.

Aim 2: Investigate if USP2 is a therapeutic target in aggressive prostate cancer.

Aim 3: Investigate the mechanisms by which USP2 promotes survival of prostate cancer.

Chapter 2:

Materials and Methods

2 Materials and Methods

Table 2.1. Oligo sequences and information

Oligo Name	Sequence (5' to 3')	Annealing Temperature (°C)	Type of target
FKBP5 F	AAAAGGCCAAGGAGCAACAAC	55	cDNA
FKBP5 R	TTGAGGAGGGGCCGAGCTT	55	cDNA
SYP Forward	TTAGTTGGGGACTACTCCTCG	61.1	cDNA
SYP Reverse	GGCCCTTTGTTATTCTCTCGGTA	61.1	cDNA
Beta-Actin F	GGCCAACCGCGAGAA	55	cDNA
Beta-Actin R	ATCACGATGCCAGTGGTACG	55	cDNA
USP2a F	CTGCCCTGAATACCTGGTCTG	57.1	cDNA
USP2a R	TCGGTAGGTTGGGCTGATGAT	57.1	
USP2b F	CCTGCTGCTCTCCACCTTC	57.1	cDNA
USP2b R	AAGCACGTGTTCCCAAGGTTTC	57.1	
USP2 CHIP F (region 1)	GTCACGGCTATTGGCTTGTT	55	Genomic DNA
USP2 CHIP R (region 1)	CGTGTGACATTCCAGTCCAC	55	Genomic DNA
USP2 CHIP F (region 2)	TGAAATTGCCACTCTTGCTG	55	Genomic DNA
USP2 CHIP R (region 2)	TGGCAGACTCATCTGCAAAC	55	Genomic DNA

G1 USP2a F1	GACTCTACCAAACGGCATCC	55 to 60	Plasmid sequencing
G1 USP2a R1	TGTCCTCGCGTTCCAGATAC	55 to 60	
M13 F	GTAAAACGACGGCCA	55 to 60	Plasmid sequencing
M13 R	AGGAAACAGCTATGAC	55 to 60	
Puromycin F1	AGAACTCTTCCTCACGCG	64	Plasmid sequencing
Puromycin R1	CTTCATCTGTTGCTGCGC	64	
TF-USP2a F1 primer	GATGGATTGTATGCGGCTCT	55	mRNA
TF-USP2a R1 primer	GCTTGCTTGTCTGATTCGG	55	
ENO2 F primer	TGGTGAAGGAAGCCATCGAC	55	cDNA
ENO2 R primer	GGTCCCCAGTGATGTATCGG	55	
SYP F primer	TTAGTTGGGGACTACTCCTCG	60	cDNA
SYP F primer	GGCCCTTTGTTATTCTCTCGGTA	60	
ZO-1 F primer	CTGGGCTCTTGGCTTGCTAT	55	cDNA
ZO-1 R primer	GTCTCCGCCTGCTGTTTTTG	55	
Vimentin F	GAGAACTTTGCCGTTGAAGC	55	cDNA
Vimentin R	GCTTCCTGTAGGTGGCAATC	55	

Table 2.2. Descriptions of chemicals and reagents

Reagent	Supplier	Catalogue Number
2-Chloroacetamide	Sigma Aldrich	C0267-100G
7-AAD	Invitrogen	A1310
Alisertib (Aurora A inhibitor)	TargetMol	T2241
AnnexinV-PE	BD Pharmingen	556421 (200 tests)
Ammonium Bicarbonate	Sigma Aldrich	09830 Bio-Ultra grade
Bradford assay reagent	Biorad	500-0006
BSA (bovine serum albumin)	Sigma Aldrich	A9647
Calcium chloride (anhydrous, granular)	Sigma Aldrich	C1016 – 100 grams
Calcium Chloride	BDH Chemicals	10070
Chloroform	Sigma Aldrich	C2432
cOmplete mini EDTA-Free Roche (easypack; 30 tablets) (for every 10mL of lysis buffer)	Sigma Aldrich	Roche #04 693 159 001
DAPI	Sigma Aldrich	MBD0015-1mL
5 α -Dihydrotestosterone (DHT) (dissolved in ethanol)	Sigma Aldrich	D5027
DMEM	ThermoFisher Scientific	11995073
DMSO (dimethyl sulfoxide)	Sigma Aldrich	D2650
DMSO (dimethyl sulfoxide) (sterile filtered; meets EP and USP testing specifications)	Sigma Aldrich	D2438 – 50mL
Docetaxel CAS 114977-28-5	Med Chem Express	HY-B0011-100mg
Dithiothreitol (DTT)	Sigma Aldrich	D0632
Dulbecco's Phosphate Buffered Saline (DPBS) – suitable for cell culture	Sigma Aldrich	D8537
Dynabeads Protein A (30mg/mL)	Invitrogen	10002D
Ethanol, molecular grade	Scharlau	ET00110500
ECL Clarity	BioRad	1705061
ECL Select	BioRad	RPN2235
FBS (Fetal bovine serum)	Sigma Aldrich or Cell Sera	14M357
Gateway BP Clonase II Enzyme mix	Invitrogen	11789100
GelRed Nucleic Acid Gel stain 10 000X	Biotium Adela Scientific	GTS41003
Glycerol	Chem Supply	GA010-2.5L-P
Hanks' Balanced Salt Solution	Sigma Aldrich	H9394 – 500mL
HEPES (1M)	Gibco	15630-080
iQ SYBR Green Supermix	BioRad	170-8885
iScript cDNA synthesis kit	BioRad	170-8891

Lipofectamine RNA iMax	ThermoFisher Scientific	13778-150
Low Bind Tubes (1.7mL)	Axygen	MCT175LC
Luria agar (Miller's LB agar)	Sigma	L-3147
NucleoSpin Plasmid (for mini-prep of plasmids)	Macherey Nagel	74058850
NucleoBond Xtra Midi EF	Macherey-Nagel	74042010
1M Magnesium chloride (0.2µm filtered)	Invitrogen	AM9530G
ML364 (USP2 inhibitor)	Med Chem Express	HY-100900
ML364 (USP2 inhibitor) (used for mice work)	TargetMol	T3555
Nitrocellulose membrane	Amersham Protran	GE10600018
Nitrocellulose membrane	Amersham Protran	GE10600016
OptiMEM	ThermoFisher Scientific	31985070
Poly(ethylene glycol glycol) BioUltra 400 (i.e. PEG 400)	Sigma Aldrich	91893 – 250mL - F
0.1% (w/v) Poly-L-Lysine in water	Sigma Aldrich	P8920
Polysorbate 80	Sigma Aldrich	59924
Ponceau S	Sigma Aldrich	P3504
RNeasy mini kit	Qiagen	74104
RPMI 1640	Sigma Aldrich	R8758
RPMI 1640 phenol red free	Sigma Aldrich	R7509
3M Sodium acetate pH5.5	Invitrogen	AM9740
5M Sodium chloride (0.2µm filtered)	Invitrogen	AM9760G
TrypLE Express Enzyme	Gibco	12605010
Trypsin EDTA	Sigma Aldrich	T4049
Trypsin (Pierce Trypsin Protease MS Grade)	Pierce	LTS90058
TE Buffer pH 8.0 (0.2µm filtered)	Invitrogen	AM9849
Tween 20	Sigma Aldrich	P7949
Xenolight D-Luciferin	Perkin Elmer	122799 – 1 gram
XT-MOPs	Biorad	1610788

2.1 Maintenance of prostate cancer cell lines

Prostate cancer cell lines LNCaP, VCaP and PC3 were obtained from the American Type Culture Collection (ATCC; Rockville, MD, USA) and castrate resistant prostate carcinoma cell lines V16D^{CRPC}, MR49F^{ENZR} and MR42D^{ENZR} were kindly gifted to us from Prof. Amina Zoubeidi's laboratory. These castrate-resistant cells were derived through serial grafting of LNCaP cells in castrated mice that were also treated with 10mg/kg enzalutamide daily, after which cell lines were generated from castration-resistant and enzalutamide-resistant tumours (Bishop et al., 2017, Toren et al., 2016). MR49F^{ENZR} and MR42D^{ENZR} cells were cultured in RPMI 1640 medium (Sigma #R0883) supplemented with 10% fetal bovine serum (FBS) and 10 μ M enzalutamide. The characteristics of cell lines used in this project are described in **Table 2.3**. All cell lines were maintained at 37°C in 5% CO₂ atmosphere.

Table 2.3. A summary of the distinguishing characteristics for the cell lines used in this project.

Cell-line	Originated from	AR status	Other relevant mutations/characteristics
LNCaP	Lymph node lesion	<p>Mutated AR: Has a T878A gain-of-function mutation in the AR's LBD (Veldscholte et al., 1990) A promiscuous androgen receptor (Veldscholte et al., 1990)</p> <p>T878A mutation allows AR to be activated by DHEA, estradiol, progesterone, cyproterone acetate, flutamide and nilutamide (Wadosky and Koochekpour, 2016)</p>	<p>PTEN^{-/-} This mutation is associated with increased chance of biochemical recurrence after prostatectomy in patients' cohort, resulting in CRPC (Li et al., 1997, Krohn et al., 2012)</p>
MR49F	An enzalutamide-resistant LNCaP derivative (Bishop et al., 2017)	<p>Its AR has both a T878A and F877L gain-of-function mutations (Bishop et al., 2017).</p> <p>The F877L mutation is implicated in conferring resistance to anti-androgens (Bishop et al., 2017, Coleman et al., 2016, Joseph et al., 2013, Korpál et al., 2013, Balbas et al., 2013).</p>	<p>Weakly responsive to androgens (Bishop et al., 2017); Enzalutamide resistant (Bishop et al., 2017)</p>
MR42D	An Enzalutamide-resistant LNCaP derivative (Bishop et al., 2017)	Same mutated AR as LNCaP (Bishop et al., 2017)	Enzalutamide resistant (Wadosky and Koochekpour, 2016);

			Does not express PSA; has reduced expression of canonical AR-regulated genes; has increased expression of neural transcription factor BRN2, neural cell adhesion molecule 1 (NCAM1) and terminal neuroendocrine markers, such as neuron-specific enolase (NSE), synaptophysin (SYP), chromogranin A (CGA) (Bishop et al., 2017, Davies et al., 2021).
VCaP	A prostate tumour that had metastasized to the bone (Makkonen et al., 2011)	Expresses wildtype AR and AR-variants AR is amplified (Makkonen et al., 2011)	Highly sensitive to androgen Sensitive to castration and Enzalutamide (Makkonen et al., 2011)
PC3	A prostate tumour that had metastasized to the bone (Tai et al., 2011)	AR-negative (Tai et al., 2011)	Growth is not affected by androgen withdrawal, resistant to AR-targeted therapies (Tai et al., 2011) Expresses neuroendocrine markers (Tai et al., 2011)
DU145	A prostate tumour that had metastasized to the brain (Wadosky and Koochekpour, 2016)	AR-negative (Wadosky and Koochekpour, 2016)	Castrate-resistant and resistant to AR-targeted therapies (Wadosky and Koochekpour, 2016)
C42B	An castration-resistant LNCaP derivative (Spans et al., 2014)	Same mutated AR as LNCaP (Spans et al., 2014)	Insensitive to hormones (Thalmann et al., 2000) Expresses PSA (Thalmann et al., 2000)

22Rv1	<p>An epithelial PCa cell-line that was derived from an androgen-dependent CWR22 xenograft which had been grown in mice, then castrated and relapsed (Pretlow et al., 1993).</p>	<p>Mutated AR: Has a H875Y gain-of-function mutation in the AR's LBD (Sramkoski et al., 1999, Wadosky and Koochekpour, 2016). The H875Y mutation allows the AR to be a promiscuous receptor in a patient's prostate tumour (Vasudevamurthy et al., 2017) and is implicated in resistance to AR-antagonists (Doamekpor et al., 2023).</p>	<p>Weakly stimulated by DHT (Sramkoski et al., 1999). Castration resistant, but still sensitive to Enzalutamide Has gene rearrangements within the <i>AR</i> gene that results in increased expression of AR variants (Li et al., 2011)</p>
-------	--	--	---

2.2 Generation of LNCaP cells over-expressing USP2

2.2.1 Insertion of triple FLAG tagged USP2a gene block into pDONR221 vector.

The triple FLAG-tagged USP2a gene block was designed and ordered from Singapore Integrated DNA Technology (IDT). 3uL of 25ng/uL triple FLAG tagged USP2a gene block (TF-USP2 g-block) was added to the mixture of 1uL 1g/L pDONR221 plasmid and 1uL BP Clonase was added to a PCR-clean tube, according to manufacturer's protocol (Gateway BP Clonase II from Life Tech, Cat #11789020) (**Table 2.2**), to generate the TF-USP2 entry vector (**Figure 2.1** and **Figure 2.2**).

The *Stb13 E.coli* cells (Invitrogen Catalogue C7373-03) were transformed with the BP reaction. SOC media (**Table 2.5**) was added to the transformed bacterial cells and allowed to recover at 37°C. The transformed bacterial cells were then plated onto LB agar plates (Sigma L-3147) containing 50 µg/mL kanamycin and incubated at 37°C overnight. Colonies were picked and grown in LB broth with 5mL LB broth with 50 µg/mL kanamycin overnight at 37°C. Plasmid DNA was extracted from the cultures using NucleoSpin Plasmid (Macherey Nagel Cat# 74058850). The resulting vector (**Figure 2.1**) was digested by *EcoRV* enzyme to confirm the insertion of the g-block.

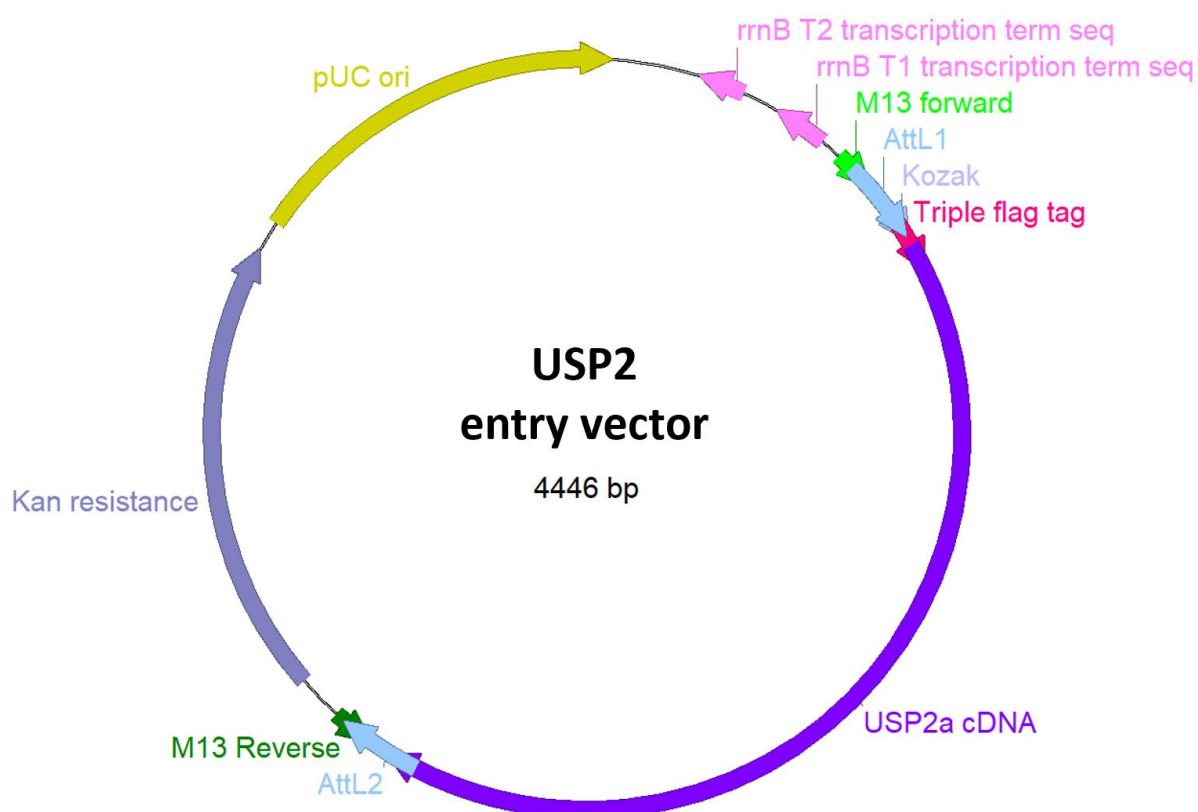


Figure 2.1. The pENTR-TF-USP2a contains the g-block inserted into the pDONR221 vector through recombination at the AttB sites present in the g-block and AttP sites present in the pDONR221 vector using BP Clonase enzyme (Invitrogen Gateway BP Clonase II Enzyme mix).

2.2.2 Insertion of TF-USP2 transgene from a Gateway entry clone into a destination vector

The pJS64 destination vector contains a constitutively active MND promoter to drive expression of the TF-USP2 transgene and the mPGK promoter to drive the expression of the hygromycin resistance gene. To generate the final lentiviral TF-USP2 overexpression vector (Figure 2.3), a reaction was set up comprising 1 μ L of destination vector (pJS64), 1 μ L of pENTR-TF-USP2 vector and 1 μ L of LR Clonase II enzyme (Invitrogen, Catalogue 11791-020) (Figure 2.2). The reaction was incubated overnight at 25°C in the thermal cycler. After the overnight incubation, 1 μ L of Proteinase K was added to each sample to terminate the reaction and the samples were then incubated at 37°C for 10 minutes.

The *Stb13 E.coli* cells (Invitrogen Catalogue# C7373-03) were transformed with the LR reaction in a 1 mm cuvette. SOC media was added to the transformed bacterial cells and allowed to recover at 37°C. The transformed bacterial cells were then plated onto LB agar plates (Sigma L-3147) containing 100 μ g/mL ampicillin and incubated at 37°C overnight. Colonies were picked and grown in LB broth with 5 mL LB broth with 100 μ g/mL ampicillin overnight at 37°C. Plasmid DNA was extracted from the cultures using NucleoSpin Plasmid (Macherey Nagel Cat# 74058850). The resulting overexpression vector (Figure 2.3) were digested by *EcoRI* enzyme to confirm the insertion of the TF-USP2 g-block into the destination vector. Once the correct vector been confirmed by *EcoRI* digestion, the sequences flanking the TF-USP2 transgene were sent for sequencing. The results of the sequencing were then aligned to the parental vector *in silico*.

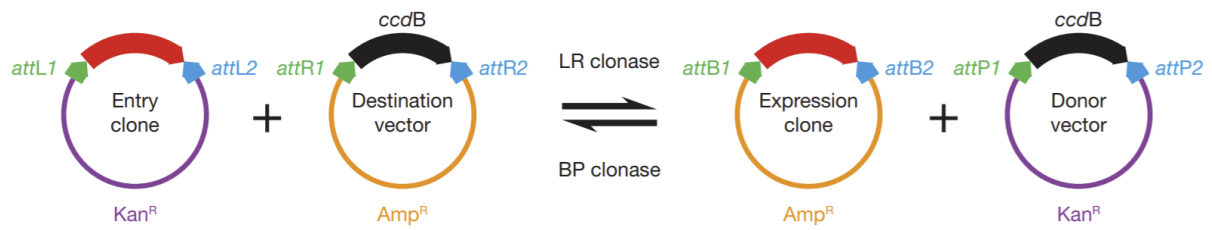


Figure 2.2. The insertion of the triple FLAG tagged USP2 fusion gene (TF-USP2) from the entry clone into the destination vector happens through the recombination at the *AttL* and *AttR* sites on the entry clone and destination vector respectively.

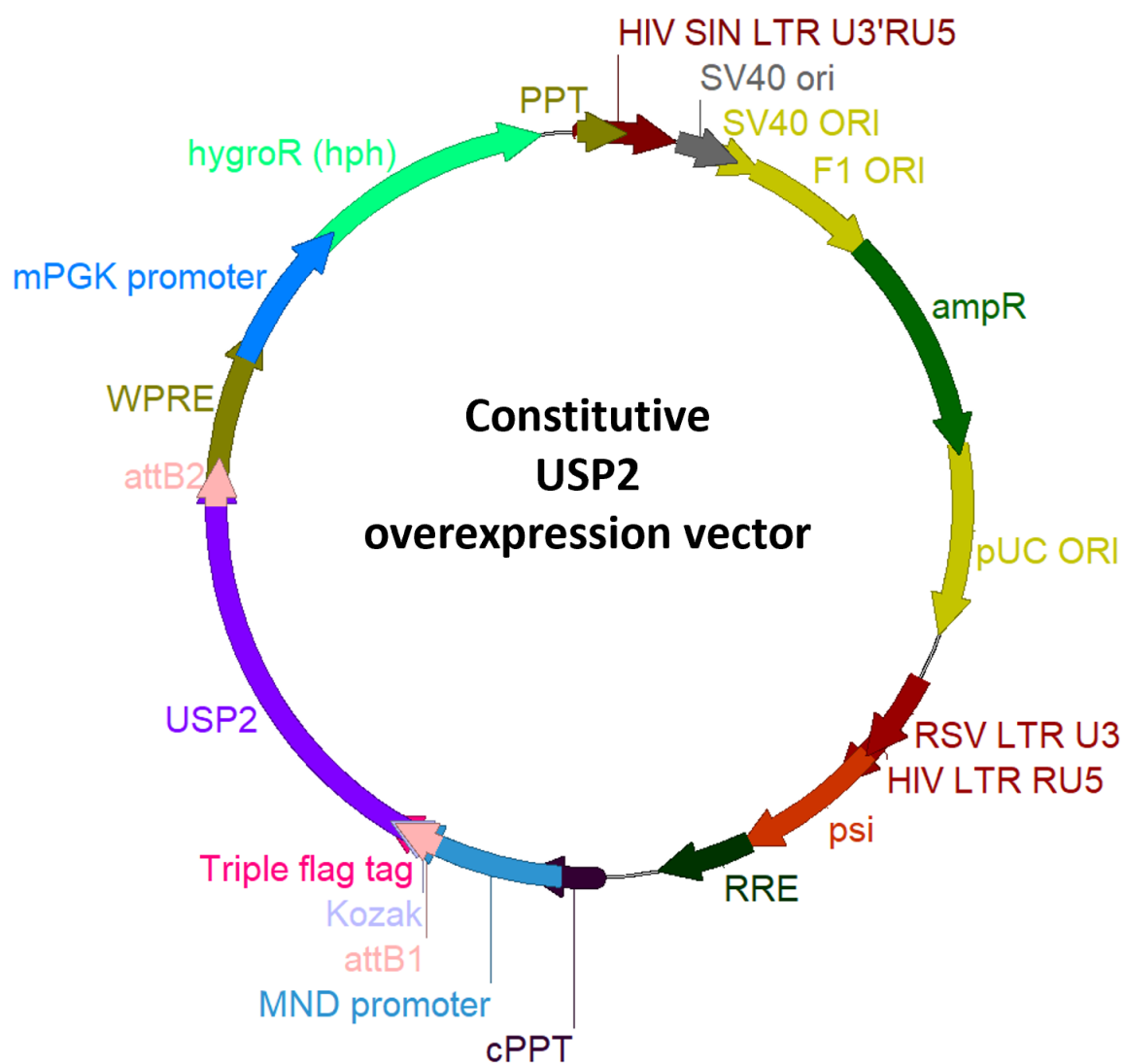


Figure 2.3. The diagram depicts the FLAG-USP2 expression vector generated from the LR reaction between the pENTR-TF-USP2a entry clone and the destination vector, MND-DEST mPGK-hygro. The FLAG-tagged USP2 transgene is now under the constitutive MND promoter. Other important features included in this expression vector are the origin of replication, the components that are part of the lentiviral transduction system and the constitutive mPGK promoter that drives the expression of the Hygromycin resistance gene, which functions as a selection marker.

2.3 Lentiviral transduction of LNCaP cells

A total of 20µg of DNA of the transfer package (final expression vector) and 2nd generation packaging lentiviral vectors (psPAX2 and pMD2.G) were transfected in a molar ratio of 4.8:3:1.6 respectively into 15 million HEK293T/17 cells, which were seeded into a T75 flask one day prior to transfection. pMD2.G was a gift from Didier Trono (Addgene plasmid # 12259 ; <http://n2t.net/addgene:12259> ; RRID:Addgene_12259). psPAX2 was a gift from Didier Trono (Addgene plasmid # 12260 ; <http://n2t.net/addgene:12260> ; RRID:Addgene_12260). The transfection reagent used was polyethylenimine (PEI) (Polysciences CAS# 49553-93-7) and the molar ratio of DNA to PEI was 1:3.1. The supernatant was changed after the transfection to remove the transfection reagent. The viral supernatant was then harvested after 48 hours and filtered through a 0.45 µm PVDF filter.

Lentiviruses were transduced into prostatic adenocarcinoma LNCaP cells with 6µg/mL polybrene (final concentration) (Also known as Hexadimethrine Bromine from Sigma, Cat# H9268). The volume of lentiviruses chosen for transduction resulted in the multiplicity of infection (MOI) to be approximately 1. The transduced LNCaP cells were then treated with one month of hygromycin selection to successfully select for USP2-overexpressing cells (LNCaP-USP2-OE) and the corresponding control cells. These transduced LNCaP-USP2-OE cells were confirmed to be overexpressing the FLAG-tagged USP2 protein, which was validated via Western blot by probing with the FLAG primary antibody.

2.4 Preparation of protein samples for Western blotting

Cells were typically grown in 6-well plates or 10cm dishes for extraction of proteins. Cells were washed with 1mL cold PBS and 110 μ L of RIPA lysis buffer (pH 7.4) (**Table 2.5**) were added to each well of a 6-well plate, followed by 5 minutes incubation on ice. Cells were scraped from wells and collected in 1.5mL Eppendorf tubes on ice. Cell lysates were spun at maximum speed and the supernatant containing proteins was collected. Protein concentration of each lysate was assessed using Bradford assay (Biorad Catalogue# 5000006). Protein lysates were stored at -80°C.

2.4.1 Sodium Dodecyl Sulfate Polyacrylamide Gel Electrophoresis (SDS-PAGE)

Protein samples were made up in a final concentration of 1X loading dye and heated at 95°C for 5 minutes. 20 to 40 μ g of denatured proteins were loaded into each well of a pre-cast SDS-PAGE gel (Criterion XT Bis-Tris or Criterion TGX Stain-free). The gels were run with the appropriate running buffer at 150V for 1 hour or until the dye front had run off the gel. The information on SDS-PAGE gels and their corresponding running buffers is described in **Table 2.4**. Precision Plus Protein Dual Color Standards (Biorad #1610374) was used as a standard protein ladder.

2.4.2 Western blotting

Transfer of proteins from SDS-PAGE gels to nitrocellulose membrane (Amersham Protran GE10600018) was conducted at 400mA for 1 hour using 1X transfer buffer (Table 2.2). Membranes were then blocked for 1 hour in 5% (w/v) skimmed milk in PBS and washed thrice for 3 minutes each in PBS Tween (PBST) prior to the addition of primary antibodies. Primary antibodies were made up in 3% (w/v) skim milk in PBST. Membranes were left overnight in the primary antibodies at 4°C with gentle agitation on a rocker. After washing the blot thrice in TBST, the corresponding secondary antibody tagged with a horseradish peroxidase enzyme (HRP) in TBST was added for 1 hour at room temperature, rocking. The membranes were then washed thrice in TBST. ECL solution (BioRad #1705061) was added on top of the membrane before the membrane was imaged on the Biorad Chemidoc MP imaging system and analysed using Image Lab Software. Protein expression was determined by densitometry measurements. The following information is described in **Table 2.5**, **Table 2.6** and **Table 2.7**: 10X transfer buffer, the primary and secondary antibodies.

Table 2.4. Description of SDS-PAGE gels and running buffers.

SDS-PAGE	Corresponding Running Buffer
Criterion XT Pre-cast Gels/ Extended shelf-life, 10% Bis-Tris, 18-well (BioRad #345-0112)	XT MOPS 20X Running Buffer pH 6.9 (BioRad # 1610788)
Criterion XT Pre-cast Gels/ Extended shelf-life, 4 to 12%, 18-well comb (BioRad #345-0124)	
Criterion TGX Stain-free, 10% polyacrylamide, 18-well (Biorad #5678034)	To run the TGX stain-free gels, a 1 in 10 dilution of the 10X Tris/Glycine/SDS running buffer. This 10X running buffer contains: 75g Tris (Sigma 7-9 #T1378), 360g Glycine (Sigma #G8898) 25g SDS (Molecular weight = 288.38g/mol, Sigma #L3771) in 2.5L of reverse osmosis (RO) water.
Criterion TGX Stain-free, 4 to 15% polyacrylamide, 18-well (BioRad # 5678084)	

Table 2.5. Recipes for solutions and buffers

Solution / Buffer	Final concentrations / amounts
SOC media	1% (w/v) Tryptone 1% (w/v) Yeast Extract 85.5mM NaCl 20mM Glucose
RIPA lysis buffer (pH 7.4)	10mM Tris 150mM NaCl 1mM EDTA 1% (w/v) TritonX-100 1X cOmplete mini protease inhibitor (Cat. # 11836153001)
10X transfer buffer	360 grams Glycine (Sigma #G8898) 77.5 grams Tris (Sigma 7-9 # T1378) 2.5L reverse osmosis (RO) water
6X Western loading buffer	0.27M Tris-Cl 10.3% SDS 35% glycerol (v/v) 6% b-mercaptoethanol (v/v) 0.05% bromophenol blue (v/v)

Table 2.6. Description of primary antibodies used for Western blotting in this study.

Primary antibody dilutions	Expected molecular weight
10mL Flag (Sigma #F1804) mouse monoclonal primary antibody diluted 1 in 2000 in 3% BSA in TBST	Approximately 68 kDa To probe for Flag-tagged USP2 protein
Aurora A (CST D3E4Q) rabbit monoclonal primary antibody diluted 1 in 1000 in 3% BSA in TBST	Approximately 48 kDa
Cyclin D1 (DAKO M3642) rabbit monoclonal primary antibody diluted 1 in 1000 in 3% BSA in TBST	Approximately 36kDa
FASN (Santa Cruz SC-20140) rabbit polyclonal primary antibody diluted 1:1000 (milk in TBST)	Approximately 250 kDa
AR (Abcam #ab108341 ER179) rabbit monoclonal primary antibody diluted 1 in 1000 in 5% skim milk in TBST	Approximately 110kDa
FKBP5 (Abcam #ab126715) rabbit monoclonal primary antibody diluted 1 in 1000 in 5% skim milk in TBST	Approximately 50kDa

Table 2.7. Description of secondary antibodies used in this study.

Name of secondary antibody	Supplier and catalogue number
Goat anti-mouse IgG highly cross-adsorbed secondary antibody with conjugated horseradish peroxidase (HRP)	Thermo Fisher (Catalogue #A16078)
Goat anti-rabbit IgG highly cross-adsorbed secondary antibody with conjugated horseradish peroxidase (HRP)	Thermo Fisher (Catalogue #A16110)

2.5 RNA extraction from prostate cancer cell lines

To isolate RNA from cells grown in 6-well plates, cell supernatant was removed from wells and cells were harvested in 1mL Trizol per well into 1.5mL PCR-clean Eppendorf tubes. 200 μ L of chloroform was added per sample, and then samples were vigorously shaken by hand for 15 seconds before a 10-minute incubation at room temperature. The samples were then centrifuged at 12,000g for 15 minutes at 4°C to isolate the upper aqueous layer. 400 μ L of the aqueous layer was transferred to a PCR-Clean 2mL tube. The following reagents were added to the aqueous layer in sequential order: 2.5 volume of 100% ethanol (which equates to $2.5 \times 400\mu\text{L} = 1000 \mu\text{L}$), 0.1 volume of 5M NaCl (which equates to $0.1 \times 400 \mu\text{L} = 40 \mu\text{L}$), a final concentration of 10mM MgCl₂ in a total volume of 1.44mL of reaction and 2 μ L of Glyco-Blue (Life Technologies). Samples were mixed and incubated overnight at -20°C, followed by spinning down at maximum speed for 30 minutes at 4°C. RNA pellets were then washed with 80% ethanol and air-dried at room temperature before being resuspended in 50 μ L nuclease-free water. RNA concentration and purity were quantified using a Nanodrop. Samples were stored at -80°C until further use.

2.6 Reverse transcription of mRNA to generate complementary DNA (cDNA)

RNA was treated with TURBO DNase (Invitrogen Catalogue #AM1907) to remove any contaminating genomic DNA that can interfere with downstream applications according to the manufacturer's instructions. Each RNA pellet was washed with 1mL of 75% ethanol and then dried before being resuspended in TE Buffer, pH7.0 (Ambicon Cat #9860) and quantified.

1000ng of DNase-treated RNA samples were reverse transcribed into complementary DNA (cDNA) in a total volume of 20 μ L per reaction using the iScript™ cDNA Synthesis Kit (Bio-Rad Cat#1708891). The cDNA reaction mix was incubated in a thermocycler using the following protocol: priming for 5 minutes at 25°C, 20 minutes of reverse transcription at 46°C and 1 minute of reverse transcriptase inactivation at 95°C.

2.7 Quantitative real-time PCR

Quantitative RT-PCR (qRT-PCR) was performed in three technical replicates for each cDNA sample. For each 10 μ L reaction in a 384-well plate, 5 μ L of 2X iQ SYBR Green Supermix (Biorad Catalogue# 1708887) and 2 μ L diluted cDNA was included. The cDNA was diluted at least 1 in 4 with nuclease free water. Sequences of primers are described in **Table 2.1**.

GAPDH or Actin levels were used for normalisation of qRT-PCR data according to the BioRad RT-qPCR method. The qPCR data was analysed using the software called BioRad CFX Manager.

2.8 Trypan blue cell viability assays for siRNA transfections

Cell viability was assessed for prostate cancer cells treated with siRNAs and drugs or when USP2 was overexpressed. The following drugs were tested in this study: enzalutamide (Focus Bioscience #HY-70002), ML364 (Focus Bioscience #HY-100900), alisertib (Assay Matrix #T2241) and docetaxel (Focus Bioscience #HY-B0011). For the transfection experiments, cells were reverse transfected with siRNAs targeting human USP2a transcript and seeded in triplicates. The siRNA used for the negative control was the “AllStars Negative Control” siRNA

(20nmol from Qiagen, Catalogue# 1027281). Live and dead cells were manually counted using a hemacytometer at the appropriate time points. Using a haemocytometer, cell viability was determined by the exclusion of Trypan blue in live cells.

Chapter 3:

**USP2 is a novel driver of
lethal prostate cancer and
mediator of therapy resistance**

3 USP2 is a novel driver of lethal prostate cancer and mediator of therapy resistance.

3.1 Introduction

This chapter aims to identify genes that are upregulated in response to AR antagonists as a means to provide new insight into uncover mechanisms of resistance to AR-targeted therapies in prostate cancer. Several studies have investigated mechanisms of resistance by conducting RNA-sequencing of enzalutamide-treated prostate cancer cell lines, such as LNCaP and C4-2 (Zhao et al., 2016, Yuan et al., 2019, Svensson et al., 2017). However, the disadvantages of using cell lines are that they lack tissue architecture and the immediate tumour microenvironment (Risbridger et al., 2018, Centenera et al., 2018a). Employing models that more accurately model the human condition, such as patient derived explants (PDEs), will provide more clinically relevant information. PDEs are small pieces of cancer tissue that are grown on gelatine sponges (Risbridger et al., 2018, Centenera et al., 2018a). The advantages of using PDEs are that tissue architecture and androgen signalling are maintained to allow for the study of androgen-regulated genes in real patient tissues (Risbridger et al., 2018, Centenera et al., 2018a). Histopathological assessment of tissue architecture and cellular appearance, between PDEs and the uncultured tumour tissue from surgery, showed that PDEs can be cultured for up to 6 days on gelatine sponges (Centenera et al., 2018a). The tumour microenvironment was also maintained in the PDEs (Centenera et al., 2018a). So far, PDEs have been mainly used for the assessment of drug efficacy and can be used for multiple other applications, such as investigating uptake of enzalutamide in tumours over time using

mass spectrometry, delivering siRNAs in porous silicon nanoparticles (pSiNPs), and inhibiting genes- and proteins-of-interest via shRNAs and drugs (Mutuku et al., 2019, Tieu et al., 2021, Centenera et al., 2018a, Gillis et al., 2013, Gillis et al., 2021).

In this chapter, we conducted RNA sequencing of PDEs treated with enzalutamide and identified *USP2* as a gene that was upregulated in response to enzalutamide. Our subsequent investigation of *USP2* revealed that it was repressed by androgen signalling, upregulated in AR-independent neuroendocrine prostate cancer, and could mediate resistance to AR-targeted therapies and chemotherapy.

3.2 Materials and Methods

3.2.1 Tissue collection from a matched normal to tumour cohort

Prostate tissues were collected with written informed consent from patients undergoing radical prostatectomy at St Andrew’s hospital, Adelaide, Australia, through the Australian Prostate Cancer BioResource. These patients had no previous treatments prior to radical prostatectomy. A longitudinal section of each tissue was removed before being cultured *ex vivo* (described below). Half of the samples were snap frozen and the remainder were fixed in formalin and paraffin embedded for assessment by a pathologist. Ethical approval for tissue collection and experimentation was obtained from St Andrew’s and the University of Adelaide Human Research Ethics committees. All experiments with patient material were performed in accordance with the National Health and Medical Research Council of Australia guidelines. Histopathologic features of all tumours used in this study are detailed in Table 3.1 (Butler et al., 2021).

Table 3.1. Description of patients’ tumours described in this study.

Patient ID	Age at RP	Pre-RP PSA	1° Gleason	2° Gleason	Total Gleason
32717	70.7	16	3	4	7
32732	66.7	7	3	4	7
32743	67.3	18.6	4	4	8
32747	57.6	6.9	3	4	7
32755	64.2	5.6	3	3	6
32760	70.6	6.5	3	4	7
32764	67.1	8.1	3	4	7
32771	66.5	5.7	3	4	7
32800	59.2	1.8	3	4	7
32802	69.1	7	4	3	7
32804	70.3	7.9	4	3	7
32840	50.6	8.6	3	4	7

3.2.2 *Ex vivo* culture of human prostate tumours

Patient prostate tumours were cultured in accordance with techniques established previously described by the laboratory of my supervisor, Prof Lisa Butler (Centenera et al., 2012). Prostate cancer tissue in the form of 8mm biopsy cores were obtained with written informed consent through the Australian Prostate Cancer BioResource from men undergoing radical prostatectomy. The tissue was cut into 1 mm³ pieces and cultured in triplicates on pre-soaked Gelfoam sponges (80 x 125mm Pfizer 1205147) in 24-well plates containing 500uL RPMI-1640, 10% FBS, antibiotic/antimycotic solution, 0.01mg/mL hydrocortisone and 0.01mg/mL insulin (Sigma). Vehicle or 10 µM or 50 µM enzalutamide was added into each well and the tissues were cultured at 37°C for 48 hours before being preserved in RNAlater (Invitrogen) or formalin-fixed and paraffin embedded. Total RNA was extracted using a RNeasy mini kit (Qiagen #74104) according to manufacturer's instructions.

Libraries for RNA sequencing were generated using 800 ng of RNA and a TruSeq Stranded Total RNA Library Prep Kit (Illumina #20020596), according to manufacturer's instructions. Sequencing was carried out at the South Australian Health and Medical Research Institute Genomics Facility using an Illumina NextSeq 500 (single read 75bp v2 sequencing chemistry). The quality and number of reads for each sample were assessed with FastQC v0.11.3 (Andrews, 2010) . Adaptors were trimmed from reads, and low-quality bases, with Phred scores < 28, were trimmed from ends of reads, using Trimgalore v0.4.4 (Krueger, 2012). Trimmed reads of <20 nucleotides were discarded. Reads passing all quality control steps were aligned to the hg38 assembly of the human genome using TopHat v2.1.1 (Kim et al., 2013) allowing for up to two mismatches. Reads not uniquely aligned to the genome were discarded. HTSeq-count v0.6.1 (Anders et al., 2015) was used with the union model to assign

uniquely aligned reads to Ensembl Hg38.86-annotated genes. Data were normalized across libraries by the trimmed mean of M-values (TMM) normalization method, implemented in the R v3.5.0, using Bioconductor v3.6 EdgeR v3.20.9 package (Robinson et al., 2010). Only genes expressed at count-per-million value greater than 10 in at least 2 samples per group were retained for further analysis. Differential expressed genes were selected based on the robust version of the quasi-likelihood negative binomial generalized log-linear model (Lun et al., 2016), with false discovery rate (FDR) set at 0.05.

3.2.3 Androgen and AR-antagonist treatment of androgen responsive cell lines

Prior to androgen treatment, LNCaP and VCaP cells were cultured in PRF-RPMI media containing 10% dextran charcoal coated FBS (DCC-FBS) and 2mM L-Glutamine (Gibco), sometimes referred to as androgen depleted media, for 72 hours. The cells were then treated with 10nM dihydrotestosterone (DHT) or 10 μ M enzalutamide (Enz) or both in androgen depleted media. For anti-androgen treatments, cells were cultured in full serum for 72 hours before treatment with 10 μ M Enz in full serum.

3.2.4 Measurements of neurite lengths

The lengths of neurite extensions were measured using the NeuronJ plugin (Meijering et al., 2004) in Fiji/ImageJ (Schindelin et al., 2012). At least 5 images were taken per technical replicate (n = 3). More than 200 neurite lengths per cell type were traced and measured.

Neurite lengths from three biological sets of replicates were measured. Representative images with overlaid neurite traces in magenta were presented.

3.2.5 Chromatin immunoprecipitation qPCR (ChIP-qPCR)

LNCaP cells were seeded at a density of 3×10^6 per 15cm plate in media supplemented with 10% Dextran charcoal stripped (DCC) FBS for 72 hours before treatment with 10nM DHT or control for 4 hours. The cells were then cross-linked with formaldehyde and snapped frozen. ChIP was performed as previously described in (Paltoglou et al., 2017). 2 μ L DNA was used in 10 μ L qPCR reactions for ChIP-qPCR. The negative control 2 (NC2) has been validated as a region that AR does not bind to when cells were treated with DHT (Jia et al., 2008).

3.2.6 Single-sample Gene Set Enrichment Analysis (ssGSEA)

To generate AR activity score, a set of AR-regulated genes was obtained from (Sowalsky et al., 2018). For the NEPC scores, the list of genes commonly upregulated or downregulated in NEPC were obtained from (Beltran et al., 2016). ssGSEA (Barbie et al., 2009) was implemented using the Broad Institute's public platform, Gene Pattern (Reich et al., 2006), using rank normalisation and default parameters.

Table 3.2. Publicly available clinical data on patient's tumours or xenografts that were downloaded from GEO.

Dataset	Description	RNA Sequencing / Microarray	Number of samples	Reference
GSE48403	Locally advanced or metastatic prostate tumours from patients given ADT	RNA sequencing	7 matched tumours from patients before and after given ADT	(Rajan et al., 2011)
GSE5091	Tumours from mice prostates following castration and supplemented with androgen	Microarray	5 mice per group	(Wang et al., 2007)
GSE70079	Primary prostate tumours	AR ChIP-Sequencing	7 normal prostate tissue, 13 primary prostate tumours	(Pomerantz et al., 2015)
GSE130408	Castrate resistant patient derived xenografts (PDXs)	AR ChIP-Sequencing	13 CRPC PDXs	(Pomerantz et al., 2020)
GSE137775	LNCaP cells (an androgen dependent PCa cell line) treated with 4 days of DMSO or Enz	AR ChIP-Sequencing	2 replicates in each group	(Hwang et al., 2019)
GSM1249447	LNCaP cells treated with 4 hours of either	H3K27ac ChIP-Seq		(Hazelett et al., 2014)

	control or 10nM DHT			
SU2C 2019	Metastatic prostate tumours	RNA Sequencing	213 castrate resistant prostate tumours and 22 neuroendocrine prostate tumours	(Abida et al., 2019)
GSE99381	Metastatic prostate tumours	RNA sequencing	34 castrate resistant prostate tumours and 15 neuroendocrine prostate tumours	(Beltran et al., 2016)
Bluemn et al. (2017)	Metastatic prostate tumours	RNA sequencing	Number of prostate tumours with the following features: 58 AR+ NE- 9 AR- NE- 11 AR+ NE+ 7 AR- NE+	(Bluemn et al., 2017)
TCGA PRAD	Normal prostate tissue, Primary prostate tumours	RNA Sequencing	52 normal tissues 419 tumour tissues	(Abeshouse et al., 2015)
GSE90891	Mouse models representing epithelial to neuroendocrine plasticity	RNA sequencing	4 Pten ^{f/f} 13 Pten ^{f/f} ; Rb1 ^{f/f} 6 Pten ^{f/f} ; Rb1 ^{f/f} ; Trp53 ^{f/f}	(Ku et al., 2017)

3.3 Results

3.3.1 USP2 is upregulated in response to AR-targeted therapy.

The chapter aimed to identify factors that might confer resistance to the clinically used anti-androgen, enzalutamide. Patient-derived explants (n=12) were treated *ex-vivo* with 10 μ M or 50 μ M enzalutamide for 48 hours. These prostate tumours were stained for Ki67, which is a proliferation marker, and the percentage of the tumour section positive for Ki67 was quantified. Although the responses to enzalutamide were heterogenous, all tumours had a significant overall reduction in Ki67 staining after treatment with 10 μ M Enz and there was a further reduction with 50 μ M Enz (**Figure 3.1A**). This indicated that the AR antagonist was inhibiting growth of prostate cancer cells. RNA sequencing was then used to evaluate the transcriptomes of tumours treated with vehicle, 10 μ M and 50 μ M enzalutamide. The gene set enrichment analysis (GSEA) plot showed a decrease in androgen receptor signalling with enzalutamide treatment, thereby providing evidence that enzalutamide is effectively inhibiting AR activity as expected (**Figure 3.1B**).

A complete evaluation of the transcriptomic response to Enz in primary tumour PDEs is being undertaken (Lisa Butler, personal communication) but is beyond the scope of this project. However, one gene of interest that we observed to be upregulated by enzalutamide was *USP2* (**Figure 3.1**). *USP2* mRNA levels increased by more than 2-fold in response to 10 μ M or 50 μ M Enz (**Figure 3.1C**). We were interested in *USP2* because of its function in cleaving ubiquitin groups from its oncogenic substrates and thereby preventing them from degradation in the proteasome (**refer to Chapter 1 Section 1.15**). These preliminary results

indicated that USP2 might be regulated by the androgen receptor signalling pathway in prostate cancer and have a role in mediating cell survival in response to enzalutamide.

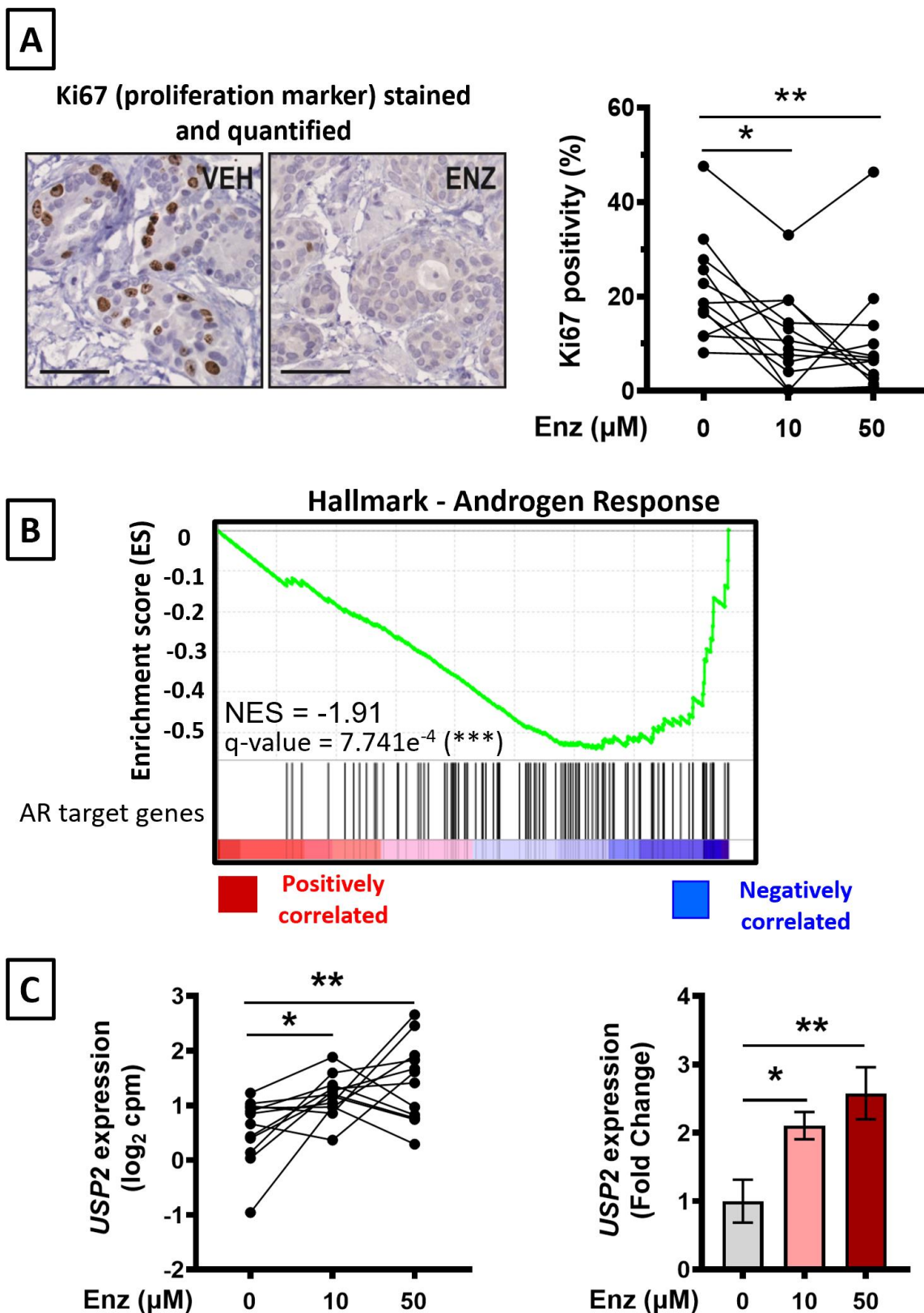
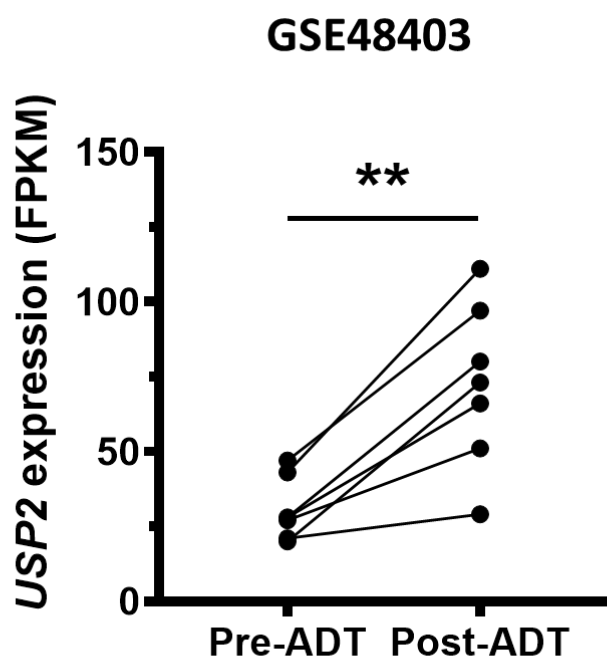


Figure 3.1. USP2 expression increased in patient-derived explants PDEs after 48 hours of enzalutamide treatment. (A) Ki67 expression, which is a proliferation marker, decreases after

48 hours of 10 μ M and 50 μ M Enz. (B) The GSEA plot showed an overall decrease in androgen response when PDEs were treated with enzalutamide. (C) USP2 expression is increased when patient derived explants were given 10 μ M Enz and further increased with 50 μ M Enz. Expression units for graph on left are counts per million (cpm, log₂), whereas the graph on the right shows fold-change (vehicle set to 1, error bars are \pm standard deviation). Statistical analyses in A and C were conducted via paired One-Way ANOVA. P-values ≤ 0.05 (*); ≤ 0.01 (**).

To confirm USP2 upregulation in response to AR-targeted therapies, published transcriptomic datasets were interrogated. In the Rajan *et al.* (2015) cohort (GSE48403) (**Table 3.2**), which comprised of patient-matched tumours pre- and post- 22 weeks of ADT (luteinising hormone-releasing hormone agonists plus an anti-androgen), *USP2* was significantly elevated after ADT (**Figure 3.2A**). Additionally, *USP2* expression was increased in the prostates of mice following surgical castration of their testes (GSE5901) and reduced in the prostates of castrated mice given testosterone (**Figure 3.2B**) (Wang et al., 2007). Collectively, these findings provide evidence that USP2 is increased after castration *in vivo*.

A



B

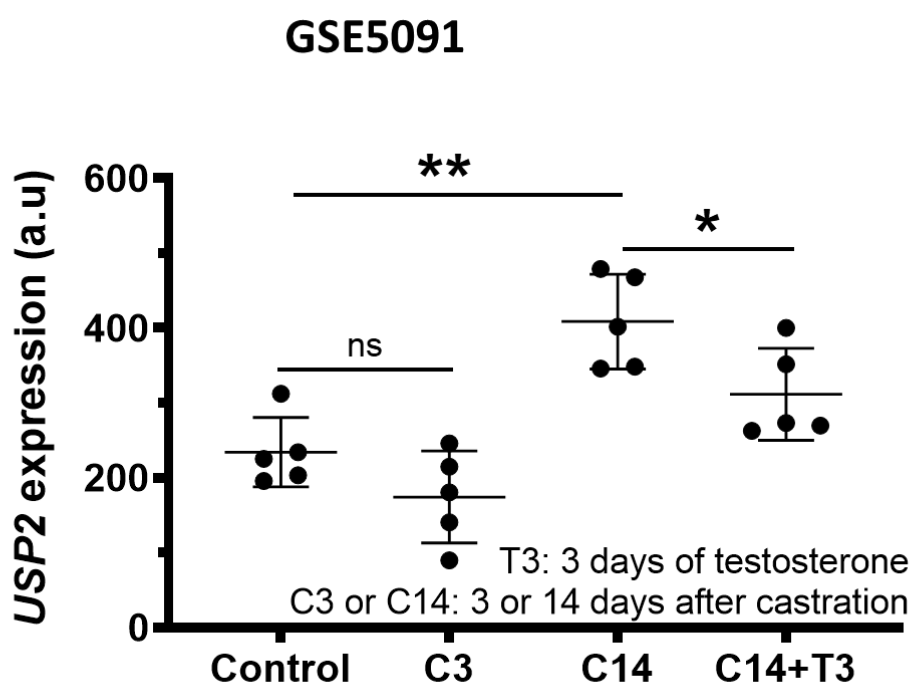


Figure 3.2. *USP2* expression is upregulated in response to AR-targeted therapy. (A) *USP2* expression is increased in patients following ADT (GSE48403, n = 7 tumours analysed pre- and post-ADT) (Table 3.2) (Rajan et al., 2011). FPKM, fragments per kilobase of exon per million mapped fragments. (B) *USP2* expression is increased in the prostates of mice 14 days after

surgical castration of the testes (C14) and decreased after castrated mice were given 3 days of testosterone treatment (T3) (GSE5901) (n = 5 mice per group) (**Table 3.2**) (Wang et al., 2007). The abbreviation “a.u.” stands for arbitrary units. Statistical analyses were conducted via paired t-test in (A) or One-Way ANOVA in (B). P-values ≤ 0.05 (*); ≤ 0.01 (**). Mean \pm standard deviation (SD) for each group was shown.

To experimentally investigate the relationship between AR activity and USP2 we used a panel of *in vitro* models. We found that *USP2* mRNA levels are higher in neuroendocrine-like PCa cell lines, such as neuroendocrine-like MR42D cells and PC3 cells, than in androgen-dependent adenocarcinoma cell lines (LNCaP and VCaP) (**Figure 3.3**). Addition of the AR antagonist, enzalutamide, significantly increased *USP2* expression in androgen dependent LNCaP and VCaP cells (**Figure 3.4**). Conversely, the androgen 5 α -dihydrotestosterone (DHT) significantly decreased *USP2* expression in LNCaP cells (**Figure 3.4**). Expression of the *KLK3* gene, a well-described gene that is upregulated by AR, validated the treatments in these experiments (**Figure 3.4**). These results confirmed the finding from PDEs and our data mining that *USP2* expression is repressed by AR activity.

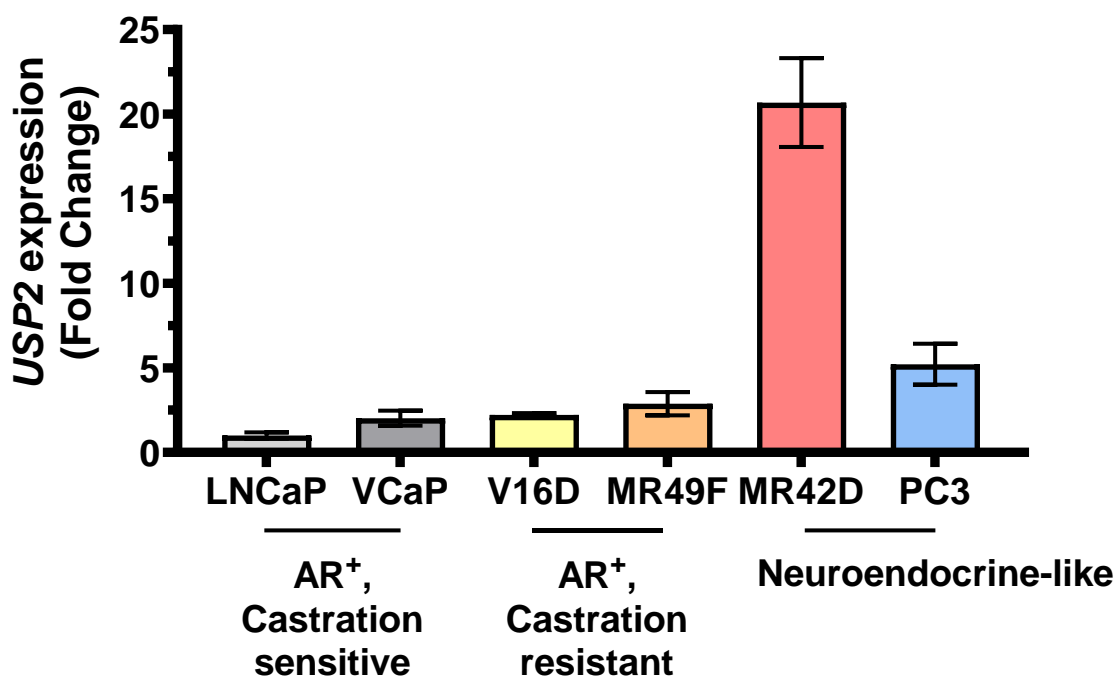


Figure 3.3. *USP2* expression is the highest in castrate resistant PCa (CRPC) cell lines. The *USP2* expression was checked across a panel of PCa cell lines cDNA. 1000ng of RNA from each cell line was reverse transcribed into cDNA and equal amounts of cDNA was loaded into the quantitative PCR (qPCR). For each cell line, the *USP2* mRNA levels were then normalised to the expression of housekeeping gene, GAPDH, and calculated as a fold change to the normalised *USP2* expression in LNCaP cells. Mean \pm standard error mean (SEM) from each group were shown, n = 3.

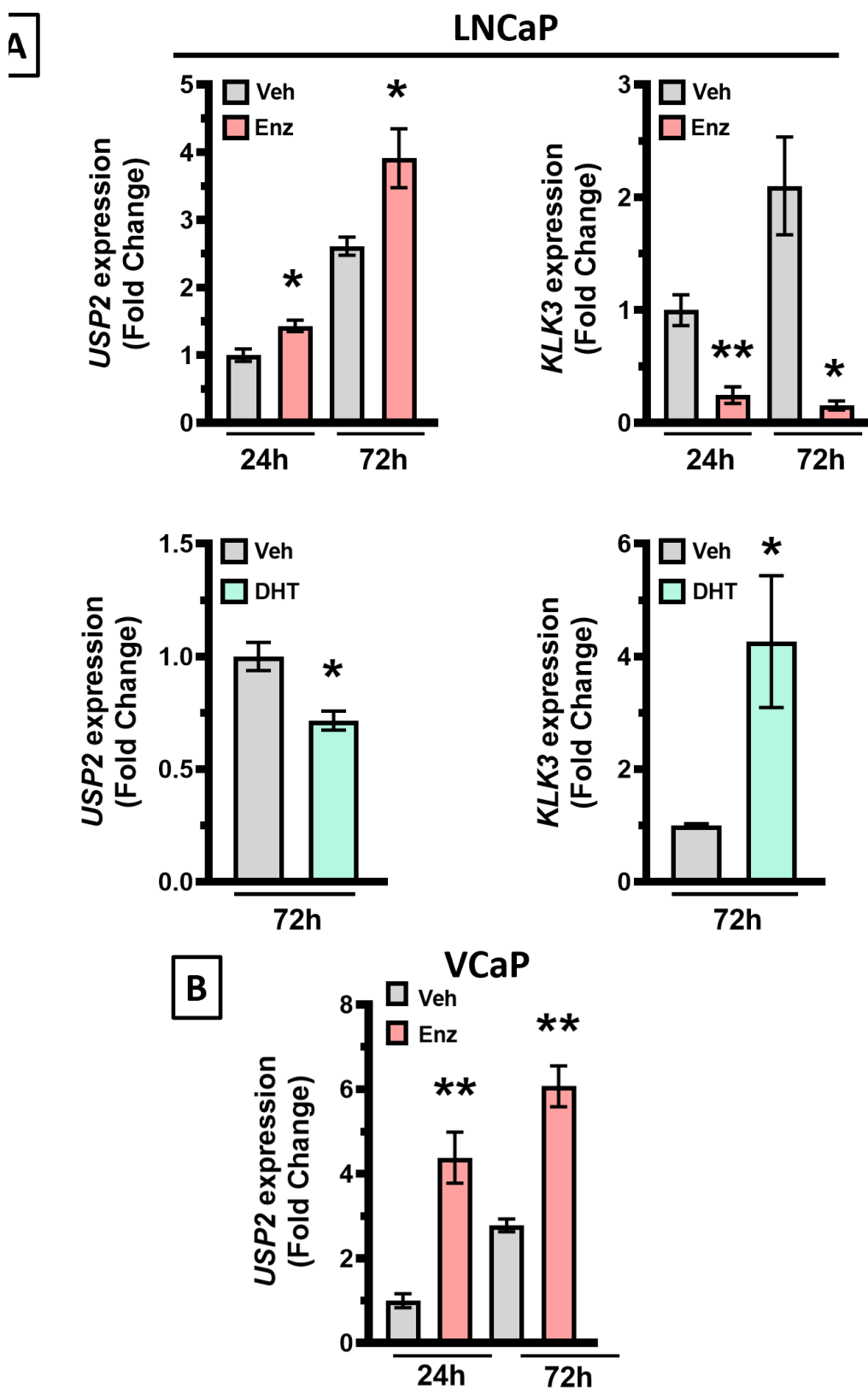


Figure 3.4. USP2 expression is upregulated by anti-androgen and repressed with androgen. The androgen dependent PCa cell lines, LNCaP in (A) and VCaP in (B), were treated with 24

and 72 hours of 10 μ M Enz in 10% full serum or androgen DHT in 10% charcoal-stripped serum (CSS). The expression data was normalised to the expression of the reference GAPDH levels and then calculated as a fold change to the corresponding vehicle controls. Statistical analyses were conducted via unpaired t-test. P-values ≤ 0.05 (*); ≤ 0.01 (**). Mean \pm standard error mean (SEM) for each group was shown, n = 3.

To investigate if *USP2* is directly regulated by AR, four publicly available ChIP-seq datasets were interrogated. Data mining of three cohorts that performed chromatin-immunoprecipitation sequencing using AR antibody (AR ChIP-seq) revealed an apparent loss of AR binding peak proximal to the *USP2* promoter in primary prostate tumours (Pomerantz et al., 2015) and castrate-resistant PDXs (Pomerantz et al., 2020) when compared to normal prostates and in LNCaP cells treated with Enz (GSE137775) (Hwang et al., 2019) (**Figure 3.5A**). Interestingly, in those cohorts, there appears to be a second loss of an AR binding peak, which indicates a distal cis-regulatory element that the androgen receptor can bind and directly repress the transcription of the *USP2* gene (**Figure 3.5A**) (Hwang et al., 2019, Pomerantz et al., 2015, Pomerantz et al., 2020). Additionally, mining of H3K27ac ChIP-seq data, which is a marker of active enhancers and promoters, from LNCaP cells treated with androgens revealed a suppression of the H3K27ac signal at approximately the same location as the putative AR binding site that is distally located to the *USP2* promoter (**Figure 3.5B**) (GSM1249447). These observations indicate that AR may bind to the *USP2* gene and directly regulate its expression. To obtain further evidence for this hypothesis, AR ChIP-qPCR was conducted on LNCaP cells treated with 10nM androgens for 4 hours and demonstrated a slight significant fold enrichment at that putative proximal AR binding site (region 1) identified near the *USP2* promoter (**Figure 3.5C**). AR ChIP-qPCR was also conducted on LNCaP cells treated with 10 μ M Enz and showed there was a significant reduction in enrichment at the distal proximal AR binding site (region 2) (**Figure 3.5D**). Therefore, the results indicated that AR could be directly regulating *USP2* transcription.

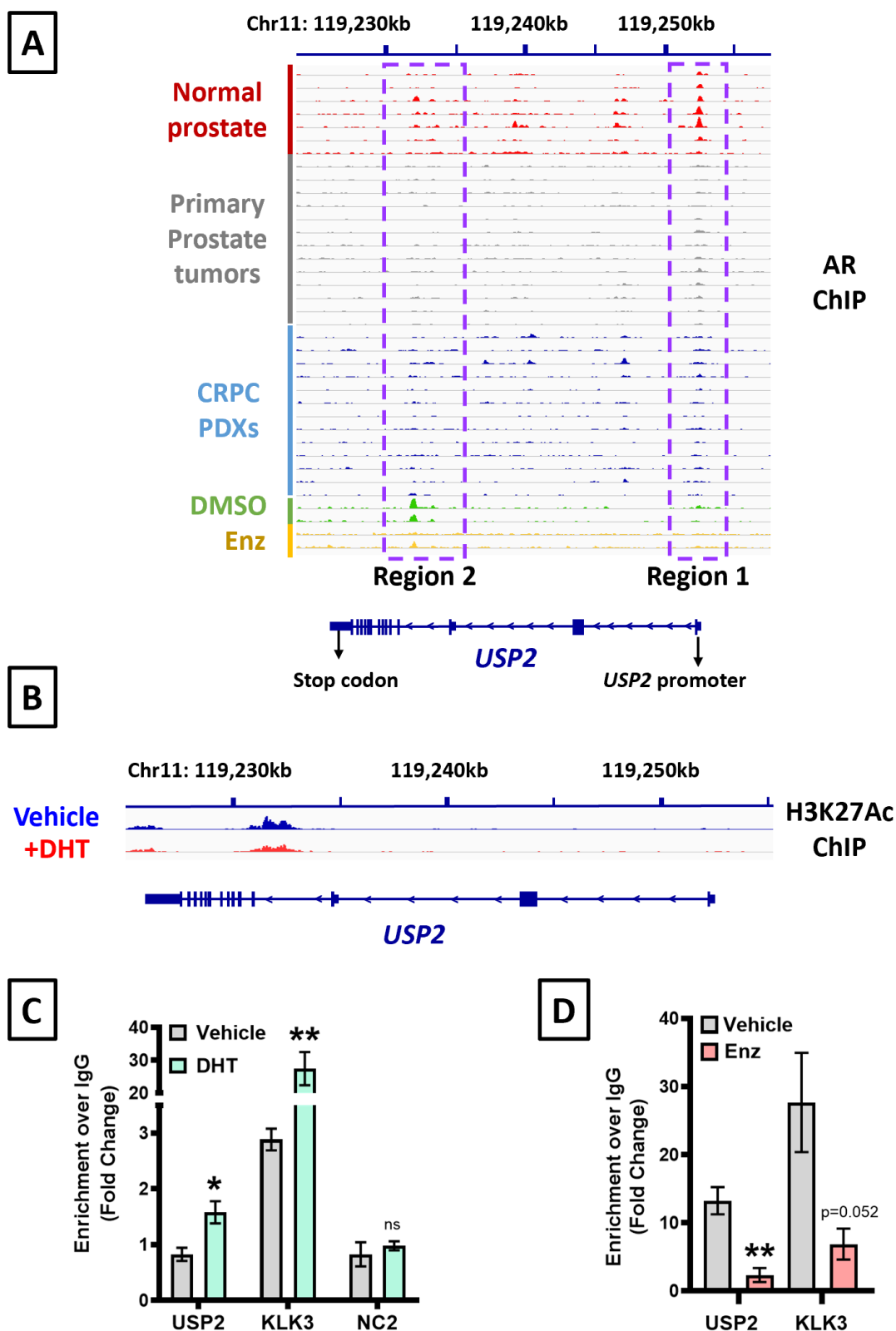


Figure 3.5. The *USP2* gene may be directly repressed by the AR. (A) This is a genome-wide AR-binding in normal prostate epithelium, primary tumour tissue, castrate resistant PCa PDXs

and LNCaP cells treated with DMSO or enzalutamide for 96 hours in full serum. Representative 30-kb areas surrounding the *USP2* gene are shown. Each track depicts the AR binding intensities for a given sample, elucidated from AR ChIP-seq. Regions of the genome that are highlighted within the purple boxes are regions that AR may be directly binding to regulate the *USP2* gene. The data range is set at a minimum of 0 and a maximum of 2.5. (B) Each track depicts the signal intensities of H3K27Ac modifications in the genome of LNCaP cells treated with or without androgen DHT. The raw files from the H3K27Ac ChIP-seq in LNCaP cells were downloaded from GSM1249447 and processed by A/Prof. Selth (**Table 3.2**). (C) ChIP-qPCR analysis demonstrates AR binding at *USP2* gene locus proximal to *USP2* promoter in LNCaP cells after treatment with androgens. Statistical analysis was conducted via unpaired two-tailed student t-test. P-values ≤ 0.05 (*); ≤ 0.01 (**). Mean \pm standard error mean (SEM) for each group was shown, n = 3. (D) ChIP-qPCR analysis demonstrates loss of AR binding at *USP2* gene locus distally located to *USP2* promoter in LNCaP cells after treatment with enzalutamide. Statistical analysis was conducted via unpaired two-tailed student t-test. P-values ≤ 0.01 (**).

3.3.2 USP2 is associated with neuroendocrine PCa.

Neuroendocrine prostate cancer is a subtype of castrate resistant PCa that loses dependence on the androgen receptor (Davies et al., 2021, Aggarwal et al., 2018, Labrecque et al., 2019, Wang et al., 2021b) (refer to **Chapter 1 Section 1.9.2**). Given the earlier key finding that USP2 expression is suppressed by AR, it is hypothesised that USP2 would be upregulated in AR-independent prostate tumours. Data mining of clinical transcriptomic datasets (SU2C 2019; Beltran et. al., Nature Medicine 2016; GSE99381) (**Table 3.2**) revealed that *USP2* expression is significantly upregulated in patients with NEPC as compared to patients with CRPC adenocarcinoma (**Figure 3.6A-C**) (Abida et al., 2019, Beltran et al., 2016, Bluemn et al., 2017). In a panel of PDXs established through the Melbourne Urological Research Alliance (MURAL) (Lawrence et al., 2018), which we had access through collaboration, *USP2* expression is significantly higher in PDXs that have neuroendocrine features (**Figure 3.6D**). *USP2a* is the canonical transcript from the *USP2* gene (Graner et al., 2004). Collectively, these data indicate that *USP2* is upregulated in clinical neuroendocrine prostate cancer.

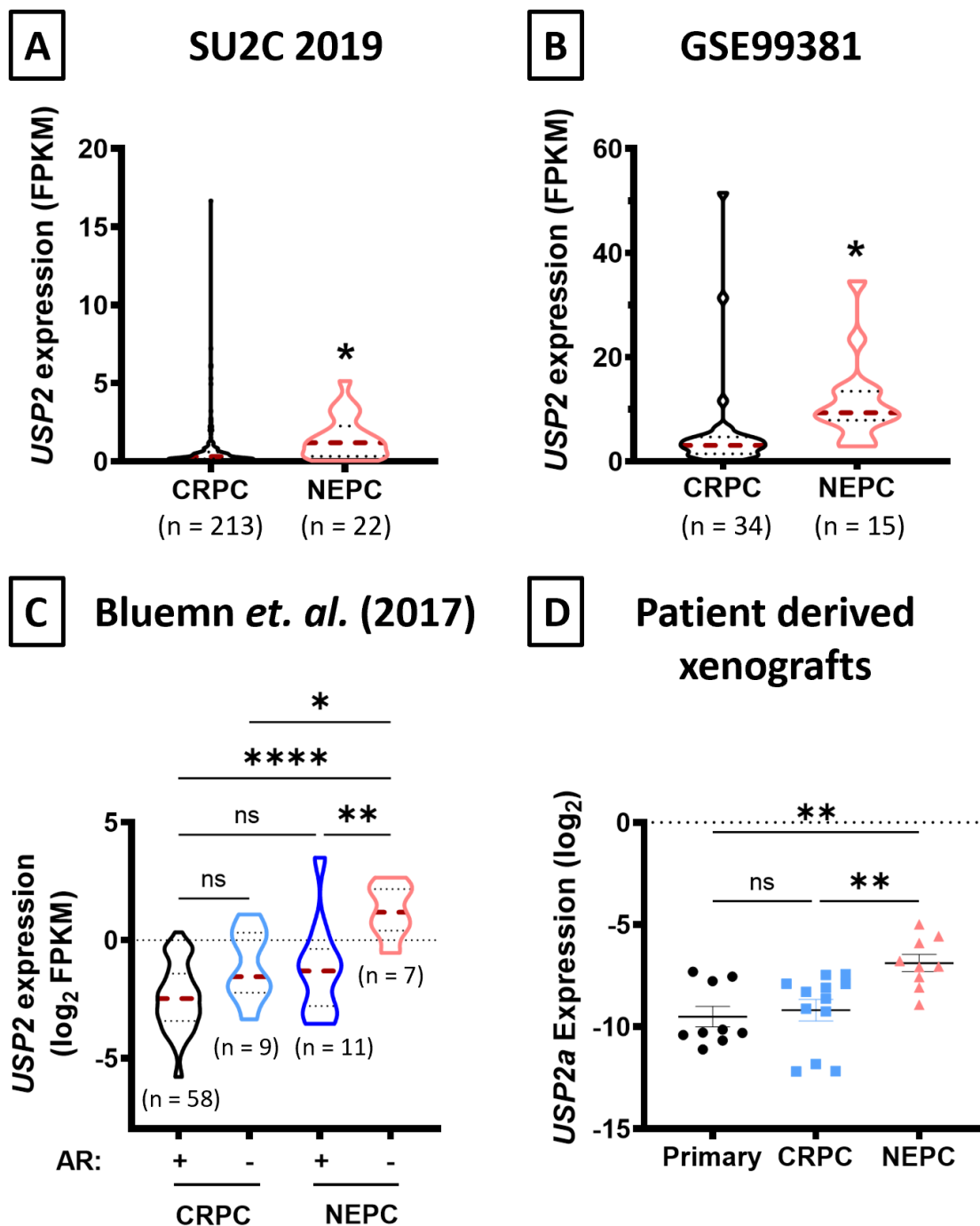


Figure 3.6. *USP2* expression is elevated in neuroendocrine prostate cancer (PCa). *USP2* expression is higher in patients with neuroendocrine PCa in several large cohorts of patients with metastatic PCa (**Table 3.2**): (A) Stand Up 2 Cancer (SU2C 2019) (B) Beltran *et. al.* (2016)

and (C) Bluemn *et. al.* (2017). The results are plotted as violin plots and the median of each violin plot is represented as a dotted red line with the interquartile range represented as dotted black lines. (D) *USP2a* expression is higher in neuroendocrine patient-derived xenografts. Mean \pm standard deviation (S.D) for each group was shown. All statistical analyses were conducted via unpaired two-tailed student t-test or one-way ANOVA, p-values ≤ 0.05 (*); ≤ 0.01 (**); ≤ 0.001 (***) ; ≤ 0.0001 (****).

The relationships between *USP2* expression and AR activity or neuroendocrine phenotypes were next evaluated in primary prostate cancer. We calculated AR activity and NEPC scores using ssGSEA and well-characterised AR- and NEPC-associated gene sets curated by Sowalsky *et. al.* (Cancer Research, 2018) and Beltran *et. al.* (Nature Medicine, 2016) respectively. Elevated *USP2* expression in patient tumours was positively associated with genes elevated in NEPC (**Figure 3.7A**) and negatively associated with genes downregulated in NEPC (**Figure 3.7B**). These observations are in concordance with elevated *USP2* expression sharing an inverse relationship with low AR activity (**Figure 3.7C**). Collectively, these data demonstrated that *USP2* is associated with the neuroendocrine phenotype and loss of AR activity.

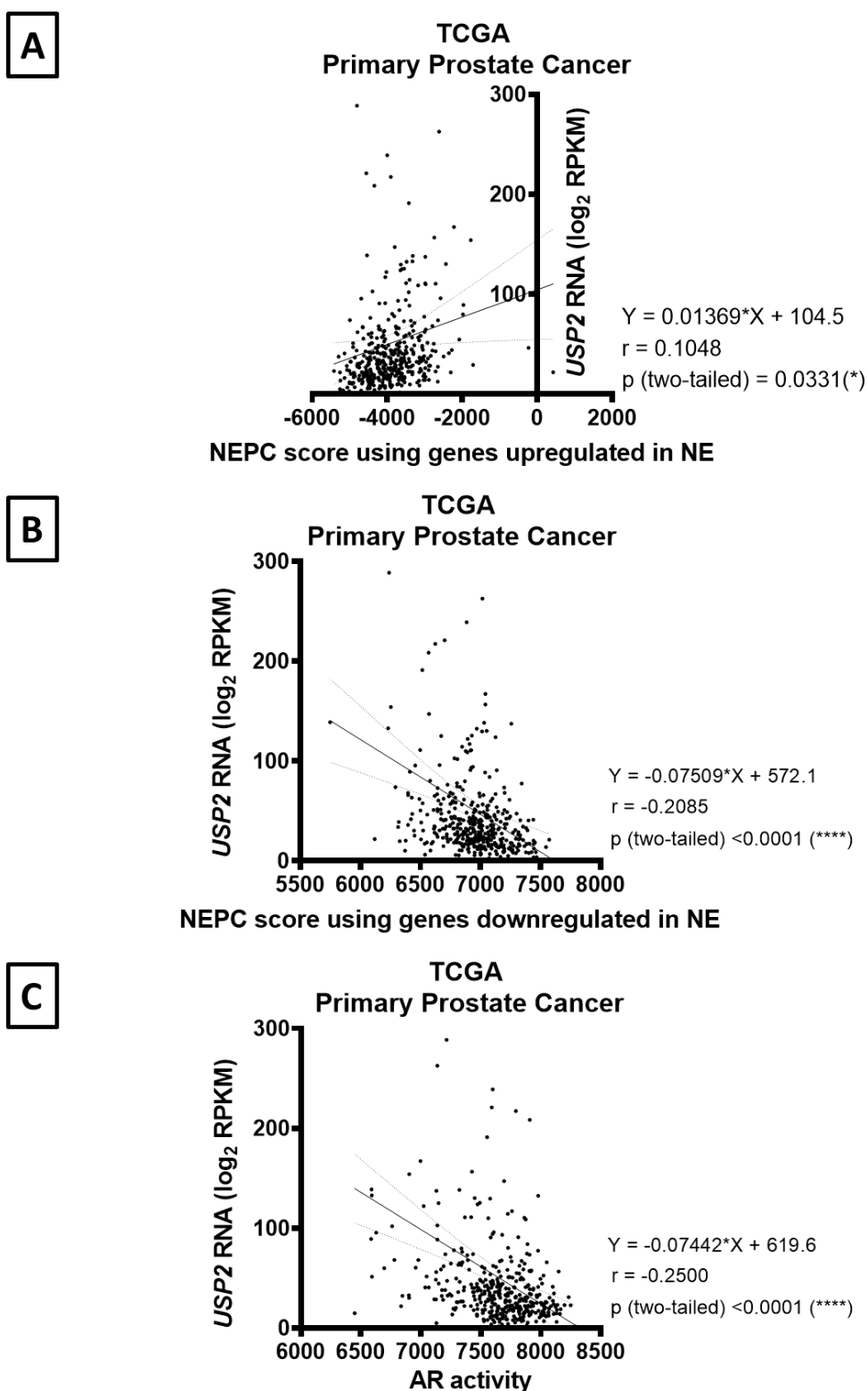


Figure 3.7. Increasing *USP2* expression directly correlated with increasing NEPC score and inversely correlated with increasing AR activity. (A) The NEPC score per patient was

calculated based on the expression of genes that were upregulated in neuroendocrine PCa using single sample Gene Set Enrichment Analysis (ssGSEA). (B) The NEPC score per patient was calculated based on the expression of genes that were downregulated in neuroendocrine PCa using single sample Gene Set Enrichment Analysis (ssGSEA). The lists of genes in (A) and (B) were curated by Beltran *et. al.* (2016). (C) Decreasing *USP2* expression correlated with increasing AR activity. AR activity was calculated using a list of canonical AR-regulated genes curated by Sowalsky *et. al.* (2018). Linear regressions were plotted to investigate the relationships between the y- and x-variables. The sample correlation coefficient (r) was also shown for each correlation and their p-values were calculated to investigate if their relationships were significant.

3.3.3 *USP2* is upregulated during the evolution to neuroendocrine prostate cancer.

Androgen-sensitive adenocarcinoma cells, such as LNCaP, can be induced into a neuroendocrine-like phenotype via trans-differentiation when grown in androgen-depleted conditions (Yuan et al., 2006, Zhang et al., 2018b, Juarranz et al., 2001, Shen et al., 1997, Sánchez et al., 2020, Fernandes et al., 2021). The growth of cells in androgen-depleted conditions mimic the microenvironment that prostate cancer cells are in when the patient is undergoing androgen deprivation therapy (ADT) (Crawford et al., 2019). As expected, there was significant upregulation of the well-established neuroendocrine marker *Synaptophysin* (*SYP*) when LNCaP cells were grown in androgen-depleted conditions (**Figure 3.8**). Importantly, *USP2a* expression was also significantly upregulated during this trans-differentiation process at all the time points tested (**Figure 3.8**). This data indicates that *USP2* is upregulated when PCa cells evolved into a neuroendocrine-like state.

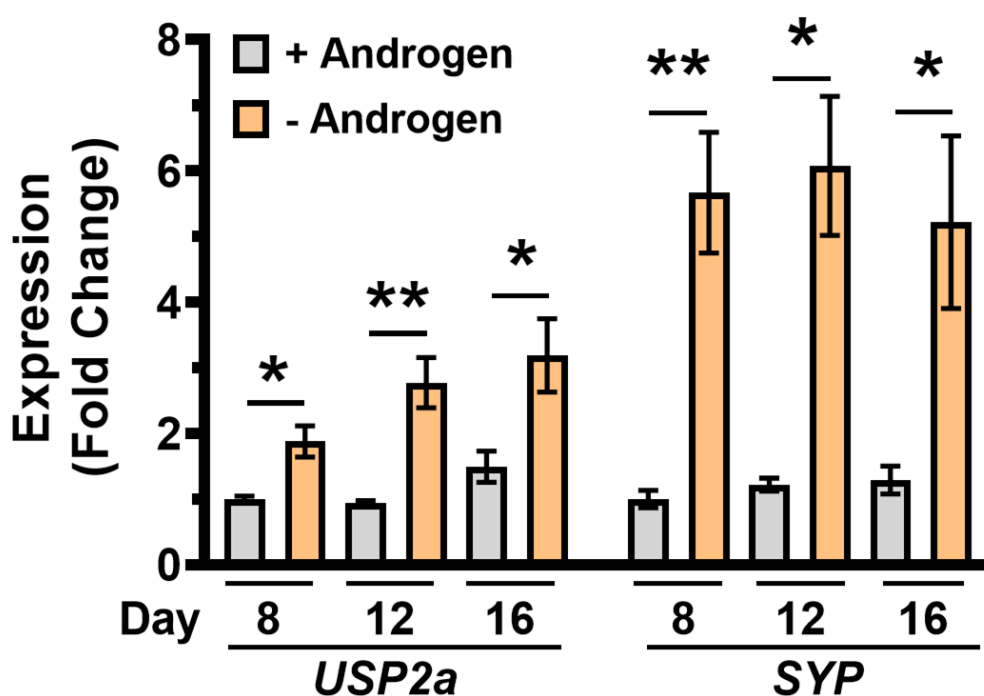
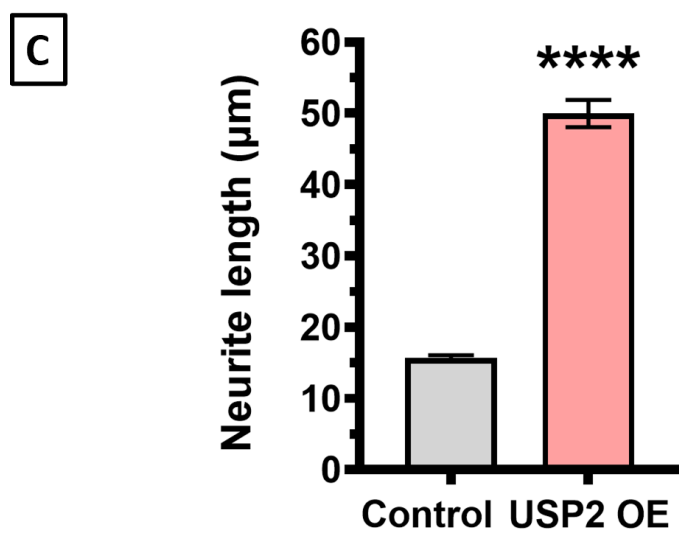
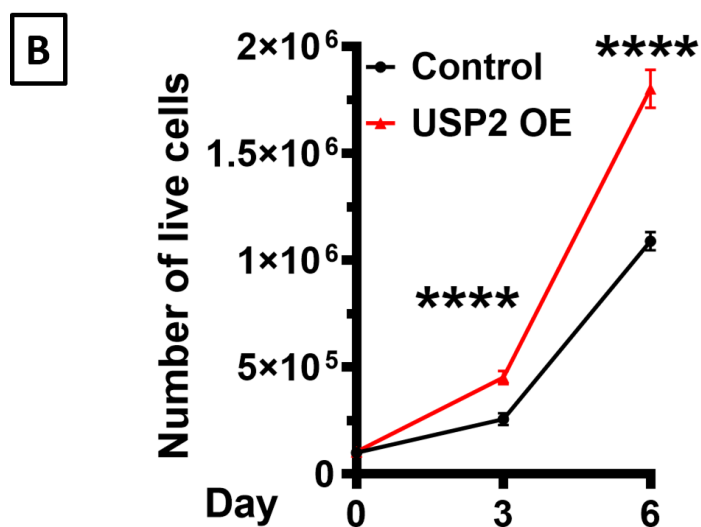
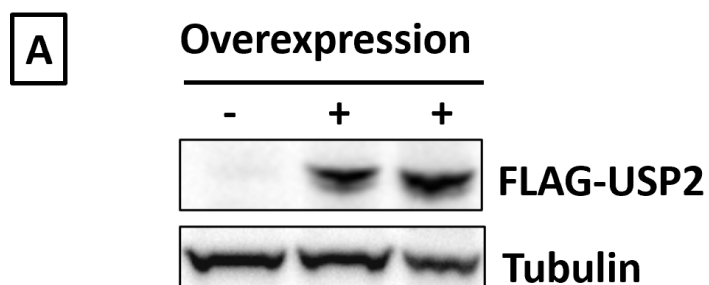


Figure 3.8. Increased *USP2a* expression is associated with neuroendocrine prostate cancer phenotype. The expression of *SYP* (a classic neuroendocrine marker) and *USP2a* increased when LNCaP cells were grown in androgen-deplete conditions, which induced the evolution of a neuroendocrine phenotype in-vitro. Statistical analysis was conducted via unpaired two-tailed student t-tests between androgen-replete and androgen-deplete conditions at each timepoint, p-values ≤ 0.05 (*); ≤ 0.01 (**). Mean \pm standard error mean (SEM) was shown, n=4.

3.3.4 Overexpressing USP2 induces a neuroendocrine phenotype.

To investigate if USP2 can drive the emergence of neuroendocrine-like PCa, a FLAG-tagged form of USP2 was over-expressed in adenocarcinoma LNCaP cells, a model earlier shown to have the lowest *USP2* expression (**Figure 3.3**). USP2 overexpression was confirmed by Western blotting with a FLAG-specific antibody (**Figure 3.9A**). LNCaP cells overexpressing USP2 (LNCaP-USP2-OE) exhibited a growth advantage in full serum conditions (**Figure 3.9B**). Neurites are projections from cancer cells that have been used to indicate a neuronal or neuroendocrine (NE) phenotype (Yuan et al., 2006, Shen et al., 1997, Sánchez et al., 2020). Interestingly, LNCaP-USP2-OE cells had longer neurites than control cells (**Figure 3.9C**), supporting the idea that USP2 could promote a NE phenotype. Additionally, overexpression of USP2 resulted in the induction of neuroendocrine differentiation and epithelial-to-mesenchymal transition as determined by the significant upregulation of the neuroendocrine marker *Enolase 2 (ENO2)* and mesenchymal marker *Vimentin (VIM)*, and the significant downregulation of the epithelial marker *Zonula occludens-1 (ZO-1)* (**Figure 3.10**). The NE marker *Synaptophysin (SYP)* exhibited modest upregulation in the USP2-OE cells, although its change in expression was not statistically significant ($p = 0.0695$). Although there was a modest upregulation of *SYP*, it appears to be biologically relevant. Collectively, these results demonstrate that USP2 can induce features of EMT and drive the acquirement of neuroendocrine features.



D

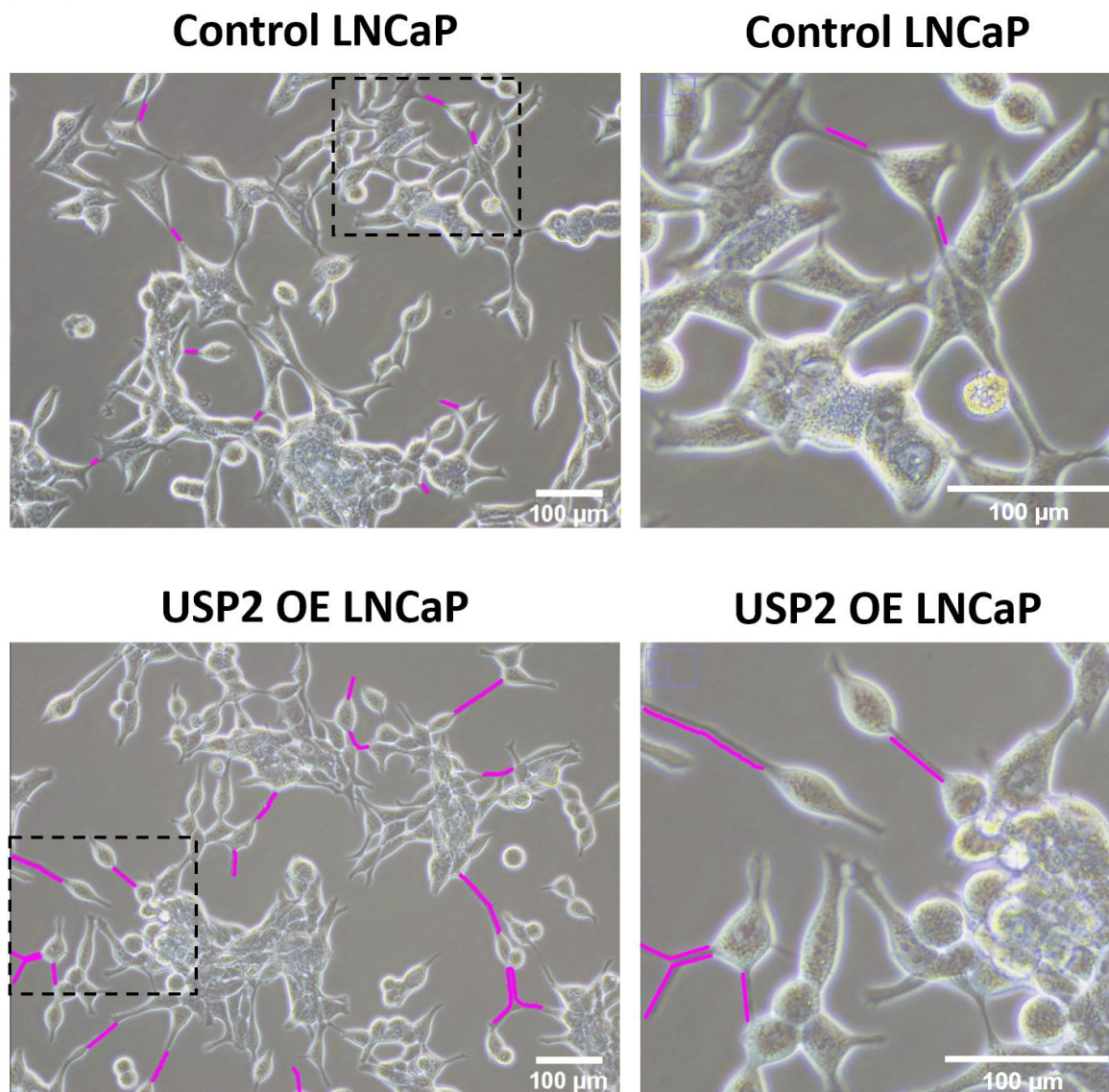


Figure 3.9. USP2 drives the development of the neuroendocrine-like phenotype. (A) LNCaP cells were transduced with lentiviruses to enable stable over-expression of FLAG-USP2 fusion protein or a control (neon fluorescent protein). (B) Overexpressing USP2 in LNCaP cells conferred a growth advantage in full serum. Cells were grown in full serum media under standard growth conditions and counted on day 3 and 6 of experiment. Live and dead cells were assessed via Trypan blue exclusion. Statistical analysis was conducted via unpaired One-Way ANOVA, p -value ≤ 0.0001 (****). Mean \pm standard deviation (S.D) from each group were shown, $n=3$. (C) USP2-OE LNCaP cells had longer neurites. At least 200 neurites per cell type

were measured using NeuronJ software in ImageJ. Mean \pm standard error mean (SEM) from each group were shown, n=3. Statistical analysis was conducted via unpaired two-tailed student t-test, p-value \leq 0.0001 (****). (D) Representative phase contrast images of control LNCaP cells overexpressing the neon transgene or USP2 were shown. Neurites were traced in magenta. Images were taken using the 20X objective lens.

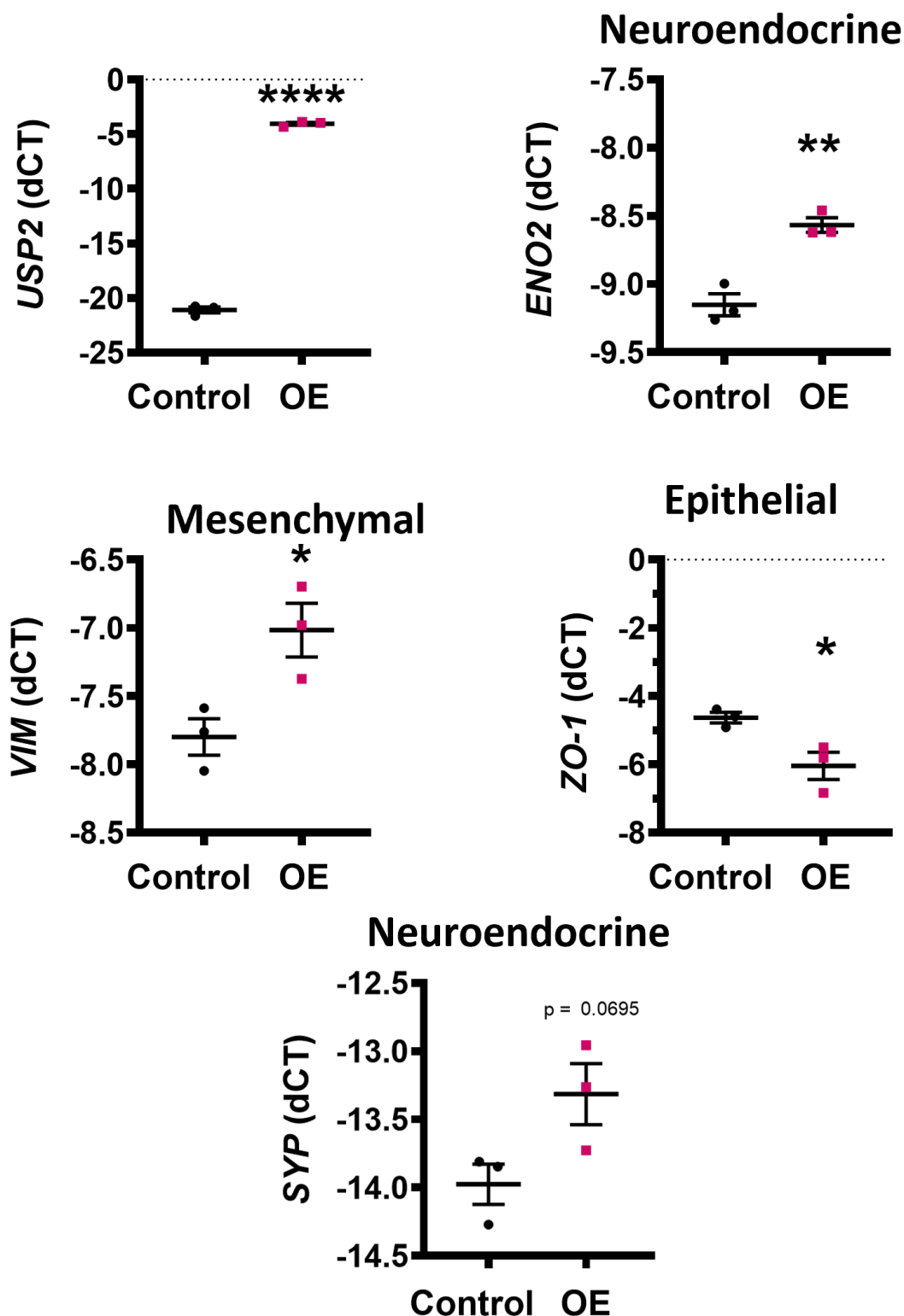


Figure 3.10. Elevated levels of USP2 expression in adenocarcinoma LNCaP induced lineage plasticity and induced the EMT pathway. The expressions of the well-established neuroendocrine-marker *Enolase 2* (*ENO2*), mesenchymal marker *Vimentin* (*VIM*), epithelial

marker *Zonula occludens-1* (*ZO 1*) and *Synaptophysin* (*SYP*) were measured in LNCaP cells overexpressing USP2 in full serum. Statistical analysis was conducted via unpaired two-tailed student t-test, p-values ≤ 0.05 (*); ≤ 0.01 (**); ≤ 0.001 (***) ; ≤ 0.0001 (****). The abbreviation “dCT” is delta CT.

3.3.5 Elevated levels of USP2 in adenocarcinoma LNCaP mediates resistance to AR-targeted therapy and chemotherapy.

The aggressive NEPC typically has a reduced dependence or even lost dependence on the AR signalling pathway, thereby acquiring resistance to AR-targeted therapies (Davies et al., 2020, Davies et al., 2021, Davies et al., 2018, Ku et al., 2019, Aggarwal et al., 2018, Beltran et al., 2016). Therefore, it is hypothesised that overexpression of USP2 and subsequent acquisition of NE features could alter the responsiveness of PCa cells to inhibitors of the AR signalling axis. Overexpression of USP2 conferred a growth advantage in the absence of androgens (**Figure 3.11A**). Importantly, LNCaP cells overexpressing USP2 were less sensitive to Enz-induced growth inhibition (**Figure 3.11B**). Collectively, these findings indicate the prostate cancer cells with elevated levels of USP2 could have a clinically relevant significance with respect to resistance to AR-targeted therapies.

Docetaxel is an approved therapy for patients with metastatic CRPC (Berthold et al., 2008, Tannock et al., 2004, James et al., 2016, Kyriakopoulos et al., 2018). However, chemotherapy is never curative; all tumours will eventually become resistant (Berthold et al., 2008, Tannock et al., 2004, James et al., 2016, Kyriakopoulos et al., 2018). To assess if PCa cells expressing high levels of USP2 are resistant to chemotherapies, LNCaP cells overexpressing USP2 were given docetaxel. Docetaxel binds to β -tubulins and promotes its assembly into microtubules, while simultaneously inhibiting its disassembly (Imran et al., 2020, Azarenko et al., 2014). This results in the stabilisation of microtubules and consequently the cell cycle is arrested, which eventually leads to cell death (Imran et al., 2020, Azarenko et al., 2014). LNCaP cells overexpressing USP2 exhibited increased survival compared to control cells (**Figure 3.12A**) and were protected from docetaxel-induced cell death (**Figure 3.12B**).

These results indicate that high expression of USP2 could mediate PCa cell resistance to chemotherapy by conferring longer survival. This phenomenon is posited to arise as a consequence of USP2's ability to drive the development of the neuroendocrine phenotype, which is resistant to chemotherapy (Davies et al., 2018, Beltran and Demichelis, 2021).

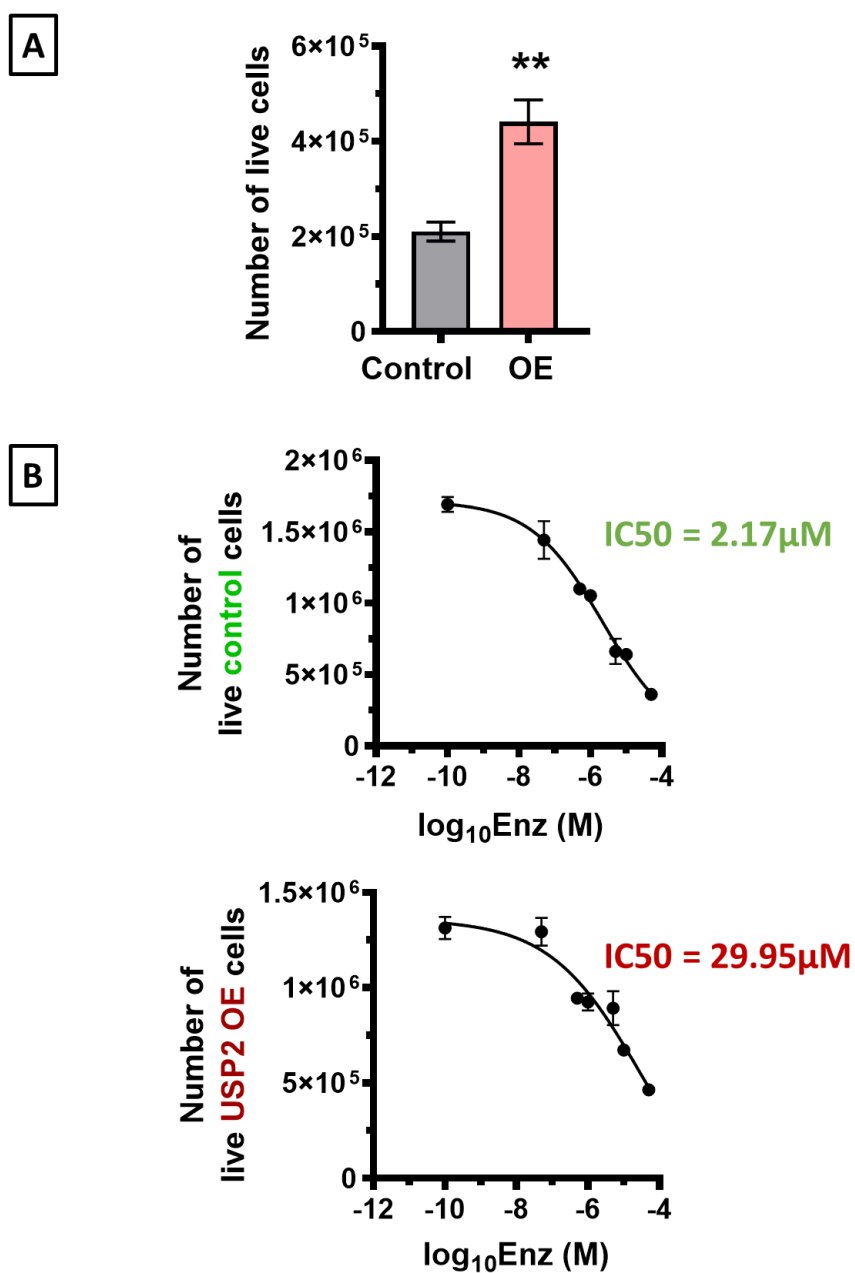


Figure 3.11. Overexpressing USP2 in LNCaP cells conferred growth advantage in androgen-depleted conditions and with enzalutamide treatment. (A) Equal numbers of control LNCaP cells (which over-express the neon fluorescent protein) or USP2 overexpressing (OE) LNCaP cells (200,000 cells/6-well) were grown in androgen-depleted media for 4 days, after which cells were counted. (B) Equal numbers of control and USP2 overexpressing (OE) cells were seeded in 6-well plates (250,000 cells/6-well) and left to grow for 24 hours, after which they were treated with indicated concentrations of enzalutamide for 3 days. For (A) and (B), the

number of live and dead cells were assessed via Trypan blue exclusion. IC50 values were calculated based on the number of live cells. Statistical analysis was conducted via unpaired two-tailed student t-test, p-values ≤ 0.01 (**). Mean \pm standard deviation (S.D) from each group were shown, n=3.

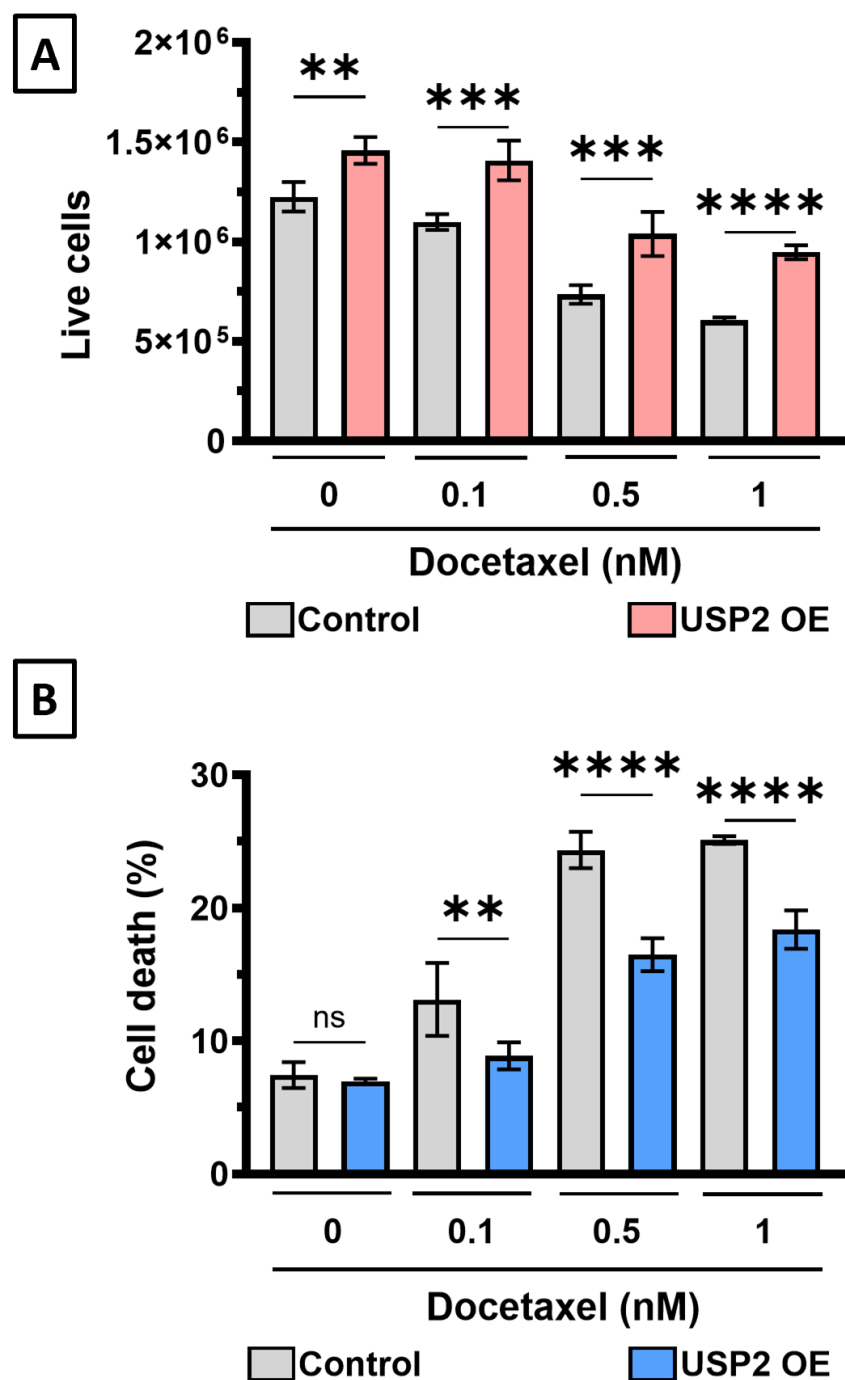


Figure 3.12. Elevated levels of USP2 in LNCaP cells confers survival advantage when treated with of the chemotherapeutic drug, Docetaxel. (A-B) Overexpressing USP2 in LNCaP cells resulted in enhanced growth (A) and reduced death (B) in response to Docetaxel. The number of live and dead cells were assessed via Trypan blue exclusion after 72 h. Statistical analysis was conducted using One-way ANOVA, p-value ≤ 0.01 (**); ≤ 0.001 (***) ; ≤ 0.0001 (****).

3.3.6 Aurora kinase A, Cyclin D1 and FAS appears to be stabilised by USP2 in adenocarcinoma LNCaP cells overexpressing USP2.

Several USP2 substrates have been identified in other types of cancers, including Cyclin D1 and Aurora kinase A (Kim et al., 2012, Shi et al., 2011). Cyclin D1 is an oncoprotein important in the proliferation of bladder cancer cells (Kim et al., 2012). AURKA is an important oncoprotein in mitosis, metastasis and the EMT pathway in bladder, pancreatic and breast cancer, and a key driver of neuroendocrine prostate cancer (Jeong et al., 2015, Shi et al., 2011, Beltran et al., 2019). AURKA also functions in the regulation of microtubule organisation during neurite extension in neurons (Mori et al., 2009). To ascertain whether Cyclin D1, Aurora kinase A and FAS are substrates of USP2 in prostate cancer, the expression levels of these proteins were investigated in LNCaP cells overexpressing USP2. Overexpression of USP2 resulted in an increase in Cyclin D1, Aurora kinase A and FAS expression in LNCaP cells (**Figure 3.13** and **Figure 3.14**). Since USP2 over-expression could mediate the acquisition of neuroendocrine features, we evaluated whether this was associated with a change in AR expression or activity. However, the expression of AR and its target gene encoding FKBP5 remained unchanged in the presence of USP2 overexpression in LNCaP cells (**Figure 3.14**). Collectively, these results suggest that Cyclin D1, AURKA and FAS are putative substrates of USP2 in prostate cancer cells.

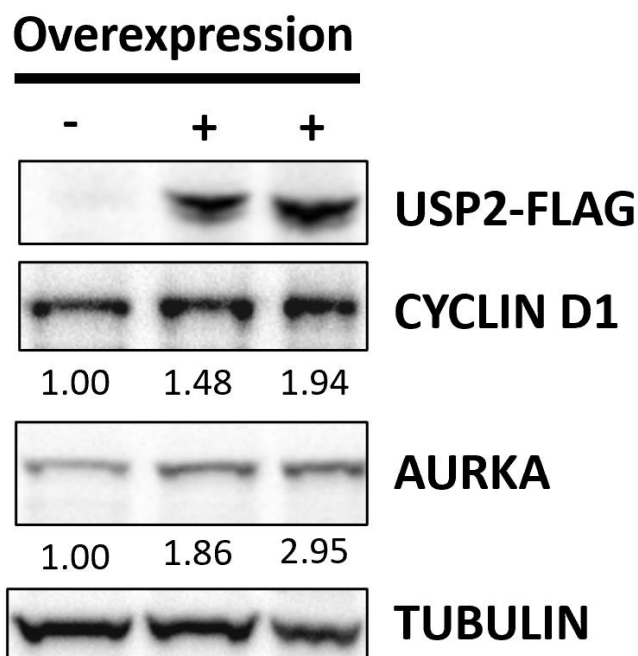


Figure 3.13. Overexpression of USP2 in LNCaP cells resulted in increased levels and stability of putative USP2 substrates in LNCaP cells, such as Cyclin D1 and Aurora A. Equal amounts of proteins per sample was loaded into each lane and the housekeeping protein, Tubulin, was shown as a loading control. (-) refers to control LNCaP cells overexpressing the neon transgene, while (+) refers to LNCaP cells overexpressing USP2. Bands were quantitated using Biorad Image software. The protein signals were normalised to the corresponding housekeeping genes and calculated as a fold change to control. Two biological replicates of USP2-OE LNCaP cells were shown.

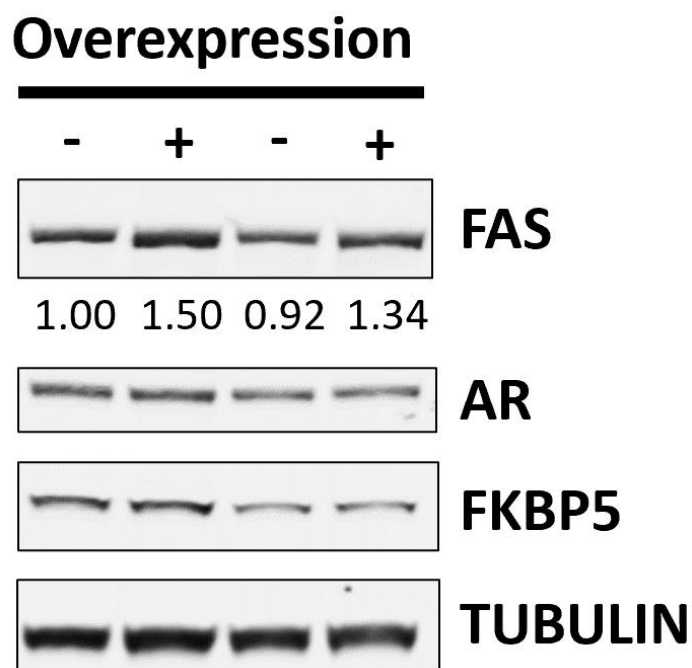


Figure 3.14. Constitutive overexpression of USP2 in LNCaP cells resulted in increased levels of putative substrate FAS, yet AR and FKBP5 levels remain unchanged. Equal amounts of proteins per sample was loaded into each lane and the housekeeping protein, Tubulin, was shown as a loading control. (-) refers to control LNCaP cells overexpressing the neon transgene, while (+) refers to LNCaP cells overexpressing USP2. Bands were quantitated using Biorad Image software. The protein signals were normalised to the corresponding housekeeping genes and calculated as a fold change to the first control. Two biological replicates of each cell type were shown.

3.3.7 USP2 expression is elevated in tumours with loss of PTEN, RB1 and P53

Mutations in tumour suppressor genes can result in induction of lineage plasticity in prostate tumours. Concurrent loss of TP53 and RB1 functions were present in 39% of metastatic castrate-resistant prostate adenocarcinomas and 74% of metastatic treatment emergent NEPC (Mu et al., 2017, Beltran et al., 2016). Mechanistically, concurrent loss of TP53 and RB1 strongly correlated with increased SOX2 expression, which suggested that active TP53 and RB1 inhibited its expression (Mu et al., 2017). Increased SOX2 expression was then able to induce lineage plasticity of prostate cancer cells, which resulted in the development of neuroendocrine PCa (Mu et al., 2017, Aparicio et al., 2016, Tan et al., 2014).

The phenomenon of lineage plasticity driven by tumour suppressors was corroborated by mouse models of PCa (Ku et al., 2017). Concurrent loss of RB1 and P53 in mouse prostate tumours (*Pten*^{null}) led to increased expression of EZH2 and SOX2, which induced a stem cell-like epigenetic environment and was associated with acquisition of a neuroendocrine phenotype (Ku et al., 2017). This observation was corroborated by other *in vitro* cell line studies (Kareta et al., 2015, Bohrer et al., 2010, Bracken et al., 2003, Hong et al., 2009). Tumours with loss of function mutations in the *Pten* and *Rb1* genes (*Pten*^{f/f}; *Rb1*^{f/f}) or in the *Pten*, *Rb1* and *Trp53* genes (*Pten*^{f/f}; *Rb1*^{f/f}; *Trp53*^{f/f}) also had reduced AR levels and sensitivity to enzalutamide (Ku et al., 2017). We examined transcriptomic data from these mouse models and found that *USP2* expression was significantly increased in these *Pten*^{f/f} *Rb1*^{f/f} tumours and *Pten*^{f/f} *Rb1*^{f/f} *Trp53*^{f/f} tumours (**Figure 3.15**). The results suggests that *USP2* is elevated in mouse tumours with deletions of these tumour suppressor genes. These results support the hypothesis that *USP2* is upregulated in neuroendocrine PCa.

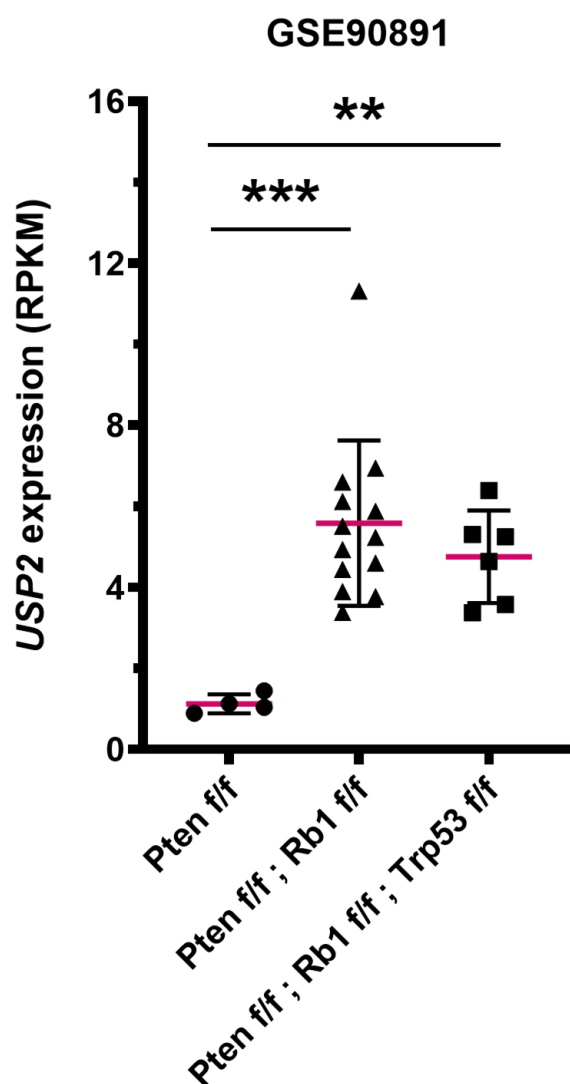


Figure 3.15. USP2 expression is the highest in prostate tumour models representing epithelial-neuroendocrine plasticity. Tumours were harvested from mouse models of prostate cancer with single, double, or triple loss of function mutations in the Pten, Rb1 and Trp53 genes. RNA-sequencing data is from GSE90891 (**Table 3.2**). Statistical analyses were conducted via unpaired One-Way ANOVA. P-values ≤ 0.01 (**); ≤ 0.001 (***). Mean \pm standard deviation (S.D) from each group were shown. The mean of each group is shown in red.

3.3.8 Lack of a suitable USP2 antibody hinders research on this factor

The lack of a specific and sensitive USP2 antibody is a major issue for research into this factor (Priolo et al., 2006, Graner et al., 2004). During this project, six different USP2 antibodies were examined, and none were able to detect endogenous USP2 or the FLAG-USP2 fusion protein that was expressed in LNCaP cells (**Table 3.3**). The majority of these antibodies detected many non-specific bands or no bands at the right size (**Figure 3.16, Figure 3.17** and **Table 3.3**). For example, the USP2 N-term (Abcepta) antibody, which in theory should be able to detect the USP2a isoform, was demonstrated to be unable to detect overexpression of Flag-tagged USP2a. The flag-tagged USP2a band detected by the flag primary antibody is also not at the same location as the band detected by the USP2 N-term (Abcepta) antibody, thereby validating that that USP2 antibody is not specific to USP2a. Collectively, this highlights the strong need for an USP2 antibody.

Table 3.3. Description of all USP2(a) antibodies being tested in this project.

USP2 Primary Antibodies	Evidence that the antibody is not specific
USP2 (Abcam AB66556) rabbit polyclonal	No band at the right size.
USP2 (Abcam AB168945) mouse polyclonal	One non-specific band at approximately the right size
USP2 (Thermofisher PA5-98234) rabbit polyclonal	Multiple non-specific bands at approximately the right size
USP2 C-term L523 (Abcepta AP2131c) rabbit polyclonal	2 bands were also seen at the approximately the 60kDa mark. There was also no band at the approximately 70kDa mark, as stipulated by manufacturer's protocol.
USP2 N-term (Abcepta AP2131a) rabbit polyclonal	Overexpression of flag tagged USP2a could not be detected.
USP2 (Proteintech 10392-1-AP) rabbit polyclonal	Multiple non-specific bands were detected. There was also no detection of flag tagged USP2a overexpression.

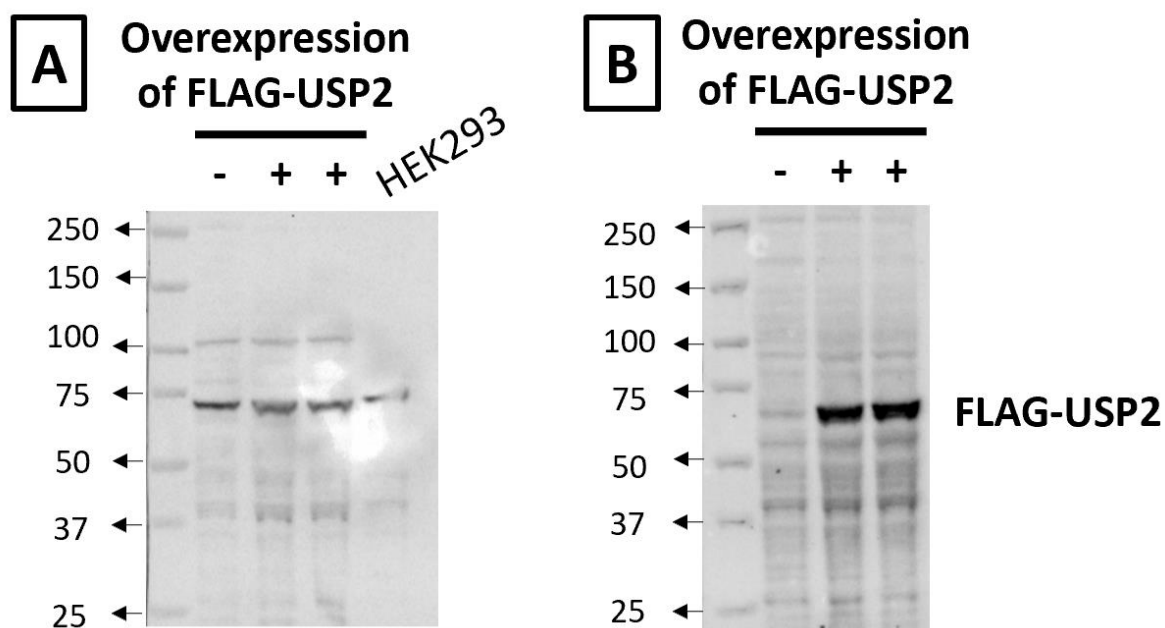


Figure 3.16. The USP2 N-term primary rabbit antibody (Abcepta) is not detecting USP2a. Each lane contained 40µg of protein. (A) Blot was incubated with 1:1000 dilution of the USP2 N-term (Abcepta catalogue number AP2131a) or (B) Flag antibody overnight shaking at 4°C, before being probed with 1:1000 dilution of secondary anti-rabbit antibody for 1 hour at 25°C and then imaged. (-) refers to control LNCaP cells overexpressing the neon transgene, while (+) refers to LNCaP cells overexpressing USP2. HEK293 lysate was run as a positive control, in accordance with manufacturer's protocol. The prominent band in blot (A) is unlikely to be USP2a since it is not at the right size.

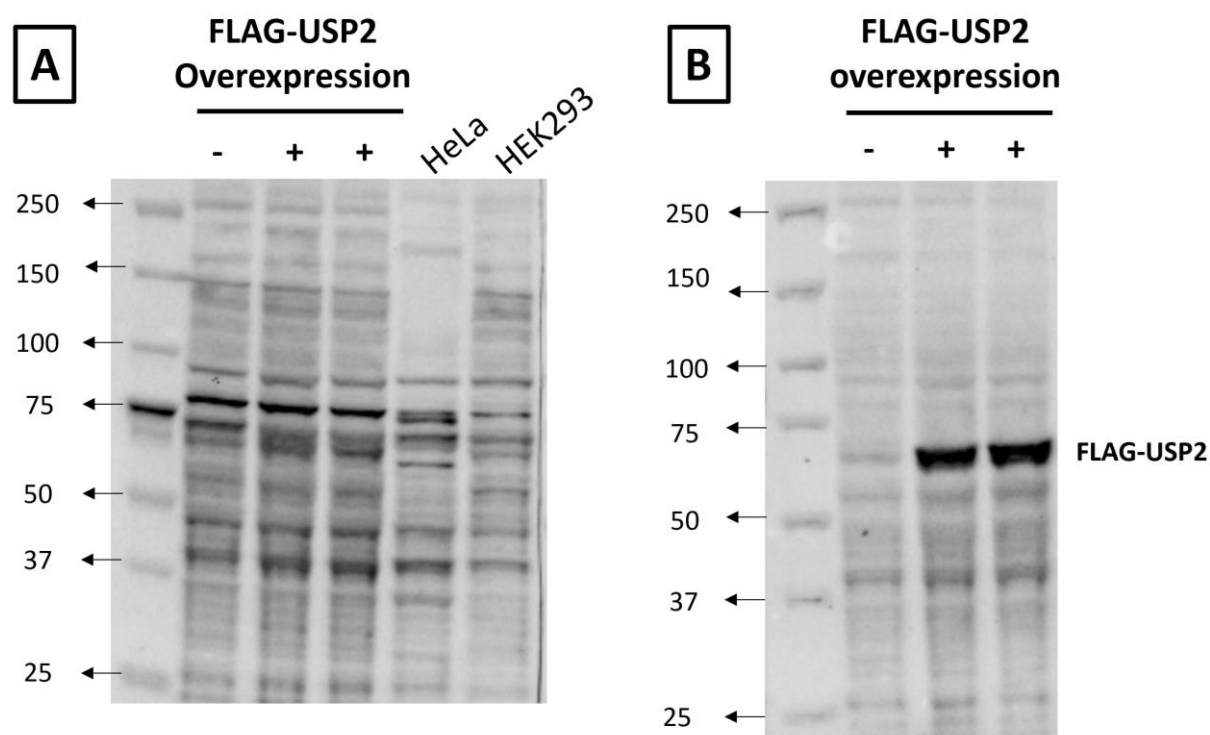


Figure 3.17. The USP2 (Proteintech 10392-1-AP) primary rabbit antibody (Abcepta) is not detecting USP2a. Each lane contained 40 μ g of protein. Blot (A) was incubated with 1:1000 dilution of the USP2 (Proteintech 10392-1-AP) or (B) Flag antibody overnight shaking at 4°C, before being probed with 1:1000 dilution of secondary anti-rabbit antibody for 1 hour at 25°C and then imaged. HeLa and HEK293 lysates were run as a positive control, in accordance with manufacturer’s protocol.

3.4 Discussion

The mechanism(s) that mediate prostate cancer cell resistance to enzalutamide is poorly understood (Labrecque et al., 2019, Aggarwal et al., 2018, Davies et al., 2021). This chapter demonstrates that the *ubiquitin specific protease 2 (USP2)* is an AR-repressed gene and elevated in NEPC and that it can directly drive the neuroendocrine phenotype and resistance to standard-of-care therapies. To the best of our knowledge, this is the first ubiquitin specific protease that is reported to drive the neuroendocrine phenotype. These findings are significant because they establish USP2 as a novel therapeutic target.

USP2 was found to be repressed by the androgen receptor, perhaps in a manner mediated by direct AR binding to the USP2 promoter. There appears to be a common theme that genes directly repressed by AR become important drivers of prostate cancer progression and therapy resistance when they are de-repressed after the AR pathway is inhibited (Davies et al., 2021, Kregel et al., 2013, Mu et al., 2017, Bishop et al., 2017), with key examples being *EZH2*, *SOX2*, *BRN2* and *FOXA2* (Davies et al., 2021, Kregel et al., 2013, Mu et al., 2017, Bishop et al., 2017, Han et al., 2022). Overall, these findings are important because they suggest that *USP2* is a novel AR-repressed gene that gets de-repressed with enzalutamide and potentially drives cancer progression.

We modelled elevated USP2 expression in LNCaP cells, a classic AR-driven adenocarcinoma model. Overexpression of USP2 resulted in the induction of a neuronal-like morphology, upregulated classic neuroendocrine markers and conferred a growth advantage in AR-targeted therapies. These results are in concordance with typical treatment-induced clinical neuroendocrine PCa, whereby prostatic adenocarcinoma become androgen-independent and acquire a neuroendocrine phenotype during long-term ADT (Bluemn et al.,

2017, Aggarwal et al., 2018, Abida et al., 2019). Our findings suggest that USP2 is not only a marker of NEPC but can also drive the development of the neuroendocrine phenotype.

Prostate adenocarcinoma LNCaP cells overexpressing USP2 conferred resistance to chemotherapeutic drug, docetaxel. This finding can be clinically important as docetaxel is the standard first-line chemotherapy for patients with CRPC and NEPC (Aparicio et al., 2016, Lavoie et al., 2019, Tannock et al., 2004, Petrylak et al., 2004, Culine et al., 2007). Therefore, the results provide additional rationale for USP2 as an appealing target for patients with neuroendocrine prostate cancer.

We believe that USP2 promotes therapy resistant and NE phenotypes by stabilising key oncoproteins, such as Aurora kinase A and Cyclin D1. Aurora kinase A has been shown to be an important regulator of mitosis, metastasis and the EMT pathway, and driver of NEPC (Wan et al., 2008, D'Assoro et al., 2014, Willems et al., 2018, Beltran et al., 2019, Beltran et al., 2011). Furthermore, inhibiting AURKA in NEPC with underlying retinoblastoma 1 (RB1) loss, which is a common alteration, was synthetically lethal and resulted in a drastic growth retardation of NEPC xenografts (Gong et al., 2019, Oser et al., 2019). Meanwhile, high Cyclin D1 expression in tumours was associated with poor prognosis and invasion (Ahmed et al., 2020, Fusté et al., 2016, Gansauge et al., 1997). Overall, the results imply that through USP2 stabilisation of Aurora kinase A and Cyclin D1, USP2 can regulate castration-resistance and the switch to a neuroendocrine phenotype. Our results also suggest that USP2 can be mediating therapy resistance through stabilisation of other novel substrates that have yet to be identified. This provides additional rationale for targeting USP2 in NEPC.

LNCaP cells overexpressing USP2 upregulated the mesenchymal marker *Vimentin* (*VIM*) and downregulated the epithelial marker *Zonula occludens-1* (*ZO-1*), indicating that

elevated levels of USP2 expression is also associated with features of EMT. Induction of EMT has been associated with castration resistance (Sun et al., 2012, Davies et al., 2020, Pak et al., 2019, Crowley et al., 2021). Furthermore, Sun *et. al.* (2012) demonstrated that the EMT pathway is induced in the prostate tissues and in the LuCAP35 xenografts of castrated mice and in patients given androgen deprivation therapy. Given that the molecular mechanisms driving neuroendocrine lineage plasticity and epithelial are similar, it is not surprising that EMT-associated transcription factors have been implicated in NEPC (Davies et al., 2020, Davies et al., 2018) (refer to **Chapter 1 Section 1.9.2**). TWIST is an important transcription factor in the EMT pathway that has also been implicated in the development of both mesenchymal and neuroendocrine phenotypes (Davies et al., 2018, Davies et al., 2020). TWIST was also identified as a substrate of USP2 in bladder cancer (Liu et al., 2022, He et al., 2019). We propose that investigating TWIST as a substrate of USP2 in prostate cancer is warranted.

Interestingly, other USPs including USP10, USP12, USP22 and USP26 have been reported to be positively regulated by the androgen receptor and increased expression of these USPs resulted in increased AR stability and activity (Takayama et al., 2018, Draker et al., 2011, Burska et al., 2013, McClurg et al., 2015, Schrecengost et al., 2014, Dirac and Bernards, 2010). Our findings contrast with these earlier studies and suggest that AR is inhibiting the expression of USP2. Our findings also identified that USP2 do not stabilise AR, thereby implying that there is no feedback loop between USP2 and AR.

The major findings of this chapter are corroborated by similar findings in non-prostatic cancer studies. Several studies have reported that USP2 deubiquitylates its substrates, such as AURKA and Cyclin D1, and stabilises them (Shi et al., 2011, Liu et al., 2013, Kim et al., 2012,

Davis et al., 2016, Zhang et al., 2020a). Through USP2 stabilisation of its substrates, USP2 can modulate cancer cell survival, cell proliferation and the EMT pathway (Silva et al., 2009, Zhang et al., 2020a, He et al., 2019, Stevenson et al., 2007, Shi et al., 2011, Kim et al., 2012, Liu et al., 2013) (refer to **Chapter 1 Section 1.15**). Overall, our major findings further strengthen a role for USP2 as a key player in cancer progression.

Importantly, our findings are significant because we have identified USP2 as a potential driver of the neuroendocrine phenotype. ADT is the current standard first-line treatment for patients with prostate cancer (Huggins and Hodges, 1972). However, there is an apparent increase in the incidence rates of NEPC in recent years (Scher et al., 2012, Fizazi et al., 2012). This may be partially explained by the introduction of more potent inhibitors during ADT and before or after chemotherapy (Scher et al., 2012, Fizazi et al., 2012). Therefore, there exists a need to identify other drivers of therapy resistance, such as USP2.

The first strength of this study is that USP2 was investigated in a range of prostate cancer cell models representing different stages of the disease. The second strength of this study is that USP2 was also investigated in large clinical or prostate cancer xenograft cohorts. Another strength of this study is that USP2 was also investigated in patient tumours that were treated with enzalutamide short-term. Collectively, the use of prostate cancer cell line and clinical models enables our research on USP2 to be clinically relevant.

We acknowledged that a limitation of this study is the lack of a specific USP2 antibody. This has limited our efforts in investigating endogenous USP2 protein levels in prostate cancer cell lines and tumours. The lack of a specific USP2 antibody could explain the discrepancies observed in our study with two studies that initially showed USP2 to be upregulated by AR activated with androgens (Graner et al., 2004, Priolo et al., 2006). To partially overcome this

antibody issue, we generated cells overexpressing a FLAG-tagged form of USP2. This model enabled us to investigate the biological outcomes of USP2 after manipulation of its expression in prostate cancer. An alternative approach could have been a quantitative Tandem mass spectrometry (MS/MS) method specifically designed for detection of USP2 (Liebler and Zimmerman, 2013).

In summary, this present first-in-field study identifies USP2 as a novel AR-repressed gene that is a driver of therapy resistance and development of the neuroendocrine phenotype when it is de-repressed after the AR pathway is inhibited. Overall, our findings rationalise USP2 as an attractive novel therapeutic target to treat NEPC, which lacks effective therapies.

Chapter 4:

**Targeting USP2 in advanced prostate
cancer suppresses tumour growth and
de-stabilises its onco-substrates**

4 Targeting USP2 in advanced prostate cancer suppresses tumour growth and destabilises its onco-substrates

4.1 Introduction

In Chapter 3, we demonstrated that USP2 directly drives the emergence of neuroendocrine prostate cancer. In this chapter, we aimed to evaluate the utility of targeting USP2 as a novel therapeutic strategy for this aggressive, therapy-resistant disease subtype castration-resistant prostate cancer (CRPC).

Patients with treatment emergent NEPC are often treated with systemic therapy regimens used for small cell lung cancer (SCLC) (Beltran and Demichelis, 2021, Davies et al., 2020, Yamada and Beltran, 2021). NEPC shares several clinical, pathologic and molecular similarities with SCLC (Berchuck et al., 2021, Davies et al., 2020, Epstein et al., 2014, Wang et al., 2021b). Both cancer types tend to be initially responsive to platinum-based chemotherapy with response rates of ~60-66.6% (Sella et al., 2000, Papandreou et al., 2002). The National Comprehensive Cancer Network (NCCN) has now recommended that patients with NEPC be treated with a combination of cabazitaxel with carboplatin, which is a platinum-based chemotherapeutic drug (Aparicio et al., 2013).

However, new therapies for treatment emergent NEPC are still urgently required. Platinum-based chemotherapy fails to be effective long-term for these patients (Davies et al., 2020, Beltran and Demichelis, 2021, Wang et al., 2021b). Current therapies are ineffective in

patients with castrate resistant prostate cancer and neuroendocrine prostate cancer. Therefore, there exists a need for identification of new drivers of NEPC to develop new targeted treatment. This chapter will investigate USP2 as a new druggable target in therapy-resistant prostate cancer.

4.2 Materials and Methods

4.2.1 Transient RNA interference

The siRNAs targeting the human *USP2a* RNA, which is the canonical transcript transcribed from the *USP2* gene, were designed and purchased from Millennium Science. These siRNAs were reverse transfected at a final concentration of 20 nM using Lipofectamine RNAiMax (Invitrogen Cat. No. 13778150) according to manufacturer's protocol.

The sequences of the siRNAs targeting human *USP2* mRNA are:

5'-UAGUUCUCCAGGUAGUCGA-3' and 5'-AUUCUGUGUAGCGCUUCAG-3'

The siRNA used for the negative control is the "AllStars Negative Control" siRNA (20nmol from Qiagen, Catalogue# 1027281).

4.2.2 Trypan blue cell viability assays

Cell viability in response to *USP2* knockdown was assessed using Trypan blue assays. Triplicate wells of prostate cancer cells were reverse transfected using RNAiMAX Lipofectamine (Invitrogen Cat# 13778150) in accordance with manufacturer's instructions. 250,000 MR42D cells/well or 150 000 PC3 cells/well were transfected with 20nM of either the siRNAs targeting the human *USP2a* transcript or the negative control siRNA at the point of seeding. Live and dead cells were manually counted using a hemacytometer after 72 hours of transfection. Using a hemacytometer, cell viability was determined by the exclusion of Trypan blue in live cells.

Cell viability in response to ML364, Docetaxel or Alisertib was assessed using Trypan blue assays. Prostate cancer cells, such as MR42D, PC3 and LNCaP, were seeded at the appropriate densities on Day “-2” such that cells in the vehicle treatments will reach 80% confluence on day of harvest. All drug treatments were for 72 hours, except for IC50 assays where PC3 cells were treated with ML364 for 48 hours.

4.2.3 Cell viability assays using an Incucyte

Cell viability was also measured using an Incucyte platform. Dead cells were stained with 100 μ M SytoxGreen Invitrogen (Catalogue #S7020), which was prepared by diluting a 5 mM stock in RPMI. The nuclei of live cells were stained with a 1 in 2000 dilution of Nuclight Rapid Red dye (Sartorius Catalogue #EBS-9500-4717). The percentage of confluence or amount of red signal was used to measure growth of cells.

4.2.4 AnnexinV-PE and 7AAD flow cytometry

MR42D cells in 6-well plates were collected in 1X binding buffer. Cells were stained with 1 μ L 7-AAD (Invitrogen Cat# A1310) and 2 μ L AnnexinV-PE (BD Pharmingen Cat# 556421) in 1x binding buffer as described in (Gillis et al., 2021). Samples were then analysed using the CytoFlex-S flow cytometry machine and CytExpert software.

4.2.5 Orthotopic xenograft model

Male NOD/SCID/IL2rynull (NSG) mice received intraprostatic injections of 1×10^6 PC3 cells overexpressing luciferase (PC3-luciferase) in 10 μ L of PBS. These mice were given daily

intraperitoneal injections of 30mg/kg ML364 (or vehicle control). D-Luciferin (potassium salt from Perkin Elmer) solution was injected weekly into these mice at 100mg/kg to image the growth of the intraprostatic-grafted PC3-luciferase cells over time. Bioluminescence is reported as the average of detected photons per second from the region of interest. At the end of the experiment, tumours were excised, and half were snap frozen while the other half was formalin fixed and paraffin embedded. All animal procedures were approved by the SAHMRI Animal Ethics Committee (approval number SAM-21-042) in accordance with the guidelines of the National Health and Medical Research Council of Australia (NHMRC).

4.3 Results

4.3.1 Pharmacological inhibition of USP2 reduced cell viability and increased cell apoptosis of neuroendocrine-like prostate cancer cells

We first evaluated a pharmacological small molecule inhibitor of USP2, ML364 (Davis et al., 2016) in several prostate cancer cell lines. ML364 was recently characterised to be a reversible inhibitor of USP2 (Davis et al., 2016). The specificity of ML364 was demonstrated using a Kinomescan assay, which showed that it did not bind to 102 other kinases, including Aurora A/B and cyclin dependent kinases (CDK2, 3, 4, 5, 7, 8, 9 and 19) (Davis et al., 2016).

The three cell lines (MR42D, PC3 and LNCaP) represent the different prostate cancer phenotypes observed in the clinic with regards to their aggressive and metastatic nature (Aggarwal et al., 2018, Labrecque et al., 2019, Davies et al., 2021) (**Table 2.3**). MR42D is an AR-positive LNCaP derivative that is resistant to enzalutamide (Bishop et al., 2017, Davies et al., 2020); it is PSA-negative and has reduced expression of other canonical AR-regulated genes (Bishop et al., 2017, Davies et al., 2020, Davies et al., 2021) and is considered to be a model that represents partial transition from an epithelial to a neuroendocrine phenotype (Davies et al., 2021, Chaves et al., 2021, Nolan et al., 2015). Meanwhile, PC3 is regarded as more neuroendocrine-like PCa than MR42D (Tai et al., 2011, Zhang et al., 2011, Uysal-Onganer et al., 2010). Both models express neuroendocrine markers such as chromogranin A (CGA), neuron specific enolase (NSE), neural cell adhesion molecules (NCAM1), ENO2 and SYP (Bishop et al., 2017, Davies et al., 2021). Treatment of the three PCa cell lines with ML364

significantly reduced cell viability and increased cell death in a dose-dependent manner (**Figure 4.1**). The representative half-maximal inhibitory concentrations (IC₅₀) of ML364 calculated in MR42D, PC3 and LNCaP were 1.611 μ M, 1.894 μ M and 3.302 μ M respectively (**Figure 4.1**). Based on the IC₅₀ calculations, the results suggested that MR42D and PC3 cells were more sensitive to USP2 inhibition than LNCaP cells. These findings were corroborated by orthogonal cell growth/death assays using an Incucyte system (**Figure 4.2**). Moreover, there was significant induction of cell death when neuroendocrine-like MR42D and PC3 cells were treated with ML364 concentrations greater than 5 μ M. In contrast, concentrations greater than 10 μ M of ML364 were required to significantly induce cell death in LNCaP cells (**Figure 4.1** and **Figure 4.2**). Therefore, we focussed our attention on the neuroendocrine-like prostate cancer models.

ML364 caused apoptosis of PCa cells, as demonstrated by staining of cells with 7AAD and AnnexinV-PE (**Figure 4.3**). A dose dependent increase in percentage of apoptotic cells was observed in MR42D treated with ML364 (**Figure 4.3**). However, we cannot rule out that ML364 causes other types of cell death including autophagy, necrosis, ferroptosis and necroptosis (Green and Llambi, 2015, Strasser and Vaux, 2020).

**Androgen insensitive / androgen independent,
neuroendocrine-like**

**Androgen responsive,
luminal adenocarcinoma**

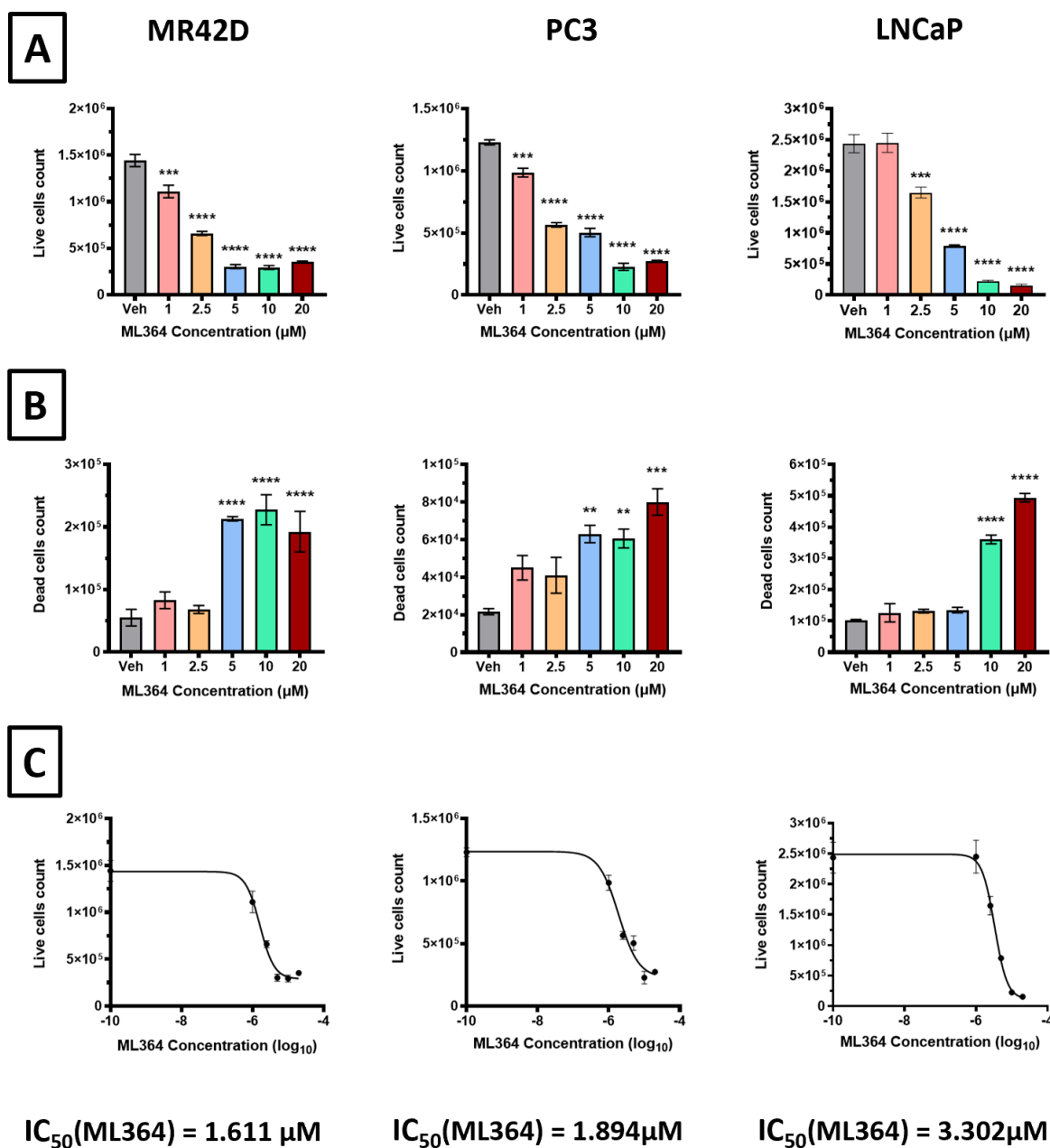


Figure 4.1. Pharmacological inhibition of USP2 with ML364 as a potential treatment for aggressive prostate cancer. (A, B) Pharmacological inhibition of USP2 by the drug ML364 resulted in reduced cell viability (A) and increased cell death (B) of three prostate cancer (Pca) cell lines as assessed using Trypan blue exclusion assays. The Pca cell lines tested were enzalutamide-resistant MR42D, AR-negative PC3 and the androgen-dependent LNCaP cells

cultured in full serum media. (C) The half maximal inhibitor concentration of ML364 in each cell line was also calculated. Mean \pm standard deviation (S.D) from each group of three independent replicates were shown, $n = 3$. The representative IC50s and cell viability data from two biological replicates are shown.

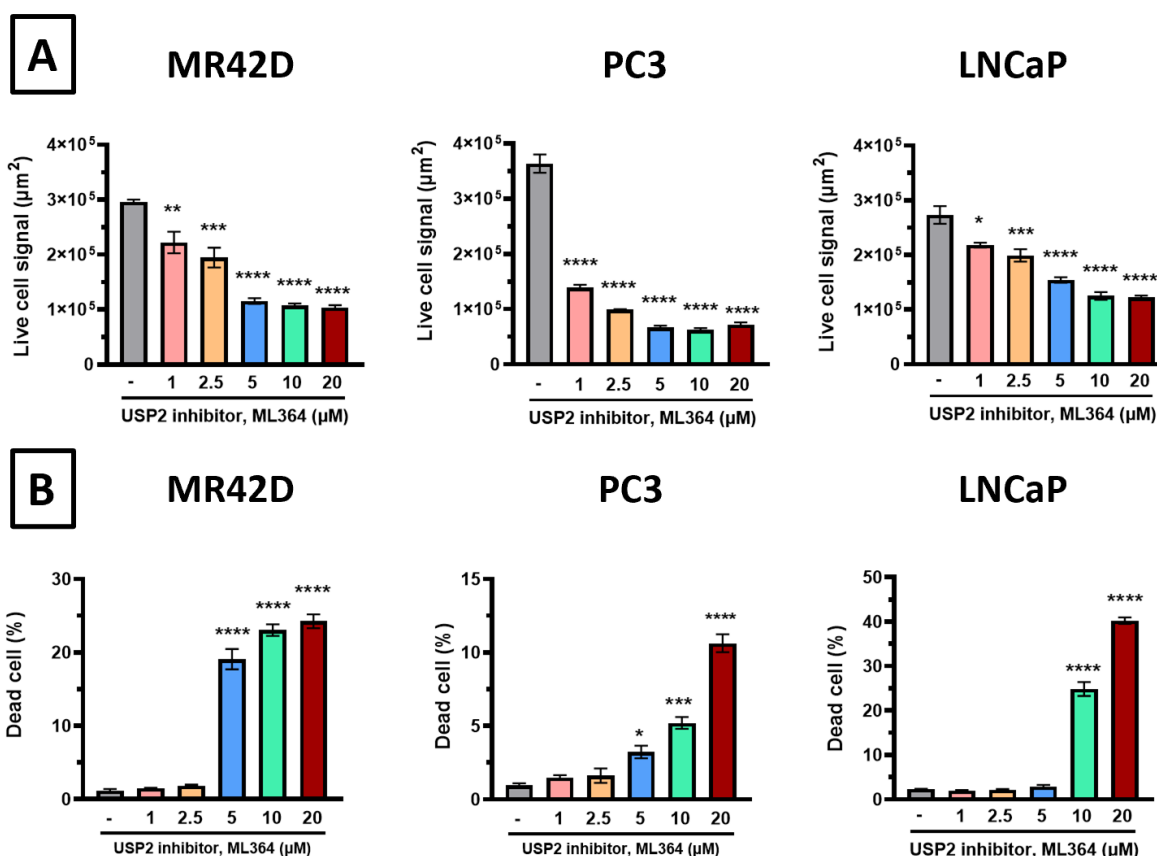


Figure 4.2. The USP2 inhibitor, ML364, reduced cell viability and induced cell death in several prostate cancer cell lines in a dose dependent manner. (A) Cell death induced by ML364 was measured over time by Sytox Green (B) Live cell signals in the experiments were detected by Nuclight RFP over time and represented as a confluence area mask. Decrease in confluence area correlated with decrease in percentage of live cells. Statistical analysis was conducted via unpaired One-Way ANOVA, p-values ≤ 0.05 (*); ≤ 0.01 (**); ≤ 0.001 (***) ; < 0.0001 (****). Mean \pm standard deviation (S.D) from each group of three independent replicates were shown, $n = 3$.

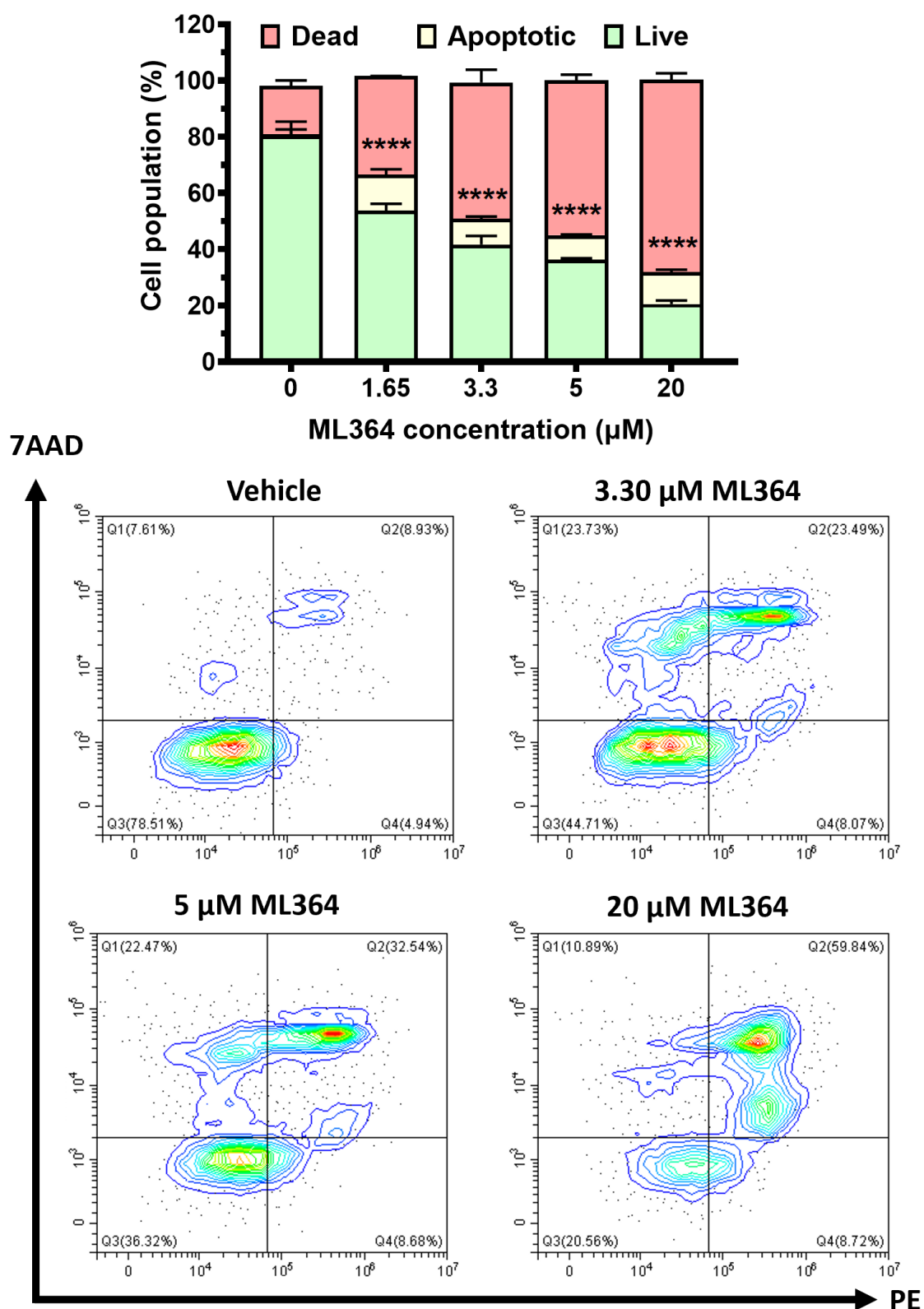


Figure 4.3. The USP2 inhibitor, ML364, induces cell apoptosis when neuroendocrine-like MR42D cells were treated with increasing concentrations of ML364. Statistical analysis was

conducted via unpaired One-Way ANOVA, p-values ≤ 0.05 (*); ≤ 0.01 (**); < 0.0001 (****). Mean \pm standard deviation (S.D) from each group of three independent replicates were shown, n = 3.

4.3.2 Knockdown of USP2 inhibits growth and induced death of PCa cells.

Given the utility of inhibiting USP2 with the pharmacological drug, ML364, we next evaluated siRNAs as an alternative method to reduce USP2 activity. To identify if inhibiting USP2 in neuroendocrine-like prostate cancer (PCa) cells reduces cell viability, USP2 was knocked down using siRNAs in androgen-insensitive MR42D and AR-negative PC3 cell line models (**Figure 4.4**). In view of this, knockdown of USP2 mRNA with two highly effective siRNAs (**Figure 4.4A**) significantly reduced cell viability (**Figure 4.4B**) and increased cell death (**Figure 4.4C**) in both neuroendocrine-like PCa cell lines. These results suggest that USP2 is important for the growth and survival of PCa cells.

Notably, both pharmacological (**Figure 4.1**, **Figure 4.2** and **Figure 4.3**) and genetic (**Figure 4.4**) inhibition of USP2 elicited the same phenotype effect. These observations provide evidence that both the siRNAs and ML364 are acting on target i.e. by inhibiting/suppressing USP2. Moreover, they provide further rationale for targeting USP2 using ML364 as a novel therapy for NEPC.

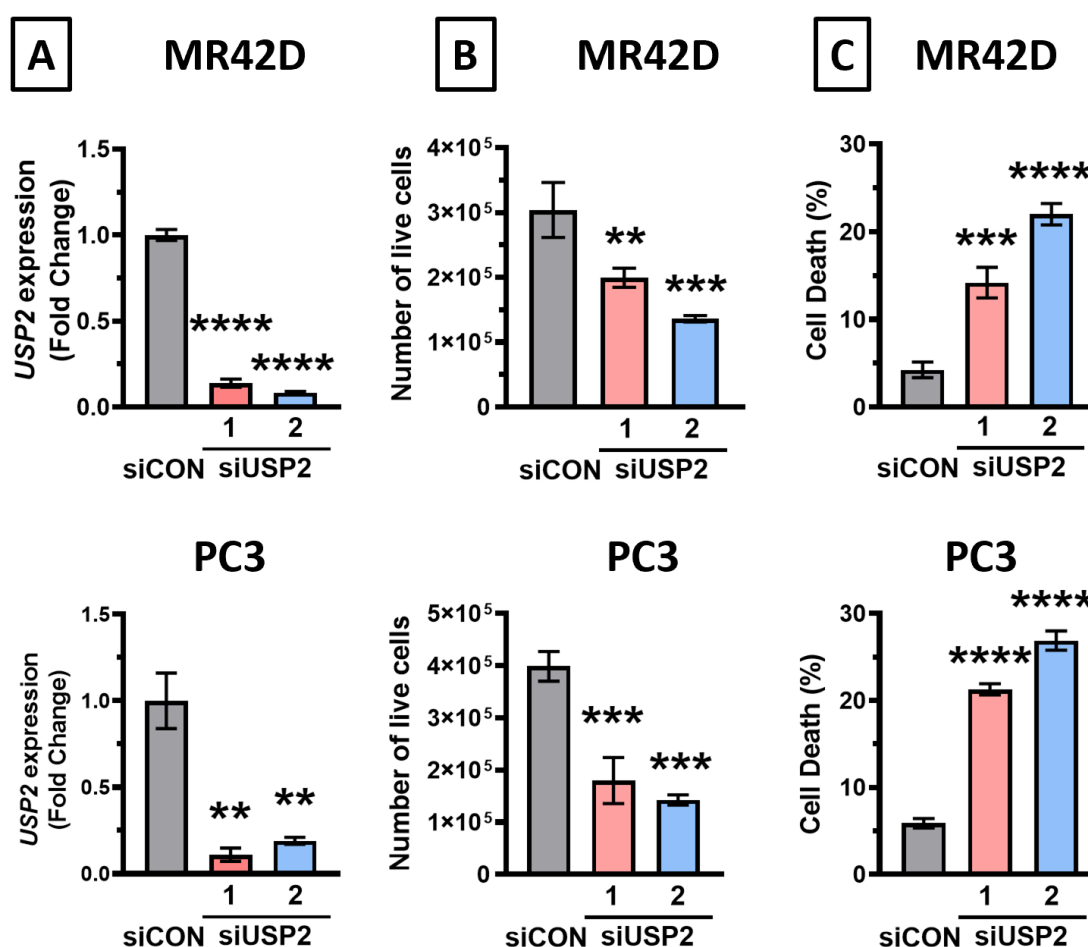


Figure 4.4. Genetic manipulation of USP2a resulted in reduced cell viability and increased cell death of neuroendocrine-like prostate cancer cells. (A) Knockdown of the *USP2a* mRNA by two different siUSP2s in the androgen-insensitive MR42D cells and AR-null PC3 cells was successful. mRNA values were represented as a fold change of the scrambled control (siCON). (B) Knocking down USP2a resulted in a decrease in number of live cells, as determined by Trypan blue assay. (C) Knocking down USP2a resulted in increase in percentage of cell death, as determined by Trypan blue assay. Cell death was calculated as a percentage of the number of dead cells over the total number of cells. For A-C, statistical analysis was conducted via unpaired One-Way ANOVA, p-values ≤ 0.01 (**); ≤ 0.001 (***) ; ≤ 0.0001 (****). Mean \pm standard deviation (S.D) from each group of three independent replicates were shown, n = 3.

4.3.3 *In vivo* activity of a small molecule inhibitor of USP2, ML364

Given the impressive efficacy of ML364 *in vitro*, we next evaluated this USP2 inhibitor *in vivo*. More specifically, PC3-luciferase xenografts were growth orthotopically (i.e. within the prostate) of immunodeficient NSG mice. Treatment of the mice with ML364 resulted in significant retardation of PC3-luciferase tumour growth (**Figure 4.5A**). Additionally, the ML364 treatment did not result in any significant change in the weights of mice (**Figure 4.5B**), suggesting that it did not cause any major toxicity.

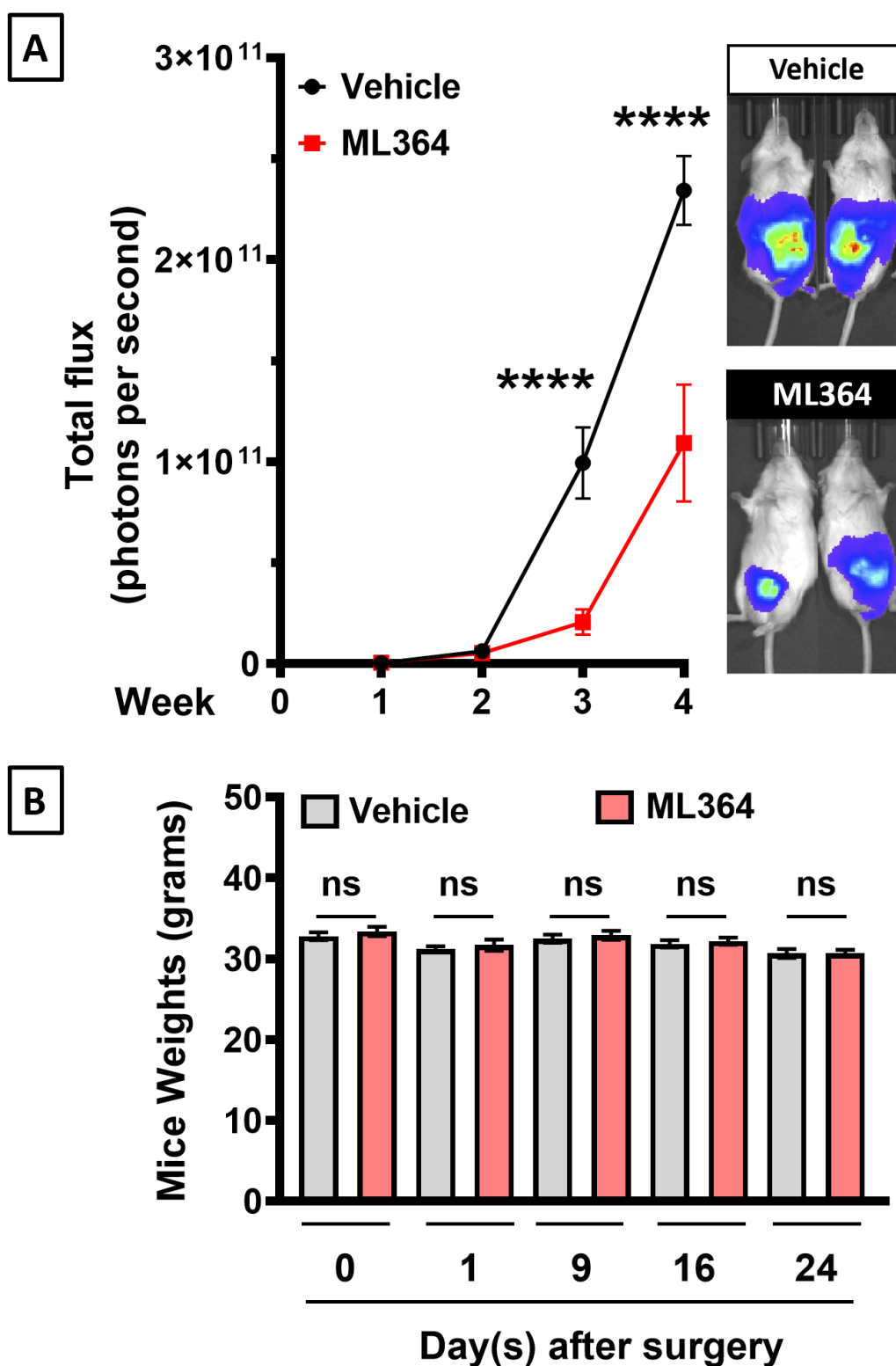


Figure 4.5. A small molecule inhibitor of USP2, ML364, significantly reduced growth of neuroendocrine-like tumours in an orthotopic PC3-luciferase xenograft model. (A) Growth of PC3-luciferase tumours over time in response to treatment. Mice were given

intraperitoneal injections of 30mg/kg ML364 (or vehicle control) daily. Imaging and analysis of the luminescence for each mouse was conducted using the IVIS Spectrum in vivo Imaging System (by PerkinElmer). Bioluminescence of the PC3-luciferase tumours were measured in photons per second. Two representative images from each group were presented. (B) The ML364 treatment did not induce any significant weight loss when compared to mice given the vehicle treatment. Statistical analysis conducted via One Way ANOVA, p-values < 0.0001 (****); > 0.05 (not significant, ns). Mean \pm standard error mean (SEM) from each group were shown, $n \geq 6$ per group.

4.3.4 Aurora kinase A, Cyclin D1 and FAS may be putative substrates of USP2 in prostate cancer.

As described in Chapter 1, USP2 stabilises many oncoproteins in prostate cancer and other cancer types. In particular, we were interested in Aurora kinase A, Cyclin D1 and fatty acid synthase (FAS), since these are known substrates of USP2 in other cancer types and our own results demonstrated increased levels of these proteins when USP2 was over-expressed in LNCaP cells.

To verify that targeting USP2 influences the levels of Aurora kinase A and Cyclin D1, we undertook Western blotting. Knockdown of USP2 in neuroendocrine-like PCa cells, such as MR42D and PC3, resulted in a drastic decrease in AURKA expression (**Figure 4.6**). Similarly, when USP2 was pharmacologically inhibited by a small molecule USP2 inhibitor ML364, the expression of AURORA A, CYCIN D1 and FAS were greatly reduced in a dose dependent manner (**Figure 4.7A**). Reduction in expression of these putative USP2 substrates began as early as 24 hours of ML364 treatment (**Figure 4.7B**).

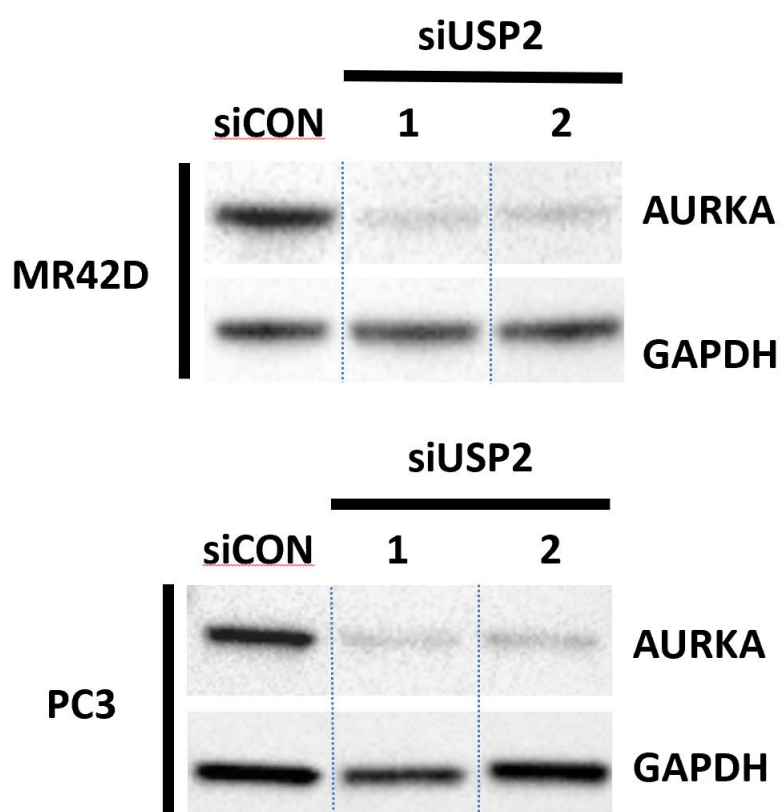
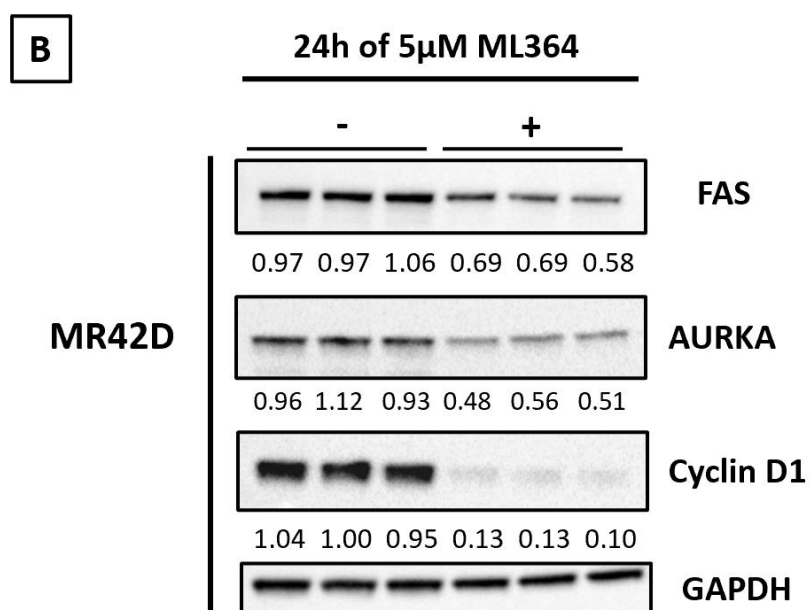
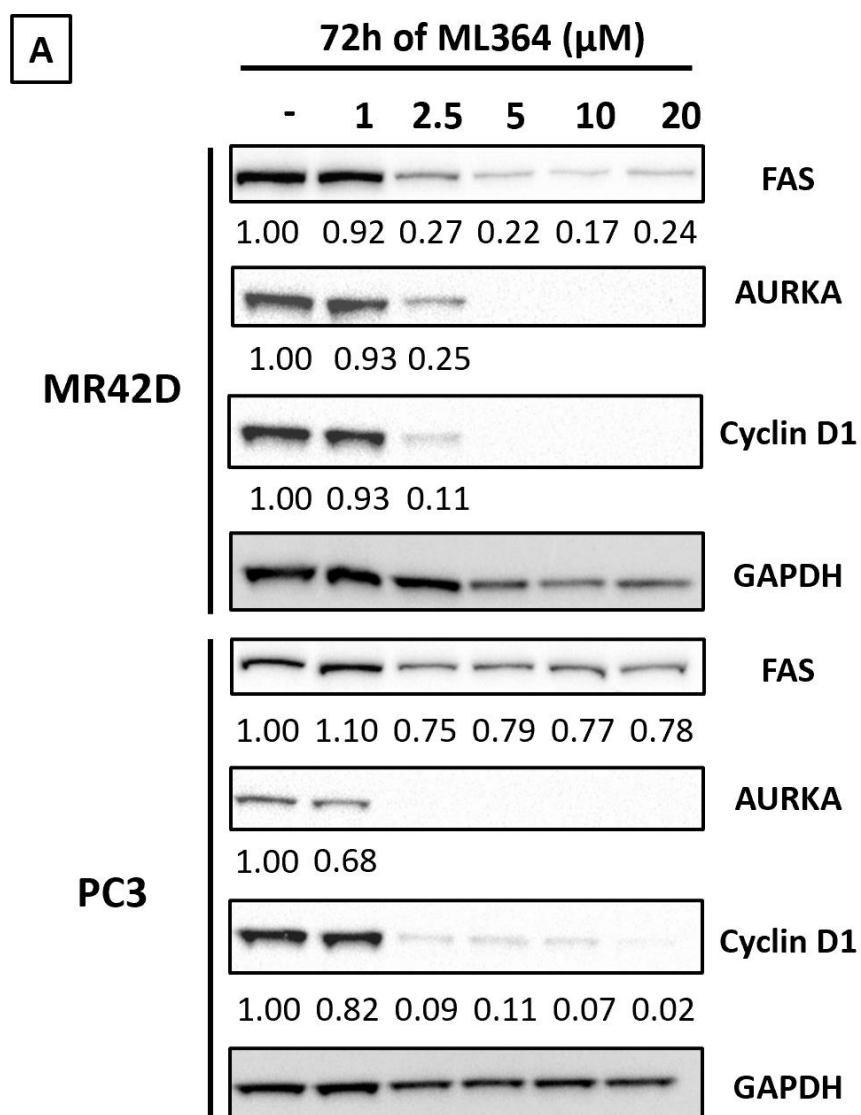


Figure 4.6. Knocking down of USP2 resulted in decreased protein levels of Aurora kinase A in the androgen-insensitive MR42D and AR-null PC3 cells. Cells were transiently transfected with two distinct siRNAs targeting *USP2* for 72 hours. Equal amounts of proteins per sample was loaded per lane and the housekeeping protein, GAPDH, is shown as a loading control.



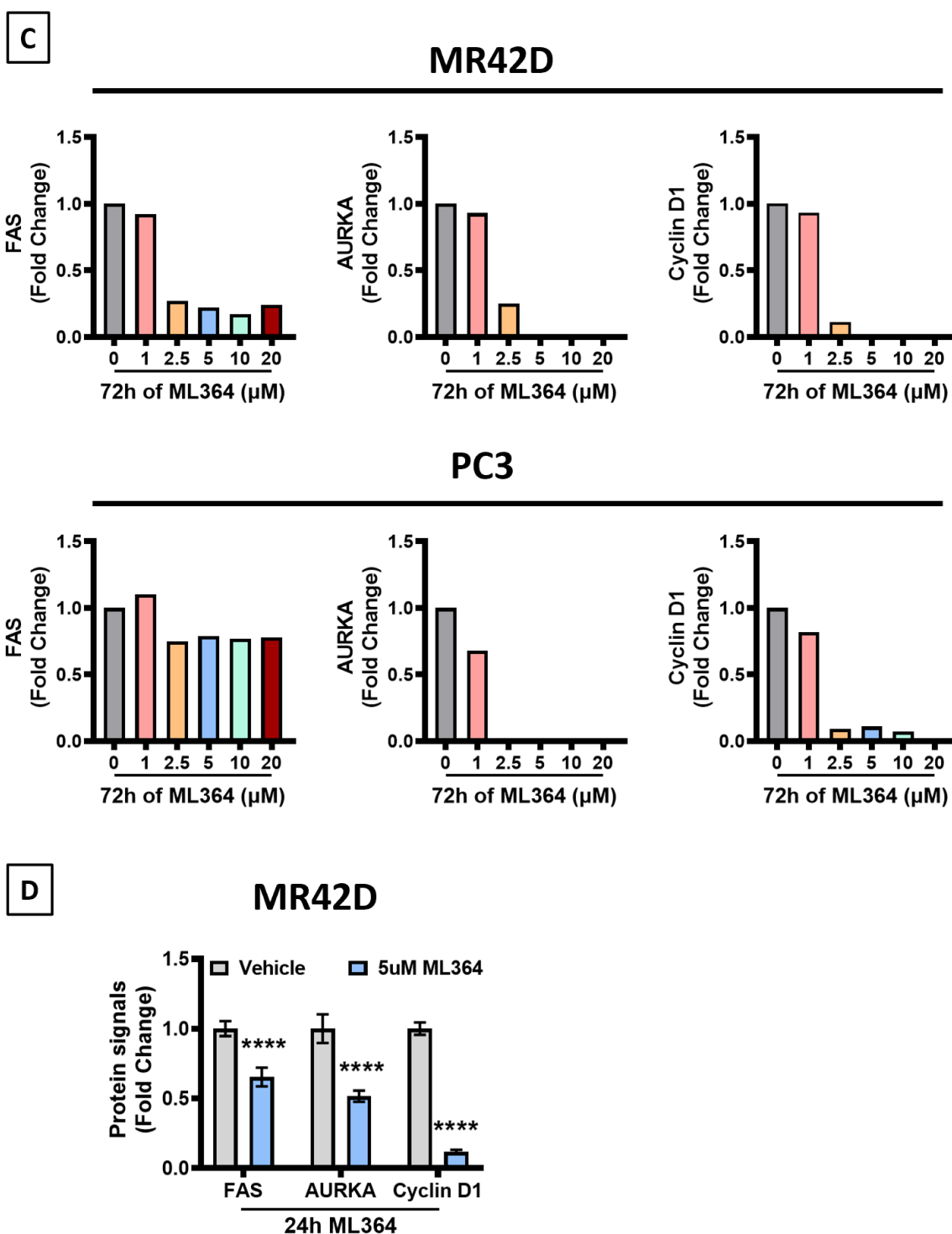


Figure 4.7. Inhibition of USP2 reduced the protein levels of FAS, Aurora kinase A and Cyclin D1. (A&C) FAS, Cyclin D1 and Aurora kinase A expression levels were reduced when neuroendocrine-like PCa cells were treated with different concentrations of ML364 for 72 hours. Quantitation of protein signals was conducted by measuring the intensity of the

protein bands in ImageLab. The intensity of each protein band was then normalised to the corresponding GAPDH and then calculated as a ratio to the control. (B&D) The kinetics of USP2 inhibition in MR42D cells by ML364 began after 24 hours of 5 μ M ML364 treatment. Equal amounts of proteins per sample was loaded into each lane and the housekeeping protein, GAPDH, was shown as a loading control. Quantitation of protein signals was conducted by measuring the intensity of the protein bands in ImageLab. The intensity of each protein band was then normalised to the corresponding tubulin.

4.3.5 LNCaP cells expressing elevated levels of USP2 were more sensitive to Aurora A inhibition.

Given the importance of USP2 for maintaining Aurora kinase A protein levels (**Figure 4.6** and **Figure 4.7**), we postulated that cells with high expression of USP2 – and hence stabilisation of Aurora kinase A – might be more sensitive to an Aurora A kinase inhibitor. To test this hypothesis *in vitro*, LNCaP cells stably overexpressing USP2, which exhibit acquisition of NEPC features and increased levels of Aurora kinase A (see Chapter 3), were treated with Alisertib. Alisertib is a specific Aurora kinase A inhibitor that has been tested in a clinical trial for patients with NEPC (Beltran et al., 2019). LNCaP cells overexpressing USP2 were more sensitive to Alisertib than control cells, both in terms of cell growth (**Figure 4.8**) and death (**Figure 4.8**). This suggests that USP2-OE LNCaP cells developed a heightened sensitivity to the Aurora kinase inhibitor, Alisertib.

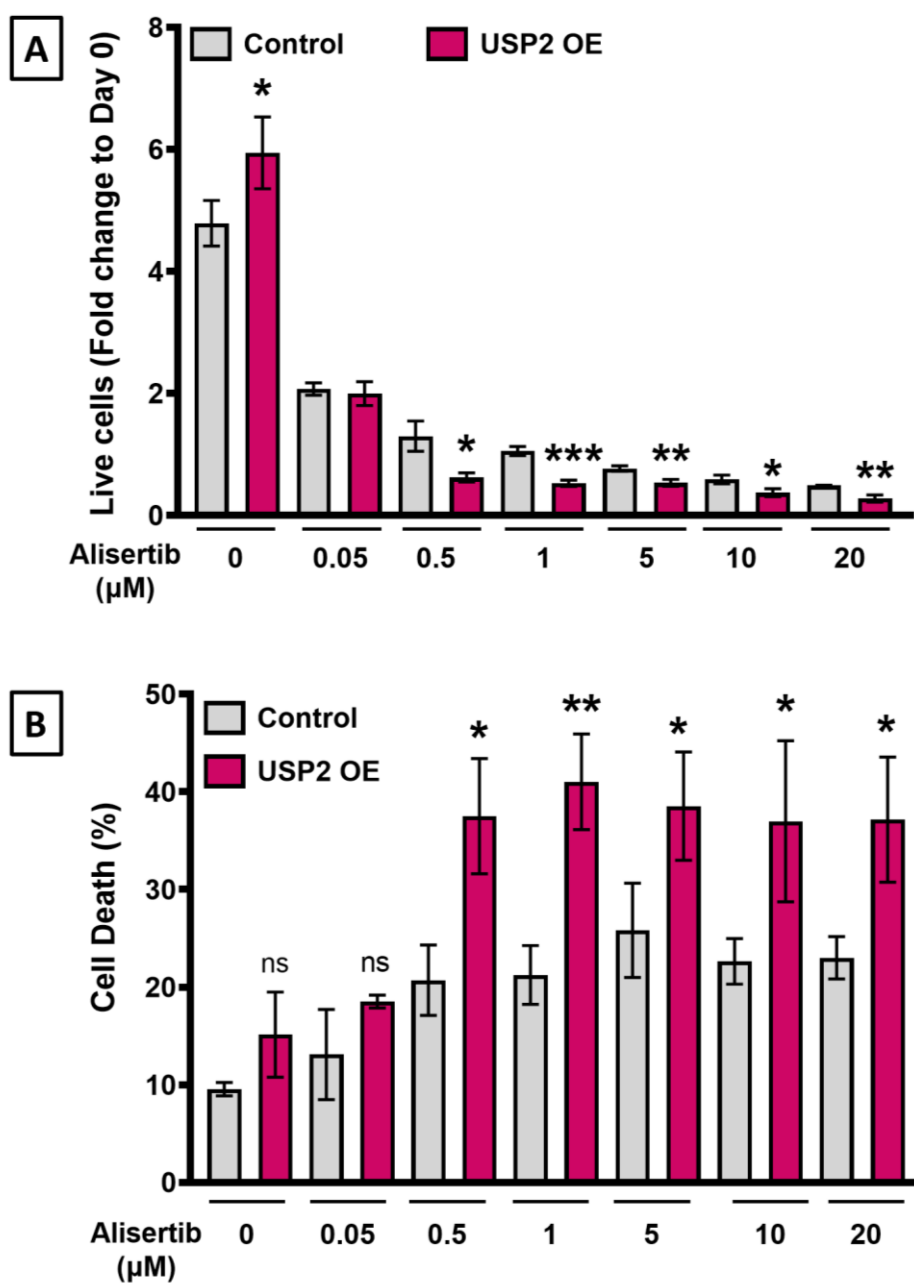


Figure 4.8. Overexpressing USP2 in LNCaP sensitises cells to Aurora kinase A inhibition by the small molecule inhibitor, called Alisertib. (A) When treated with Alisertib, LNCaP cells overexpressing USP2 had a lower number of live cells than control, which is measured as a fold change to Day 0 count of live cells. (B) LNCaP cells overexpressing USP2 experienced greater cell death than control cells, when treated with Alisertib. The number of live and dead cells were counted via hemacytometer and live cells excluded Trypan blue. Fold change of live cells was calculated as a ratio of the number of live cells on Day 3 to the average number of

live cells on Day 0. Cell death was calculated as the percentage of dead cells over the total number of live and dead cells. Statistical analyses were conducted via unpaired t-tests between control and LNCaP cells overexpressing USP2, p-values ≤ 0.05 (*); ≤ 0.01 (**); ≤ 0.001 (***); > 0.05 (not significant). Mean \pm standard deviation (S.D) from each group of three independent replicates were shown, $n = 3$.

4.4 Discussion

Current AR-targeted strategies inevitably result in the development of CRPC (Aggarwal et al., 2018, Davies et al., 2020). One mechanism of resistance to AR-targeted therapies is the acquisition of an AR-independent, neuroendocrine-like phenotype (Smith et al., 2018a, Smith et al., 2015, Wong et al., 2008, Ben-Porath et al., 2008, Davies et al., 2021, Aggarwal et al., 2018). Using a range of prostate cancer cell lines and prostate tumours that model different stages of the disease, this chapter builds on the key findings of Chapter 3 and provides more evidence that USP2 is a potential therapeutic target in NEPC.

Genetic and pharmaceutical inhibition of USP2 significantly reduced cell viability of a diverse range of prostate cancer cell lines. Supporting our hypothesis, the data suggest that the two NEPC-like models used in this study, MR42D and PC3, were more sensitive than LNCaP to USP2 inhibition. Additionally, this is the first study that demonstrated a significant reduction of tumour growth in an orthotopic xenograft model of neuroendocrine-like prostate cancer when USP2 was pharmacologically inhibited using a small molecule inhibitor of USP2, ML364. Our major finding is consistent with two previous studies of aggressive solid tumour models (He et al., 2019, Zhang et al., 2020a). In those two studies, inhibition of USP2 by ML364 resulted in significant growth reductions of basal-like breast and triple negative breast tumours (He et al., 2019, Zhang et al., 2020a).

Furthermore, our study is the first to demonstrate that ML364 did not cause a reduction in the weights of mice. Measurement of mice weight is the most basic measure of drug safety. ADME of a drug stand for absorption, distribution, metabolism, and excretion. The preliminary ADME results of the activity, pharmacokinetic properties, and safety profile for ML364 suggested that it is a good drug candidate for *in vivo* models (Davis et al., 2016).

The stability of ML364 in mouse plasma and mouse and human liver microsomes were reported to be at 100%, 61% and 84% respectively within 30 minutes of the microsome assay ($t_{1/2}$) (Davis et al., 2016), which indicates reasonable stability of the drug (Davis et al., 2016, Dybing, 1973, Obach, 1999, Poulin et al., 2012, Sohlenius-Sternbeck et al., 2010). Therefore, our results and the preliminary ADME results collectively suggest that USP2 is a promising drug candidate that warrants further evaluation as a novel treatment for NEPC. However, we acknowledged that the mice could have experienced early pre-diabetes, dyslipidemia or other early toxicity as no additional measurements were taken.

Notably, inhibition of USP2 reduced the protein levels of Aurora kinase A, FAS, and Cyclin D1 in multiple prostate cancer cell lines. These results, in combination with the findings from Chapter 3, strongly suggest that Aurora kinase A, FAS, and Cyclin D1 are USP2 substrates in prostate cancer. Reduction of these USP2 substrates in prostate cancer were observed within 24 hours of ML364 treatment. Given that the *in vitro* and *in vivo* pharmacokinetics of a drug shares a positive linear relationship (Rojas Gómez and Restrepo Valencia, 2015), our results also imply that the pharmacokinetics of ML364 can occur within 24 hours *in vivo*. However, it must be acknowledged that further *in vivo* analyses such as the rapid assessment of compound exposure (RACE) (McAnally et al., 2012) and a comprehensive analysis of pharmacokinetics *in vivo* must be conducted (White, 2000).

This chapter demonstrates that USP2 is a good protein candidate to target in prostate cancer due to its ability to stabilise Aurora kinase A. This kinase is of great interest because it has been identified as a driver of NEPC (Beltran et al., 2011, Davies et al., 2020). Aurora kinase A is important for mitosis, and the duplication and maturation of centrosomes (Liu and Ruderman, 2006, Asteriti et al., 2015). Aurora kinase A has also been found to be associated

with the epithelial-to-mesenchymal transition (D'Assoro et al., 2014, Liu et al., 2016) and with chemotherapy-resistance (Anand et al., 2003, Sun et al., 2014). The *AURKA* gene is often amplified and overexpressed in treatment emergent neuroendocrine PCa (Mosquera et al., 2013, Beltran et al., 2011). Collectively, these studies suggest that Aurora kinase A is important in NEPC. Therefore, we propose that one key mechanism of action of USP2 in NEPC is to stabilise Aurora kinase A.

Given the importance of Aurora kinase A as a driver in the development of NEPC (Beltran et al., 2011, Aparicio et al., 2016), a small molecule inhibitor, Alisertib, was tested in a phase II clinical trial (Beltran et al., 2019). Unfortunately, Alisertib improved progression-free survival in only four out of sixty patients in that clinical trial (Beltran et al., 2019). Our study demonstrated that LNCaP cells with elevated levels of USP2 developed enhanced *in vitro* sensitivity to inhibition of AURORA A as compared to control cells (**Figure 4.8**). This phenomenon can be partly explained by the increased Aurora kinase A expression in these USP2-OE LNCaP cells, and potentially a greater reliance on Aurora kinase A as a knock-on effect. Given that USP2-OE LNCaP cells resembles NEPC phenotypically and that USP2 directly drives the development of a neuroendocrine-like phenotype (refer to chapter 3), our results imply that prostate tumours with high USP2 expression can be treated with Alisertib. Thus, we propose that USP2 could be used as a selection marker to stratify patients for treatment, which may improve patient outcomes in trials of Alisertib. This hypothesis could be tested in patient-derived xenografts, which have a range of USP2 levels (**Figure 3.6D**). Moreover, our results suggest that a combinatorial inhibition of USP2 (with ML364) and Aurora kinase A (with Alisertib) is a rational combination therapy that might also sensitise neuroendocrine prostate cancer cells to chemotherapy.

One of the strengths of this study is that USP2 was evaluated as a target in multiple prostate cancer cell lines with a diverse range of phenotypes. Prostate adenocarcinoma LNCaP cells are luminal epithelial cells that are androgen responsive, while PC3 and the LNCaP-derived MR42D are neuroendocrine-like PCa cells that are androgen insensitive. The objective of choosing those three PCa models (LNCaP, MR42D and PC3) is that these models represent the heterogeneity of therapy-resistant prostate cancer that can plausibly arise as multiple “conduits” to terminal state NEPC (Labrecque et al., 2019, Aggarwal et al., 2018, Davies et al., 2021). However, we acknowledge that ML364 should be tested in additional models, most importantly the gold-standard in the field, which is NEPC patient derived xenografts.

Another strength is that ML364 was evaluated in mice grafted with neuroendocrine-like PCa cells in their prostate glands. This type of preclinical mouse model enables us to assess the efficacy of ML364 in an organ-specific tumour environment, which best mimics the pathology, metastasis, and prostate cancer progression in humans (Nassar et al., 2020, Li et al., 2020, Zhang et al., 2018a).

We acknowledge that we have not conclusively shown that Aurora kinase A is a key mediator of USP2 action. Therefore, we suggest conducting further experiments to conclusively demonstrate that putative mechanism. A potential experiment can be knocking down USP2 in neuroendocrine-like PCa (such as MR42D cells), followed by overexpressing Aurora kinase A in those cells and document any rescue of phenotype. The objective of this future experiment is to investigate if AURKA is a direct substrate of USP2 and acts downstream of USP2. Another important future work can be to identify other novel substrates of USP2. This can enable a comprehensive understanding of the mechanism(s) by

which USP2 utilises to mediate epithelial-neuroendocrine plasticity; this work will be described in Chapter 5, which discusses proteomic and transcriptomic analyses of PCa cells following manipulation of USP2 expression and activity.

Chapter 5:

Integrative omics to define USP2

function in prostate cancer

5 INTEGRATIVE OMICS TO DEFINE USP2 FUNCTION IN PROSTATE CANCER

5.1 Introduction

The ubiquitin-proteasome system (UPS) manages degradation of intracellular proteins through substrate recognition by ubiquitin ligases, conjugation of ubiquitin and degradation of ubiquitinated substrates by proteasomes (Borg and Dixit, 2017, Komander et al., 2009). Ubiquitinated proteins can be de-ubiquitinated by deubiquitylating enzymes (DUBs) (Harrigan et al., 2018, Komander et al., 2009, Rajkumar et al., 2005). Among the 79 putative DUBs encoded by the human genome, the ubiquitin-specific proteases (USPs) make up the largest family of DUBs (Pal et al., 2014, Harrigan et al., 2018).

Notably, we have identified USP2 to be important and dysregulated in prostate cancer. To the best of our knowledge, we have shown for the first time that USP2 is upregulated in patients' primary tumours in response to AR-targeted therapies and in NEPC (refer to chapter 3). We are also the first to show that USP2 directly drives the neuroendocrine phenotype and mediates resistance to AR-targeted therapy and chemotherapy (refer to chapter 3). In chapter 4, we validated USP2 as a *bona fide* therapeutic target in aggressive prostate cancer. While several novel substrates of USP2 have been identified and investigated in prostate cancer (refer to chapter 3 and 4), it is imperative that other novel substrates of USP2 be identified to elucidate the resistance mechanism(s) by which USP2 mediates its effects.

Proteomics- and transcriptomics-based techniques have often been employed in cancer studies to identify potential mechanisms of resistance (Lenchine et al., 2021, Liu et al., 2018a, Gillis et al., 2021). To elucidate the substrates of USPs using omics, studies had labelled the proteome with radiolabelled amino acids and conduct quantitative proteome or ubiquitinome (Heidelberger et al., 2016, Liu et al., 2018a). Label-free proteomics of the immunoprecipitant to identify substrates of the USP has also been conducted (Liu et al., 2018a).

In this chapter, an integrative omics strategy to identify the substrates and functions of USP2 in prostate cancer is described. More specifically, we conducted mass spectrometry-based proteomics and transcriptional profiling (RNA sequencing) following manipulation of USP2 expression. Integration of these -omics approaches had provided the first comprehensive evaluation of USP2 function in prostate cancer and yielded a set of putative substrates that can be interrogated in future work.

5.2 Methods

5.2.1 Proteomics

2 million MR42D cells were seeded in full serum media per 10cm dish prior to a 24-hour treatment with 5 μ M ML364 (n = 5) or vehicle control (n = 5). LNCaP cells overexpressing USP2 (USP2-OE) or neon (control) transgenes were seeded in full serum media (n = 5) at the appropriate densities: 1.1 million cells or 1.8 million cells in a 10cm dish for a 4 day or 3 day growth. For both sets of proteomics experiments, cells were washed with PBS and then harvested in 0.7 mL of lysis buffer (50 mM Tris-HCL pH 8.0) and 1x cOmplete mini EDTA-free protease inhibitors (Roche Catalogue# 04693124001). Protein lysates were homogenised using a Dounce homogeniser and a final concentration of 1% (w/v) Dodecylmaltoside (DDM) was added per sample.

The Flinders Omics Facility then carried out EZQ protein assay (Invitrogen Catalogue# R33200) to quantitate protein concentrations. 10 μ g of proteins per lysate were reduced with 100 mM ammonium bicarbonate (Sigma #09830 Bio-Ultra Grade) and 10 mM TCEP-HCL (Millipore CAS 51805-45-9) for 30 minutes at 56°C to reduce the proteins. The reduced proteins were then alkylated with 20 mM chloroacetamide (Sigma #C0267) for 30 minutes at room temperature. The alkylated proteins were digested with trypsin at ratio of 1:50 (protein to trypsin) in a total volume of 200 μ L overnight at 37°C. The trypsinisation reaction was quenched using 0.1% Formic acid. The digested peptides were cleaned up using C18 StageTips and eluted using 80% acetonitrile in 0.1% formic acid. In-house stage tips were made by inserting 3x 1.25mm C18 disks (PK20 Empore Octadecyl C18, Sigma 66883-U) followed by 3x 1.4mm disks into an Axygen maxyum recovery 200 μ L tip (T-200-C-L). Peptides were separated

using reversed phase liquid chromatography, which is a type of high-performance liquid chromatography (HPLC). Peptide precursors were identified using data acquired via mass spectrometry 1 (MS1) and MS2 scans. Identification of peptides were carried out via data-dependent and data-independent acquisition of peptide precursors and analysed against a spectral library. The mass spectrometry model for both proteomics experiments was Dionex Ultimate 3000 UPLC (ThermoFisher Scientific). The spectral library database file used was: uniprot-Homo+sapiens+(Human)+[9606]_08-2021.fasta. For both proteomics experiments, peptides were enriched using an in-house 40 cm 75µm inner diameter fused silica capillary packed with 1.9 µm ReproSil-Pur C18 beads (Dr. Maisch, Ammerbuch, Germany) was used. The uHPLC gradient was 0.3 µL per minute. In the first proteomics experiment, where MR42D cells were treated with DMSO or ML364, peptides were analysed using the Exploris data dependent and independent analysis methods. In the second proteomics experiment, where USP2 was constitutively overexpressed in LNCaP cells, peptides were analysed using the Lumos data dependent and independent analysis methods.

In the first proteomics experiment, the proteins were calculated as a ratio of the protein expression in the ML364 treatment group over the control group. In the second proteomics experiment, the proteins were calculated as a ratio of the protein expression in the USP2-OE LNCaP cells over the control group. In both proteomics experiments, candidate proteins are proteins with absolute \log_2 fold change > 0.5 and a q-value ≤ 0.05 .

Pathway Enrichment Analyses

The entire list of proteins was inserted into the Gene Set Enrichment Analysis (GSEA) tool. Pathways enriched in the LNCaP-USP2-OE cells (i.e. USP2 up) or the LNCaP-USP2-neon

cells (i.e. USP2 down) were identified using GSEA. The following databases from MSigDB (Subramanian et al., 2005) were selected for assessment by GSEA: Hallmarks, KEGG, Reactome, Wikipathways, Transcription factor targets, Computational gene sets, Gene Ontology and Oncogenic signature.

The list of significantly elevated or reduced proteins were inserted into the ClueGO tool (Bindea et al., 2009). The following databases from MSigDB (Subramanian et al., 2005) were selected for assessment by GSEA: KEGG, Reactome, Wikipathways, and Gene Ontology.

5.2.2 RNA sequencing

LNCaP cells constitutively overexpressing USP2 (LNCaP-USP2-OE) or the neon control transgene (LNCaP-control) were seeded in full serum media in 6-well plate format. They were then harvested in Trizol at the appropriate time points. Three biological replicates from consecutive passage numbers, each of which were a pool of 3 technical replicates from that passage, were processed for RNA sequencing. Total RNA was extracted using a RNeasy mini kit (Qiagen #74104) according to manufacturer's instructions.

RNA sequencing was done by the South Australian Genomic Centre (SAGC). The quality and quantity of RNA samples was assessed using LabChip GX Touch 24 and Qubit respectively. Next-generation RNA sequencing libraries were constructed according to the Nugen Universal Plus mRNA-seq protocol and include 15 cycles of amplification. Equimolar pools were prepared and converted to MGI compatible libraries. Illumina to MGI library conversion was carried out using the MGIEasy Universal Library Conversion kit, part no. MGI1000004155. Libraries were sequenced (single-end) on the MGI DNBSEQ-G400 large Flow cell platform at the South Australian Genomics Centre (SAGC). The run had produced reads of 471.1 million lengths with an average Q30 of 92.75%.

Bioinformatics analysis of RNA-sequencing data

The following data processing and analysis was carried out by Dr. Marri from Flinders Centre for Innovation in Cancer (FCIC, South Australia). The resulting FASTQ files averaging 75 million reads per sample were analysed and quality checked using FastQC program (<http://www.bioinformatics.babraham.ac.uk/projects/fastqc>). Reads were mapped against the human reference genome (hg38) using the STAR spliced alignment algorithm (Dobin et al., 2013) (version 2.5.2b with default parameters). The reads were assigned to each exon region based on the human genome annotation from the GENCODE (<https://www.genecodegenes.org/>) and assigned reads were summarised as counts using the featureCounts (v.1.6.4) tool (Liao et al., 2014). The counts were normalized and PCA plots generated using the pcaExplorer package (Marini and Binder, 2019) in R (v.4.2; <https://www.R-project.org/>).

Differential gene expression analysis was done using the DESeq2 program (Love et al., 2014) in R (v.4.2; <https://www.R-project.org/>). Briefly, DESeq2 uses a Wald test for statistically significant testing. The Wald test p values from the genes that pass the independent filtering step are adjusted for multiple testings using the Benjamini-Hochberg test. Benjamini-Hochberg adjusted p values of < 0.05 were considered statistically significant. DESeq2 reports a log₂FoldChange for the differential expression of each gene. Differentially expressed genes were defined by a log₂FoldChange of > 1 or < -1 . Volcano plots were generated using the EnhancedVolcano R package (<https://bioconductor.org/packages/release/bioc/html/EnhancedVolcano.html>).

Pathway Enrichment Analyses

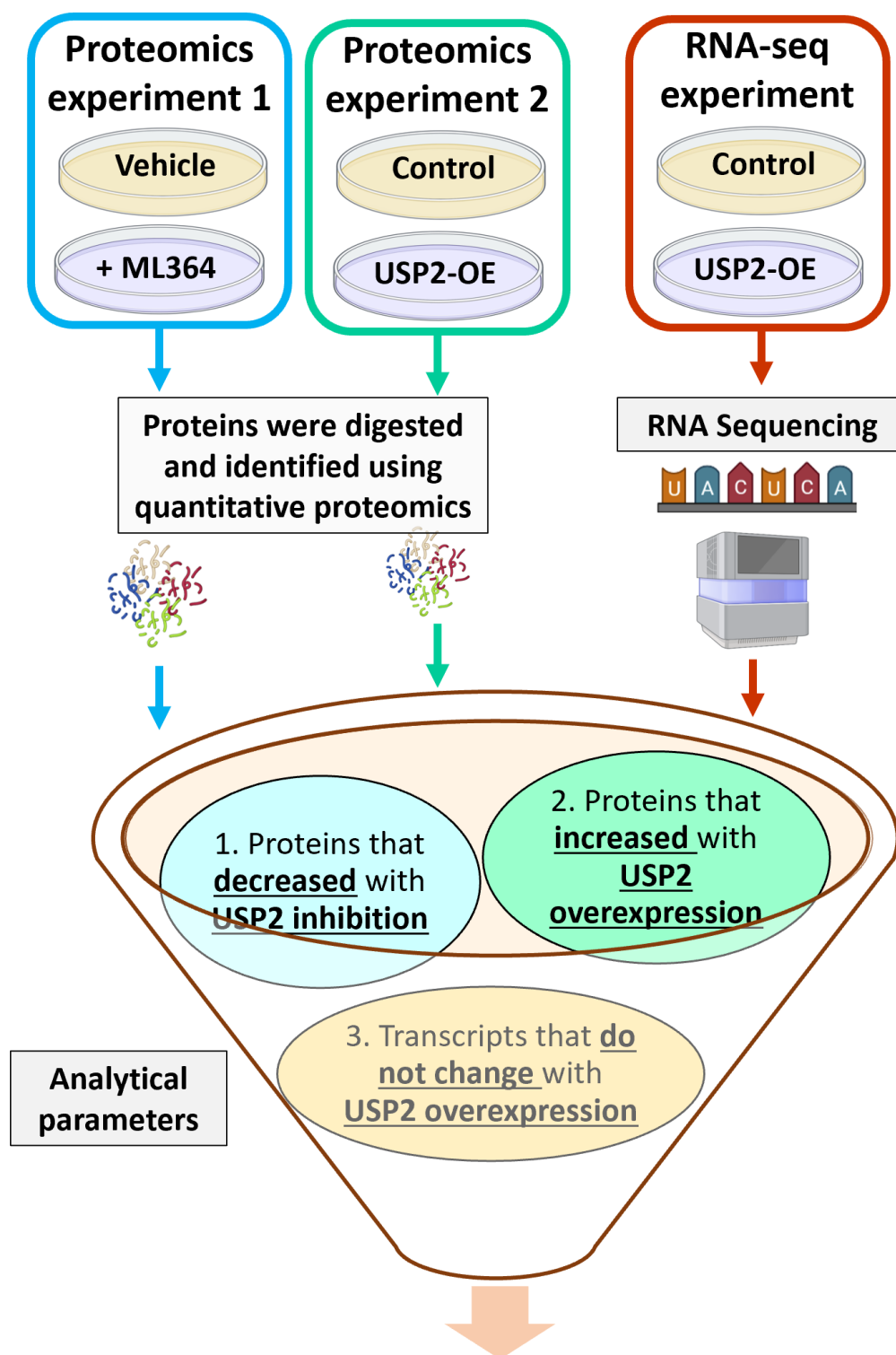
The gene lists were filtered to only include protein-coding genes. Subsequently, pathways enriched in the LNCaP-USP2-OE cells (i.e. USP2 up) or the LNCaP-neon cells (i.e. USP2 down) were identified using Gene Set Enrichment Analysis (GSEA). The following databases from MSigDB (Subramanian et al., 2005) were selected for assessment by GSEA: Hallmarks, KEGG, Reactome, Wikipathways, Transcription factor targets, Computational gene sets, Gene Ontology and Oncogenic signature.

The list of significantly upregulated or downregulated genes were inserted into the ClueGO tool (Bindea et al., 2009). The following databases from MSigDB (Subramanian et al., 2005) were selected for assessment by GSEA: KEGG, Reactome, Wikipathways, and Gene Ontology.

5.3 Results

5.3.3 Overview of experimental strategy to identify USP2 substrates

We devised a strategy to robustly identify USP2 substrates and activities in prostate cancer cells (**Figure 5.1**). This strategy relied on mass-spectrometry-based analysis of proteomes when USP2 is inhibited in neuroendocrine-like MR42D cells and when USP2 is overexpressed in the adenocarcinoma LNCaP cells, combined with RNA-sequencing of the USP2-OE LNCaP cells (**Figure 5.1**). Integration of these three experiments would identify proteins that decreased with USP2 inhibition and increased with USP2 overexpression, with a further filtering step being to identify proteins that did not exhibit altered expression at the transcript level (**Figure 5.1**). In other words, factors exhibiting changes at the mRNA level but not the protein level are unlikely to be a substrate. RNA-seq can also provide additional insights into how the overall transcriptome is altered and whether this is related to the neuroendocrine phenotype, including potential changes to activity of transcription factors. Below, the results of these experiments, including integration of the distinct datasets, are described in more detail.



To identify novel potential substrates of USP2

Figure 5.1. Schematic diagram depicting the overall experimental approach for quantitative proteomics and transcriptomics in this study. The analytical parameters to identify novel potential substrates of USP2 are described in chronological order.

5.3.4 Analyses of the global proteome in MR42D cells treated with the USP2 inhibitor, called ML364.

To systematically identify proteins that were altered when USP2 was inhibited in neuroendocrine-like prostate cancer cells, the total proteome was profiled in MR42D cells treated for 24 hours with 5 μ M ML364 or a vehicle control. Principal component analysis (PCA) revealed that the proteome of the MR42D cells treated with ML364 was distinct from MR42D cells treated with vehicle and there was little variation between replicates (**Figure 5.2**).

The average number of protein groups detected per sample was 3395 (**Table 5.1**). The minimum percentage of detected protein groups was 94.05% (**Table 5.1**), thereby indicating that the data was robust.

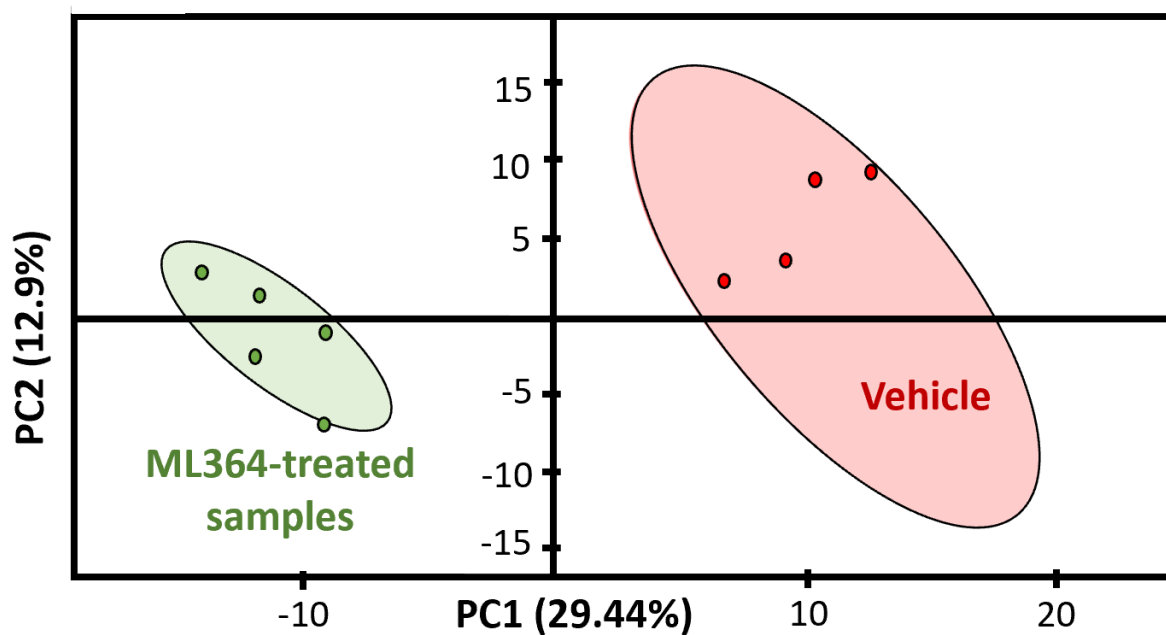


Figure 5.2. Principal component analysis of the global proteomes from MR42D cells treated with vehicle (control) versus 5 μ M ML364. The 95% confidence interval used to group the samples were indicated by the probability ellipsoids.

Table 5.1. Number of protein groups detected in MR42D cells treated with vehicle (DMSO) versus ML364.

Number of protein groups detected in MR42D cells treated with vehicle versus ML364				
	Sample name	Number of protein groups detected	Total number of protein groups across all samples	Percentage of protein groups detected
1	Control replicate 1	3371	3549	94.98%
2	Control replicate 2	3434	3549	96.76%
3	Control replicate 3	3435	3549	96.79%
4	Control replicate 4	3461	3549	97.52%
5	Control replicate 5	3443	3549	97.01%
6	ML364-treated replicate 1	3338	3549	94.05%
7	ML364-treated replicate 2	3373	3549	95.04%
8	ML364-treated replicate 3	3341	3549	94.14%
9	ML364-treated replicate 4	3393	3549	95.60%
10	ML364-treated replicate 5	3364	3549	94.79%

A volcano plot was plotted to showcase the changes in protein abundance in response to inhibition of USP2 by ML364. The proteins that had significant changes in expression are indicated in red dots (**Figure 5.3**). These candidate proteins had absolute $\log_2(\text{fold change}) > 0.5$ and $q\text{-values} \leq 0.05$. This analysis revealed that there were a greater number of proteins that were significantly downregulated than upregulated: 57 proteins were significantly upregulated (**Supplementary Table 7.1**), while 476 proteins were significantly downregulated with USP2 inhibition in MR42D cells (**Figure 5.3; Supplementary Table 7.2**). This finding may reflect the function of USP2 in maintaining stability of its protein substrates.

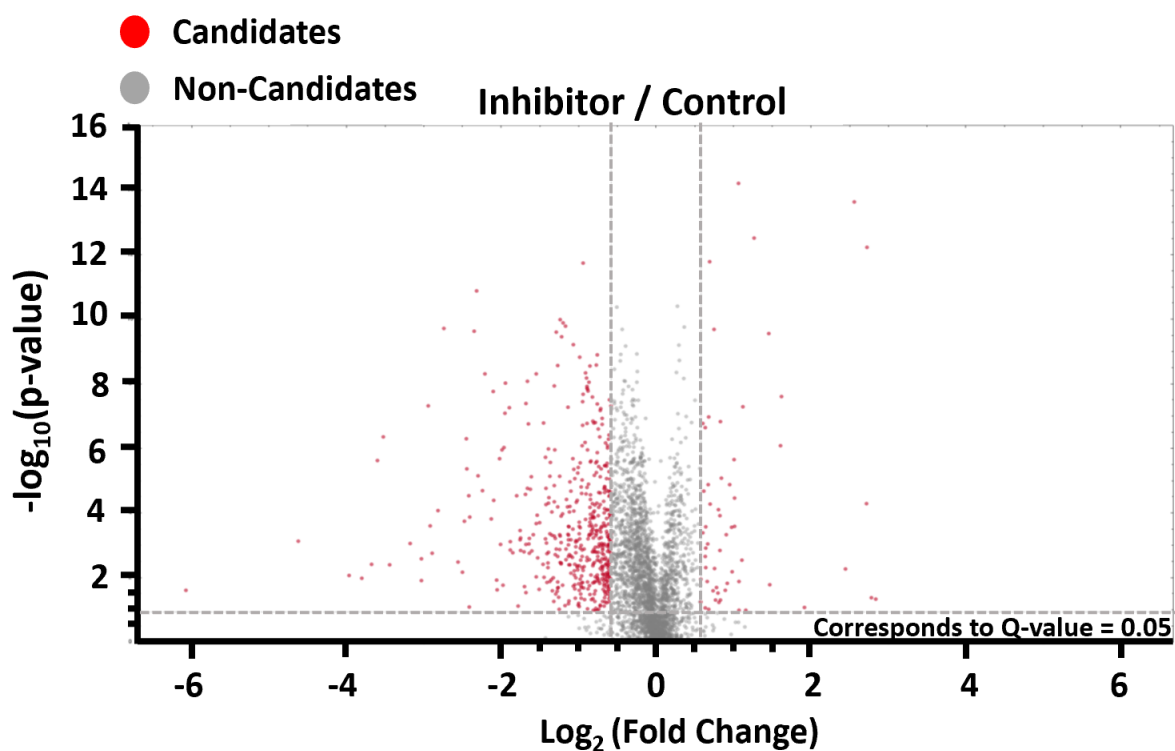


Figure 5.3. Volcano plot of the proteins at different abundance levels were identified between the MR42D cells treated with 24 hours of 5 μ M ML364 and the control group. These proteins were calculated as a ratio of the protein expression in the ML364 treatment group over the control group. Each dot represents a protein. Candidate proteins are proteins with absolute $\log_2(\text{fold change}) > 0.5$ and $q\text{-value} \leq 0.05$, shown as red dots. The threshold line corresponds to $q\text{-value} = 0.05$.

To gather insight into the possible biological functions of USP2, Gene Set Enrichment Analysis (GSEA) was used to identify pathways altered in the proteomics data. GSEA is a powerful enrichment tool to interpret mass spectrometry-based proteomics and RNA sequencing (Zito et al., 2021, Subramanian et al., 2005). Pathways enriched using GSEA that had an FDR-adjusted p-value less than 0.25 were determined to be enriched, a cutoff that has been determined to identify biologically relevant pathways previously (Subramanian et al., 2005). We also used another enrichment tool called ClueGO (Bindea et al., 2009) to investigate the list of proteins that were significantly reduced or increased. ClueGO has been used to interpret mass spectrometry-based proteomics in cancer cells (Liu et al., 2018a). Pathways enriched using the ClueGO tool that have adjusted p-values less than 0.05 were selected for this study, according to the suggested workflow (Liu et al., 2018a).

Gene Set Enrichment Analysis (GSEA) revealed an enrichment of cell cycle pathways that were significantly downregulated (FDR adjusted p-value < 0.05) with USP2 inhibition in MR42D cells (**Figure 5.4A**). The enriched cell cycle pathways that were inhibited were the Hallmark “E2F targets” and Hallmark “G2/M checkpoint” pathways with normalised enrichment scores of -2.04 and -1.65 respectively (**Figure 5.4A**). The Hallmark “G2/M checkpoint” collection was a list of genes encoding proteins important for cell cycle progression, while the Hallmark “E2F targets” pathway contained a list of cell cycle related targets of E2F transcription factors (Liberzon et al., 2015, Subramanian et al., 2005).

Meanwhile, analyses via GSEA and ClueGO also revealed enrichment of DNA repair and mitochondrial translation pathways that were downregulated (**Figure 5.4B, Figure 5.5**). With GSEA, the “DNA repair” and “mitochondrial translation” Reactome pathways have normalised enrichment scores of -1.64 and -1.55 respectively (**Figure 5.4B**). The “DNA repair”

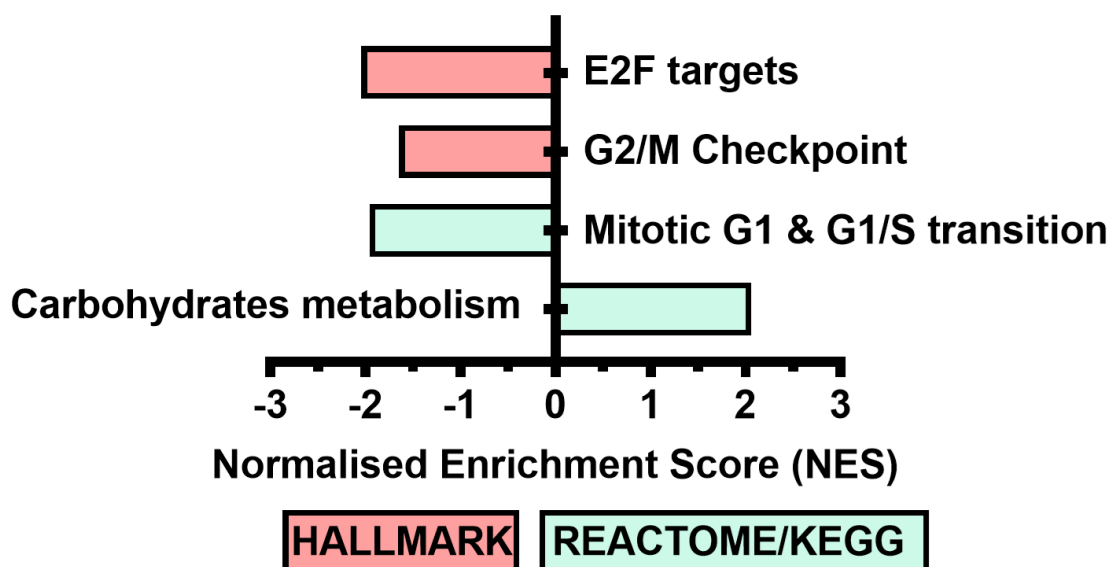
Reactome pathway (R-HAS-73894) ensures the integrity of the cellular genome is maintained (Curtin, 2012, Lindahl and Wood, 1999). The “mitochondrial translation” Reactome pathway represents proteins that are encoded in the genome and translated by the mito-ribosomes on the inner mitochondrial membrane (Hällberg and Larsson, 2014, Lightowlers et al., 2014).

Notably, there was enrichment of the glycolysis pathway in the set of proteins that were significantly reduced in neuroendocrine-like MR42D cells treated with ML364 (**Figure 5.5**). Other notable pathways that were suppressed with ML364 include fatty acid metabolism, extracellular matrix assembly, chaperone-mediated protein folding, ERAD pathway and canonical WNT signalling pathway (**Figure 5.5**).

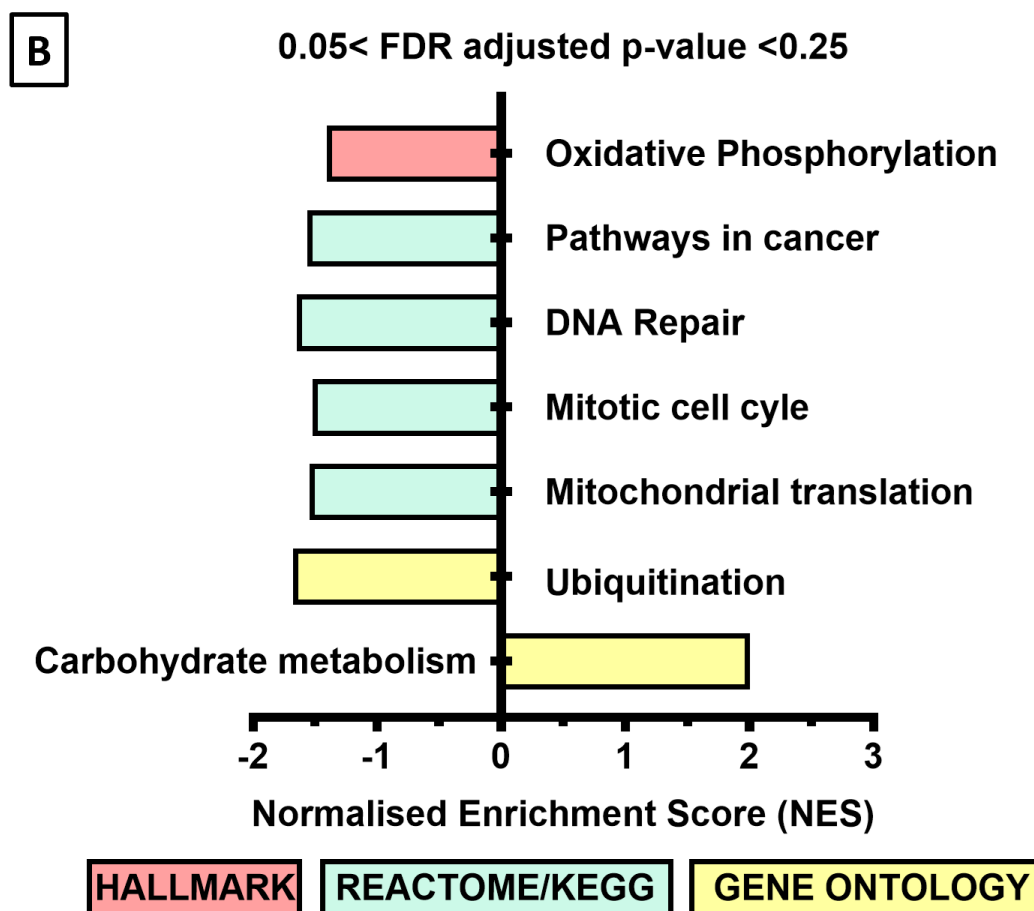
In contrast, there was enrichment of pathways that metabolised cellular energy reserves, such as glycogen, with proteins that were significantly upregulated in MR42D cells treated with ML364 (**Figure 5.6**). Collectively our analyses revealed new associations of USP2 with cellular functions, such as cell cycle, DNA repair, mitochondrial translation, protein chaperones, fatty acid metabolism and WNT signalling in neuroendocrine-like prostate cancer cells.

A

FDR adjusted p-value < 0.05



Name of pathway	NES	FDR adjusted p-value
E2F targets	-2.04	<0.0001
G2/M checkpoint	-1.65	0.0382
Mitotic G1 and G1/S transition	-1.95	0.0195
Metabolism of carbohydrates	2.06	0.0417



NAME	NES	FDR adjusted p-value
Oxidative phosphorylation	-1.41	0.1252
Pathways in cancer	-1.56	0.1404
DNA repair	-1.64	0.1826
Mitotic cell cycle	-1.52	0.1884
Mitochondrial translation	-1.55	0.1973
Ubiquitination	-1.68	0.2043
Carbohydrate metabolism	2.00	0.0792

Figure 5.4. GSEA analysis of proteomics data from MR42D cells exposed to 5 μ M ML364 revealed inhibition of cell cycle pathways. (A) The pathways displayed are significantly enriched (FDR-adjusted p-value < 0.05). (B) The pathways displayed are significant (0.05 < FDR-adjusted p-value < 0.25). For (A) and (B), the entire proteomic dataset (i.e. all proteins detected) were used as an input in GSEA.

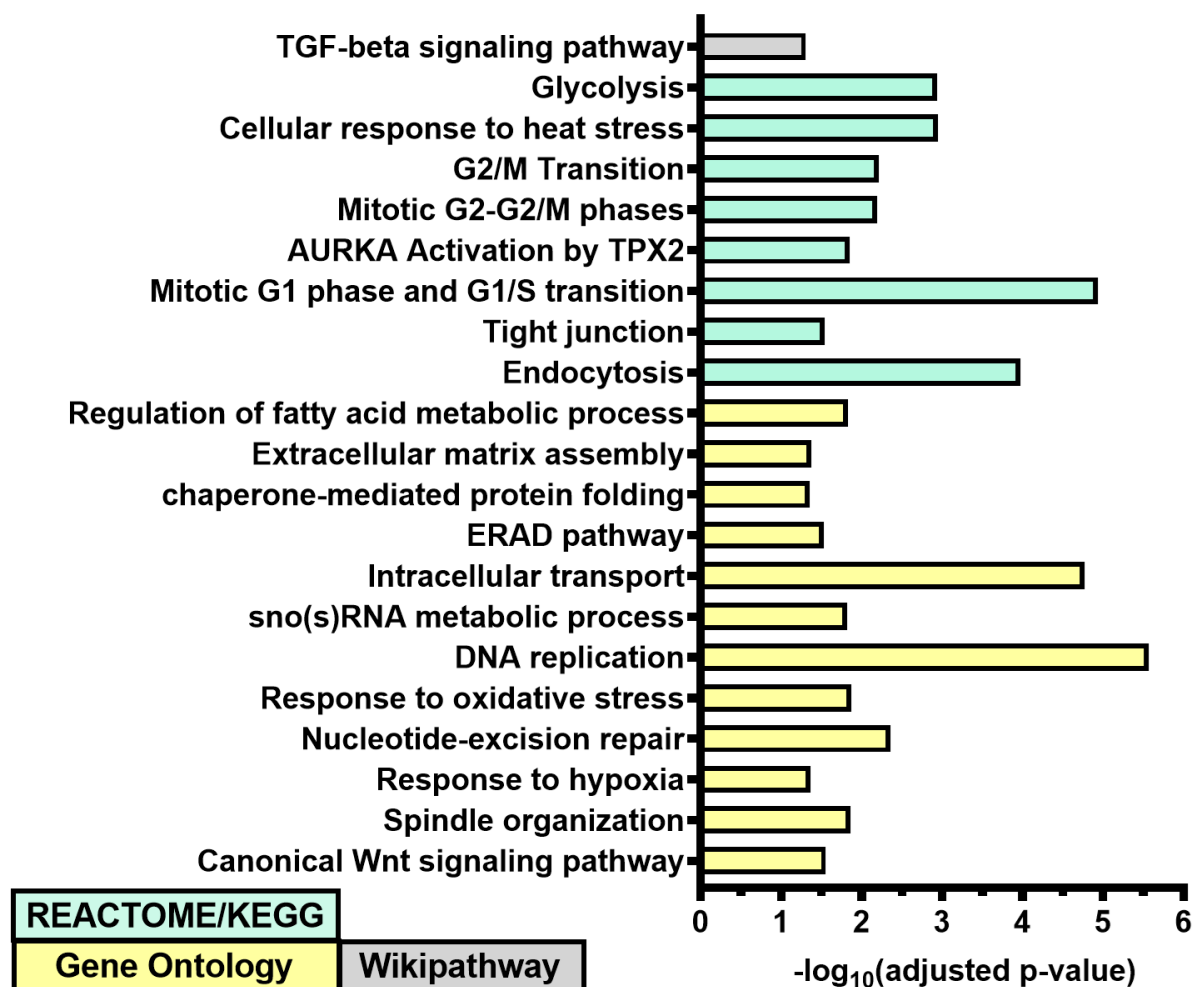


Figure 5.5. Inhibition of USP2 in neuroendocrine-like PCa cells is associated with an inhibition of glycolysis, cell cycle and fatty acid metabolism. Pathway enrichments via ClueGO were conducted using the list of proteins that were significantly reduced in MR42D cells treated with 24 hours of ML364 (adjusted p-value < 0.05).

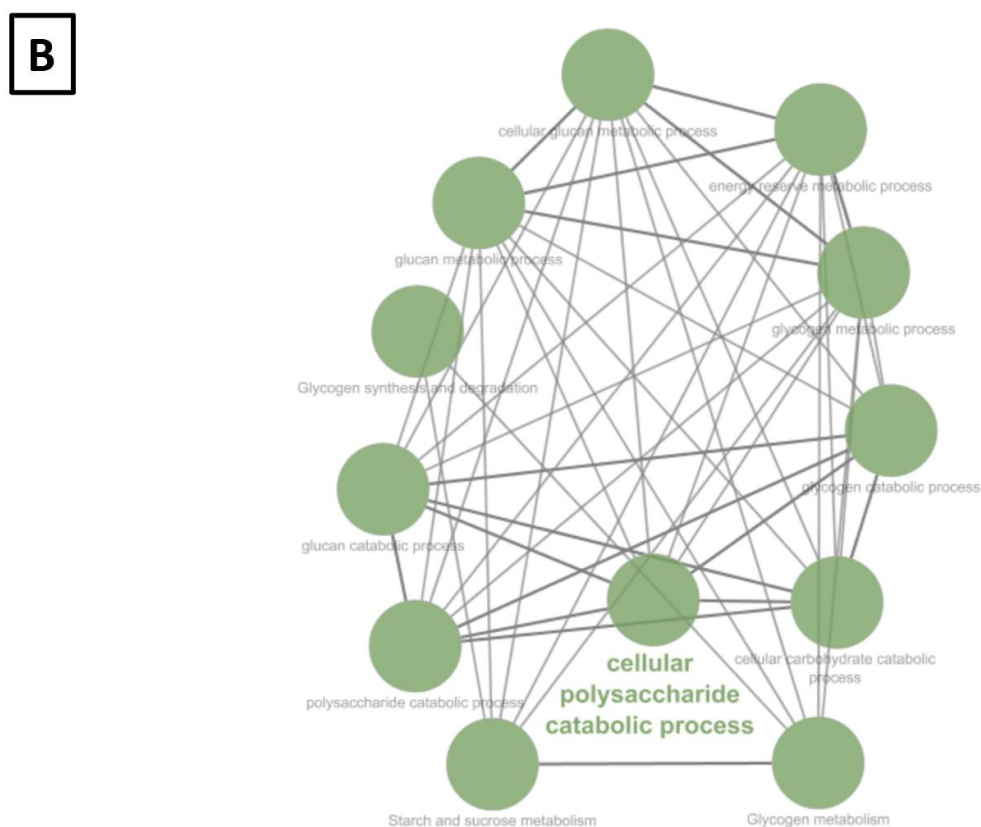
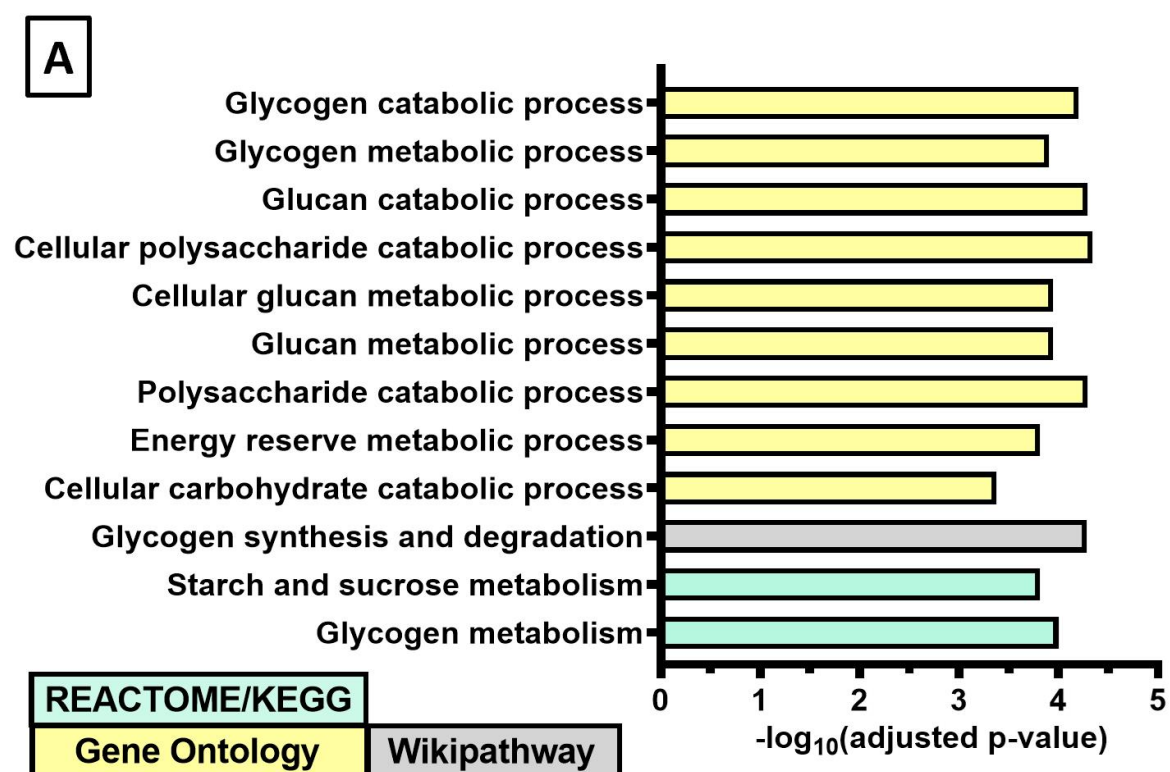


Figure 5.6. Inhibition of USP2 in neuroendocrine-like PCa cells is associated with an activation of cellular polysaccharide catabolic process. (A) Pathway enrichments via ClueGO

were conducted using the list of proteins that were significantly upregulated in MR42D cells treated with 24 hours of ML364 (adjusted p-value < 0.05). (B) Pathways related to the cellular polysaccharide catabolic process were highlighted. The larger the size of the node, the higher the enrichment significance of the terms. The thicker the connecting line, the stronger the association strength between the terms.

5.3.5 Analyses of the global proteome when LNCaP cells overexpressed USP2

The global proteome was also profiled in LNCaP cells overexpressing USP2 (USP2-OE) or the neon transgene (control). Principal component analysis (PCA) distinguished the proteome of USP2-OE LNCaP cells from the control cells (**Figure 5.7**). The relatively low variance accounted by the combination of the two most important principal components signals that the proteomes from the two cell types are very distinct (**Figure 5.7**).

The average number of protein groups detected per sample was 3997 (**Table 5.2**). The minimum percentage of detected protein groups was 90.01% (**Table 5.2**), thereby indicating that the data was robust.

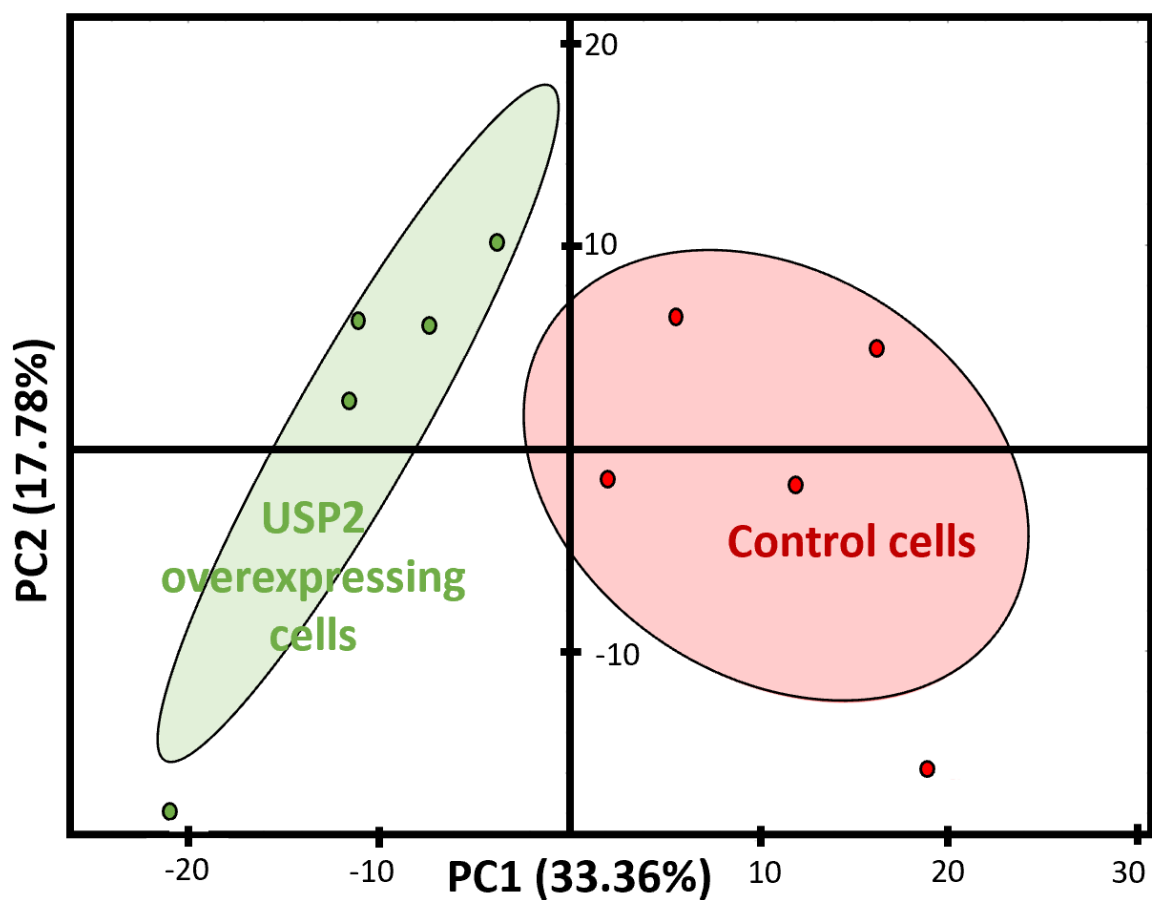


Figure 5.7. Principal component analysis of the global proteome differentiated the global proteome profiles of the LNCaP cells overexpressing USP2 (USP2-OE) versus control cells overexpressing the neon transgene. The probability ellipsoids represent the 95% confidence interval used to group the samples.

Table 5.2. Number of protein groups detected in the LNCaP overexpressing the neon transgene (control) or USP2 (USP2-OE) when these cells were grown in media supplemented with full serum.

Number of protein groups detected in the control LNCaP cells versus LNCaP cells overexpressing USP2				
	Sample names	Number of protein groups detected	Total number of protein groups across all samples	Percentage of protein groups
1	Control LNCaP replicate 1	3984	4254	93.65%
2	Control LNCaP replicate 2	4075	4254	95.79%
3	Control LNCaP replicate 3	4127	4254	97.01%
4	Control LNCaP replicate 4	4067	4254	95.60%
5	Control LNCaP replicate 5	3963	4254	93.16%
6	USP2-OE LNCaP replicate 1	3829	4254	90.01%
7	USP2-OE LNCaP replicate 2	3976	4254	93.46%
8	USP2-OE LNCaP replicate 3	3948	4254	92.81%
9	USP2-OE LNCaP replicate 4	4068	4254	95.63%
10	USP2-OE LNCaP replicate 5	3942	4254	92.67%

The volcano plot depicted the changes in protein abundance in response to overexpression of USP2 in androgen dependent LNCaP cells (**Figure 5.8**). There were 137 proteins that were significantly upregulated (average \log_2 fold change > 0.5) (**Figure 5.8; Supplementary Table 7.3**) and 448 proteins that were significantly downregulated (average \log_2 (fold change) < -0.5) (**Figure 5.8; Supplementary Table 7.4**). Candidate proteins that have absolute \log_2 (fold change) ≥ 0.05 and q-values ≤ 0.05 and are denoted in red dots (**Figure 5.8**). It is postulated that the proteins that are more highly expressed in the USP2-OE LNCaP cells than control cells could be enriched as USP2 substrates. Therefore, we mainly focused on the pathways that were activated within this class of proteins.

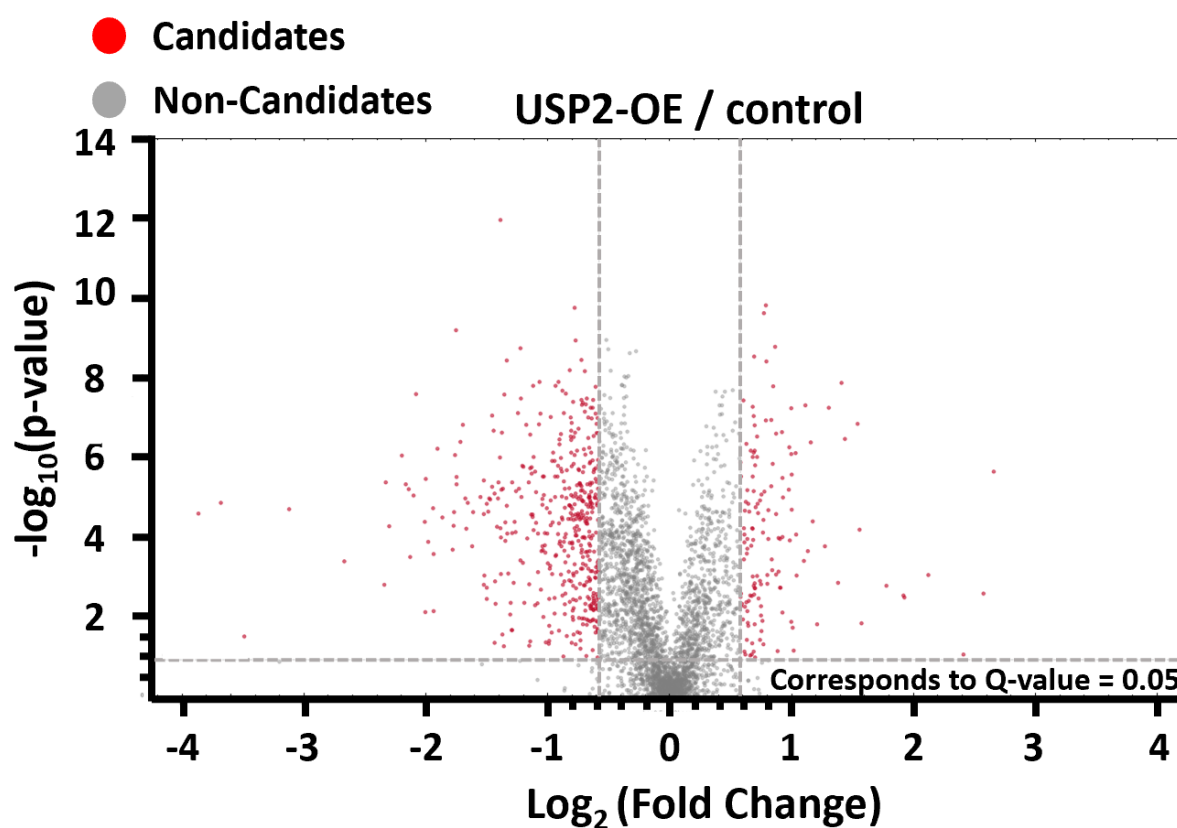


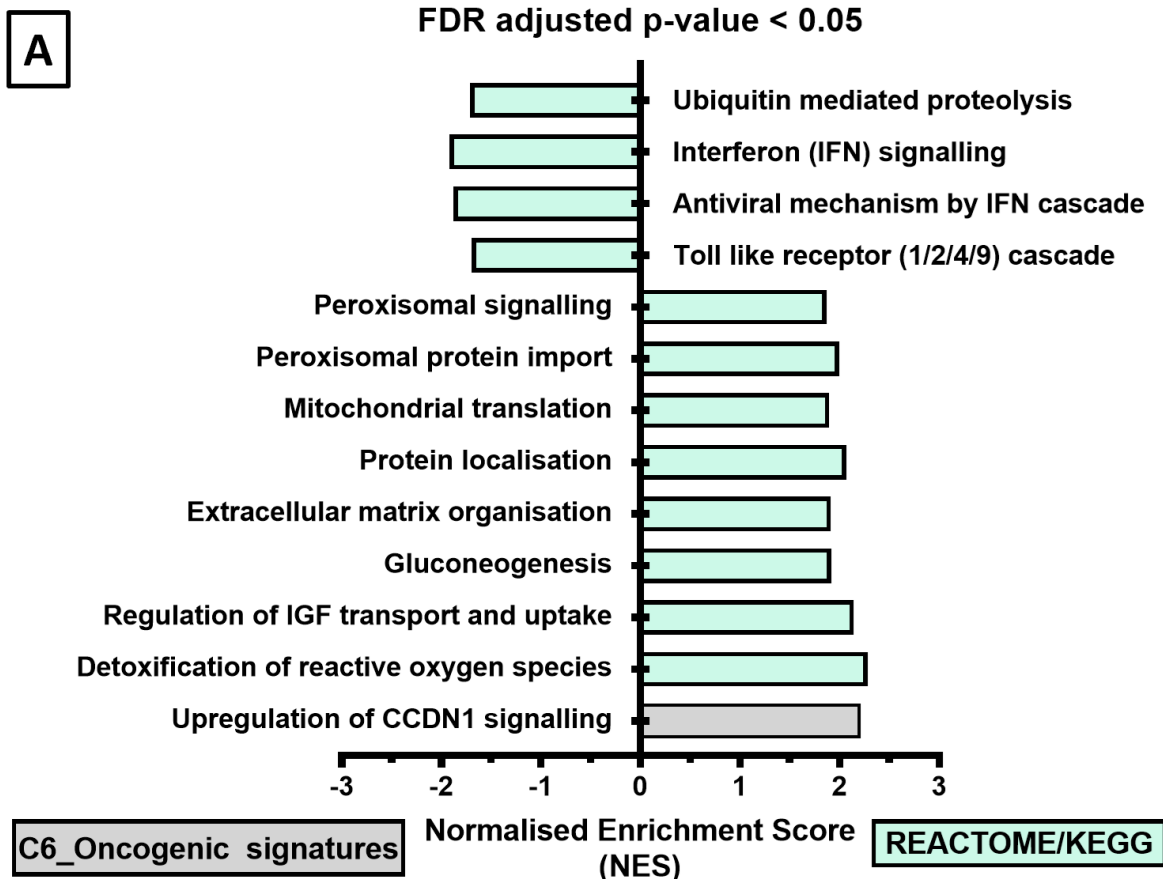
Figure 5.8. Volcano plot of proteins at different abundance levels were identified between the USP2-OE LNCaP cells and the control group. These proteins were calculated as a ratio of the protein expression in the USP2-OE LNCaP cells over the control group. Candidate proteins are proteins with absolute $\log_2(\text{fold change}) > 0.5$ and a $q\text{-value} \leq 0.05$, shown as red dots. The threshold line corresponds to $q\text{-value} = 0.05$.

GSEA analysis of the global proteomes from LNCaP cells overexpressing USP2 revealed the following pathways to be significantly and positively enriched (FDR-adjusted p-value < 0.05 and normalised enrichment score > 0): Cyclin D1 signalling, peroxisomal signalling and import of peroxisomal proteins, translation and import of mitochondrial proteins, protein localisation, extracellular matrix organisation, gluconeogenesis, regulation of the transport of insulin growth factor and detoxification of reactive oxygen species (**Figure 5.9A**). GSEA pathway analyses also suggested USP2 to play a role in RAF1 signalling, fatty acid metabolism and reactive oxygen species (ROS) (0.05 < FDR-adjusted p-value < 0.25 and normalised enrichment score > 0) (**Figure 5.9B**).

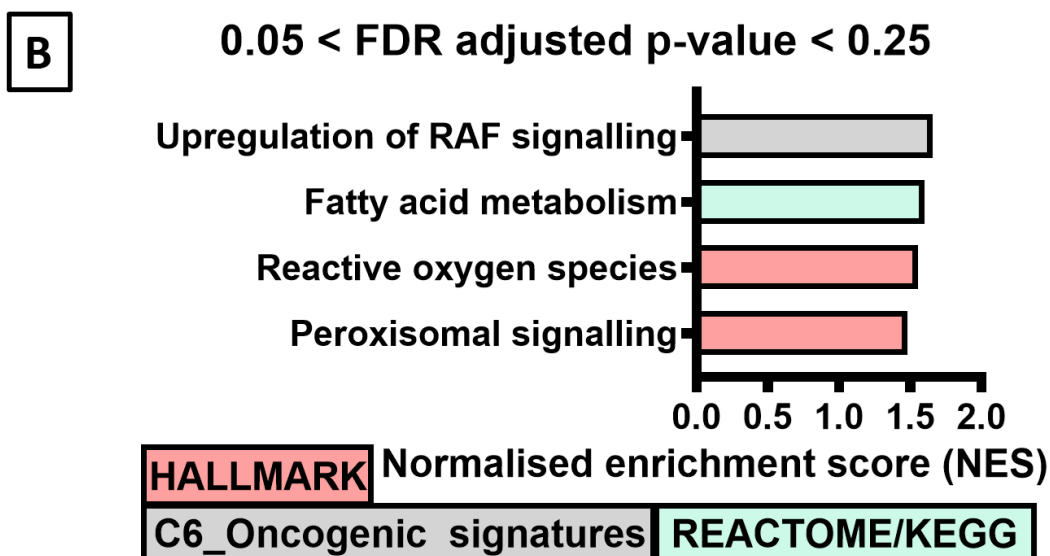
Findings using the ClueGO tool were generally similar to that obtained by GSEA (**Figure 5.10**). There were enrichments of lipid metabolism pathways, suggesting that USP2 might be a positive regulator of lipid metabolism (**Figure 5.10**). There were also enrichments of translation and import of mitochondrial proteins, and chaperone-mediated protein folding (**Figure 5.10**). Other notable pathway enrichments were detoxification of reactive oxygen species, neuron projection regeneration and positive regulation of histone H3-K4 methylation (**Figure 5.10**). This indicated that USP2 might be involved in the ROS pathway and regulating neuron projections and methylation. Importantly, there was enrichment of protein deubiquitination with the proteins that were significantly increased in USP2-OE LNCaP cells (**Figure 5.10**). This supports the role of USP2 as a deubiquitinating enzyme in prostate cancer cells.

GSEA also revealed enrichment of several downregulated pathways that were previously not associated with elevation of USP2 in prostate cancer (**Figure 5.9**). High expression levels of USP2 in LNCaP cells was associated with downregulation of interferon

signalling and the antiviral mechanism by IFN signalling cascade (**Figure 5.9**). These enrichments were supported by the ClueGO analyses (**Figure 5.11**). The Toll like receptor (1/2/4/9) signalling cascades were also downregulated in these USP2-OE LNCaP cells (**Figure 5.9**). Additionally, elevated expression of USP2 resulted in a negative enrichment for ubiquitin-mediated proteolysis, specifically the ubiquitin conjugating enzyme activity and protein K48-linked ubiquitination pathways (**Figure 5.9, Figure 5.11**).



Pathway Enriched	NES	FDR adjusted p-value
Ubiquitin mediated proteolysis	-1.71	0.0310
Interferon (IFN) signalling	-1.92	0.0294
Antiviral mechanism by IFN cascade	-1.88	0.0139
Toll like receptor (TLR1/2/4/9) signalling	-1.69	0.0284
Peroxisomal signalling	1.87	0.0377
Peroxisomal protein import	1.99	0.0073
Mitochondrial translation	1.90	0.0095
Protein localisation	2.06	0.0058
Extracellular matrix organisation	1.91	0.0099
Gluconeogenesis	1.92	0.0114
Regulation of IGF transport and uptake	2.14	0.0054
Detoxification of reactive oxygen species	2.28	0.0034
Upregulation of CCDN1 signalling	2.21	<0.0001



Pathway enriched	NES	FDR adjusted p-value
Upregulation of RAF signalling	1.66	0.1083
Fatty acid metabolism	1.60	0.1124
Reactive oxygen species	1.55	0.2211
Peroxisome signalling	1.48	0.1744

Figure 5.9. GSEA pathway analysis of the altered proteome in response to USP2 overexpression in LNCaP cells revealed novel associations with upregulation of **CCDN1 signalling and fatty acid metabolism**. (A) The pathways presented were significantly enriched (FDR-adjusted p-value <0.05). (B) The pathways presented were significantly enriched ($0.05 < \text{FDR-adjusted p-value} < 0.25$).

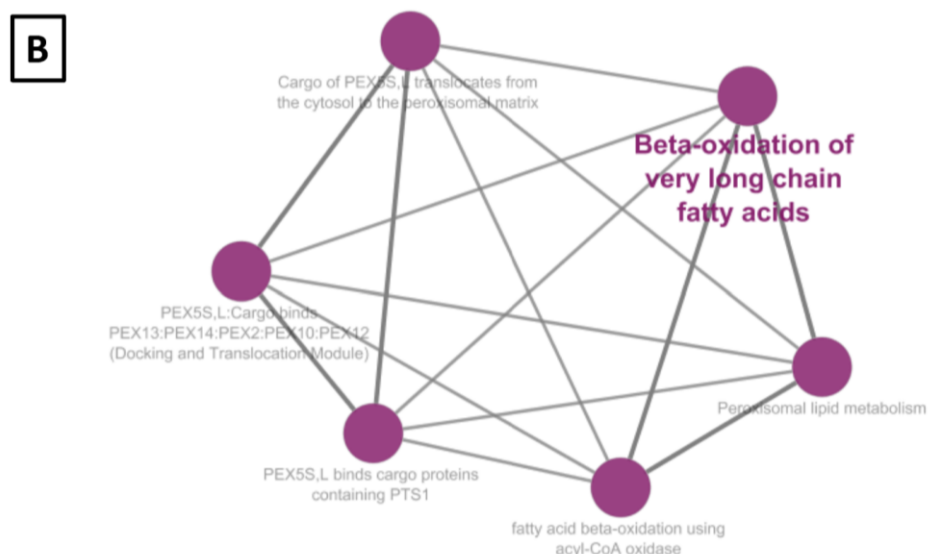
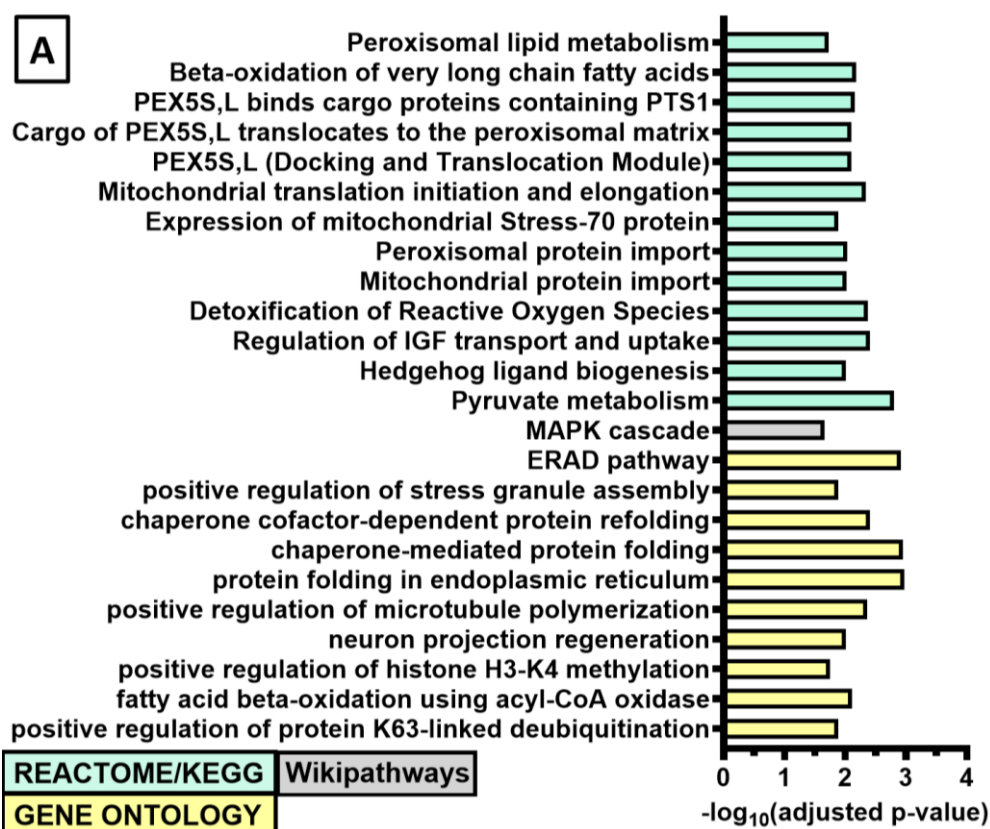
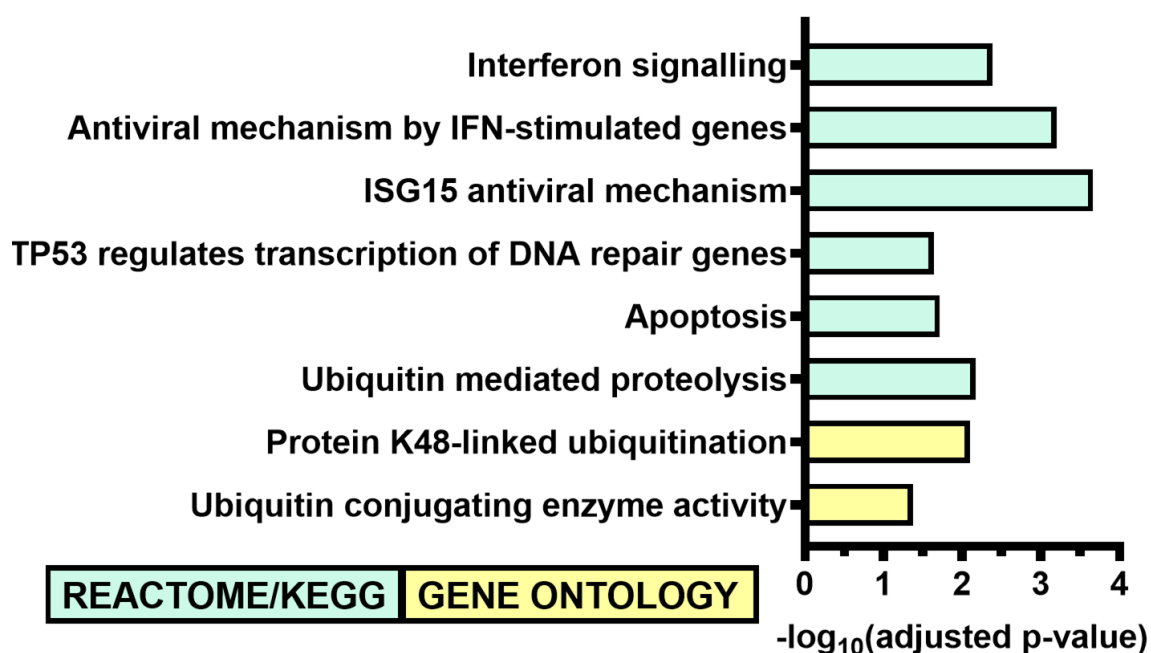


Figure 5.10. Elevated USP2 expression in LNCaP cells is associated with activation of neuroendocrine-associated signalling and lipid metabolism. (A) Pathway analyses via ClueGO was conducted using the list of proteins that were significantly elevated in the USP2-OE LNCaP cells. Displayed pathways are significantly enriched (adjusted p-value < 0.05). (B)

Pathways related to beta-oxidation of very long chain fatty acids were highlighted. The larger the size of the node, the higher the enrichment significance of the terms. The thicker the connecting line, the stronger the association strength between the terms.

A



B

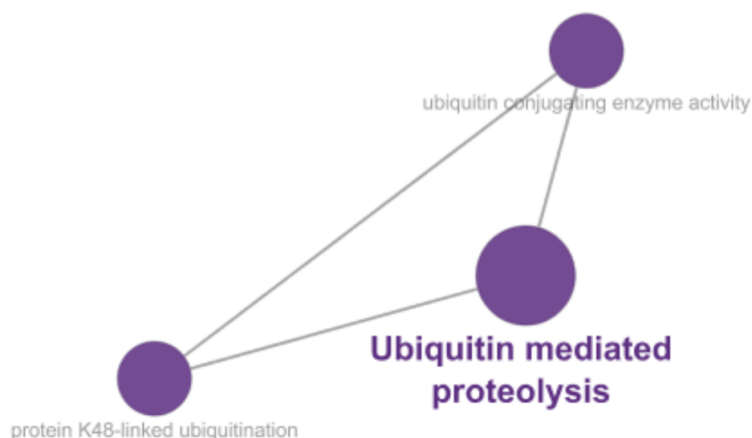


Figure 5.11. Elevated USP2 expression in LNCaP cells is associated with inhibition of protein ubiquitination, apoptosis, and interferon signalling. (A) Pathway analyses via ClueGO was conducted using the list of proteins that were significantly reduced in the USP2-OE LNCaP cells. Displayed pathways are significantly enriched (adjusted p-values < 0.05). (B) Pathways related to ubiquitin mediated proteolysis were highlighted. The larger the size of the node, the higher the enrichment significance of the terms. The thicker the connecting line, the stronger the association strength between the terms.

5.3.6 Analyses of the global transcriptome when LNCaP cells overexpress USP2

To identify transcripts that had significant changes in expression in LNCaP cells when USP2 is elevated, RNA-seq was used to profile the transcriptome in LNCaP cells overexpressing USP2 (USP2-OE) or the neon transgene (control). Across the six samples, the average number of mapped reads was 73.2 million, which corresponds to an average of 97.82% mapped reads (**Table 5.3**). The minimum percentage of mapped reads in the transcriptomics data was 97.42% (**Table 5.3**). Despite the variability between replicates, the principal component analysis (PCA) still categorised the transcriptomes of the USP2-OE LNCaP cells and the control LNCaP cells as two distinct groups (**Figure 5.12**).

Table 5.3. Number of transcripts detected in the LNCaP overexpressing the neon transgene (control) or USP2 (USP2-OE) when these cells were grown in media supplemented with full serum.

Sample Name	Total Reads	Mapped Reads	Mapped Reads (%)	Uniquely mapped (%)	Multi mapped (%)	Unmapped reads	Unmapped (%)
Control Replicate 1	7.24E+07	7.07E+07	97.63%	90.80%	6.83%	1.72E+06	2.37%
Control Replicate 2	7.40E+07	7.24E+07	97.88%	92.25%	5.64%	1.57E+06	2.12%
Control Replicate 3	7.19E+07	7.02E+07	97.70%	92.15%	5.55%	1.65E+06	2.30%
USP2-OE Replicate 1	8.67E+07	8.45E+07	97.42%	92.28%	5.14%	2.24E+06	2.58%
USP2-OE Replicate 2	7.30E+07	7.16E+07	98.17%	91.42%	6.75%	1.34E+06	1.83%
USP2-OE Replicate 3	7.10E+07	6.97E+07	98.12%	91.18%	6.94%	1.34E+06	1.88%

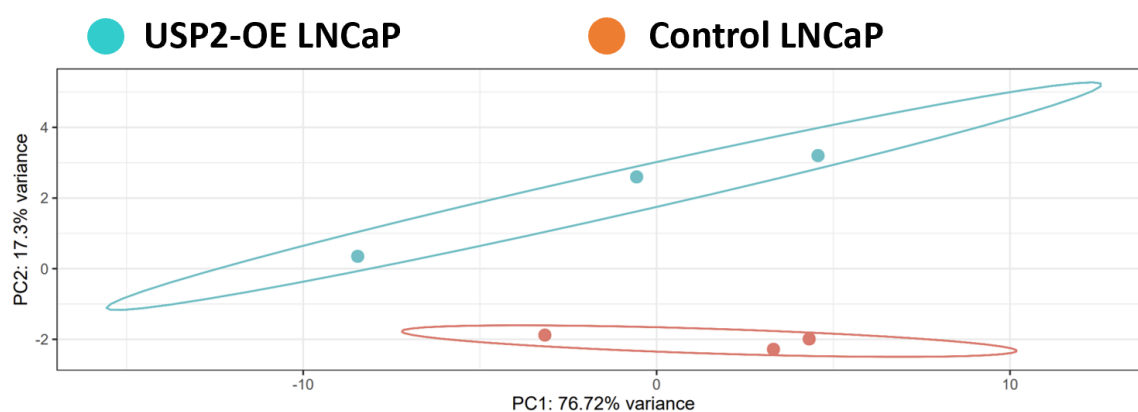


Figure 5.12. Principal component analysis of the global transcriptome grouped the transcriptomes of the LNCaP cells overexpressing USP2 (USP2-OE) and LNCaP cells overexpressing the neon transgene (control) into two clear clusters. The probability ellipsoids indicate the 95% confidence interval used to group the samples.

The volcano plot depicted the changes in transcript abundance in response to overexpression of USP2 in adenocarcinoma LNCaP cells (**Figure 5.13**). There were 433 transcripts that were significantly upregulated and 358 transcripts that were significantly downregulated (**Figure 5.13; Supplementary Table 7.5**).

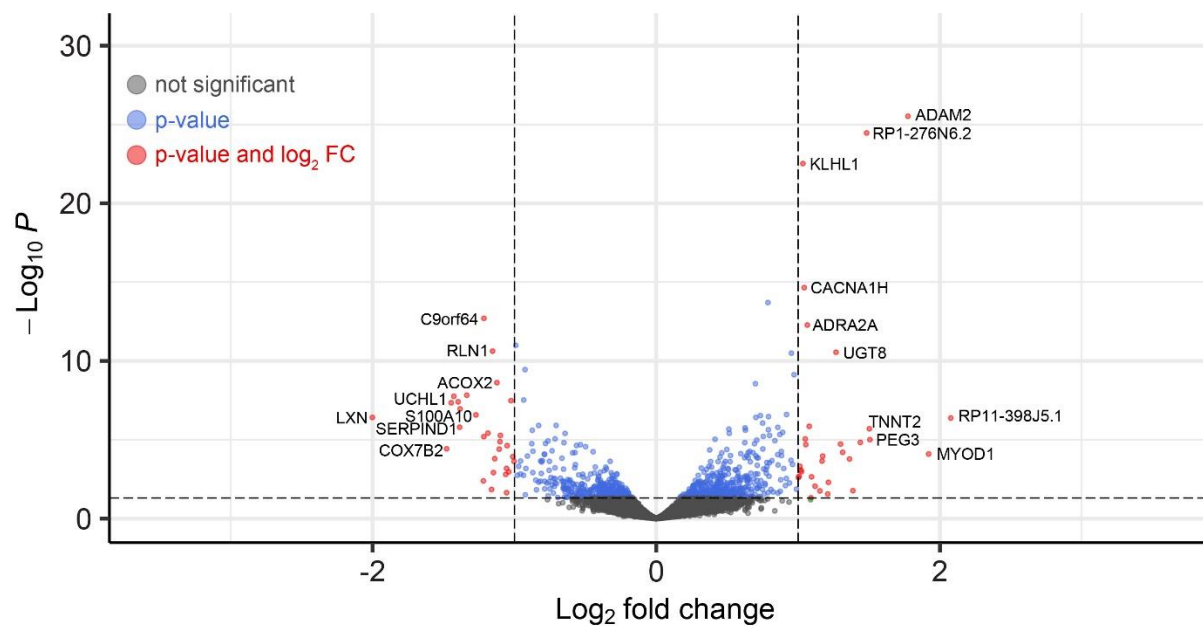
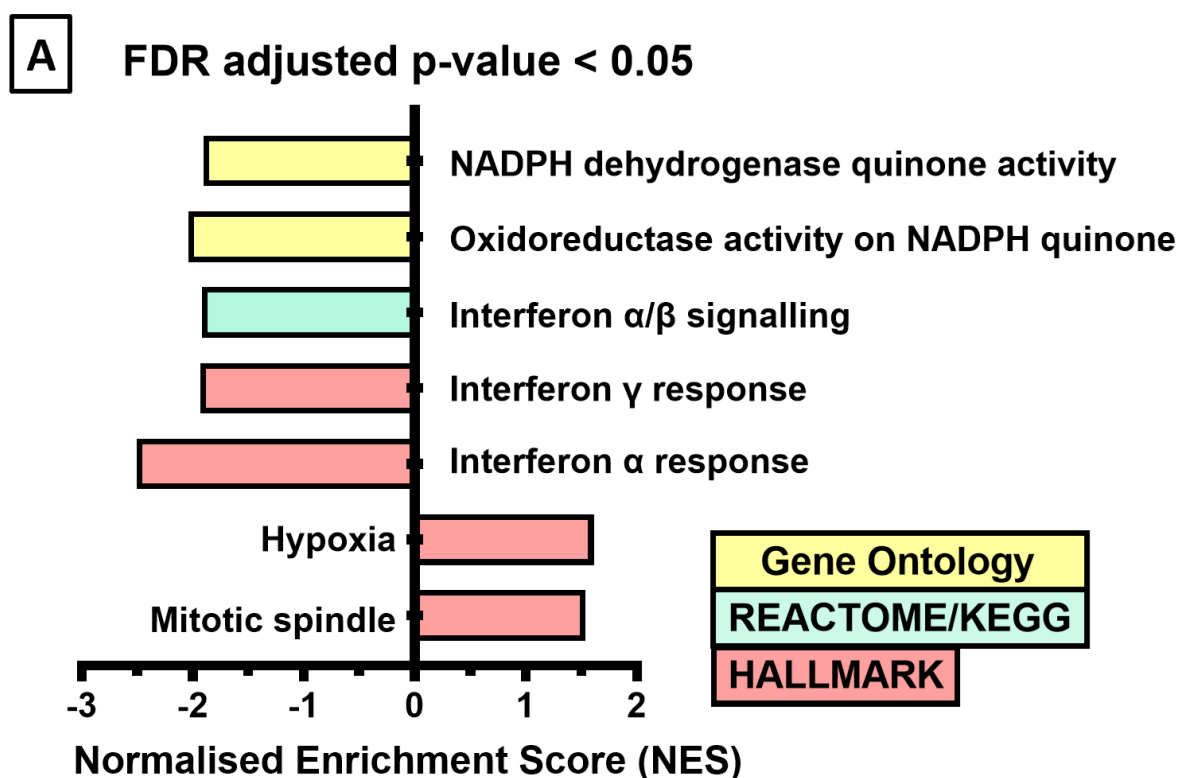


Figure 5.13. Volcano plot of transcripts at different abundance levels between the USP2-OE LNCaP cells and the control LNCaP cells. These transcripts were calculated as a ratio of the transcript levels in the USP2-OE LNCaP cells over the control group. The transcripts that had \log_2 (fold change) ≥ 1 and p-value < 0.05 were indicated in red dots.

GSEA analysis of the transcriptomic data was conducted to systematically identify the biological pathways that USP2 can influence. This strategy revealed that hypoxia and mitotic spindle pathways were significantly positively enriched in LNCaP cells overexpressing USP2 (FDR-adjusted p-value <0.05) (**Figure 5.14**). A lower parameter (FDR-adjusted p-value < 0.05) was chosen due to the moderate variation observed among replicates (**Figure 5.12**). Furthermore, these GSEA analyses were supported by the ClueGO analyses of proteins that were significantly increased or reduced (**Figure 5.15** and **Figure 5.16**).

Pathway analyses, via ClueGO, of transcripts that were significantly increased in USP2-OE LNCaP cells unveiled enrichment of glycolysis, fatty acid metabolism, neuron/cell projection and mesenchymal cell migration (**Figure 5.15**). There was also enrichment of cellular response to hypoxia and signalling pathways, such as the HIF-1, EGFR, ERBB, MAPK, Hippo and WNT signalling pathways (**Figure 5.15**).

Regarding the transcripts that were significantly reduced in USP2-OE LNCaP cells, pathway analyses via ClueGO uncovered enrichment of interferon signalling and expression of interferon-induced genes (**Figure 5.16**). This supported the negative enrichment of interferon signalling when the global transcriptome of USP2-OE LNCaP cells was analysed using GSEA (**Figure 5.14**). These results also supported the GSEA and ClueGO analyses on the proteomes of USP2-OE LNCaP cells (**Figure 5.9, Figure 5.11**).



B

Pathway name	NES	FDR-adjusted p-value
NADPH dehydrogenase quinone activity	-1.90	0.0204
Oxidoreductase activity on NADPH quinone	-2.04	0.0022
Interferon α/β signalling	-1.92	0.0124
Interferon γ response	-1.93	< 0.0001
Interferon α response	-2.50	< 0.0001
Hypoxia	1.61	0.0424
Mitotic spindle	1.54	0.0320

Figure 5.14. GSEA analysis of transcriptomic data conducted on LNCaP cells overexpressing USP2 (USP2-OE) versus LNCaP cells overexpressing the neon transgene (control) revealed associations of USP2 with inhibition of Interferon signalling and activation of hypoxia and

mitotic spindle pathways. (A) The pathways presented are significantly enriched (FDR-adjusted p-value < 0.05). (B) Further description on the normalised enrichment scores (NES), FDR-adjusted p-values for the enriched pathways shown in (a).

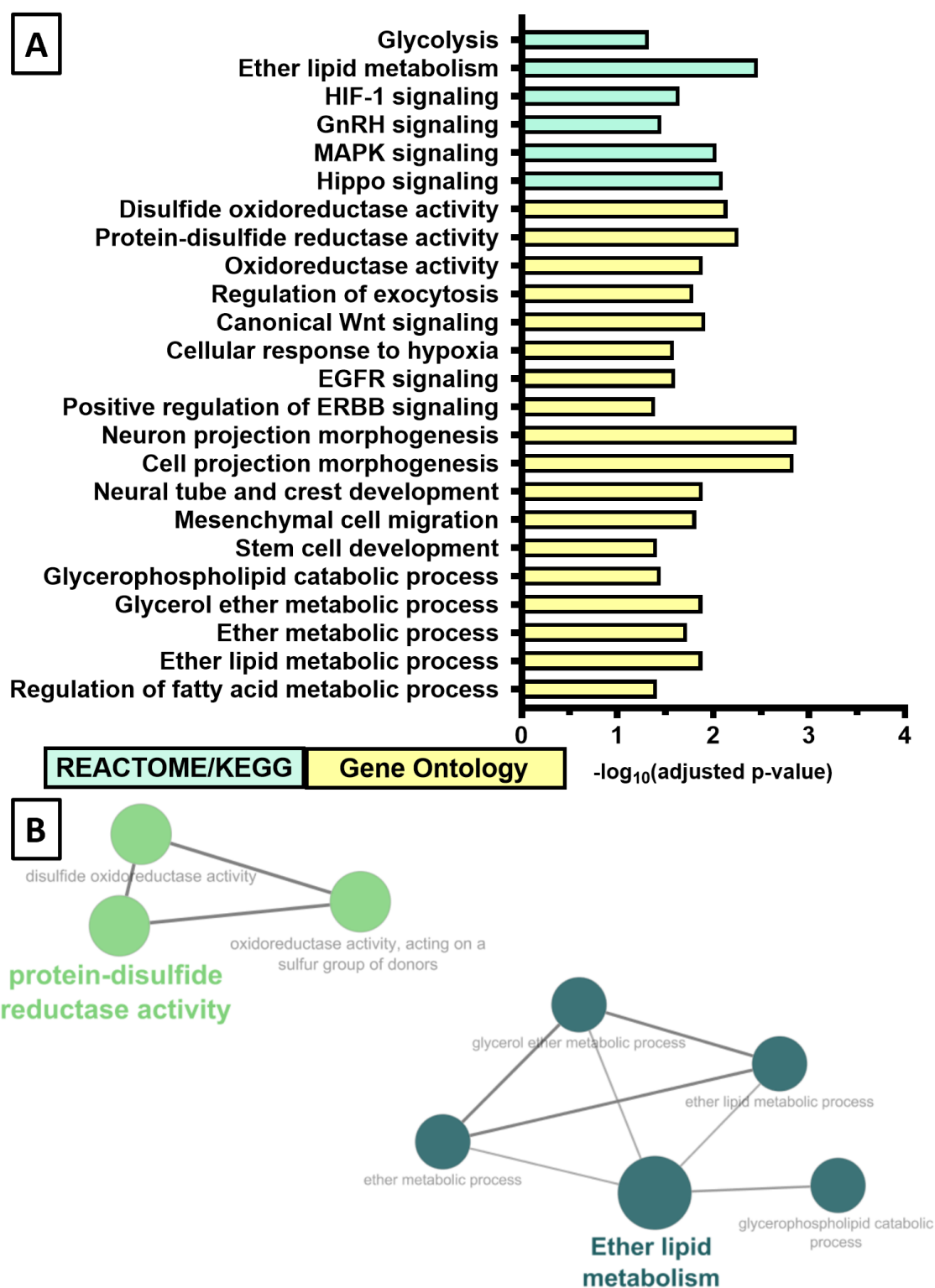
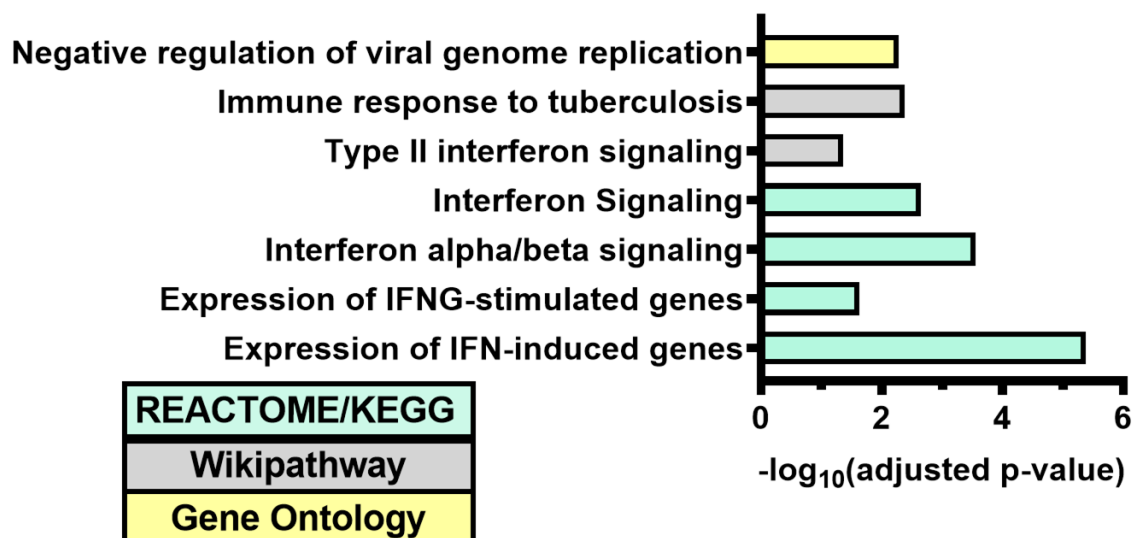


Figure 5.15. Elevated USP2 expression in LNCaP cells is associated with activation of neuroendocrine-associated signalling and fatty acid metabolism. (A) Pathway analyses via ClueGO was conducted using the list of genes that were significantly elevated in USP2-OE

LNCaP cells. Displayed pathways are significantly enriched (adjusted p-values < 0.05). (B) Pathways related to protein-disulfide reductase activity and ether lipid metabolism were highlighted. The larger the size of the node, the higher the enrichment significance of the terms. The thicker the connecting line, the stronger the association strength between the terms.

A



B

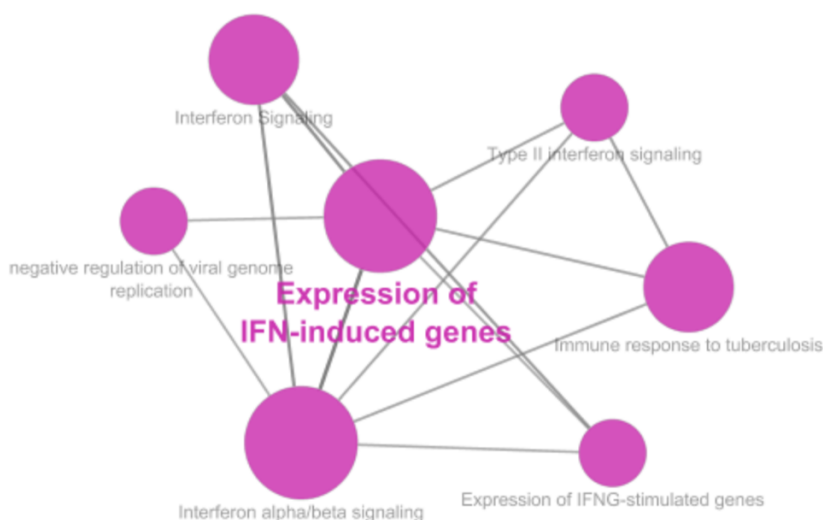


Figure 5.16. Elevated USP2 expression in LNCaP cells is associated with inhibition of interferon signalling and expression of interferon-induced genes. (A) Pathway analyses via ClueGO was conducted using the list of genes that were significantly reduced in USP2-OE LNCaP cells. Displayed pathways are significantly enriched (adjusted p-values < 0.05). (B) Pathways related to expression of IFN-induced genes were highlighted. The larger the size of the node, the higher the enrichment significance of the terms. The thicker the connecting line, the stronger the association strength between the terms.

5.3.7 Integration of the three sets of proteomics and transcriptomics

expression data

As a first step to integrate the data from the 3 separate -omics experiments, we overlapped the proteins that were found to be reduced in cells treated with ML364 and elevated in LNCaP cells overexpressing USP2. There were 13 proteins that overlapped between the two sets of proteomes (**Figure 5.17A**). We then incorporated the transcriptomic data and found no significant changes in transcript levels between the experimental and control groups for those high priority candidates (FDR-adjusted p-values close to 1) (**Table 5.4**). The cellular functions associated with those 13 protein candidates were described (**Figure 5.18**), with several of these proteins being associated with chemotherapy resistance and neuroendocrine tumours. The roles of these proteins were further discussed in Chapter 5 Section 5.4.

There were 585 genes encoding proteins that overlapped between the proteome and transcriptome of USP2-OE LNCaP cells. Out of those 585 genes, the transcription of only 2 genes were significantly changed (\log_2 fold change > 1 and p-value < 0.05) (Table 5.5). Those two genes were *GAGE1* and *PEG3* (**Table 5.5**). This indicates that *GAGE1* and *PEG3* are not regulated by USP2, as USP2 functions at the post-translational level through the removal of ubiquitin groups from proteins.

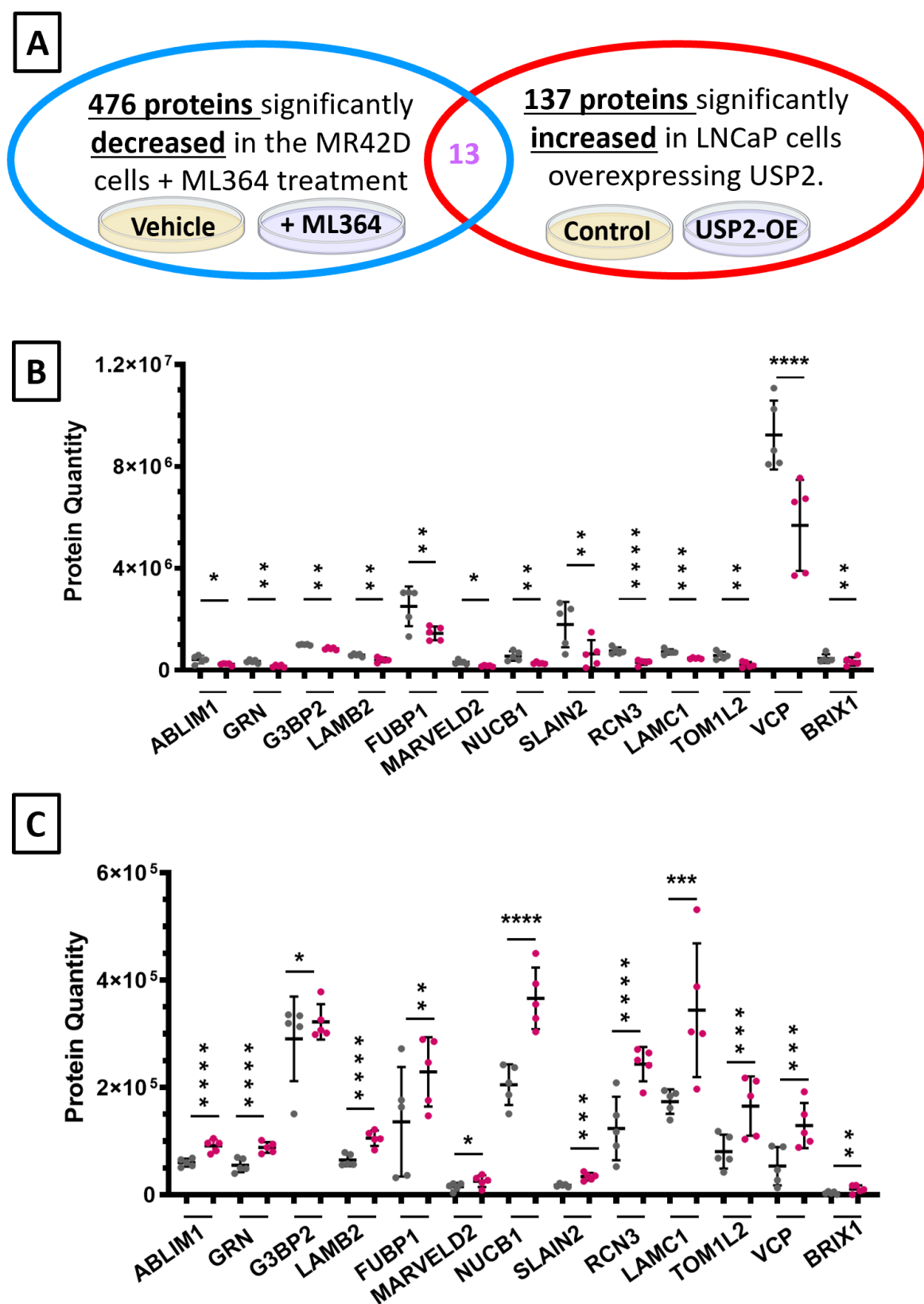


Figure 5.17. Thirteen proteins were identified as potential novel USP2 substrates. (A) Venn diagram showing the overlap between the two sets of proteomes. The first set of proteome

was the list of 476 proteins that were significantly reduced (average log₂ fold change < -0.5) in MR42D cells treated with 24 hours of 5uM ML364. The second set of proteome is the list of 137 proteins that were significantly increased (average log₂ fold change > 0.5) in LNCaP cells overexpressing USP2. (B) Each of the 13 overlapping proteins had reduced expression in MR42D cells treated with ML364. Statistical analysis was conducted via t-test, FDR-adjusted p-values ≤ 0.05 (*); ≤ 0.01 (**); ≤ 0.001 (***); < 0.0001 (****). (C) Each of the 13 overlapping proteins had increased expression in LNCaP cells overexpressing USP2. Statistical analysis was conducted via t-test, FDR-adjusted p-values ≤ 0.05 (*); ≤ 0.01 (**); ≤ 0.001 (***); < 0.0001 (****).

Table 5.4. Changes in transcript levels encoding potential substrates of USP2.

Protein Name	Gene (formula)	log ₂ (FoldChange)	p-value	q-value
ABLIM1	<i>ABLIM1</i>	0.1779	0.3380	0.9988
GRN	<i>GRN</i>	-0.1648	0.4058	0.9988
G3BP2	<i>G3BP2</i>	0.1552	0.5863	0.9988
LAMB2	<i>LAMB2</i>	0.1035	0.4097	0.9988
FUBP1	<i>FUBP1</i>	0.0312	0.8571	0.9988
MARVELD2	<i>MARVELD2</i>	-0.0280	0.8928	0.9988
NUCB1	<i>NUCB1</i>	-0.0293	0.8828	0.9988
SLAIN2	<i>SLAIN2</i>	0.0802	0.6738	0.9988
RCN3	<i>RCN3</i>	0.3956	0.0598	0.9180
LAMC1	<i>LAMC1</i>	0.1313	0.4235	0.9988
TM1L2	<i>TOM1L2</i>	-0.1966	0.0380	0.7767
VCP	<i>VCP</i>	-0.0912	0.2921	0.9988
BRX1	<i>BRX1</i>	-0.1545	0.1621	0.9988

Proteins	Resistance			Literature
ABLIM1				
PGRN				(Klupp et al., 2021, Barbu et al., 2016)
G3BP2				(Fournier et al., 2010, Gareau et al., 2011, Schwed-Gross et al., 2022)
LAMB2				
FUBP1				(Venturutti et al., 2016, Liu et al., 2020)
MARVELD2				
NUCB1				(Ejtehadifar et al., 2023, Tsukumo et al., 2007)
SLAIN2				
RCN3				
LAMC1				
TM1L2				(Bucher-Johannessen et al., 2019)
VCP				
BRX1				(Paulson et al., 2018)

- Associated with chemotherapy resistance
- Associated with immunotherapy resistance
- Associated with neuroendocrine tumours

Figure 5.18. Several of these thirteen high-priority candidates as USP2 substrates were associated with neuroendocrine tumours and resistance to chemotherapy and immunotherapy. The other protein candidates remained unexplored in relation to neuroendocrine tumours, chemotherapy, or immunotherapy.

Table 5.5. Two genes were identified to have significantly changed transcript levels ($\log_2\text{foldchange} > 1$ and $p\text{-value} < 0.05$). These genes were identified by overlapping the transcriptome of USP2-OE LNCaP cell line with its proteome.

Genes	log2FoldChange	p-value
<i>GAGE1</i>	-1.10	1.32E-05
<i>PEG3</i>	1.51	9.84E-06

5.4 Discussion

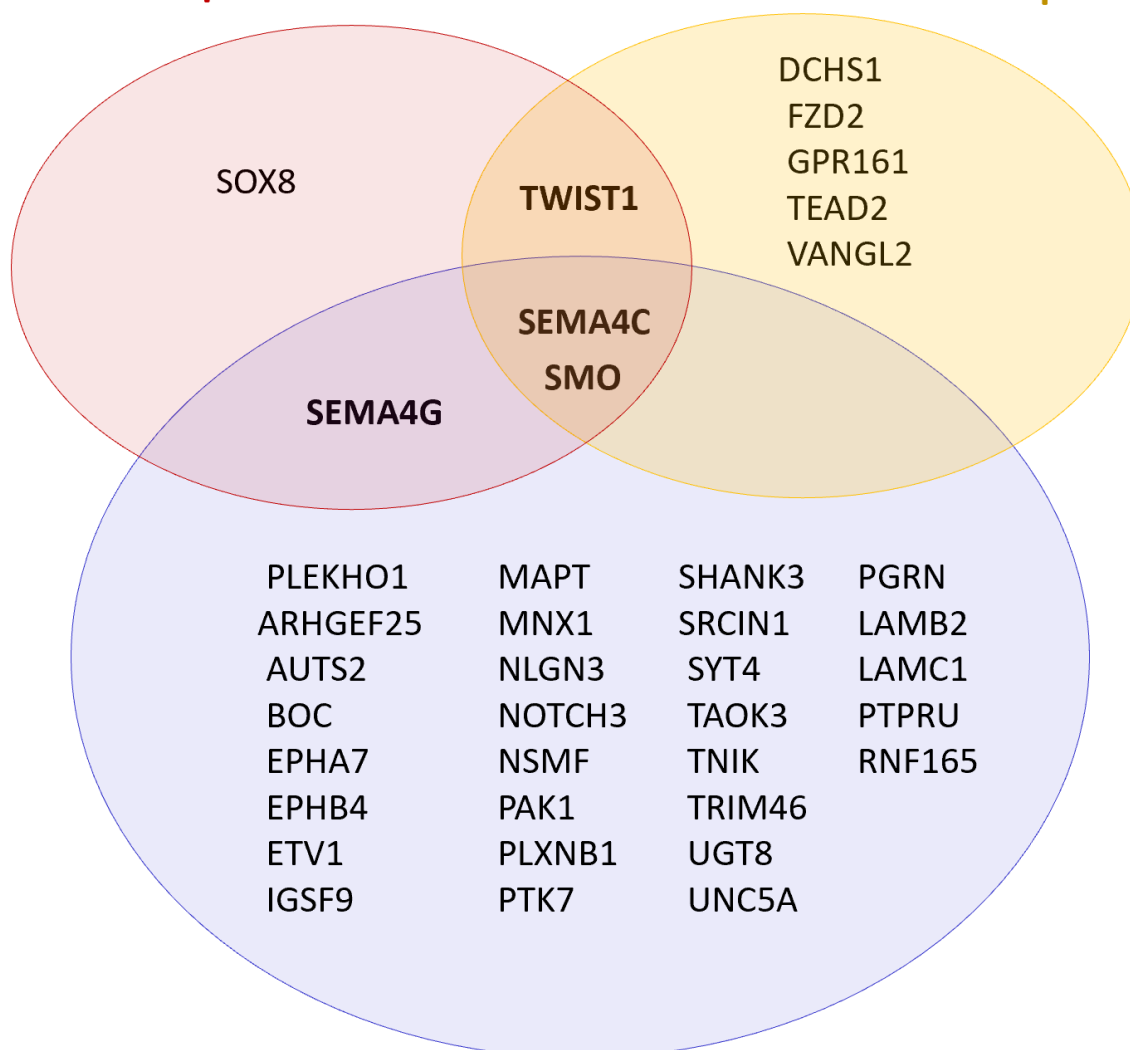
Despite our findings in Chapters 3 and 4, the precise mechanism(s) that USP2 utilises in prostate cancer to drive resistance against AR-targeted therapy and chemotherapy remain to be fully determined. In this chapter, using a series of omics experiments, we found that USP2 can be involved in a plethora of signalling pathways. Consistently, elevated USP2 expression was associated with activation of protein de-ubiquitination, which is to be expected given its enzymatic activity. Additionally, pathway analyses revealed associations of USP2 with cellular pathways such as neuroendocrine, lipid metabolism and cell cycle; these findings are significant because they support the results in Chapter 3 and 4.

Elevation of USP2 in LNCaP cells resulted in a significant activation of neuroendocrine-associated pathways (**Figure 5.10** and **Figure 5.15**). These pathways include neuron projection regeneration, neural crest development, stem cell development, mesenchymal cell, and glycolysis. Neuron projections from cancer cells indicate a neuronal or neuroendocrine (NE) phenotype (Yuan et al., 2006, Shen et al., 1997, Sánchez et al., 2020). Furthermore, a major fraction of human prostatic neuroendocrine cells and neuroendocrine tumours was identified to be neural crest-derived (Szczyrba et al., 2017, Gammill and Weichert, 1973, Adams and Bronner-Fraser, 2009, Rosai, 2011). Additionally, treatment induced NEPC exhibits metabolic reprogramming towards aerobic glycolysis (Ahmad et al., 2021, Wang et al., 2019, Choi et al., 2018). A more detailed dissection of the neuroendocrine-associated proteins/transcripts that are regulated by USP2, which were identified in this chapter from both the proteomics and transcriptomics experiments and summarised in **Figure 5.19**, will undoubtedly provide more insight into its function. For example, by identifying factors enriched in several of the major

neuroendocrine-associated pathways (**Figure 5.19**), we could prioritise TWIST1, SEMA4C, SEMA4G and SMO as factors that may play influential roles downstream of USP2 in mediating cell plasticity. PGRN/GRN and LAMB2 are also of high interest as they are part of the thirteen high priority putative substrates of USP2 (**Figure 5.18**). Collectively, our omics results suggest that elevated USP2 expression is associated with neuroendocrine signalling and these results support the findings that USP2 is a driver of the neuroendocrine phenotype in prostate cancer (refer to chapter 3 and 4).

Mesenchymal stem cell development

Neural tube development



Neuron projection morphogenesis and regeneration

Figure 5.19. Neuroendocrine- and mesenchymal-related factors that are increased with upregulation of USP2 expression in LNCaP cells.

Inhibition of USP2 by ML364 resulted in a significant downregulation of cell cycle pathways, such as G2M checkpoint and E2F targets (**Figure 5.4A**). Conversely, elevated levels of USP2 in the androgen dependent LNCaP cells resulted in significant upregulation of cell cycle pathways, such as mitotic spindle, Cyclin D1 and RAF signalling (**Figure 5.5** and **Figure 5.9**). The upregulation of mitotic spindle pathways can be facilitated by the increased expression of Aurora kinase A (AURKA). AURKA is important for the assembly and orientation of mitotic spindles (Liu and Ruderman, 2006, Asteriti et al., 2011). Meanwhile, Cyclin D1 can complex with CDK4/6 (Topacio et al., 2019, Otto and Sicinski, 2017) and activate the transcriptional activity of E2F transcription factors to promote cell cycle progression (Hurford et al., 1997, Ohtani et al., 1995). Activation of the E2F signalling can also further amplify the Cyclin D1 signalling pathway (Lee et al., 2000, Hydbring et al., 2016, Ohtani et al., 1995). Activation of the RAF signalling pathway often results in enhanced cellular proliferation, increased protein synthesis and reduced sensitivity to agents that induces apoptosis (Steelman et al., 2011, Wang and Proud, 2002). Collectively, our proteome data supports our key findings in previous chapters that increased expression of Cyclin D1 and Aurora kinase A in LNCaP cells overexpressing USP2 is important for cell viability and proliferation.

Elevation of USP2 levels in LNCaP cells resulted in a positive enrichment of peroxisomal (**Figure 5.9**) and fatty acid metabolism pathways (**Figure 5.5, Figure 5.10, Figure 5.15**). Lipid metabolism is often dysregulated in prostate cancer (Butler et al., 2021, Hoy et al., 2021), while peroxisomes are essential for the oxidative metabolism of both linear and branched forms of very long chain fatty acids (vLCFAs) (≥ 22 carbons) (Singh et al., 1992, Lazarow and De Duve, 1976, Mihalik et al., 1995) (Morita and Imanaka, 2012, Jakobs and

Wanders, 1995) into long-chain acyl-CoA fatty acids and acetyl-CoA that can fuel proliferation of cancer cells and tumorigenesis (Butler et al., 2021, Hoy et al., 2021, Jakobs and Wanders, 1995). Additionally, dysregulation of lipid metabolism has been associated with the development of resistance to AR antagonists (Lin et al., 2021) and chemotherapy (Scheinberg et al., 2023, Butler et al., 2020, Rysman et al., 2010, Hoy et al., 2021, Princová et al., 2023, Wilson et al., 2022). Our results suggests that USP2 might be regulating the stability of enzymes important in lipid metabolism, such as acyl-CoA oxidase 1 (ACOX1), catalase (CAT) and peroxisomal 2,4-dienoyl-CoA reductase (DECR2). Through USP2 stabilisation of these enzymes, USP2 can promote cancer proliferation, survival and resistance to AR-antagonist and chemotherapy.

Elevated expression of USP2 in LNCaP cells resulted in a negative enrichment with innate immunity signalling cascades, such as Toll like receptor(s) (TLRs) and interferon (IFN) (**Figure 5.11, Figure 5.16**). In many studies, TLR signalling had been demonstrated to exert an anti-tumour effect (Javaid and Choi, 2020, Brignole et al., 2010, Urban-Wojciuk et al., 2019, Xun et al., 2021, Meyer and Stockfleth, 2008, Krieg, 2007, Karapetyan et al., 2020). Downregulation of TLR signalling in USP2-OE LNCaP cells could partly explain the downregulation of interferon signalling cascade (Xun et al., 2021). Cancer cells often downregulate IFN signalling to evade the anti-tumour effects of IFN (Boukhaled et al., 2021, Budhwani et al., 2018, Alavi et al., 2018). Interferons could inhibit the angiogenesis of tumour cells (Berger et al., 2011, Kitamura et al., 2015, Boukhaled et al., 2021, Katlinskaya et al., 2016). Downregulation of IFN could also promote the establishment of an immune privileged tumour microenvironment (Katlinski et al., 2017, Hirata et al., 2019) and has been associated with immunotherapy resistance (Katlinski et al., 2017, Alavi et al., 2018, Uehara et al., 2017,

Zhang et al., 2020b, Liang et al., 2018). Therefore, our results suggest that USP2 can partly mediate an aggressive phenotype and the development of therapy resistance through stabilising factors important in the inhibition of innate immunity pathways.

Inhibition of protein ubiquitination pathways were significantly enriched when MR42D cells were treated with ML364 (**Figure 5.4**) or when USP2 is overexpressed in LNCaP cells (**Figure 5.9, Figure 5.11**). For the former finding, inhibition of the ubiquitination pathway might arise because of high levels of accumulated protein ubiquitination in cells, where USP2 is unable to cleave ubiquitin molecules from its substrates. For the latter finding, inhibition of the ubiquitination pathway might arise because of cross talk between USP2 and ubiquitin ligases (Oh et al., 2011, Zhang et al., 2021).

By comparing the two sets of proteomics data and the transcriptomic data, we identified thirteen high-priority candidate substrates of USP2. Several of these proteins, such as Progranulin (PGRN), Ras-GTPase activating protein SH3 domain-binding protein 2 (G3BP2), Far upstream element-binding protein 1 (FUBP1), Nucleobindin-1 (NUCB1) and TOM1-like protein 2 (TM1L2), have been associated with chemotherapy resistance. Progranulin is highly expressed in colorectal tumours from patients who had undergone neoadjuvant chemotherapy and is associated with impaired overall survival of patients (Klupp et al., 2021). G3BP2 is a core protein involved in the formation of stress granules (SG) that can mediate resistance against chemotherapy (Fournier et al., 2010, Gareau et al., 2011) in osteosarcoma (U2OS) and mouse embryonic fibroblasts (MEFs) (Schwed-Gross et al., 2022). FUBP1 is highly expressed in ERBB2+ breast tumours and is associated with significantly shorter disease-free survival for patients (Venturutti et al., 2016, Liu et al., 2020). FUBP1 can target matrix metalloproteinase 2 (MMP2) and c-Myc to enhance breast cancer metastasis and resistance

to chemotherapy, such as cisplatin (Liu et al., 2020), or to drugs that are typically used in conjunction with chemotherapy (Venturutti et al., 2016). NUCB1 can activate breast cancer cell metastasis by promoting the trafficking of MMPs along the Golgi apparatus. NUCB1 was identified as a potential drug resistance biomarker in diffuse large B cell lymphoma (Ejtehadifar et al., 2023). Through NUCB1 inhibition of the activating transcription factor 6 (ATF6), NUCB1 can suppress the unfolded protein response (UPR) (Tsukumo et al., 2007), which can result in the dampening of UPR-induced apoptosis (Ejtehadifar et al., 2023). Methylation of the *TOM1L2* gene in testicular cancer was found to be higher in patients who received cisplatin-based chemotherapy than untreated, and had been associated with increased risk of developing metabolic syndrome and relapse of cancer (Bucher-Johannessen et al., 2019). Collectively, USP2 is posited to mediate chemotherapy resistance through stabilising these high-priority candidates.

Several of these high-priority candidates are also associated with neuroendocrine tumours and immunotherapy resistance. Barbu *et. al.* (2016) suggested that Progranulin (PGRN) was associated with neuroendocrine tumours. PGRN was upregulated in the tumours of MEN1+/- mouse and in the serum of patients with pancreatic neuroendocrine tumours (Barbu et al., 2016). Another factor associated with neuroendocrine tumours is BRX1 (Paulson et al., 2018). *BRX1* was identified via single cell RNA-sequencing to be elevated in a patient with relapsed Merkel cell carcinoma, which is a type of neuroendocrine skin cancer (Paulson et al., 2018). Furthermore, this patient had been treated with immunotherapy prior to relapse, thereby associating BRX1 with immunotherapy resistance (Paulson et al., 2018). As a result, USP2 is postulated to orchestrate the development of the neuroendocrine phenotype through stabilising these high-priority candidates.

A strength of this study is the ability to compare and integrate different sets of -omics data. A limitation of this study is that the protein/gene candidates are yet to be further validated. Future work can be conducted to validate some of the protein candidates as direct substrates of USP2 in prostate cancer. This objective can be achieved by immunoprecipitation of the FLAG-USP2 fusion protein and probing for the protein candidates via Westerns. Alternatively, we could use an affinity-based ubiquitinated peptide enrichment proteomics approach to systematically quantify the ubiquitinome changes after manipulations of USP2 expression in the neuroendocrine-like MR42D cells.

In summary, the analyses of the proteomics and transcriptomics data unveiled new potential roles of USP2 in pathways such as neuroendocrine differentiation, lipid metabolism, cell cycle and interferon signalling in prostate cancer. These analyses also demonstrated that USP2 is also associated with cellular processes such as the epithelial-to-mesenchymal transition. These mechanisms posit USP2 as an important factor for influencing prostate cancer growth and progression. Critically, our omics analyses were consistent with USP2 function as a de-ubiquitylating enzyme and its importance in cancer (refer to chapter 1 section 1.13 and 1.15).

Chapter 6: Discussion

6 Discussion

Prostate cancer (PCa) is the fourth most diagnosed cancer in the world, with the highest incidence occurring in Australia and New Zealand. The growth of prostate tumours relies on the activation of the androgen receptor by male sex hormones, called androgens (Centenera et al., 2018b). Therefore, the standard-of-care treatment for patients with metastatic PCa is androgen deprivation therapy (ADT), which inhibits AR activity (Huggins et al., 1941, Cornford et al., 2017) (**Chapter 1 section 1.8.2**). However, these patients will eventually develop a lethal therapy-resistant form of the disease, termed castration-resistant prostate cancer (CRPC) (Centenera et al., 2018b). The AR signalling axis is altered in CRPC to confer resistance to AR-targeted therapies (**Chapter 1 section 1.9.1**) (Centenera et al., 2018b).

A subset of CRPC may evade inhibition of AR by ADT through becoming AR-independent, which is termed as neuroendocrine PCa (NEPC). Treatment-emergent neuroendocrine PCa occurs in approximately 15 to 20% of patients with adenocarcinoma CRPC (Bluemn et al., 2017, Aggarwal et al., 2018, Abida et al., 2019, Beltran and Demichelis, 2021, Wang et al., 2021b, Zhang et al., 2020c, Yao et al., 2021).

The body of work described in this thesis stemmed from the urgent need to identify drivers of resistance to AR-targeted therapies, including those factors that cause the emergence of NEPC. We were fortunate to have access to a transcriptomic dataset in which patients' tumours were treated *ex vivo* with a clinical AR antagonist, enzalutamide. This dataset revealed that *Ubiquitin specific protease 2 (USP2)* was upregulated in response to enzalutamide (Chapter 3 Figure 3.1). Given the many examples of USPs having oncogenic roles in various tumour types (Chapter 1), this led to the hypothesis that USP2 is important for the growth and survival of prostate cancer and can mediate resistance to AR-targeted

therapies and a project aimed at testing that hypothesis. Our findings demonstrated that USP2 is upregulated in response to AR-targeted therapies, drives epithelial-neuroendocrine plasticity via major alterations to the PCa proteome and transcriptome and can be targeted to inhibit PCa growth (**Figure 6.1**).

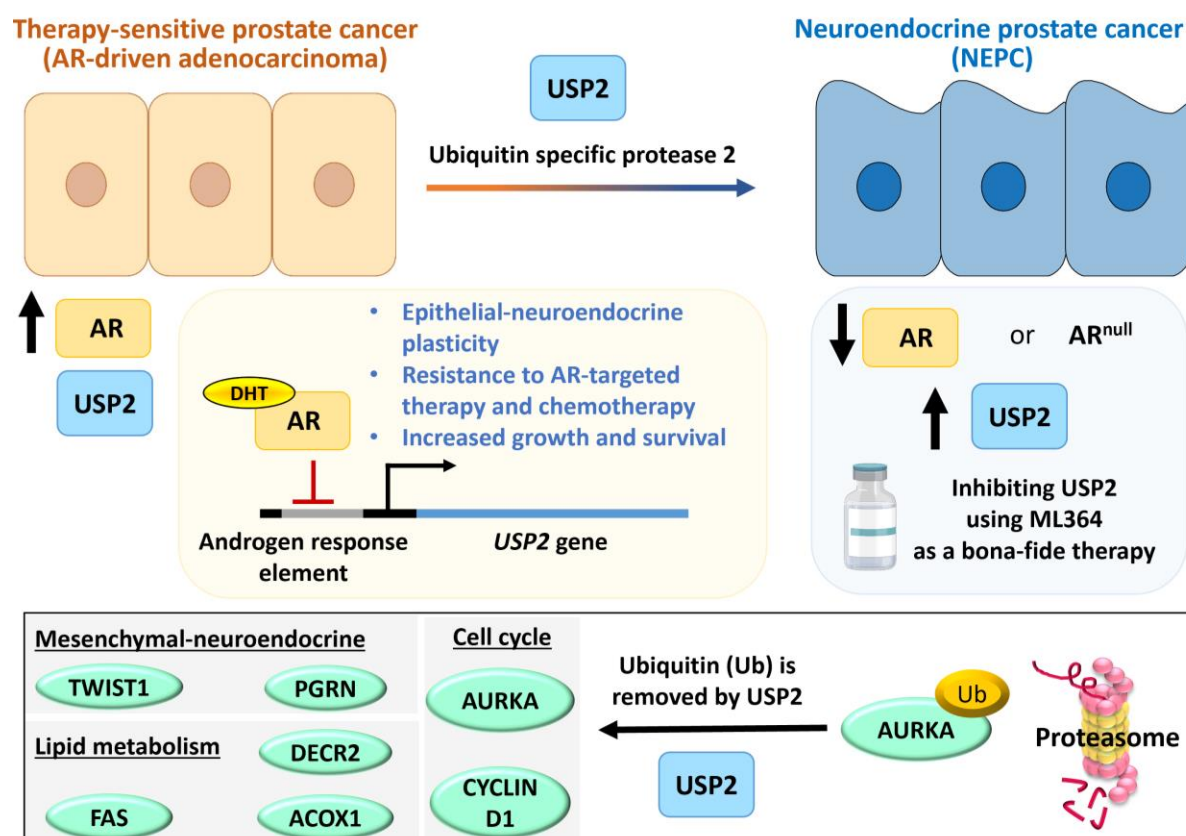


Figure 6.1. Diagram summarising the key findings in my PhD dissertation. The activated androgen receptor (AR) is identified to inhibit *USP2* expression. Conversely, AR inhibited by enzalutamide resulted in an increase in *USP2* expression in patient tumours. Elevated *USP2* expression in LNCaP cells (*USP2*-OE) resulted in induction of epithelial-neuroendocrine plasticity, resistance to AR-targeted therapy and chemotherapy and increased growth and survival. The effects of *USP2* could be mediated through *USP2* stabilisation of its substrates. Inhibiting *USP2* in a mouse model of AR-null PC3 cells was effective, thereby suggesting the potential of ML364 as a bona-fide therapy.

6.1 USP2 can drive the development of treatment-emergent neuroendocrine phenotype and confers therapy resistance.

This is the first study demonstrating that *USP2* expression as being increased in patient tumours and prostate cancer cell lines treated with AR-targeted therapies (Chapter 3). Conversely, treatment with DHT resulted in reduction in *USP2* expression (Chapter 3). This phenomenon is unlike the findings for other USPs, such as *USP10*, *USP12*, *USP22* and *USP26* (Takayama et al., 2018, Draker et al., 2011, Burska et al., 2013, McClurg et al., 2015, Schrecengost et al., 2014, Dirac and Bernards, 2010). Those USPs were reported to be positively regulated by the androgen receptor, and increased expression of those USPs also resulted in increased AR stability and activity (Takayama et al., 2018, Draker et al., 2011, Burska et al., 2013, McClurg et al., 2015, Schrecengost et al., 2014, Dirac and Bernards, 2010).

There is an apparent trend that AR-repressed genes become important drivers of prostate cancer progression and therapy resistance after the AR pathway is inhibited. A classic example of a gene that is de-repressed after the AR pathway is targeted is *EZH2* (Davies et al., 2021). The de-repression of *EZH2* resulted in the induction of lineage infidelity and plasticity, which promotes emergence of treatment-resistant tumours with neuroendocrine features (Davies et al., 2021). Another classic example is the master neural transcription factor, *BRN2* (Bishop et al., 2017). *BRN2* was demonstrated to mediate resistance to enzalutamide and is required for neuroendocrine differentiation (Bishop et al., 2017). Similarly, the body of work in this thesis suggest that *USP2* is a novel AR-repressed gene that following enzalutamide treatment, its expression is de-repressed and potentially drives cancer progression.

To the best of our knowledge, this is also the first study to demonstrate USP2 as a direct driver for neuroendocrine differentiation and orchestrator of the epithelial-to-mesenchymal (EMT) transition in prostate cancer. In the context of the broader literature, several USPs have been associated as mediators of EMT in non-prostatic types of cancer. Examples of these USPs are USP1 (Meng and Li, 2022) , USP3 (Fan et al., 2019, Fang et al., 2018) , USP4 (Zhang et al., 2012, Pu et al., 2022) , USP5 (Xue et al., 2020) , USP7 (Zeng et al., 2019) , USP9X (Chen et al., 2019) , USP13 (Gao et al., 2020) , USP15 (Xu et al., 2018, Zhong et al., 2021) , USP17 (Yildirim et al., 2019) , USP18 (Cai et al., 2020, Song et al., 2021) , USP21 (Chen et al., 2017b) , USP22 (Zhang et al., 2017) USP47 (Silvestrini et al., 2020, Choi et al., 2017). Mechanistically, USP5, USP7 and USP15 can induce EMT through the activation of WNT/ β -catenin signalling pathway (Xue et al., 2020, Zeng et al., 2019, Zhong et al., 2021). Given that USP2 is associated with positive enrichment with WNT signalling pathway (chapter 5), it is postulated that USP2 could be inducing EMT through activation of WNT signalling in prostate cancer. However, USP2 is the only ubiquitin-specific protease to be implicated as driver for both the neuroendocrine phenotype and EMT.

Future work could be conducted to provide further evidence that USP2 directly drives the neuroendocrine phenotype. The first proposed experiment is to culture LNCaP cells in androgen deprived conditions and inhibit USP2 using ML364. The objective of the experiment is to investigate whether USP2 is required for the acute transition into the neuroendocrine phenotype. The second proposed experiment is to conduct chromatin immunoprecipitation sequencing (ChIP-seq) for H3K27-trimethylation (H3K27me3) and H3K4-trimethylation (H3K4me3). The experimental objective is to determine if there was a switch from the repressive H3K27me3 mark to the active H3K4me3 mark near the promoters of stem cell

reprogramming factors and neuroendocrine lineage markers as described in (Shamma et al., 2013). Given that inactivation of RB1 and PTEN correlated with increased *USP2* expression in prostate tumour models (**Figure 3.15**) and there is enrichment of histone H3-K4 methylation in *USP2*-OE LNCaP cells (**Figure 5.10**), these results provide rationale to conduct the aforementioned ChIP-seq.

The third proposed experiment is to assess *USP2* in *in vivo* prostate carcinoma models of epithelial-neuroendocrine plasticity such as mouse models of prostate adenocarcinoma containing loss of function mutations in the tumour suppressor genes *Pten*, *Rb1* genes and *Trp53* gene (*Pten^{f/f} RB1^{f/f} Trp53^{f/f}*). Loss of PTEN, RB1 and P53 resulted in the induction of lineage plasticity of prostate adenocarcinoma into neuroendocrine PCa and the development of resistance to anti-androgen therapy (Ku et al., 2017). The objective of the *Pten^{f/f} RB1^{f/f} Trp53^{f/f}* mouse model is to assess if deletion or inhibition of *USP2* can block tumour growth, progression, and emergence of NEPC. The expression of AR, luminal lineage markers and neuroendocrine lineage markers and AR activity can be measured to investigate if inhibition of *USP2* can reverse or suppress lineage transformation of NEPC variants *in vivo*.

Other future experiments can be to conduct single-cell RNA sequencing (scRNA-seq) on prostate tumours. These prostate tumours could be harvested from the *in vivo* PCa models of epithelial-neuroendocrine (*Pten^{f/f}; Rb1^{f/f}; Trp53^{f/f}*) followed by deletion or inhibition of *USP2* by ML364 or si*USP2*. scRNA-seq can classify, characterise, and distinguish the transcriptomes of each cell and this can enable identification of various functional cell populations in the neuroendocrine prostate tumour (Jovic et al., 2022). The primary objective of this experiment is to identify signatures of NEPC in these tumours following manipulations of *USP2*. The secondary experimental objective is to investigate the cellular network directing

neuroendocrine trans-differentiation following USP2 manipulations in patients' tumours. Overall, the single-cell characterisation of the spatiotemporal dynamics of neuroendocrine prostate tumours can offer new perspective on USP2 as a potential novel prognostic biomarker of NEPC.

6.2 USP2 is a bona fide therapeutic target in prostate cancer.

Importantly, we demonstrated the utility of a small molecule USP2 inhibitor, ML364, in an orthotopic xenograft model of neuroendocrine-like prostate cancer treated with ML364 as well as multiple *in vitro* models (chapter 4). An important finding of the *in vivo* study was that ML364 did not cause any overt toxicity (chapter 4). Preliminary results of the ML364's stability and ADME (adsorption, distribution, metabolism and excretion) also indicate favourable bioavailability for *in vivo* models (Davis et al., 2016). Given the anti-cancer activity of ML364 in prostate cancer models *in vitro* and *in vivo* (chapter 3, 4 and 5), we propose that this pharmacological inhibitor of USP2 could eventually be tested in clinical trials.

Prior to investigating USP2 inhibitor(s) in patients with NEPC, the pharmacodynamics and pharmacokinetics of the drug and in combination with AR-targeted therapy and chemotherapy must be evaluated in animal models (McAnally et al., 2012, White, 2000). The additive effect of these drug combinations will also be assessed concurrently in these models. Given that USP2 is also implicated in other systems, such as metabolic regulation (Kitamura and Hashimoto, 2021), we acknowledge that the potential side effects of systemic USP2 inhibition may adversely affect its clinical utility. Therefore, we propose targeted delivery (Tieu et al., 2021, Dmochowska et al., 2023) of ML364 to prostate tumours can be an option to explore in mice models.

Assessing the acute toxicity of the drug can be implemented using two different animal species (one rodent and one non-rodent) (Parasuraman, 2011). This can be followed by assessing the acute and sub-chronic toxicity of the drug with repeated doses of the drug for a minimum of 28 and 90 days respectively (Parasuraman, 2011). The purpose of these safety trials in animal models of prostate cancer is to measure variations in the body weight, biochemical, cardiovascular, and behavioural changes (Parasuraman, 2011, Kpemissi et al., 2020, Rodríguez-Lara et al., 2019). Risk assessments of the drug, such as the lowest observed adverse effect level (LOAEL) (Dorato and Engelhardt, 2005, Sahota et al., 2016), no observed adverse effect (NOAEL) (Dorato and Engelhardt, 2005, Sahota et al., 2016) and minimum anticipated biological effect level (MABEL) can also be calculated to provide a holistic and comprehensive assessment of ML364 prior to clinical trials (Agoram, 2009, Muller et al., 2009, Sahota et al., 2016).

If ML364 has favourable pharmacokinetic and pharmacodynamic properties individually and in combination with AR-targeted therapy and chemotherapy, it can be recommended to be given in phase 1 clinical trials. The primary objective of the phase 1 clinical trial is to assess safety of ML364 in combination with AR-targeted therapies or chemotherapy. The secondary objective is to assess efficacy of ML364 in humans by documenting progression-free survival and overall survival over time. Our findings suggest that early phase clinical trials of ML364 could utilise combination treatment strategies with chemotherapies, Alisertib and/or AR-targeted therapies. The rationale for combinatorial treatments of ML364 with AR-targeted therapy and chemotherapy is that current AR-targeted therapies or chemotherapies remain ineffective long term (Aggarwal et al., 2018, Yamada and Beltran, 2021, Abida et al., 2019). Furthermore, inhibition of USP2 by ML364 is

posited to sensitise CRPC tumours to chemotherapy when used in conjunction with Docetaxel, which targets the microtubules (Imran et al., 2020, Azarenko et al., 2014). The working hypothesis that stemmed from the body of work described in this dissertation is that USP2 is important in the progression to CRPC and NEPC. Therefore, we envision that the assessment of ML364 with AR-targeted therapy or chemotherapy in phase 1 clinical trial will comprise of patients with metastatic PCa, CRPC and NEPC. Patients with high levels of USP2 and/or Aurora A expression could be prioritised for this clinical trial as a means to improve patient responses, as described in Section 4.4.

6.3 Integrative omics reveals new functions of USP2

The proteomics and transcriptomics analyses identified enrichment of pathways such as neuroendocrine signalling, cell cycle and lipid metabolism (chapter 5). These pathway associations have not been previously linked to USP2 activity in cancer. The cell cycle pathways that were enriched in USP2-OE LNCaP cells included enhanced Cyclin D1 signalling and mitotic spindle (chapter 5), which supported the enhanced expression of Cyclin D1 and Aurora kinase A identified in USP2-OE LNCaP cells (chapter 4). The results suggest that these pathways can be important in enabling prostate cancer cells to acquire an aggressive phenotype and develop resistance against chemotherapy and AR-targeted therapy. The results also highlight that USP2 can be an important mediator of classic resistance mechanisms, thereby emphasising the benefit of targeting USP2 in prostate cancer.

Through the integration of three sets of proteomics and transcriptomics data, thirteen proteins were identified as putative substrates of USP2 (chapter 5). Several of these putative substrates (such as PGRN (Klupp et al., 2021), G3BP2 (Fournier et al., 2010, Gareau et al.,

2011, Schwed-Gross et al., 2022), FUBP1 (Venturutti et al., 2016, Liu et al., 2020), Nucleobindin-1 (NUCB1) (Ejtehadifar et al., 2023, Tsukumo et al., 2007) and TOM1-Like protein 2 (TM1L2) (Bucher-Johannessen et al., 2019) had been associated with chemotherapy resistance in non-prostatic cancers. PGRN and BRX1 were also associated with neuroendocrine tumours in non-prostatic cancers (Barbu et al., 2016, Paulson et al., 2018). Therefore, USP2 is posited to mediate its resistance to chemotherapy and drive lineage plasticity through stabilising at least some of these factors. Validating whether these are direct substrates of USP2, using strategies described in Chapter 5 section 5.4, is an important next step for this research project.

Future work needs to be conducted to elucidate how USP2 mediates epithelial-neuroendocrine plasticity. It is posited that USP2 mediates its effects through stabilisation of its substrates. A potential experiment can be knocking down USP2 in neuroendocrine-like PCa (such as MR42D and PC3 cells), followed by overexpressing a putative substrate (such as PGRN) in those cells and document any rescue of phenotype. The objective of this future experiment is to investigate if PGRN is a direct substrate of USP2 and acts downstream of USP2. These rescue experiments can also be conducted in other prostate cancer models, such as organoids, that are more clinically relevant to patient tumours. However, it is expected that only a partial rescue of phenotype will be observed, since USP2 has many substrates. Therefore, it is likely that to completely rescue the phenotype, a combination of putative USP2 substrates is required to be simultaneously overexpressed in PCa cells when USP2 activity is decreased. Collectively, these experiments can enable systematic evaluation of the importance of USP2 in prostate cancer.

6.4 Overall conclusion

In summary, the research conducted in the course of my PhD has demonstrated that USP2 plays an important role in prostate cancer growth, survival and resistance to therapy. We provide evidence that elevated expression of USP2 in response to AR-targeted therapies drives therapy resistance and the emergence of a neuroendocrine phenotype. In addition, our work demonstrates the plausibility of using ML364 as a treatment for aggressive NEPC. It is proposed that the body of work in this dissertation could, in the long term, lead to new therapeutic strategies to treat lethal prostate cancer.

Chapter 7: Appendices

7 Appendices

7.1 Proteomics data from MR42D cells treated with ML364

Supplementary Table 7.1. Expression data of proteins that are significantly elevated in MR42D cells treated with either DMSO or 5 μ M ML364 for 24 hours.

Comparison (group1/group2)	Gene encoding the detected protein	Log2 fold change	q value
Inhibitor / Control	A2M	0.847868432	3.15E-05
Inhibitor / Control	ACP6	0.676641925	4.59E-05
Inhibitor / Control	AFP	0.978019069	0.000418339
Inhibitor / Control	AGL	1.623953017	4.40E-07
Inhibitor / Control	AMDHD2	1.01070011	1.22E-05
Inhibitor / Control	ANGEL2	1.112853314	0.002514041
Inhibitor / Control	ARHGEF10	0.580186942	0.007233307
Inhibitor / Control	ARMC1	0.69238317	3.16E-10
Inhibitor / Control	ARRB1	0.805892096	0.000163887
Inhibitor / Control	CD44	0.636780573	0.039547547
Inhibitor / Control	CHCHD2	1.066126794	6.36E-12
Inhibitor / Control	CTH	0.748778983	1.33E-08
Inhibitor / Control	DCAF13	1.015616424	9.11E-05
Inhibitor / Control	DDOST	0.826626562	0.000224746
Inhibitor / Control	EHD1	0.832886534	0.024725432
Inhibitor / Control	FARS2	2.840083886	0.023503267
Inhibitor / Control	GDF15	2.722989041	1.52E-10
Inhibitor / Control	GDPGP1	1.071009229	0.008313174
Inhibitor / Control	GYS1	2.559605569	1.20E-11
Inhibitor / Control	HOGA1	0.620393933	6.32E-05
Inhibitor / Control	ITIH2	0.606122898	0.000562926
Inhibitor / Control	LAS1L	1.012951524	0.000395446
Inhibitor / Control	MALT1	0.582548149	0.027212758
Inhibitor / Control	MAN2C1	0.983124211	0.004782565
Inhibitor / Control	MAP3K7IP1	0.740090283	0.014129825
Inhibitor / Control	MOCS2	1.158218879	0.045139464
Inhibitor / Control	MRRF	1.074628244	0.045839467
Inhibitor / Control	MYO18A	0.779535493	0.011861202
Inhibitor / Control	NARS1	0.798910094	0.016352185

Inhibitor / Control	NIFUN	0.769194207	0.024683582
Inhibitor / Control	NOLC1	0.909357609	0.000627453
Inhibitor / Control	NR2C2AP	0.697757177	0.00012309
Inhibitor / Control	NUDCD3	0.758721892	0.004005506
Inhibitor / Control	PBEF1	0.605982102	1.63E-06
Inhibitor / Control	PGAM5	0.682026658	1.18E-06
Inhibitor / Control	PLG	1.611509631	5.90E-06
Inhibitor / Control	PON2	0.813935973	0.028117137
Inhibitor / Control	PPP2CB	0.646402577	0.001281632
Inhibitor / Control	PYGB	1.460135494	1.51E-08
Inhibitor / Control	PZP	0.827223081	0.001464264
Inhibitor / Control	RAB25	2.717396586	0.000120206
Inhibitor / Control	RP11-78J21.1	0.66058764	0.008266084
Inhibitor / Control	SEPHS2	0.639233924	2.07E-06
Inhibitor / Control	SEPT7	0.637004277	0.00202707
Inhibitor / Control	SHC1	2.450524859	0.004108322
Inhibitor / Control	SLU7	0.895518923	0.01364849
Inhibitor / Control	SPTBN1	0.922565815	0.009329085
Inhibitor / Control	SQSTM1	1.124826409	6.77E-07
Inhibitor / Control	STBD1	0.950932382	4.59E-05
Inhibitor / Control	STXBP5L	0.67902916	0.043755906
Inhibitor / Control	SUMO2	0.670775793	0.00102607
Inhibitor / Control	TDP2	2.78046992	0.021586196
Inhibitor / Control	TMED9	1.470511337	0.010101828
Inhibitor / Control	VDAC3	0.645896567	0.000412785
Inhibitor / Control	WDR12	0.83364116	1.49E-06
Inhibitor / Control	ZHX3	1.919858771	0.038981611
Inhibitor / Control	ZNF447	0.643989651	0.003828089

Supplementary Table 7.2. Expression data of proteins that are significantly reduced in MR42D cells treated with 5 μ M ML364 for 24 hours (average log₂ fold-change < 0.5).

Comparison (group1/group2)	Gene encoding the detected protein	AVG Log ₂ Ratio	q value
Inhibitor / Control	AAMP	-0.875700108	7.78E-04
Inhibitor / Control	AAR2	-0.8521253	1.78E-02
Inhibitor / Control	AASDHPPT	-0.581162884	0.000601606
Inhibitor / Control	ABLIM1	-0.604797714	1.09E-02
Inhibitor / Control	ABR	-0.967573307	1.11E-03
Inhibitor / Control	ABRAXAS2	-0.601457618	0.001053289
Inhibitor / Control	ACTR10	-0.605493119	2.19212E-05
Inhibitor / Control	ACTR5	-1.288710249	1.36E-03
Inhibitor / Control	ACYP1	-2.411497445	0.037058481
Inhibitor / Control	ADAT3	-0.606701317	0.011372564
Inhibitor / Control	ADD1	-1.241581685	6.22E-04
Inhibitor / Control	ADNP	-1.126680703	2.05E-03
Inhibitor / Control	ADRBK1	-0.713068056	7.26E-07
Inhibitor / Control	AFG3L2	-0.647397444	0.007429025
Inhibitor / Control	AIP	-0.628379927	0.001145607
Inhibitor / Control	ALKBH7	-2.298861203	2.76835E-05
Inhibitor / Control	ANKRD39	-1.389925545	6.93E-06
Inhibitor / Control	ANKZF1	-1.686530925	7.54909E-05
Inhibitor / Control	APOC3	-0.675953445	7.89E-03
Inhibitor / Control	AR	-0.796562114	2.70E-05
Inhibitor / Control	ARHGEF16	-0.891345107	0.00213639
Inhibitor / Control	ARNT	-0.668612211	0.000195843
Inhibitor / Control	ASAH1	-0.664041652	0.021749449
Inhibitor / Control	ASDURF	-0.848250792	7.71903E-05
Inhibitor / Control	ASF1B	-1.454898306	0.003139708
Inhibitor / Control	ATG3	-0.612717166	6.46505E-05
Inhibitor / Control	ATL2	-0.991520092	0.000399778
Inhibitor / Control	ATN1	-0.603371472	0.000742159
Inhibitor / Control	ATP1B1	-0.587245163	0.000819567
Inhibitor / Control	ATP5MF-PTCD1	-0.609782854	0.000732036
Inhibitor / Control	ATPAF1	-0.691640918	0.00446091
Inhibitor / Control	ATPAF2	-2.937359093	6.60122E-07
Inhibitor / Control	ATRN	-1.048640046	0.010018289
Inhibitor / Control	ATXN10	-0.588726821	2.08E-04
Inhibitor / Control	AVEN	-0.638490377	1.16E-02
Inhibitor / Control	BAX	-0.801895989	1.60E-03
Inhibitor / Control	BCAM	-1.06517488	0.010739264

Inhibitor / Control	BCKDHA	-0.740645755	6.87171E-05
Inhibitor / Control	BCL9L	-4.621058467	8.80E-04
Inhibitor / Control	BID	-0.743866655	0.000223662
Inhibitor / Control	BIRC6	-1.973283612	0.010385927
Inhibitor / Control	BOD1L1	-0.756994495	0.006811818
Inhibitor / Control	BRCA1	-1.532308328	2.20E-04
Inhibitor / Control	BRD2	-0.885310315	0.008637943
Inhibitor / Control	BRD4	-0.734080159	0.000762904
Inhibitor / Control	BRD8	-1.962900483	6.34936E-06
Inhibitor / Control	BRIX1	-0.66971428	0.00947206
Inhibitor / Control	BUB1B	-1.033051468	1.19E-03
Inhibitor / Control	BUD23	-1.545854453	3.43E-04
Inhibitor / Control	BZW1	-2.473988606	0.000307725
Inhibitor / Control	C12orf57	-0.601576962	5.17153E-07
Inhibitor / Control	C18orf25	-1.753647066	0.000503867
Inhibitor / Control	C1orf48	-1.604371134	0.00150076
Inhibitor / Control	CAMK2N1	-2.098471536	3.19746E-07
Inhibitor / Control	CAMSAP1	-0.628284557	7.77E-03
Inhibitor / Control	CAPRIN1	-0.760888117	0.000115768
Inhibitor / Control	CASP7	-1.265006884	0.000142511
Inhibitor / Control	CCDC32	-1.165016565	1.33115E-08
Inhibitor / Control	CCDC86	-1.111826522	0.000136835
Inhibitor / Control	CCNA2	-0.618368746	0.017238109
Inhibitor / Control	CCNB1	-1.342923879	0.000187094
Inhibitor / Control	CCNT1	-2.053169857	0.013443258
Inhibitor / Control	CDC123	-1.500008765	0.000329811
Inhibitor / Control	CDC2L5	-1.245948204	2.82246E-05
Inhibitor / Control	CDC40	-0.963303463	0.010915942
Inhibitor / Control	CDC42EP4	-0.768842141	0.000501413
Inhibitor / Control	CDK1	-0.945173656	1.75812E-06
Inhibitor / Control	CDK2	-0.805304923	0.000741634
Inhibitor / Control	CDK4	-0.919145286	0.023804183
Inhibitor / Control	CDK5RAP3	-2.124991756	0.00026717
Inhibitor / Control	CEBPZ	-0.76377085	0.000508552
Inhibitor / Control	CENTG3	-0.799514561	0.001396571
Inhibitor / Control	CEP170B	-1.243251557	0.001392089
Inhibitor / Control	CETN2	-0.75519255	8.41874E-06
Inhibitor / Control	CHAF1B	-1.586249654	0.00061587
Inhibitor / Control	CHP	-3.522301521	3.60884E-06
Inhibitor / Control	CKS1B	-1.416929515	0.000126549
Inhibitor / Control	CKS2	-2.237413543	6.23113E-05
Inhibitor / Control	CLASP2	-0.791740457	0.017490246
Inhibitor / Control	CLMN	-0.719615787	7.04058E-05
Inhibitor / Control	CLPX	-0.635419828	0.000169549

Inhibitor / Control	CMSS1	-0.639089173	0.009869162
Inhibitor / Control	CNOT3	-2.316952367	1.92474E-09
Inhibitor / Control	COL4A3BP	-0.904724187	7.31961E-05
Inhibitor / Control	COL6A1	-0.721462637	0.001132614
Inhibitor / Control	COPG2	-0.593940143	0.019762472
Inhibitor / Control	COPRS	-0.837804843	0.005777901
Inhibitor / Control	CSDE1	-0.638641867	1.57838E-05
Inhibitor / Control	CTNNBIP1	-1.368388435	0.008341076
Inhibitor / Control	CTU1	-0.618861987	0.003936595
Inhibitor / Control	CWC27	-1.251726798	0.043396857
Inhibitor / Control	DCAF11	-1.050025787	0.012611063
Inhibitor / Control	DCAF7	-2.737325039	1.33115E-08
Inhibitor / Control	DCTN5	-1.125821914	0.026390226
Inhibitor / Control	DDA1	-0.660926051	1.5614E-05
Inhibitor / Control	DDR GK1	-0.616342279	0.00331263
Inhibitor / Control	DDX23	-0.934041963	0.01201724
Inhibitor / Control	DENND1B	-0.585324711	0.000236366
Inhibitor / Control	DERA	-0.623307018	0.008213208
Inhibitor / Control	DHX38	-0.639993023	0.000259541
Inhibitor / Control	DHX8	-0.7908878	0.02691966
Inhibitor / Control	DIAPH1	-1.124710897	0.000405485
Inhibitor / Control	DIDO1	-0.631664589	0.005677016
Inhibitor / Control	DLGAP5	-0.74891896	0.002061559
Inhibitor / Control	DNAJA1	-0.691563909	1.25002E-06
Inhibitor / Control	DNAJA3	-0.596953497	0.002832977
Inhibitor / Control	DNAJB2	-0.602029133	0.005741672
Inhibitor / Control	DNAJC19	-0.631448104	0.003056447
Inhibitor / Control	DNM1L	-0.623204645	0.001539649
Inhibitor / Control	DNPEP	-0.611464201	0.014358799
Inhibitor / Control	DOM3Z	-0.812330543	0.000229462
Inhibitor / Control	DRAP1	-0.613441308	0.003379886
Inhibitor / Control	DSC2	-0.85617581	0.002434465
Inhibitor / Control	DYR	-0.939628659	3.16088E-10
Inhibitor / Control	EEF1E1-BLOC1S5	-1.542958902	1.31866E-07
Inhibitor / Control	EFNB1	-0.631113443	0.00645111
Inhibitor / Control	EIF1	-1.062726339	1.91792E-05
Inhibitor / Control	EIF4G3	-1.236387766	0.000681255
Inhibitor / Control	ELMO3	-0.762660965	1.3167E-05
Inhibitor / Control	ENDOG	-1.015597578	0.000102088
Inhibitor / Control	ENO3	-1.750377584	0.00074708
Inhibitor / Control	EPB41L1	-0.846382367	0.000206043
Inhibitor / Control	ERAL1	-1.0504134	0.004584623
Inhibitor / Control	ERBB2	-1.611453004	2.92434E-05
Inhibitor / Control	ERCC1	-0.957450135	0.006107092

Inhibitor / Control	ERCC6	-0.815788051	0.022867822
Inhibitor / Control	EXOSC10	-1.697108052	0.011091728
Inhibitor / Control	FAM107B	-0.728775292	0.002604732
Inhibitor / Control	FAM111B	-0.687103827	0.001290316
Inhibitor / Control	FAM120C	-1.324057267	0.006814639
Inhibitor / Control	FAM54B	-0.751216202	0.007181818
Inhibitor / Control	FANCI	-1.053642164	0.005852957
Inhibitor / Control	FAT1	-1.265991014	0.008471066
Inhibitor / Control	FKBP8	-0.628543718	1.37164E-05
Inhibitor / Control	FLNC	-0.71933191	0.035526803
Inhibitor / Control	FNBP1	-1.255148279	0.021172373
Inhibitor / Control	FTH1	-0.680946503	0.005597378
Inhibitor / Control	FUBP1	-0.795739588	0.002839041
Inhibitor / Control	FZD6	-2.020330308	1.17912E-05
Inhibitor / Control	G3BP1	-0.625561351	5.82374E-06
Inhibitor / Control	G3BP2	-3.031234773	0.007787702
Inhibitor / Control	GADD45GIP1	-1.131902138	0.0306552
Inhibitor / Control	GAGE5	-0.950608615	0.003787547
Inhibitor / Control	GATAD2A	-0.829533872	0.024069534
Inhibitor / Control	GCFC2	-0.668212821	0.000390035
Inhibitor / Control	GIT1	-1.751369812	0.000829437
Inhibitor / Control	GLTSCR2	-0.621053804	0.006337732
Inhibitor / Control	GNB2	-0.86045424	0.000391342
Inhibitor / Control	GOLPH2	-0.797803026	0.000178481
Inhibitor / Control	GOLPH3L	-0.832341469	0.000516802
Inhibitor / Control	GPATCH11	-0.667916989	0.010470787
Inhibitor / Control	GPATCH4	-1.048825182	3.20559E-05
Inhibitor / Control	GRN	-1.239250822	0.002883857
Inhibitor / Control	GSTK1	-1.111918816	3.89817E-05
Inhibitor / Control	GTF2H2	-0.771379472	8.96012E-08
Inhibitor / Control	GTF2I	-0.822758396	4.41348E-07
Inhibitor / Control	H1-2	-0.661918663	0.006519502
Inhibitor / Control	HAUS6	-0.605364912	0.027176096
Inhibitor / Control	HBB	-2.499507515	0.004884863
Inhibitor / Control	HCTP4	-0.768810322	0.000597292
Inhibitor / Control	HEBP1	-0.884543788	2.97152E-07
Inhibitor / Control	HEL-S-2	-3.674983112	0.003134
Inhibitor / Control	HIC2	-0.73752006	1.65025E-05
Inhibitor / Control	HK2	-0.80811484	0.003099372
Inhibitor / Control	HMCES	-1.65620925	2.00313E-07
Inhibitor / Control	HMG20A	-1.143991714	0.000144414
Inhibitor / Control	HNRNPA3	-3.439071662	0.003217375
Inhibitor / Control	HOKK1	-0.911352605	0.000272144
Inhibitor / Control	HSP90AB2P	-0.674609605	0.001854399

Inhibitor / Control	HSPA1L	-1.952584338	9.49921E-07
Inhibitor / Control	HSPA8	-1.336179236	0.014034117
Inhibitor / Control	IDUA	-1.846987793	0.001666047
Inhibitor / Control	IGFBP2	-1.197421834	1.21658E-08
Inhibitor / Control	IGHMBP2	-1.157392637	9.6192E-05
Inhibitor / Control	IGKC	-1.507210312	0.013158844
Inhibitor / Control	IK	-0.78391431	0.006431255
Inhibitor / Control	IMPACT	-2.441845485	1.85889E-05
Inhibitor / Control	IPO4	-0.718598329	0.003975117
Inhibitor / Control	IPO9	-0.601683462	0.000645717
Inhibitor / Control	IRAK1	-0.633903151	0.00254405
Inhibitor / Control	JMJD1B	-0.968840082	0.002509664
Inhibitor / Control	JPT1	-1.301688878	0.001833793
Inhibitor / Control	JUP	-1.138192637	0.000604051
Inhibitor / Control	KCTD5	-0.975071196	0.000425138
Inhibitor / Control	KIAA0256	-0.669020892	0.035456597
Inhibitor / Control	KIAA1244	-0.689523043	0.026638111
Inhibitor / Control	KIAA1715	-0.600759623	0.001543147
Inhibitor / Control	KNSTRN	-1.162978641	0.0013573
Inhibitor / Control	KNTC2	-0.889907485	5.15127E-05
Inhibitor / Control	KPNA2	-0.853301059	9.03193E-08
Inhibitor / Control	KPRP	-0.666012423	0.002399017
Inhibitor / Control	KRT10	-0.608521367	0.004621353
Inhibitor / Control	KRT2	-1.1097475	0.003220448
Inhibitor / Control	KRT5	-1.525712817	0.002183583
Inhibitor / Control	KRT77	-1.677741374	0.015806209
Inhibitor / Control	KYAT1	-0.992961098	0.036379165
Inhibitor / Control	LAMB2	-0.589496783	0.006875722
Inhibitor / Control	LAMC1	-0.632307212	0.000588234
Inhibitor / Control	LAMTOR5	-0.727919299	3.60579E-06
Inhibitor / Control	LANCL2	-1.225360523	0.002916603
Inhibitor / Control	LARP4	-0.664303587	4.93557E-05
Inhibitor / Control	LARP4B	-0.830245741	0.000375073
Inhibitor / Control	LGALS3BP	-0.747403483	0.001638192
Inhibitor / Control	LGMN	-2.054186956	0.00771555
Inhibitor / Control	LMNB2	-0.614415233	0.013158844
Inhibitor / Control	LOC392748	-0.848179043	1.33968E-05
Inhibitor / Control	LONP2	-0.855845904	0.010618329
Inhibitor / Control	LSR	-0.812920345	0.000240667
Inhibitor / Control	LYPLA1	-0.626252048	0.000166022
Inhibitor / Control	LYRM4	-0.593064834	0.000239019
Inhibitor / Control	MAN2B2	-0.795708171	0.008707407
Inhibitor / Control	MANBA	-1.046641581	0.003151901
Inhibitor / Control	MAP2K4	-0.735384295	0.043626647

Inhibitor / Control	MARK2	-1.449190822	1.58393E-06
Inhibitor / Control	MARK3	-0.659275456	5.15127E-05
Inhibitor / Control	MARVELD2	-0.964010509	0.021838687
Inhibitor / Control	MAST4	-0.653992815	0.00336404
Inhibitor / Control	MCRIP1	-0.892362706	2.55819E-07
Inhibitor / Control	MCTS1	-1.261851663	0.011668535
Inhibitor / Control	MEA1	-1.081511735	0.002156046
Inhibitor / Control	MED8	-1.546267728	0.006489704
Inhibitor / Control	METAP2	-0.793722265	0.00024744
Inhibitor / Control	METTL2A	-1.405998388	0.008690662
Inhibitor / Control	MEX3C	-0.698279947	0.001013237
Inhibitor / Control	MGC11102	-0.838090733	1.31573E-05
Inhibitor / Control	MID1IP1	-1.639028485	0.001041239
Inhibitor / Control	MMADHC	-0.754704907	0.002509664
Inhibitor / Control	MMP24OS	-0.600560079	0.000844659
Inhibitor / Control	MORC2	-1.346027275	0.000630304
Inhibitor / Control	MRFAP1	-1.945439906	2.14448E-07
Inhibitor / Control	MRPL14	-0.649874048	4.87416E-06
Inhibitor / Control	MRPL16	-0.592159865	6.32211E-05
Inhibitor / Control	MRPL18	-0.608476222	0.005577429
Inhibitor / Control	MRPL22	-1.3946976	0.003787547
Inhibitor / Control	MRPL24	-2.816812911	0.000174025
Inhibitor / Control	MRPL28	-0.603764221	8.15244E-05
Inhibitor / Control	MRPL3	-0.805302974	0.000191315
Inhibitor / Control	MRPL34	-0.672115239	0.001108993
Inhibitor / Control	MRPL39	-0.778852772	0.000663851
Inhibitor / Control	MRPL47	-0.587154865	0.009951164
Inhibitor / Control	MRPS14	-1.066221241	2.97824E-08
Inhibitor / Control	MRPS15	-1.264886204	9.03193E-08
Inhibitor / Control	MRPS21	-1.703482406	0.001566181
Inhibitor / Control	MRPS26	-1.649073687	1.63159E-06
Inhibitor / Control	MRPS31	-1.892800445	7.14941E-07
Inhibitor / Control	MRPS9	-1.000412655	1.70731E-05
Inhibitor / Control	MSL1	-0.971592861	0.017526638
Inhibitor / Control	MSX2	-0.844519524	0.00061587
Inhibitor / Control	MTA2	-0.912420607	4.85947E-06
Inhibitor / Control	MTCH2	-2.911788392	0.000392412
Inhibitor / Control	MYH14	-0.643657702	0.00306427
Inhibitor / Control	MZT2B	-0.583052643	0.000944017
Inhibitor / Control	N6AMT1	-0.603726569	0.002624198
Inhibitor / Control	NAAA	-1.03222859	0.00167487
Inhibitor / Control	NAP1L1	-0.767990003	0.001621781
Inhibitor / Control	NAV1	-0.6113957	0.00035243
Inhibitor / Control	NCAPD2	-0.68770225	0.005504325

Inhibitor / Control	NCAPD3	-0.860987067	0.000602463
Inhibitor / Control	NCBP2	-1.422491761	5.51561E-05
Inhibitor / Control	NCOR2	-0.873919154	3.15584E-07
Inhibitor / Control	NDRG3	-1.036106612	0.000878035
Inhibitor / Control	NDUFA13	-1.070941903	1.17871E-05
Inhibitor / Control	NDUFA2	-1.288622167	1.43313E-08
Inhibitor / Control	NDUFAB1	-0.651577104	0.002220225
Inhibitor / Control	NDUFB10	-0.746742873	2.15965E-06
Inhibitor / Control	NDUFB4	-1.225901785	0.000228967
Inhibitor / Control	NDUFS1	-0.947528287	5.47601E-07
Inhibitor / Control	NDUFS3	-0.675435157	0.000104828
Inhibitor / Control	NDUFV1	-0.66490866	0.015055605
Inhibitor / Control	NDUFV2	-0.611615281	4.07249E-06
Inhibitor / Control	NMNAT1	-1.316447061	0.02647343
Inhibitor / Control	NOB1	-0.963848094	5.0427E-05
Inhibitor / Control	NRBP1	-0.812343231	0.000477424
Inhibitor / Control	NSA2	-1.031209572	0.000111385
Inhibitor / Control	NUCB1	-1.131084234	0.001082851
Inhibitor / Control	NUDT16	-0.786834777	0.001526474
Inhibitor / Control	NUDT3	-1.314393245	0.000672994
Inhibitor / Control	NUP153	-0.692588296	0.001082897
Inhibitor / Control	NUP58	-1.124071909	0.003285245
Inhibitor / Control	NUP88	-0.953919697	0.002018388
Inhibitor / Control	NUP93	-1.347169798	0.007495407
Inhibitor / Control	NUP98	-0.6937641	0.007165902
Inhibitor / Control	NUSAP1	-1.311859183	2.503E-07
Inhibitor / Control	OAS3	-0.811620028	0.009013902
Inhibitor / Control	OCIAD1	-0.910823894	1.31866E-07
Inhibitor / Control	OXSRI	-0.782330937	0.04678002
Inhibitor / Control	P4HA2	-0.791180568	0.000127941
Inhibitor / Control	P4HTM	-1.114195316	0.00018425
Inhibitor / Control	PAIP1	-3.030405531	0.002291421
Inhibitor / Control	PALLD	-1.88194442	0.000909124
Inhibitor / Control	PARD6B	-1.057662408	0.000175342
Inhibitor / Control	PARN	-1.411110771	0.000991441
Inhibitor / Control	PAWR	-0.630165072	0.005091834
Inhibitor / Control	PAXX	-0.783400965	0.014123473
Inhibitor / Control	PCLAF	-3.595339673	1.3026E-05
Inhibitor / Control	PDCD10	-1.676795128	0.001051634
Inhibitor / Control	PDCL3	-0.862799064	0.000652777
Inhibitor / Control	PDDC1	-1.226567144	0.003105231
Inhibitor / Control	PDIA3	-0.85365093	0.00032759
Inhibitor / Control	PDK3	-1.407550032	0.00173595
Inhibitor / Control	PDLIM2	-1.447635778	0.006658394

Inhibitor / Control	PDPR	-0.940419842	0.004467954
Inhibitor / Control	PDS5B	-1.26602767	0.00204314
Inhibitor / Control	PEX5	-0.867426126	4.46667E-05
Inhibitor / Control	PFKFB2	-1.131893505	0.000396268
Inhibitor / Control	PGGT1B	-0.658040788	0.00556813
Inhibitor / Control	PHKA1	-0.958059635	7.04058E-05
Inhibitor / Control	PIP5K1A	-1.26514448	0.012190309
Inhibitor / Control	PJA1	-0.809060073	0.045890315
Inhibitor / Control	PKIA	-0.813107199	0.000251156
Inhibitor / Control	PKIG	-0.626069933	0.000700326
Inhibitor / Control	PLK1	-1.987789726	7.20471E-06
Inhibitor / Control	PLRG1	-1.622190876	5.64232E-05
Inhibitor / Control	PML	-1.636522983	0.00170602
Inhibitor / Control	PMM1	-1.382864049	8.91402E-05
Inhibitor / Control	PMVK	-1.097385379	0.005252451
Inhibitor / Control	POLA1	-1.097967801	6.32211E-05
Inhibitor / Control	POLD2	-0.662131526	6.78596E-05
Inhibitor / Control	POLE3	-0.75854015	4.98038E-08
Inhibitor / Control	POLR2E	-0.890400368	0.002567487
Inhibitor / Control	POMP	-0.818199153	0.000421052
Inhibitor / Control	POP7	-0.587510028	6.32211E-05
Inhibitor / Control	PPFIA1	-1.385046648	0.001633507
Inhibitor / Control	PPFIA2	-1.137161199	7.0092E-07
Inhibitor / Control	PPIAL4C	-0.995835893	0.030088399
Inhibitor / Control	PPID	-0.612492743	0.001113186
Inhibitor / Control	PPP1R10	-0.603336787	0.001080078
Inhibitor / Control	PPP1R9A	-1.043604904	0.02224033
Inhibitor / Control	PPP4C	-0.889371514	1.63159E-06
Inhibitor / Control	PREPL	-0.803122791	1.58393E-06
Inhibitor / Control	PRIM1	-0.99146443	0.000324122
Inhibitor / Control	PRIM2	-0.688836893	0.003900557
Inhibitor / Control	PRKCI	-1.308094701	7.23097E-06
Inhibitor / Control	PRKCZ	-1.796937846	7.94683E-05
Inhibitor / Control	PRPF38A	-0.950522116	0.001430733
Inhibitor / Control	PRRC2B	-1.220709252	1.80257E-08
Inhibitor / Control	PSMB3	-0.987665988	0.000592534
Inhibitor / Control	PSMD5	-0.617659293	0.005461502
Inhibitor / Control	PYGO2	-1.130282468	0.000631402
Inhibitor / Control	QRSL1	-0.649720176	0.017798967
Inhibitor / Control	R3HDM4	-0.713973842	0.000542747
Inhibitor / Control	RAB27A	-1.225318524	0.000962393
Inhibitor / Control	RAB3GAP1	-0.707966125	0.000726906
Inhibitor / Control	RAB5A	-0.651727907	0.00038934
Inhibitor / Control	RAB6B	-1.27399531	0.014458761

Inhibitor / Control	RBM15B	-1.012130782	0.004356996
Inhibitor / Control	RBM3	-0.716771638	8.15188E-07
Inhibitor / Control	RCN3	-1.312339627	4.77469E-05
Inhibitor / Control	RECQL4	-0.785463317	0.008378607
Inhibitor / Control	RFC4	-0.785067348	0.001202691
Inhibitor / Control	RFK	-0.738207961	0.000147415
Inhibitor / Control	RING1	-0.929319125	0.00133965
Inhibitor / Control	RMDN1	-0.587548808	0.015338769
Inhibitor / Control	RNF187	-1.359904839	1.33968E-05
Inhibitor / Control	RNF220	-0.954308014	5.89527E-06
Inhibitor / Control	RNF40	-0.780272755	1.58239E-06
Inhibitor / Control	RPIA	-0.975042302	0.001288748
Inhibitor / Control	RPLP1	-1.037742708	0.000928203
Inhibitor / Control	RPP40	-1.395199687	0.002913304
Inhibitor / Control	RRM1	-0.670324652	0.001018135
Inhibitor / Control	RRM2	-1.239518365	1.04858E-08
Inhibitor / Control	RRP12	-0.822501102	0.001586323
Inhibitor / Control	RSBN1L	-0.717084782	0.000126549
Inhibitor / Control	RSF1	-1.204675877	0.000204674
Inhibitor / Control	RSL24D1	-0.603828263	0.022942411
Inhibitor / Control	RTF1	-1.426340046	1.13049E-05
Inhibitor / Control	RTL8C	-0.844761836	0.000262504
Inhibitor / Control	RTN4IP1	-1.291286205	0.017430092
Inhibitor / Control	RUFY1	-0.718353972	0.033449454
Inhibitor / Control	SCRIB	-0.957304499	0.008916535
Inhibitor / Control	SDCBP	-2.093997119	0.000102088
Inhibitor / Control	SEC24A	-0.853901841	0.000145033
Inhibitor / Control	SEC24B	-1.159549678	0.002451851
Inhibitor / Control	SENP8	-1.204985409	0.010190456
Inhibitor / Control	SEPTIN3	-1.03306175	0.006847668
Inhibitor / Control	SERPINI1	-0.938464528	3.8637E-07
Inhibitor / Control	SETD3	-0.589385118	0.001663241
Inhibitor / Control	SETDB1	-2.400771479	0.000237205
Inhibitor / Control	SFRP1	-0.997248486	0.009498439
Inhibitor / Control	SHROOM1	-0.760052968	0.00571024
Inhibitor / Control	SIN3A	-0.606919215	0.001354921
Inhibitor / Control	SIRT1	-0.813510209	0.003455392
Inhibitor / Control	SLAIN2	-1.131894473	0.000818167
Inhibitor / Control	SLC25A10	-1.01617363	0.003391743
Inhibitor / Control	SLC25A22	-0.957391129	0.011977333
Inhibitor / Control	SMAP1	-0.785586768	0.001549201
Inhibitor / Control	SMAP2	-1.014542002	0.000862005
Inhibitor / Control	SMARCB1	-0.846779097	9.72123E-05
Inhibitor / Control	SMARCE1	-0.70599779	0.000422972

Inhibitor / Control	SMIM20	-0.583245401	6.59823E-07
Inhibitor / Control	SNRPF	-1.018043393	0.003744466
Inhibitor / Control	SNX6	-0.592505859	0.00017118
Inhibitor / Control	SPDL1	-2.345801351	1.40955E-08
Inhibitor / Control	SPECC1L	-3.963118325	0.005974438
Inhibitor / Control	SPINT1	-2.557606816	0.002803088
Inhibitor / Control	SRR	-0.743346983	0.001188437
Inhibitor / Control	SSBP3	-0.726362698	0.000481599
Inhibitor / Control	SSNA1	-0.668330294	5.60114E-05
Inhibitor / Control	SSU72	-0.984719909	5.62271E-08
Inhibitor / Control	ST14	-2.004520761	0.001061331
Inhibitor / Control	STK32C	-0.716497446	2.86088E-05
Inhibitor / Control	STXBP2	-0.714311691	0.00277016
Inhibitor / Control	SUGT1	-0.815186631	1.48162E-06
Inhibitor / Control	SUZ12	-0.671825001	0.000335981
Inhibitor / Control	TBC1D15	-0.592570846	7.86431E-05
Inhibitor / Control	TBC1D5	-0.707726995	1.83766E-05
Inhibitor / Control	TBPL1	-0.696735913	0.003520035
Inhibitor / Control	TCAF1	-2.41347958	8.09802E-05
Inhibitor / Control	TCEAL4	-1.010536096	2.32989E-05
Inhibitor / Control	TCEAL8	-0.952152102	3.4398E-05
Inhibitor / Control	TCERG1	-1.366322222	0.000600134
Inhibitor / Control	TDRKH	-0.698211767	0.000398165
Inhibitor / Control	TENM2	-0.595467655	3.27162E-05
Inhibitor / Control	TFB2M	-0.943291369	0.008741758
Inhibitor / Control	THAP11	-0.652115489	0.014946185
Inhibitor / Control	THOC2	-1.878462526	0.001411454
Inhibitor / Control	TIMM23	-0.820243916	0.000575936
Inhibitor / Control	TIMM44	-1.746540719	0.001462218
Inhibitor / Control	TJP2	-3.17347392	0.001006946
Inhibitor / Control	TK1	-1.658185653	5.4495E-05
Inhibitor / Control	TLE1	-0.731362821	0.008068076
Inhibitor / Control	TMED8	-0.975920187	0.007254796
Inhibitor / Control	TMEM113	-0.773186505	0.000382736
Inhibitor / Control	TMEM132A	-1.390257251	0.000117656
Inhibitor / Control	TOM1L1	-2.888053399	0.001716972
Inhibitor / Control	TOM1L2	-1.409456421	0.008676148
Inhibitor / Control	TOMM34	-0.585088007	0.002243272
Inhibitor / Control	TOR1AIP1	-0.68933206	0.001418613
Inhibitor / Control	TRAF2	-1.314443484	0.000108087
Inhibitor / Control	TRAPPC3	-0.66238688	0.000156479
Inhibitor / Control	TRIM26	-1.075220767	0.00046927
Inhibitor / Control	TRIP4	-1.635528762	0.00077036
Inhibitor / Control	TRNAU1AP	-0.637090873	6.01823E-05

Inhibitor / Control	TUSC2	-0.604925483	0.027809286
Inhibitor / Control	TWSG1	-0.885369506	7.19067E-06
Inhibitor / Control	TXLNA	-0.656262769	1.5614E-05
Inhibitor / Control	TXLNG	-0.691073585	1.65049E-06
Inhibitor / Control	TYMS	-1.676553431	5.94004E-07
Inhibitor / Control	TYSND1	-0.694810685	0.003566442
Inhibitor / Control	UBAP2	-0.769608785	2.26471E-05
Inhibitor / Control	UBE2A	-0.624860044	6.56691E-06
Inhibitor / Control	UBE2B	-0.863567793	2.04786E-07
Inhibitor / Control	UBE2T	-2.2086713	1.31866E-07
Inhibitor / Control	UBE4B	-0.822113499	0.000118454
Inhibitor / Control	UBR1	-0.927910584	0.00361379
Inhibitor / Control	UBXN2A	-1.174352841	0.035070987
Inhibitor / Control	UCK2	-1.368822103	2.82246E-05
Inhibitor / Control	UQCRC2	-0.634381736	3.25181E-05
Inhibitor / Control	UQCRFS1P1	-2.447951202	4.01643E-06
Inhibitor / Control	URLC6	-0.734732237	0.001021654
Inhibitor / Control	USP11	-0.60271051	3.29664E-06
Inhibitor / Control	USP13	-0.756190997	6.07931E-07
Inhibitor / Control	USP19	-0.693736109	0.002286598
Inhibitor / Control	USP4	-1.005404401	0.033153809
Inhibitor / Control	UTP15	-1.428389692	0.000786605
Inhibitor / Control	UTP20	-0.637357627	0.000529472
Inhibitor / Control	UTP4	-0.778040242	0.040893865
Inhibitor / Control	VBP1	-0.988223266	0.003375115
Inhibitor / Control	VCP	-0.776755853	1.35602E-05
Inhibitor / Control	VPS25	-6.068716286	0.013759426
Inhibitor / Control	VPS37C	-1.297161213	0.000762904
Inhibitor / Control	WASHC5	-3.800088236	0.006879512
Inhibitor / Control	WDR18	-0.879568508	0.012724729
Inhibitor / Control	WDR37	-0.636519408	0.028928412
Inhibitor / Control	WDR6	-0.887914306	2.78412E-07
Inhibitor / Control	WNK1	-0.981263735	0.000778346
Inhibitor / Control	XPO4	-0.684250713	0.013129189
Inhibitor / Control	XRCC1	-1.778921473	0.035249769
Inhibitor / Control	YTHDF2	-0.976480971	1.37164E-05
Inhibitor / Control	ZC3HDC1	-1.100396402	0.002015679
Inhibitor / Control	ZCCHC6	-0.596284187	0.006824881
Inhibitor / Control	ZFAND1	-0.883900241	0.041540607
Inhibitor / Control	ZFYVE16	-0.616875593	0.001043339
Inhibitor / Control	ZNF316	-1.097032048	0.000831922
Inhibitor / Control	ZNF503	-0.895462093	1.73994E-07
Inhibitor / Control	ZNF511	-0.754734623	0.04560312

7.2 Proteomics data from LNCaP cells overexpressing USP2

Supplementary Table 7.3. Expression data of proteins that are significantly increased in the LNCaP cells overexpressing USP2 than the control cells (average log₂ fold-change > 0.5).

Comparison (group1/group2)	Gene encoding the detected protein	Log ₂ fold change	q value
USP2 / Neon	ACAT1	2.660392267	9.14E-06
USP2 / Neon	TRIM56	2.410814661	3.86E-02
USP2 / Neon	HSPBP1	2.123313269	0.000828341
USP2 / Neon	TXNRD2	1.926884659	2.37E-03
USP2 / Neon	BTF3	1.917889719	2.21E-03
USP2 / Neon	MCFD2	1.778259414	0.001355307
USP2 / Neon	BRIX1	1.576490665	0.008230426
USP2 / Neon	NONO	1.560970311	1.05E-04
USP2 / Neon	PAN3	1.542714383	1.58102E-06
USP2 / Neon	MTRES1	1.439331347	2.64415E-06
USP2 / Neon	DHPS	1.412166998	5.18E-07
USP2 / Neon	FBXO2	1.382160804	1.19E-03
USP2 / Neon	VCP	1.273086264	2.10E-04
USP2 / Neon	PSMA2	1.21154656	0.008659358
USP2 / Neon	CBX8	1.174302167	7.1062E-05
USP2 / Neon	HMGGA1	1.160063531	3.01961E-06
USP2 / Neon	PROSC	1.136686878	2.61E-04
USP2 / Neon	CKB	1.112852141	8.8532E-07
USP2 / Neon	PEG3	1.103351836	4.19E-04
USP2 / Neon	RBM8	1.043500432	8.35E-04
USP2 / Neon	TOM1L2	1.038057287	0.000125736
USP2 / Neon	COX17	1.034116518	4.57464E-06
USP2 / Neon	NFX1	1.017161234	0.032491694
USP2 / Neon	FKBP2	1.011343303	0.010284082
USP2 / Neon	NUCKS1	1.004583764	4.42533E-05
USP2 / Neon	ZNFX1	1.001188063	1.06116E-05
USP2 / Neon	MRPS18A	0.999248221	4.79025E-06
USP2 / Neon	HDAC2	0.997902978	0.007789045
USP2 / Neon	LAMC1	0.986849181	0.000164412
USP2 / Neon	CAT	0.982936362	3.77606E-06
USP2 / Neon	RCN3	0.978839368	1.99453E-05
USP2 / Neon	RALY	0.929253213	2.64079E-05
USP2 / Neon	SCAF11	0.927977479	0.004926573
USP2 / Neon	SLAIN2	0.926502084	1.38E-04

USP2 / Neon	HEL-S-74	0.924945151	1.20E-05
USP2 / Neon	KLK3	0.922161885	2.14E-06
USP2 / Neon	NMD3	0.91024323	0.001508422
USP2 / Neon	MKNK1	0.908378278	0.001504097
USP2 / Neon	LSM14B	0.905939224	1.51E-04
USP2 / Neon	GDF15	0.895055132	0.000699277
USP2 / Neon	POLRMT	0.893619903	0.0001449
USP2 / Neon	PRPF4B	0.886452317	0.033152029
USP2 / Neon	PHF6	0.874114965	8.12E-04
USP2 / Neon	ADGRG6	0.873729362	5.27517E-05
USP2 / Neon	EFS	0.87311539	2.18601E-06
USP2 / Neon	ADA	0.864876923	1.88937E-07
USP2 / Neon	RNPEP	0.851005243	5.18181E-07
USP2 / Neon	MYDGF	0.847575028	6.81E-06
USP2 / Neon	MGC3731	0.842797292	6.47E-04
USP2 / Neon	MRPL30	0.838852737	0.000386332
USP2 / Neon	NUCB1	0.836060809	1.38778E-06
USP2 / Neon	MPLKIP	0.834036602	1.69889E-05
USP2 / Neon	GTF3C3	0.810351076	4.43646E-05
USP2 / Neon	RNF115	0.810276329	0.000152774
USP2 / Neon	SEPTIN6	0.801849891	8.23E-04
USP2 / Neon	EXOSC4	0.800969384	0.001223237
USP2 / Neon	PPIF	0.794903136	2.44707E-07
USP2 / Neon	RYBP	0.792575464	1.43073E-06
USP2 / Neon	HSPA5	0.792335237	5.81347E-08
USP2 / Neon	NVL	0.78024688	2.14954E-05
USP2 / Neon	ERP70	0.775733185	5.87521E-08
USP2 / Neon	RRAS	0.771059423	0.023065669
USP2 / Neon	NIP30	0.769866082	6.69696E-05
USP2 / Neon	MGC20255	0.764773142	0.000116673
USP2 / Neon	GOLGA4	0.760866186	0.007426986
USP2 / Neon	PTMS	0.753705567	2.42683E-05
USP2 / Neon	MARVELD2	0.753423713	0.012164717
USP2 / Neon	FUBP1	0.751757492	0.003623807
USP2 / Neon	FLVCR1	0.750921269	0.001276496
USP2 / Neon	USP25	0.749603082	0.005588434
USP2 / Neon	MYO18A	0.74448636	0.018714078
USP2 / Neon	CALR	0.742800671	0.001079512
USP2 / Neon	VGLL4	0.74095495	2.9235E-05
USP2 / Neon	DPP7	0.731301726	0.002503435
USP2 / Neon	GNAS	0.728053813	5.03641E-05
USP2 / Neon	RNMT	0.720925562	3.43622E-05
USP2 / Neon	SHROOM3	0.720416912	2.3815E-06
USP2 / Neon	ZNF513	0.719473407	0.000871025

USP2 / Neon	WDR5	0.717409224	5.32145E-06
USP2 / Neon	DDX54	0.706907393	3.96528E-05
USP2 / Neon	LAMB2	0.702970554	7.27948E-06
USP2 / Neon	USP48	0.702620464	0.001542029
USP2 / Neon	G3BP2	0.700718352	0.044947868
USP2 / Neon	MARS2	0.700353627	0.00877759
USP2 / Neon	ACOX1	0.699855717	4.23479E-06
USP2 / Neon	CDKN2AIP	0.697727812	0.001198828
USP2 / Neon	RNF181	0.697705352	0.00152047
USP2 / Neon	RDX	0.697483175	1.59832E-06
USP2 / Neon	CARD11	0.696349841	0.002050667
USP2 / Neon	TMSB4X	0.693427541	2.2302E-07
USP2 / Neon	C2orf49	0.692129547	4.50519E-06
USP2 / Neon	NENF	0.690718649	1.2023E-06
USP2 / Neon	NEDD1	0.690535217	2.07947E-05
USP2 / Neon	FVT1	0.68972962	0.033889546
USP2 / Neon	THOP1	0.688865314	0.001359433
USP2 / Neon	HTATSF1	0.685072469	0.000158543
USP2 / Neon	hCG_2042749	0.684310298	1.14141E-05
USP2 / Neon	TRMT10A	0.68356307	0.000891101
USP2 / Neon	PRDX4	0.682802225	9.26073E-07
USP2 / Neon	JMJD6	0.682183947	9.86958E-05
USP2 / Neon	GRN	0.681172491	5.34908E-06
USP2 / Neon	MACROD1	0.680221632	0.02232844
USP2 / Neon	FH	0.678189913	9.76935E-05
USP2 / Neon	BCS1L	0.676031411	0.002252349
USP2 / Neon	DYNLL2	0.67563188	0.038563083
USP2 / Neon	PCBD2	0.669050102	0.000206634
USP2 / Neon	MANF	0.665654335	4.23479E-06
USP2 / Neon	ATP5IF1	0.660653943	0.002158112
USP2 / Neon	DCTD	0.652741932	4.75287E-05
USP2 / Neon	CIZ1	0.649445012	0.002790617
USP2 / Neon	C6orf57	0.645428508	3.42624E-05
USP2 / Neon	CWC15	0.645408509	0.009436454
USP2 / Neon	HLCS	0.64132319	0.008063617
USP2 / Neon	HAGH	0.640240965	0.000233634
USP2 / Neon	DECR2	0.637362785	0.000150697
USP2 / Neon	HSPA9	0.637072205	2.00983E-05
USP2 / Neon	OXCT1	0.636359356	0.00029424
USP2 / Neon	CKAP5	0.635153006	0.018571184
USP2 / Neon	P4HB	0.630113294	3.29797E-06
USP2 / Neon	STX4A	0.629813738	0.00302394
USP2 / Neon	ARHGEF35	0.62466333	3.14598E-05
USP2 / Neon	DTL	0.621888805	0.03855036

USP2 / Neon	MBP	0.619559336	4.56947E-05
USP2 / Neon	AADAT	0.617401959	0.003671578
USP2 / Neon	DHX16	0.614439854	0.000126979
USP2 / Neon	NELFE	0.614007707	0.00017784
USP2 / Neon	GTPBP1	0.613436043	0.034152857
USP2 / Neon	MICALL1	0.612333596	9.66759E-05
USP2 / Neon	LZIC	0.610193693	0.000386758
USP2 / Neon	ABLIM1	0.607975115	7.54743E-07
USP2 / Neon	STXBP4	0.603161624	0.006914607
USP2 / Neon	ALCAM	0.593748275	0.003218195
USP2 / Neon	SUMF2	0.588167866	1.14141E-05
USP2 / Neon	MRPS27	0.58609503	0.002001301
USP2 / Neon	FXR1	0.585483391	0.003635651
USP2 / Neon	HSPE1	0.584045693	6.55489E-06
USP2 / Neon	MRPS35	0.581874357	0.002361227

Supplementary Table 7.4. Expression data of proteins that are significantly reduced in the LNCaP cells overexpressing USP2 than the control cells (average log₂ fold-change > 0.5).

Comparison (group1/group2)	Gene encoding the detected protein	Log ₂ fold change	q value
USP2 / Neon	EARS2	-0.580018249	2.46E-04
USP2 / Neon	GPRASP2	-0.580336686	2.44E-03
USP2 / Neon	TMOD3	-0.581820105	0.000407735
USP2 / Neon	PMS2	-0.582900831	7.22E-06
USP2 / Neon	FLNB	-0.583104868	6.19E-04
USP2 / Neon	PRKACB	-0.584173833	2.81492E-05
USP2 / Neon	FHOD1	-0.585512475	0.004236663
USP2 / Neon	ANKRD44	-0.586098948	1.30E-02
USP2 / Neon	CDC123	-0.587229223	1.91283E-05
USP2 / Neon	TRIP13	-0.587899068	6.63388E-05
USP2 / Neon	KPNA6	-0.587953017	2.16E-06
USP2 / Neon	TRA2A	-0.588445816	1.08E-02
USP2 / Neon	NUP62	-0.588617864	4.38E-04
USP2 / Neon	PDLIM7	-0.588880379	0.000702033
USP2 / Neon	BTF3L4	-0.588894652	0.044497402
USP2 / Neon	DCTN5	-0.58913784	0.004018679
USP2 / Neon	MRPL11	-0.590442111	7.77E-03
USP2 / Neon	WDFY2	-0.591022776	0.011610517
USP2 / Neon	TBCD	-0.591093274	5.26E-04
USP2 / Neon	GFM2	-0.591501935	1.28E-06
USP2 / Neon	GYG1	-0.592085996	0.002283053
USP2 / Neon	PI4KA	-0.594867745	0.003573994
USP2 / Neon	RPA1	-0.595292185	3.38432E-05
USP2 / Neon	PSMD9	-0.595495681	3.65888E-05
USP2 / Neon	PFKFB2	-0.597462135	2.17283E-06
USP2 / Neon	AP1B1	-0.598208391	1.58102E-06
USP2 / Neon	SNX18	-0.598551615	0.002033619
USP2 / Neon	CSE1L	-0.598774476	1.45113E-05
USP2 / Neon	RAB24	-0.599116076	0.002747775
USP2 / Neon	MCM7	-0.600854143	0.00734249
USP2 / Neon	N6AMT1	-0.601217683	0.000563318
USP2 / Neon	LSM6	-0.603755885	0.00011744
USP2 / Neon	PHB	-0.604410758	0.013037619
USP2 / Neon	GIN51	-0.60458283	1.25E-05
USP2 / Neon	KPNB1	-0.604587332	2.43E-05
USP2 / Neon	GTF2B	-0.604853682	5.18E-07
USP2 / Neon	IDH3B	-0.604915247	0.003271366

USP2 / Neon	GET3	-0.605589781	2.65576E-05
USP2 / Neon	COG3	-0.605882306	9.45E-04
USP2 / Neon	ROCK1	-0.606727187	8.08077E-06
USP2 / Neon	TUBA4A	-0.607014507	1.14546E-06
USP2 / Neon	UBE2E1	-0.607536774	0.000732042
USP2 / Neon	MAP2K5	-0.610655294	9.21E-04
USP2 / Neon	SLC4A2	-0.611388952	0.004037866
USP2 / Neon	WUGSC:H_RG054D04.1	-0.614139674	0.009694427
USP2 / Neon	TRUB1	-0.614908269	2.60484E-05
USP2 / Neon	C9orf32	-0.616329478	8.45177E-06
USP2 / Neon	TARDBP	-0.618333999	2.68E-04
USP2 / Neon	PIK3R2	-0.62081691	2.34E-06
USP2 / Neon	NDRG3	-0.621082709	9.35335E-06
USP2 / Neon	AURKAIP1	-0.622556848	0.002512678
USP2 / Neon	BCL2L13	-0.622667684	0.001948509
USP2 / Neon	UROD	-0.623194209	0.004384945
USP2 / Neon	HSPA14	-0.623899221	0.002803587
USP2 / Neon	PATJ	-0.624123026	3.09E-03
USP2 / Neon	PNN	-0.624527801	0.004230839
USP2 / Neon	DAXX	-0.624555728	0.002224143
USP2 / Neon	SNX12	-0.626919411	7.54743E-07
USP2 / Neon	EPS8L1	-0.62740093	0.006893545
USP2 / Neon	NECAP1	-0.628917778	0.000131669
USP2 / Neon	TBC1D15	-0.629458146	4.00368E-05
USP2 / Neon	PRPF31	-0.630179598	9.26554E-07
USP2 / Neon	CUL4A	-0.631300554	5.96315E-06
USP2 / Neon	LIMD1	-0.631382291	0.031398313
USP2 / Neon	EIF3K	-0.632622302	0.000683509
USP2 / Neon	RPL22L1	-0.632710988	4.86271E-05
USP2 / Neon	PRMT7	-0.633407787	3.42624E-05
USP2 / Neon	GAGE2B	-0.63369128	0.007212707
USP2 / Neon	GNMT	-0.634339243	4.86271E-05
USP2 / Neon	PPME1	-0.635054748	1.48919E-05
USP2 / Neon	MAP4	-0.636477788	0.004017381
USP2 / Neon	CNOT1	-0.638356276	0.00325019
USP2 / Neon	MAP2K4	-0.639377975	1.30705E-06
USP2 / Neon	ACACA	-0.640623913	4.50519E-06
USP2 / Neon	ANKMY2	-0.641754269	0.000148262
USP2 / Neon	USO1	-0.641935464	2.12913E-05
USP2 / Neon	TDRKH	-0.642663577	0.003607443
USP2 / Neon	AFP	-0.646065442	0.004045748
USP2 / Neon	DPH5	-0.646708685	9.26554E-07
USP2 / Neon	JMY	-0.646837387	3.18278E-05
USP2 / Neon	HBA2	-0.647021314	0.000688461

USP2 / Neon	HSDL2	-0.647997332	3.87549E-05
USP2 / Neon	KRT79	-0.648644351	3.42624E-05
USP2 / Neon	POLD2	-0.648660604	1.46973E-05
USP2 / Neon	PTPN6	-0.649052942	0.001002552
USP2 / Neon	ATXN10	-0.649534687	1.57965E-05
USP2 / Neon	NPC1	-0.649640811	0.001595979
USP2 / Neon	TBC1D10B	-0.650298086	0.00020663
USP2 / Neon	NHLRC2	-0.650532335	6.27725E-05
USP2 / Neon	ATP6V1E1	-0.650660869	6.41153E-06
USP2 / Neon	PWP1	-0.650805391	0.007575995
USP2 / Neon	DNAAF5	-0.652039153	2.91777E-05
USP2 / Neon	AHCTF1	-0.652874527	6.75278E-06
USP2 / Neon	XRN1	-0.653433098	0.000261193
USP2 / Neon	ZZEF1	-0.654880492	2.58256E-05
USP2 / Neon	ELL	-0.655394785	0.001074808
USP2 / Neon	AGPS	-0.655901454	0.000394167
USP2 / Neon	SNX5	-0.657080513	2.64079E-05
USP2 / Neon	C6orf106	-0.657518982	2.42683E-05
USP2 / Neon	GSTK1	-0.659054814	3.87555E-06
USP2 / Neon	MCRIP1	-0.659503775	0.002599987
USP2 / Neon	GGA1	-0.659726612	0.000188067
USP2 / Neon	CRADD	-0.659988407	0.000114055
USP2 / Neon	POLR2H	-0.660187386	0.000136569
USP2 / Neon	PITPNB	-0.66166649	0.000928932
USP2 / Neon	DSTN	-0.662541113	2.64079E-05
USP2 / Neon	VPS4A	-0.664792699	1.27823E-06
USP2 / Neon	H2AZ1	-0.66514661	2.51862E-06
USP2 / Neon	ATF7IP	-0.666884225	0.000599341
USP2 / Neon	ATP1A1	-0.668281002	0.007178058
USP2 / Neon	HOOK3	-0.668330876	3.89854E-05
USP2 / Neon	CHFR	-0.668456513	0.002370165
USP2 / Neon	TYMS	-0.671914598	0.000329062
USP2 / Neon	BUB1B	-0.67261832	1.54558E-05
USP2 / Neon	MORF4L2	-0.67272291	5.04825E-05
USP2 / Neon	CASP9	-0.672871158	7.87694E-05
USP2 / Neon	TRMT61A	-0.674698166	0.000267522
USP2 / Neon	ATP6V1H	-0.676817792	0.006872489
USP2 / Neon	FNBP1	-0.677033228	0.008925182
USP2 / Neon	ATPAF2	-0.678485332	7.25509E-07
USP2 / Neon	GGA2	-0.679003205	0.001136384
USP2 / Neon	HAT1	-0.679576989	6.93793E-05
USP2 / Neon	GTF2I	-0.67966647	6.15794E-05
USP2 / Neon	MTHFD1	-0.680891155	3.52742E-05
USP2 / Neon	CGREF1	-0.682066717	0.041430798

USP2 / Neon	SPECC1L	-0.682790204	7.77823E-05
USP2 / Neon	ASL	-0.68603541	0.000275753
USP2 / Neon	NCAPD2	-0.686889734	8.8532E-07
USP2 / Neon	CAMK2G	-0.687775771	0.000505282
USP2 / Neon	SLC25A5	-0.689360908	0.004430444
USP2 / Neon	DGKH	-0.68942002	7.12981E-05
USP2 / Neon	AP3S1	-0.68957905	4.84329E-06
USP2 / Neon	GLTP	-0.692055462	0.003201879
USP2 / Neon	CYC1	-0.692521717	1.09169E-06
USP2 / Neon	UCK1	-0.692809862	2.19077E-05
USP2 / Neon	NEDD4L	-0.694115646	3.54244E-07
USP2 / Neon	RPE	-0.695932491	0.000144673
USP2 / Neon	TEX264	-0.696036571	0.001329113
USP2 / Neon	MRPL50	-0.700443069	0.001322746
USP2 / Neon	IPO4	-0.700852965	0.006589815
USP2 / Neon	EIF4A2	-0.700879327	0.000139553
USP2 / Neon	HMBS	-0.703380975	7.56213E-06
USP2 / Neon	CTU1	-0.703702096	4.01239E-06
USP2 / Neon	FDX2	-0.706464115	6.12222E-05
USP2 / Neon	TBC1D10A	-0.707679441	3.10065E-05
USP2 / Neon	ARHGAP1	-0.70781424	5.38655E-05
USP2 / Neon	NUP93	-0.708874881	9.37506E-06
USP2 / Neon	APIP	-0.709507403	0.00034192
USP2 / Neon	KBTBD7	-0.711485334	0.008773287
USP2 / Neon	PRPSAP1	-0.711580054	8.33455E-07
USP2 / Neon	GTF2A2	-0.711581556	0.000471425
USP2 / Neon	COG1	-0.712689885	0.000598914
USP2 / Neon	NOB1	-0.712818687	0.000142799
USP2 / Neon	PRMT3	-0.714027667	2.00983E-05
USP2 / Neon	MON2	-0.715848727	2.97825E-05
USP2 / Neon	SEC24C	-0.716709384	4.68583E-05
USP2 / Neon	CAMSAP3	-0.717507924	2.89971E-05
USP2 / Neon	CCDC132	-0.719873846	0.000246283
USP2 / Neon	SMC2L1	-0.720274652	8.8532E-07
USP2 / Neon	FAM49B	-0.720393822	2.44707E-07
USP2 / Neon	PHGDH	-0.720608277	1.68464E-05
USP2 / Neon	ADSL	-0.721137887	0.000278324
USP2 / Neon	NEK7	-0.722495543	7.54743E-07
USP2 / Neon	PPP2R1B	-0.72470651	6.12222E-05
USP2 / Neon	TBC1D17	-0.725968361	0.000200092
USP2 / Neon	RBM14	-0.72632692	2.04689E-05
USP2 / Neon	PDCL3	-0.727946821	0.000599341
USP2 / Neon	EIF2B3	-0.729812694	5.16164E-05
USP2 / Neon	DNM1L	-0.730604006	1.5973E-05

USP2 / Neon	ITPKB	-0.730851577	0.019330941
USP2 / Neon	NOL6	-0.731369398	0.029252653
USP2 / Neon	TRAPPC11	-0.73197131	2.55578E-05
USP2 / Neon	HNRPK	-0.733946616	0.01341644
USP2 / Neon	DDX39A	-0.734234226	0.00247343
USP2 / Neon	BCAR1	-0.734525661	6.51403E-05
USP2 / Neon	RHPN2	-0.734977131	1.49707E-05
USP2 / Neon	RAB6A	-0.73520649	0.001221161
USP2 / Neon	CASP7	-0.738737939	1.49723E-05
USP2 / Neon	POLDIP3	-0.740446945	0.00010455
USP2 / Neon	CUL1	-0.741067253	0.00640812
USP2 / Neon	UGDH	-0.741265506	8.605E-06
USP2 / Neon	PKN2	-0.741787693	5.96888E-05
USP2 / Neon	NDUFA6	-0.745579216	2.71959E-05
USP2 / Neon	MAGED2	-0.746117565	1.8928E-06
USP2 / Neon	RAB3GAP1	-0.746619578	8.29796E-06
USP2 / Neon	UBE2Q1	-0.747216907	0.00016542
USP2 / Neon	ST20-MTHFS	-0.749552496	5.11404E-05
USP2 / Neon	STARD7	-0.752850441	0.012816475
USP2 / Neon	UBE2T	-0.755245151	5.56815E-05
USP2 / Neon	AP3B1	-0.756868104	1.62836E-05
USP2 / Neon	SRSF6	-0.759050392	8.80481E-05
USP2 / Neon	TSEN2	-0.759895579	4.23479E-06
USP2 / Neon	CBL	-0.760584396	0.000703839
USP2 / Neon	LENG9	-0.761336608	0.000131669
USP2 / Neon	UBXN7	-0.762239222	2.5818E-05
USP2 / Neon	RPS6KA3	-0.767085261	6.46971E-05
USP2 / Neon	ARHGAP17	-0.767794296	0.002732576
USP2 / Neon	DDX23	-0.767855834	0.00151347
USP2 / Neon	LYSMD2	-0.769126426	0.000132044
USP2 / Neon	POLR1A	-0.769551212	0.023606167
USP2 / Neon	NCAPG	-0.769929872	5.34012E-05
USP2 / Neon	HOOK1	-0.770454778	1.65058E-07
USP2 / Neon	TRAPPC3	-0.770942651	2.32945E-05
USP2 / Neon	RPA3	-0.77210906	0.000113646
USP2 / Neon	SAE1	-0.774758265	2.13573E-06
USP2 / Neon	PARN	-0.776740775	3.52571E-05
USP2 / Neon	DDX19B	-0.777769316	5.81347E-08
USP2 / Neon	RAC1	-0.778778326	4.90504E-06
USP2 / Neon	FBS1	-0.784662836	0.004018679
USP2 / Neon	CUL2	-0.785650741	6.87083E-06
USP2 / Neon	DUSP23	-0.785690108	0.014446765
USP2 / Neon	TCF25	-0.786046823	2.43289E-06
USP2 / Neon	AP1M2	-0.786666408	6.63388E-05

USP2 / Neon	FLJ20323	-0.788135149	0.000832208
USP2 / Neon	VDAC1	-0.788821451	0.00708653
USP2 / Neon	LDAH	-0.790131494	0.002637074
USP2 / Neon	IST1	-0.790224926	0.001359745
USP2 / Neon	GAGE5	-0.790692361	0.000772153
USP2 / Neon	PPCS	-0.791130516	2.55578E-05
USP2 / Neon	PRIM1	-0.792303732	8.0487E-07
USP2 / Neon	SRSF11	-0.793011717	0.00610691
USP2 / Neon	SDSL	-0.795717631	5.57603E-05
USP2 / Neon	TUBB2A	-0.796192837	0.000230777
USP2 / Neon	UMPS	-0.796594363	4.24609E-05
USP2 / Neon	HIP1R	-0.79848747	0.000186942
USP2 / Neon	TPMT	-0.798704031	0.000177273
USP2 / Neon	LRRC40	-0.801259817	7.32916E-06
USP2 / Neon	KPNA2	-0.801311038	1.56194E-06
USP2 / Neon	GPSM1	-0.8023836	0.021511734
USP2 / Neon	CDK4	-0.804614175	4.50519E-06
USP2 / Neon	DIAPH1	-0.805152484	2.75388E-06
USP2 / Neon	EHD4	-0.806372619	2.05474E-06
USP2 / Neon	ARFGAP3	-0.807280738	2.42683E-05
USP2 / Neon	TIPRL	-0.807301526	0.001104114
USP2 / Neon	GTF3C5	-0.808728019	6.41062E-05
USP2 / Neon	NUDT16	-0.81057618	5.02289E-05
USP2 / Neon	SH3GLB1	-0.810742504	3.81106E-05
USP2 / Neon	DKFZp686H0429	-0.810792731	2.3815E-06
USP2 / Neon	DENND10	-0.810958267	1.27823E-06
USP2 / Neon	NAA30	-0.817420808	0.002918084
USP2 / Neon	STXBP2	-0.818620443	3.54244E-07
USP2 / Neon	EEF1E1	-0.8193541	3.60435E-05
USP2 / Neon	ARF6	-0.820278204	0.000179835
USP2 / Neon	UNC45A	-0.821409447	1.84782E-05
USP2 / Neon	CTDP1	-0.822260745	3.6236E-05
USP2 / Neon	FAM54B	-0.822700915	0.001059829
USP2 / Neon	NME7	-0.827017486	0.000702685
USP2 / Neon	PUF60	-0.82865418	6.43933E-05
USP2 / Neon	APPL2	-0.831276309	0.000326568
USP2 / Neon	STXBP3	-0.842617336	0.015568836
USP2 / Neon	FNBP4	-0.844387163	8.75709E-06
USP2 / Neon	MAP2K6	-0.84679106	2.65576E-05
USP2 / Neon	RCOR1	-0.848651214	0.000124987
USP2 / Neon	DPCD	-0.849027535	6.68987E-07
USP2 / Neon	FIP1L1	-0.853780701	0.000438546
USP2 / Neon	CC2D1B	-0.855607503	0.001994668
USP2 / Neon	BICD2	-0.856665507	0.003293375

USP2 / Neon	IPO11	-0.857153324	4.08215E-05
USP2 / Neon	MGC10911	-0.857916313	0.000143866
USP2 / Neon	NBEAL2	-0.858357556	0.005199542
USP2 / Neon	CDAN1	-0.859357237	1.89995E-05
USP2 / Neon	MRE11A	-0.860614672	0.001111083
USP2 / Neon	NAPG	-0.861356377	0.000254873
USP2 / Neon	EIPR1	-0.865758668	1.14243E-06
USP2 / Neon	ENTPD5	-0.866372345	0.000174913
USP2 / Neon	TTC27	-0.867659589	1.42802E-05
USP2 / Neon	NRBP1	-0.870733803	0.043142527
USP2 / Neon	ATG3	-0.875179412	0.001305226
USP2 / Neon	ARMC6	-0.876936857	6.54802E-05
USP2 / Neon	CHMP5	-0.87815725	6.22172E-07
USP2 / Neon	CHMP3	-0.878830884	0.002209886
USP2 / Neon	PYCRL	-0.882060927	9.14158E-06
USP2 / Neon	BORCS7-ASMT	-0.882639594	2.55578E-05
USP2 / Neon	ABCF2	-0.883675051	6.05543E-05
USP2 / Neon	RBM12B	-0.885560282	0.000210328
USP2 / Neon	RAB3A	-0.888968798	0.000800523
USP2 / Neon	NUP188	-0.889960969	5.45968E-06
USP2 / Neon	KPNA4	-0.891216016	8.2063E-06
USP2 / Neon	TRAFD1	-0.892422805	2.21764E-06
USP2 / Neon	SLC3A2	-0.899146597	0.00016916
USP2 / Neon	N4BP1	-0.901676085	3.36706E-06
USP2 / Neon	SLC25A3	-0.902068936	0.000186946
USP2 / Neon	IPO8	-0.903942052	2.6921E-06
USP2 / Neon	SAR1B	-0.904628635	0.011867597
USP2 / Neon	UBE2G1	-0.908038684	7.6604E-05
USP2 / Neon	ZC3H18	-0.909412248	5.18181E-07
USP2 / Neon	KPNA1	-0.912664269	7.27948E-06
USP2 / Neon	TFRC	-0.913050553	0.000123718
USP2 / Neon	SRRT	-0.919654737	1.14141E-05
USP2 / Neon	COG5	-0.929305696	0.000316867
USP2 / Neon	MAP2K1	-0.935368894	5.18181E-07
USP2 / Neon	ALDH1A3	-0.93640222	0.000329062
USP2 / Neon	EIF2AK4	-0.937504299	2.58256E-05
USP2 / Neon	C2orf76	-0.939952662	1.14141E-05
USP2 / Neon	ARFIP2	-0.941175713	6.17872E-06
USP2 / Neon	SMCHD1	-0.942207177	0.002457506
USP2 / Neon	IMPDH1	-0.943997143	0.005092719
USP2 / Neon	UBE2H	-0.956379377	4.50519E-06
USP2 / Neon	HGH1	-0.95715454	7.36264E-05
USP2 / Neon	ATP5PO	-0.961190668	0.000789755
USP2 / Neon	EIF2B1	-0.964139918	6.17872E-06

USP2 / Neon	MRPL20	-0.965134431	0.013135036
USP2 / Neon	USP9Y	-0.973490738	2.91777E-05
USP2 / Neon	RELCH	-0.974398997	1.26824E-06
USP2 / Neon	TSEN54	-0.975835275	8.49383E-05
USP2 / Neon	KIFC1	-0.97842852	0.000526257
USP2 / Neon	KIAA1217	-0.98274462	0.000600985
USP2 / Neon	CLSPN	-0.983670289	4.9646E-05
USP2 / Neon	UTP6	-0.985649865	0.009385209
USP2 / Neon	CCDC88C	-0.986336956	0.002585679
USP2 / Neon	ANXA5	-0.986847749	0.019501008
USP2 / Neon	PTPN2	-0.990494313	0.022995984
USP2 / Neon	CHTF18	-0.996918937	0.00045992
USP2 / Neon	GAGE1	-1.000677772	0.000121721
USP2 / Neon	FTH1	-1.007541796	4.12307E-05
USP2 / Neon	DEF6	-1.013857111	0.02105822
USP2 / Neon	QRSL1	-1.018268617	0.000278783
USP2 / Neon	STRBP	-1.021363094	0.000200454
USP2 / Neon	FLJ12886	-1.023974117	0.000120076
USP2 / Neon	SESN2	-1.031140424	1.14141E-05
USP2 / Neon	SCYL1	-1.031653358	2.42683E-05
USP2 / Neon	NAA25	-1.033253621	0.006028378
USP2 / Neon	EXOSC1	-1.036885856	0.000252102
USP2 / Neon	CCNK	-1.037170238	1.14141E-05
USP2 / Neon	GSTCD	-1.041114996	2.71809E-05
USP2 / Neon	HOOK2	-1.043713185	0.000207543
USP2 / Neon	NLRP2	-1.044540458	3.55238E-05
USP2 / Neon	C12orf29	-1.050639562	0.000260328
USP2 / Neon	PCBP2	-1.053305721	0.001620259
USP2 / Neon	ARHGEF1	-1.060436621	1.14243E-06
USP2 / Neon	SBDS	-1.065239517	5.18181E-07
USP2 / Neon	MAP2K2	-1.069631471	1.58788E-06
USP2 / Neon	NELFB	-1.078859877	0.000123098
USP2 / Neon	MCM3AP	-1.078906495	0.000708136
USP2 / Neon	RFK	-1.080838868	0.003145202
USP2 / Neon	KTN1	-1.094571915	7.62524E-05
USP2 / Neon	AASDHPPT	-1.09564568	2.1832E-05
USP2 / Neon	KNTC1	-1.101959116	9.13048E-06
USP2 / Neon	NUDCD1	-1.10287177	0.003462917
USP2 / Neon	POLR2K	-1.113696306	0.000105464
USP2 / Neon	GLMN	-1.115823449	5.34908E-06
USP2 / Neon	ISG15	-1.12015563	5.18181E-07
USP2 / Neon	TRIM5	-1.123145529	5.28472E-05
USP2 / Neon	SMAD2	-1.123239598	5.96888E-05
USP2 / Neon	TBC1D1	-1.131698106	9.94629E-06

USP2 / Neon	PRKCD	-1.132534229	7.67506E-06
USP2 / Neon	PITPNB	-1.135493273	5.35699E-05
USP2 / Neon	SNX1	-1.141054523	2.2492E-06
USP2 / Neon	GK	-1.143646657	0.01992956
USP2 / Neon	RAB3GAP2	-1.144591454	8.12907E-06
USP2 / Neon	RECQL	-1.14975968	0.001264002
USP2 / Neon	BCAT2	-1.152479724	0.02502073
USP2 / Neon	BAX	-1.155683073	1.46102E-05
USP2 / Neon	TBC1D13	-1.166287442	0.000147841
USP2 / Neon	DKFZp434L1715	-1.175791677	1.59832E-06
USP2 / Neon	U2SURP	-1.191124277	0.003090911
USP2 / Neon	COG7	-1.197992912	7.49668E-06
USP2 / Neon	GSTT1	-1.201980281	0.000452747
USP2 / Neon	ESRP2	-1.206800712	7.32916E-06
USP2 / Neon	BTAF1	-1.21360545	2.58993E-05
USP2 / Neon	NUDT21	-1.220327489	7.25509E-07
USP2 / Neon	PLK1	-1.223241626	0.000407735
USP2 / Neon	VTA1	-1.223879208	1.88937E-07
USP2 / Neon	DBT	-1.233294325	1.89177E-05
USP2 / Neon	DCUN1D5	-1.244558365	1.14243E-06
USP2 / Neon	PPP1CA	-1.259085244	2.09733E-05
USP2 / Neon	KIF1A	-1.261242221	0.000115591
USP2 / Neon	ASH2L	-1.268783529	7.27615E-05
USP2 / Neon	OATL1	-1.279919958	0.001188359
USP2 / Neon	ARFGF2	-1.289550151	0.000118285
USP2 / Neon	KRT9	-1.290740703	0.011781593
USP2 / Neon	TPP1	-1.291012284	1.45574E-05
USP2 / Neon	ANKRD52	-1.296201151	0.011533095
USP2 / Neon	UBE3C	-1.301599877	0.003075719
USP2 / Neon	ANLN	-1.306231583	0.005412015
USP2 / Neon	SAAL1	-1.323791567	0.000777488
USP2 / Neon	RNGTT	-1.332501388	0.000121628
USP2 / Neon	ACYP1	-1.333497982	3.69192E-05
USP2 / Neon	PPP2R5A	-1.336484899	2.44707E-07
USP2 / Neon	UBE2S	-1.346589114	0.00016739
USP2 / Neon	TIMM10	-1.346907333	7.47137E-05
USP2 / Neon	VPS16	-1.352805132	6.74098E-07
USP2 / Neon	SEC24A	-1.357709072	0.025516024
USP2 / Neon	GAMT	-1.366071697	1.89274E-05
USP2 / Neon	COPS3	-1.372619299	0.014644981
USP2 / Neon	CAPN1	-1.373295955	2.13573E-06
USP2 / Neon	TRG14	-1.379717115	1.98993E-05
USP2 / Neon	ILKAP	-1.382742701	0.000142799
USP2 / Neon	NUDT16L1	-1.38413285	0.000791021

USP2 / Neon	SON	-1.387167635	9.67061E-05
USP2 / Neon	CNP	-1.38738247	1.09019E-09
USP2 / Neon	DHX38	-1.391665742	5.4149E-06
USP2 / Neon	TPM3	-1.403740776	1.46308E-05
USP2 / Neon	TBC1D4	-1.413558063	9.08695E-05
USP2 / Neon	ULK3	-1.426809714	0.003190515
USP2 / Neon	SBNO1	-1.432729771	0.001097513
USP2 / Neon	NCBP2	-1.433143906	2.31952E-05
USP2 / Neon	WASF2	-1.435624562	0.021570505
USP2 / Neon	SEC22B	-1.441521395	2.02723E-06
USP2 / Neon	CYP11B2	-1.452934153	1.2023E-06
USP2 / Neon	MIF4GD	-1.455935314	1.71603E-05
USP2 / Neon	PSME2	-1.471552053	2.82276E-05
USP2 / Neon	PANK4	-1.479489594	2.69548E-05
USP2 / Neon	HAUS3	-1.487035642	4.77724E-05
USP2 / Neon	WDR7	-1.497102603	0.002566426
USP2 / Neon	INTS13	-1.499349121	3.42624E-05
USP2 / Neon	CSDA	-1.499388555	0.001508017
USP2 / Neon	PCBP2	-1.517458705	0.000838312
USP2 / Neon	HSPBAP1	-1.521429153	0.001300144
USP2 / Neon	MTFR1	-1.521883683	1.36182E-05
USP2 / Neon	SPC24	-1.524447597	5.22735E-05
USP2 / Neon	XPOT	-1.551735293	2.59995E-05
USP2 / Neon	CTTNBP2NL	-1.611574583	4.88889E-05
USP2 / Neon	HINT3	-1.618033109	0.000208977
USP2 / Neon	ARF4	-1.653019261	3.31419E-05
USP2 / Neon	METAP1	-1.673662861	2.67058E-05
USP2 / Neon	DTX3L	-1.693408291	1.59457E-06
USP2 / Neon	TRIM24	-1.716015677	2.97894E-06
USP2 / Neon	MRPS9	-1.745413427	1.16195E-05
USP2 / Neon	BOLA1	-1.748019437	1.54558E-05
USP2 / Neon	TRADD	-1.752500547	1.27446E-07
USP2 / Neon	UBE4B	-1.758752675	4.90504E-06
USP2 / Neon	PRNPIP	-1.769021	4.88889E-05
USP2 / Neon	SNX27	-1.769840006	8.59949E-05
USP2 / Neon	MNAT1	-1.780341662	0.000245201
USP2 / Neon	RPS6KB1	-1.864959868	6.05147E-05
USP2 / Neon	HGS	-1.902799494	4.00294E-06
USP2 / Neon	MICAL1	-1.933912657	0.000297663
USP2 / Neon	TSC22D4	-1.935127545	0.00456496
USP2 / Neon	FKBP8	-1.937858162	4.1762E-05
USP2 / Neon	FAM136A	-1.977299796	0.000174244
USP2 / Neon	ABR	-2.000290974	1.25344E-05
USP2 / Neon	AHSG	-2.003940103	0.004784791

USP2 / Neon	WDR4	-2.00741123	7.26322E-05
USP2 / Neon	PSMB6	-2.080814327	6.74098E-07
USP2 / Neon	RPL15	-2.099303587	2.45715E-05
USP2 / Neon	TARS2	-2.125364824	0.000343189
USP2 / Neon	AP1G1	-2.139634991	1.94443E-05
USP2 / Neon	TPD52L1	-2.165184821	1.54558E-05
USP2 / Neon	CYFIP1	-2.195826774	5.04678E-06
USP2 / Neon	RWDD1	-2.29904054	8.83914E-05
USP2 / Neon	HSPA8	-2.328464029	1.45555E-05
USP2 / Neon	CEP170B	-2.33991674	0.001295861
USP2 / Neon	NCOA2	-2.667138962	0.00042431
USP2 / Neon	RPL26	-3.118640041	4.27584E-05
USP2 / Neon	AP2M1	-3.488867937	0.016005231
USP2 / Neon	HEL-176	-3.678747688	3.31419E-05
USP2 / Neon	RPL29	-3.862697441	5.07001E-05

7.3 Transcriptomics data from LNCaP cells overexpressing USP2

Supplementary Table 7.5. Transcripts that were significantly increased or decreased in the LNCaP cells overexpressing USP2 versus the control cells (average log₂ fold-change > 1).

Comparison (group1/group2)	Gene	log ₂ FoldChange	pvalue
USP2 / Neon	LXN	-2.001683262	3.84E-07
USP2 / Neon	COX7B2	-1.478143646	3.74E-05
USP2 / Neon	UCHL1	-1.44569606	4.52278E-08
USP2 / Neon	SPG20	-1.427631651	1.75E-08
USP2 / Neon	RLN2	-1.397055481	3.91E-08
USP2 / Neon	SERPIND1	-1.3863634	1.59962E-06
USP2 / Neon	KRT6C	-1.383459639	1.10564E-07
USP2 / Neon	REEP2	-1.336114048	1.50E-08
USP2 / Neon	S100A10	-1.27199362	2.65182E-07
USP2 / Neon	RFX6	-1.218784683	0.004090937
USP2 / Neon	MID1	-1.215766108	6.36E-06
USP2 / Neon	C9orf64	-1.215133364	1.99E-13
USP2 / Neon	ABHD1	-1.18677331	3.81E-06
USP2 / Neon	RARRES3	-1.161331474	0.014312396
USP2 / Neon	RLN1	-1.154079304	2.37713E-11
USP2 / Neon	CDKN2B	-1.147996967	0.001209638
USP2 / Neon	GSTA2	-1.13887579	1.59E-04
USP2 / Neon	ACOX2	-1.12356052	2.38696E-09
USP2 / Neon	CYP2S1	-1.107515464	3.94E-05
USP2 / Neon	GAGE1	-1.102135651	1.32E-05
USP2 / Neon	SGK2	-1.098775595	5.27599E-06
USP2 / Neon	CYP3A5	-1.061640776	0.001584384
USP2 / Neon	NPPC	-1.055556299	0.000656832
USP2 / Neon	OAS1	-1.055167836	0.022864245
USP2 / Neon	GSTA1	-1.051622261	2.3737E-05
USP2 / Neon	PTGES	-1.039394856	0.001085485
USP2 / Neon	LIN7A	-1.024124679	3.29363E-08
USP2 / Neon	TTR	-1.011661671	0.000118084
USP2 / Neon	ANK1	-1.002691263	0.000236786
USP2 / Neon	EPDR1	-0.990772959	1.02141E-11
USP2 / Neon	ZNF608	-0.97921002	0.001792465
USP2 / Neon	FRAS1	-0.970696897	0.000485873

USP2 / Neon	PHLDA1	-0.956958029	0.001488896
USP2 / Neon	BCAS1	-0.956660862	2.23E-04
USP2 / Neon	ALPK2	-0.936072805	1.81E-03
USP2 / Neon	SPAG16	-0.934727003	3.02E-08
USP2 / Neon	NMNAT2	-0.925275158	3.56545E-10
USP2 / Neon	LAMB3	-0.923080392	0.03098579
USP2 / Neon	C17orf49	-0.918972406	6.67E-04
USP2 / Neon	GNAI1	-0.908506117	0.00010859
USP2 / Neon	NPC1	-0.877886507	1.77848E-05
USP2 / Neon	HTATIP2	-0.874207855	2.51147E-06
USP2 / Neon	CTB-119C2.1	-0.870460816	1.21E-03
USP2 / Neon	FAM110B	-0.869551601	5.33287E-05
USP2 / Neon	FBXL7	-0.850050142	0.003647835
USP2 / Neon	ABCC8	-0.84445488	0.014881216
USP2 / Neon	RP11-479H16.1	-0.829572835	1.24543E-06
USP2 / Neon	COL3A1	-0.829099141	4.91E-03
USP2 / Neon	CRYAB	-0.816938327	4.26E-03
USP2 / Neon	BRDT	-0.815786855	0.000220523
USP2 / Neon	RP11-11N9.4	-0.810444639	0.001369592
USP2 / Neon	ACE2	-0.808146433	0.000257629
USP2 / Neon	GAGE2A	-0.80268754	0.000211531
USP2 / Neon	LAMA1	-0.789784122	8.14298E-05
USP2 / Neon	HS3ST1	-0.786797314	8.60E-05
USP2 / Neon	MAF	-0.786539522	0.004280818
USP2 / Neon	SNCG	-0.786519594	0.013147113
USP2 / Neon	PLA1A	-0.780991767	1.72594E-05
USP2 / Neon	OPRK1	-0.771159414	0.005603795
USP2 / Neon	IFIT1	-0.763511562	0.03580724
USP2 / Neon	ADAM23	-0.763437925	1.19126E-05
USP2 / Neon	ACTA2	-0.756758359	0.004678313
USP2 / Neon	CCDC74A	-0.755369865	0.000867408
USP2 / Neon	SLC1A3	-0.753330519	0.000233243
USP2 / Neon	OLFM1	-0.749704049	0.013103564
USP2 / Neon	NAP1L3	-0.742333738	0.002485312
USP2 / Neon	IFITM2	-0.734706134	5.06279E-05
USP2 / Neon	GBP2	-0.734193245	0.007077536
USP2 / Neon	IFIT3	-0.725605253	0.024124059
USP2 / Neon	GUCY1B3	-0.723130112	0.002880714
USP2 / Neon	HDX	-0.717708085	0.009102613
USP2 / Neon	NAALAD2	-0.714237286	0.000602825
USP2 / Neon	PCDHB11	-0.714005845	0.005414871
USP2 / Neon	PARVA	-0.713838388	8.77187E-06
USP2 / Neon	OASL	-0.71357562	0.0029725
USP2 / Neon	CFAP69	-0.706236102	1.23442E-06

USP2 / Neon	IGF1	-0.703620218	0.006015768
USP2 / Neon	IFI6	-0.694490331	0.046041408
USP2 / Neon	AC018865.8	-0.675879111	0.002759451
USP2 / Neon	VTA1	-0.665144391	0.000147994
USP2 / Neon	RANBP3L	-0.663926916	0.004276947
USP2 / Neon	RP11-318A15.2	-0.657267777	0.012310982
USP2 / Neon	CNTNAP4	-0.654278288	0.009962499
USP2 / Neon	NFASC	-0.65404933	0.000731473
USP2 / Neon	MCMDC2	-0.653497646	0.006996828
USP2 / Neon	CTD-2314B22.1	-0.65288701	0.004235619
USP2 / Neon	SQRDL	-0.651893765	0.004927203
USP2 / Neon	CTB-131B5.4	-0.650986043	1.53106E-05
USP2 / Neon	LA16c-83F12.6	-0.650325909	0.01252239
USP2 / Neon	ID1	-0.64763659	0.043379922
USP2 / Neon	AC073869.1	-0.643895305	0.019794317
USP2 / Neon	DOCK3	-0.64301815	3.9753E-06
USP2 / Neon	DAPK1	-0.642285469	0.014198521
USP2 / Neon	TLL2	-0.640290232	0.011155098
USP2 / Neon	CHST11	-0.636028966	0.045763351
USP2 / Neon	APOL3	-0.635534176	0.012046812
USP2 / Neon	EFHC2	-0.634191702	0.0087701
USP2 / Neon	IRF1	-0.624590993	0.042553105
USP2 / Neon	DNAH2	-0.623255067	0.003359918
USP2 / Neon	RP11-39H3.2	-0.621401739	0.015666939
USP2 / Neon	GPC3	-0.616828978	0.011608806
USP2 / Neon	RP1-34B20.4	-0.616163481	0.013483874
USP2 / Neon	RP5-1096D14.2	-0.615064536	0.005021244
USP2 / Neon	AC018804.3	-0.614880645	0.004058883
USP2 / Neon	RP1-239B22.5	-0.612096273	0.029473781
USP2 / Neon	B3GALT4	-0.608976028	0.031823685
USP2 / Neon	EVA1B	-0.60771229	0.003555898
USP2 / Neon	ADAMTS15	-0.598862569	0.020856268
USP2 / Neon	PIFO	-0.598744156	0.019855457
USP2 / Neon	DMGDH	-0.597223756	0.011174232
USP2 / Neon	PLCB1	-0.591118906	0.005705738
USP2 / Neon	BAG2	-0.589768466	6.82803E-05
USP2 / Neon	PARP10	-0.582250608	0.006600628
USP2 / Neon	ANKRD22	-0.577553943	0.009203068
USP2 / Neon	KLB	-0.575951333	0.035267151
USP2 / Neon	BIRC3	-0.574935029	0.000607519
USP2 / Neon	AGAP2	-0.5746784	0.021505365
USP2 / Neon	ZDHHC14	-0.572664655	6.48433E-05
USP2 / Neon	ZNF629	-0.570693406	0.000378801
USP2 / Neon	CD177	-0.570028765	0.048175224

USP2 / Neon	SERPINB8	-0.56453495	0.047451266
USP2 / Neon	TRGC2	-0.563727878	0.027850769
USP2 / Neon	ECHDC1	-0.562359566	2.28647E-05
USP2 / Neon	PRSS23	-0.559133074	0.006858991
USP2 / Neon	CD4	-0.558111062	0.048266905
USP2 / Neon	GPR19	-0.555905705	0.035436734
USP2 / Neon	A2ML1	-0.550702892	0.016501485
USP2 / Neon	RP11-500G10.1	-0.547185695	0.001686089
USP2 / Neon	HBEGF	-0.543837889	0.013152942
USP2 / Neon	PLXNA2	-0.542400162	0.028118392
USP2 / Neon	FMO4	-0.539736521	0.020595238
USP2 / Neon	CTC-498J12.1	-0.537232981	0.01839717
USP2 / Neon	RALYL	-0.535118138	2.07221E-05
USP2 / Neon	LIF	-0.532614026	0.009647086
USP2 / Neon	NUDT7	-0.524976131	0.03769351
USP2 / Neon	ANKRD6	-0.524383275	0.006360673
USP2 / Neon	MYH15	-0.523970332	0.006216994
USP2 / Neon	IFIT2	-0.523530493	0.011936651
USP2 / Neon	MYL9	-0.523422796	0.041931218
USP2 / Neon	SDK1	-0.522539725	0.041741281
USP2 / Neon	ZNF812P	-0.518140363	0.001540088
USP2 / Neon	APOL6	-0.516639626	0.035473904
USP2 / Neon	SAT1	-0.516136134	0.002290037
USP2 / Neon	LGALS3BP	-0.512897033	0.035844761
USP2 / Neon	NNMT	-0.508638349	0.015221996
USP2 / Neon	PSMD5	-0.505150345	0.007539463
USP2 / Neon	IFI44	-0.505125443	0.018722266
USP2 / Neon	RP11-88E10.5	-0.504205809	0.02243737
USP2 / Neon	RAB27A	-0.498376049	2.76172E-05
USP2 / Neon	IGSF5	-0.48902687	0.015255093
USP2 / Neon	HIST1H2AG	-0.48384346	0.003030548
USP2 / Neon	RP11-392E22.9	-0.483103718	0.036985573
USP2 / Neon	RP11-27I1.2	-0.478584333	0.021037738
USP2 / Neon	CTC-504A5.1	-0.475870277	0.040063709
USP2 / Neon	TOX3	-0.473695153	0.023925928
USP2 / Neon	SLC36A1	-0.467794559	0.039314405
USP2 / Neon	HSD3B7	-0.463936452	0.035849543
USP2 / Neon	EPHA6	-0.463927374	0.014554331
USP2 / Neon	MAP3K14	-0.463734446	0.001500808
USP2 / Neon	SEPSECS-AS1	-0.46294138	0.017658963
USP2 / Neon	RASL11A	-0.4624443	0.016714658
USP2 / Neon	FAS	-0.458453286	0.048628989
USP2 / Neon	UBA7	-0.456288596	0.048594317
USP2 / Neon	GTSE1-AS1	-0.447939643	0.032116714

USP2 / Neon	MYEF2	-0.4457862	0.048485637
USP2 / Neon	STK33	-0.445327674	5.74528E-05
USP2 / Neon	ALDH4A1	-0.444588221	0.011116581
USP2 / Neon	DIO1	-0.443588768	0.047816825
USP2 / Neon	TSPEAR-AS2	-0.441766776	0.015030765
USP2 / Neon	RP11-120K24.3	-0.437742401	0.009327515
USP2 / Neon	LPXN	-0.436125009	0.001274075
USP2 / Neon	RPL3L	-0.43569757	0.039594342
USP2 / Neon	MSRA	-0.432734743	0.008749098
USP2 / Neon	NXN	-0.429808596	0.000536135
USP2 / Neon	COL5A2	-0.424624958	0.012538001
USP2 / Neon	MKRN2OS	-0.422062573	0.026194909
USP2 / Neon	CFAP99	-0.414117125	0.042231627
USP2 / Neon	TNFSF15	-0.411783626	0.003322144
USP2 / Neon	SP100	-0.411317036	0.004122542
USP2 / Neon	RP11-440D17.3	-0.409396875	0.040467077
USP2 / Neon	PTPRM	-0.407817513	0.009529541
USP2 / Neon	PTGR1	-0.407441504	0.002258823
USP2 / Neon	STAT5A	-0.406467284	0.015556853
USP2 / Neon	APOBEC3F	-0.406002722	0.002051726
USP2 / Neon	RP11-225L12.2	-0.404093328	0.01391944
USP2 / Neon	FBXO36	-0.403665994	0.010130992
USP2 / Neon	CD27-AS1	-0.403340719	0.025496896
USP2 / Neon	PLXDC2	-0.403192809	0.022163898
USP2 / Neon	CYSTM1	-0.400141061	0.0483339
USP2 / Neon	CYP2J2	-0.39917513	0.007812636
USP2 / Neon	VGF	-0.398390076	0.048309196
USP2 / Neon	RP11-1020A11.2	-0.396514055	0.046703915
USP2 / Neon	GPX8	-0.39615696	0.006156005
USP2 / Neon	SPSB1	-0.395048393	0.001137065
USP2 / Neon	ASRGL1	-0.393317563	0.003685224
USP2 / Neon	TRGC1	-0.392722946	0.005017878
USP2 / Neon	CCT6B	-0.392489844	0.030137764
USP2 / Neon	GPR158	-0.391319987	0.036773325
USP2 / Neon	RP11-167P11.3	-0.390852434	0.040469777
USP2 / Neon	RTN1	-0.387372868	0.019772449
USP2 / Neon	FOXD4	-0.385598846	0.012710161
USP2 / Neon	HIBCH	-0.384142197	0.007561951
USP2 / Neon	CCDC69	-0.383353834	0.023883631
USP2 / Neon	NEK11	-0.380824734	0.032866693
USP2 / Neon	CA5BP	-0.380329612	0.014735683
USP2 / Neon	ELFN1	-0.378701208	0.01402909
USP2 / Neon	HIST1H3H	-0.377319886	0.026333207
USP2 / Neon	SDC2	-0.374667068	0.006369383

USP2 / Neon	KB-1732A1.1	-0.374623856	0.020497348
USP2 / Neon	HACL1	-0.374497875	0.023515522
USP2 / Neon	TXNL4B	-0.373057915	0.018995337
USP2 / Neon	SFXN5	-0.372629141	0.005964136
USP2 / Neon	SAMD12	-0.371501697	0.009994252
USP2 / Neon	RP11-305E17.6	-0.371334708	0.024395631
USP2 / Neon	TDRD7	-0.36978011	0.016227708
USP2 / Neon	SFTPA2	-0.369125273	0.010232047
USP2 / Neon	DDO	-0.369025311	0.018553936
USP2 / Neon	EAF2	-0.368813637	0.034947234
USP2 / Neon	LAMA3	-0.367507117	0.048717674
USP2 / Neon	COL4A2	-0.366895961	0.032586273
USP2 / Neon	RP11-96O20.1	-0.366493593	0.000924146
USP2 / Neon	HIST1H2AC	-0.361594757	0.007996071
USP2 / Neon	TMEM254-AS1	-0.36062079	0.006482754
USP2 / Neon	SLC25A16	-0.359422903	0.014719511
USP2 / Neon	C1orf21	-0.355866258	0.000549917
USP2 / Neon	GPER1	-0.355170519	0.016134324
USP2 / Neon	RP11-391M1.3	-0.354827362	0.040255567
USP2 / Neon	MT-ND3	-0.353180985	0.032313773
USP2 / Neon	TBXAS1	-0.352994976	0.013575874
USP2 / Neon	RABIF	-0.352437662	0.018197832
USP2 / Neon	RP3-404F18.2	-0.35154441	0.013768819
USP2 / Neon	CC2D2A	-0.350894406	0.00072396
USP2 / Neon	ABC13-47488600E17.1	-0.350211973	0.021763506
USP2 / Neon	ATP1B1	-0.349027674	0.029302752
USP2 / Neon	MFSD6	-0.346228776	0.024380085
USP2 / Neon	STS	-0.344994244	0.039659885
USP2 / Neon	CCDC64	-0.343046166	0.005055086
USP2 / Neon	ITGA3	-0.342973534	0.046791933
USP2 / Neon	CLN5	-0.341833127	0.012949469
USP2 / Neon	RP11-817O13.8	-0.341371295	0.042643567
USP2 / Neon	DNASE2B	-0.341217317	0.040781734
USP2 / Neon	RP3-467N11.1	-0.339772837	0.042459476
USP2 / Neon	STAMBPL1	-0.339461988	0.048678831
USP2 / Neon	SLC43A2	-0.338116408	0.00902051
USP2 / Neon	NKIRAS1	-0.33429181	0.007672816
USP2 / Neon	AP001372.2	-0.332153197	0.018983166
USP2 / Neon	SLC38A7	-0.330052192	0.003303148
USP2 / Neon	FLVCR1-AS1	-0.327651315	0.043403045
USP2 / Neon	GOT2	-0.325307677	0.000234317
USP2 / Neon	TPP1	-0.325021127	0.00520724
USP2 / Neon	CDH26	-0.324010802	0.018231762

USP2 / Neon	RP11-134G8.7	-0.322219384	0.038907481
USP2 / Neon	PYROXD1	-0.321778822	0.016573213
USP2 / Neon	GNG5	-0.321231472	0.031047271
USP2 / Neon	TIGAR	-0.317313839	0.010897813
USP2 / Neon	MPHOSPH6	-0.316895877	0.001266233
USP2 / Neon	RP11-120K24.2	-0.31506277	0.0375498
USP2 / Neon	SNAPC5	-0.313851236	0.009272606
USP2 / Neon	TMEM79	-0.313799388	0.03145717
USP2 / Neon	MLYCD	-0.313194945	0.002866167
USP2 / Neon	GGCT	-0.310814585	0.011403138
USP2 / Neon	DEPTOR	-0.309994366	0.020089189
USP2 / Neon	SPATS2L	-0.309871822	0.001794496
USP2 / Neon	RP11-73M18.8	-0.309339571	0.022040882
USP2 / Neon	EMBP1	-0.30735075	0.032737993
USP2 / Neon	ADGRG1	-0.307111046	0.007041352
USP2 / Neon	SMCO4	-0.306678513	0.038152079
USP2 / Neon	RP11-259N19.1	-0.304895421	0.026959329
USP2 / Neon	RP11-332M2.1	-0.303909312	0.002787189
USP2 / Neon	COG8	-0.303046975	0.013710487
USP2 / Neon	CAPN13	-0.302757737	0.045227579
USP2 / Neon	GINS2	-0.301515848	0.008715084
USP2 / Neon	COQ2	-0.299081916	0.046554993
USP2 / Neon	LMAN2L	-0.295251554	0.013981942
USP2 / Neon	SNX7	-0.292482154	0.005465795
USP2 / Neon	ALG8	-0.29100633	0.003364418
USP2 / Neon	HSD17B11	-0.290664571	0.049656622
USP2 / Neon	AC003665.1	-0.285662512	0.033347795
USP2 / Neon	AKTIP	-0.285309363	0.02501478
USP2 / Neon	SBDS	-0.285073229	0.005699531
USP2 / Neon	PSMG1	-0.282666836	0.010022133
USP2 / Neon	CCNH	-0.280709357	0.025632826
USP2 / Neon	ORC6	-0.280266617	0.021714809
USP2 / Neon	RP5-991G20.1	-0.278423643	0.049172553
USP2 / Neon	MANEAL	-0.27841665	0.037800646
USP2 / Neon	WWP2	-0.27836531	0.001611405
USP2 / Neon	MAP1LC3B	-0.277853329	0.005235494
USP2 / Neon	DHRS7	-0.277852914	0.030774714
USP2 / Neon	NAAA	-0.277729172	0.001444935
USP2 / Neon	CAPRIN2	-0.277634385	0.032612782
USP2 / Neon	TAP1	-0.276815377	0.024165126
USP2 / Neon	APOBEC3B	-0.271540386	0.01608847
USP2 / Neon	SPRYD4	-0.271392246	0.027688469
USP2 / Neon	ITPRIP	-0.270664653	0.038992287
USP2 / Neon	GLMP	-0.264700879	0.03838151

USP2 / Neon	COQ9	-0.263321784	0.015289992
USP2 / Neon	HNF1B	-0.263110092	0.005681692
USP2 / Neon	B2M	-0.262927751	0.03171944
USP2 / Neon	AFG3L1P	-0.261493455	0.012752998
USP2 / Neon	IDI1	-0.261117073	0.010227972
USP2 / Neon	MARVELD3	-0.260982335	0.011832234
USP2 / Neon	HOMER2	-0.258878336	0.011843844
USP2 / Neon	CCZ1	-0.253181802	0.038671282
USP2 / Neon	EPN3	-0.251678676	0.041490565
USP2 / Neon	EIF2B2	-0.248743149	0.045037659
USP2 / Neon	PIGH	-0.248492688	0.015842572
USP2 / Neon	TPRG1L	-0.244947695	0.020513607
USP2 / Neon	PHF7	-0.244829083	0.038560336
USP2 / Neon	F8	-0.243879623	0.019065789
USP2 / Neon	HK1	-0.243661667	0.006967962
USP2 / Neon	RDH11	-0.243123903	0.036038677
USP2 / Neon	RDH14	-0.242984942	0.016695534
USP2 / Neon	HABP4	-0.242038357	0.029781121
USP2 / Neon	CNDP2	-0.240978919	0.011100863
USP2 / Neon	KCNN2	-0.239814917	0.010822317
USP2 / Neon	GINS3	-0.239779376	0.035252281
USP2 / Neon	C2orf76	-0.239317641	0.037033032
USP2 / Neon	VPS33A	-0.238805685	0.031281721
USP2 / Neon	RP4-591C20.9	-0.238633386	0.014375233
USP2 / Neon	ALPK1	-0.238087461	0.044836767
USP2 / Neon	HAUS4	-0.237601258	0.046635932
USP2 / Neon	WDR81	-0.234266819	0.033063955
USP2 / Neon	TANGO2	-0.231152873	0.035005019
USP2 / Neon	TMEM254	-0.230900445	0.029969605
USP2 / Neon	TMEM231	-0.229878514	0.045115745
USP2 / Neon	HSBP1	-0.228998052	0.040710634
USP2 / Neon	STXBP1	-0.224137295	0.03179422
USP2 / Neon	INTS12	-0.223982249	0.018828221
USP2 / Neon	CRLS1	-0.220126822	0.038694618
USP2 / Neon	LACTB2	-0.220045369	0.048104327
USP2 / Neon	SLC7A8	-0.219821052	0.032605059
USP2 / Neon	UGP2	-0.218480718	0.026309178
USP2 / Neon	PCYOX1L	-0.215639987	0.011829894
USP2 / Neon	PNO1	-0.215581358	0.037720449
USP2 / Neon	EEPDI	-0.215054646	0.018265043
USP2 / Neon	CIAPIN1	-0.213743734	0.036592333
USP2 / Neon	CPPED1	-0.212175594	0.032884391
USP2 / Neon	FAIM	-0.209369051	0.027228596
USP2 / Neon	PCNA	-0.208557518	0.031248826

USP2 / Neon	COG1	-0.20692663	0.041177751
USP2 / Neon	ARSD	-0.20594359	0.037234319
USP2 / Neon	SIAE	-0.205018717	0.015507534
USP2 / Neon	SETD6	-0.204843945	0.033996478
USP2 / Neon	ATG3	-0.204573468	0.030169342
USP2 / Neon	ZPR1	-0.20432473	0.043929723
USP2 / Neon	NDUFAB6	-0.203198939	0.035098766
USP2 / Neon	GUCD1	-0.202719692	0.025287668
USP2 / Neon	CHKA	-0.20186989	0.037614718
USP2 / Neon	TERF2IP	-0.196781409	0.022619931
USP2 / Neon	TOM1L2	-0.196582282	0.037981956
USP2 / Neon	AUH	-0.196282466	0.035573391
USP2 / Neon	HIGD1A	-0.196064534	0.048117044
USP2 / Neon	VAMP3	-0.195854383	0.023933829
USP2 / Neon	PLPP6	-0.192557133	0.036348367
USP2 / Neon	TLDC1	-0.190427899	0.04237356
USP2 / Neon	HSDL2	-0.182698626	0.04418382
USP2 / Neon	RTCA	-0.17610742	0.041152316
USP2 / Neon	SLC44A2	-0.166189736	0.046628843
USP2 / Neon	PBX2	0.165170627	0.048803139
USP2 / Neon	CANT1	0.17292983	0.039673817
USP2 / Neon	JAG2	0.184262779	0.035750755
USP2 / Neon	THRA	0.192918842	0.028156674
USP2 / Neon	PLXNB1	0.19805946	0.04021376
USP2 / Neon	RAB11FIP4	0.209004019	0.029201604
USP2 / Neon	DIRAS1	0.225443252	0.033436858
USP2 / Neon	PTK7	0.225542517	0.021919509
USP2 / Neon	SEPT3	0.226294435	0.032362547
USP2 / Neon	CEP290	0.22899983	0.026957809
USP2 / Neon	TTYH3	0.232406879	0.047947957
USP2 / Neon	C1RL	0.232420733	0.019454819
USP2 / Neon	FAM53B	0.232610338	0.01325269
USP2 / Neon	TARSL2	0.232933056	0.038145645
USP2 / Neon	CASKIN1	0.236867686	0.030174037
USP2 / Neon	TTC6	0.238143923	0.028727463
USP2 / Neon	ANKRD10	0.239426371	0.035374483
USP2 / Neon	RP11-569G13.1	0.241268255	0.045083643
USP2 / Neon	DNAJC22	0.242512291	0.0452932
USP2 / Neon	PTPRU	0.24465631	0.018487432
USP2 / Neon	SOX8	0.250720237	0.013133154
USP2 / Neon	GATA2	0.250963729	0.023644475
USP2 / Neon	DCUN1D2	0.254718242	0.035112494
USP2 / Neon	CBX2	0.255036251	0.020440523
USP2 / Neon	PDIA4	0.25762726	0.008442993

USP2 / Neon	KIAA0922	0.257710674	0.031345636
USP2 / Neon	TP73-AS1	0.259863583	0.007959205
USP2 / Neon	CAMKK2	0.261807736	0.010092626
USP2 / Neon	NECTIN4	0.262255544	0.011578505
USP2 / Neon	PNISR	0.263988055	0.007785927
USP2 / Neon	ULBP1	0.267349808	0.033142796
USP2 / Neon	NSMF	0.269917323	0.030812369
USP2 / Neon	FADS2	0.272291707	0.015021992
USP2 / Neon	AC126544.4	0.273442184	0.007515462
USP2 / Neon	TMEFF2	0.273970877	0.014114933
USP2 / Neon	H3F3A	0.274592726	0.003822032
USP2 / Neon	ARNT2	0.274901907	0.018167479
USP2 / Neon	DNAJC15	0.275767432	0.038000526
USP2 / Neon	MIA3	0.276238379	0.019888431
USP2 / Neon	PHF21A	0.276906414	0.022614257
USP2 / Neon	FAM63A	0.279671088	0.034103425
USP2 / Neon	BPNT1	0.282719055	0.024455085
USP2 / Neon	MNX1	0.283382366	0.023372882
USP2 / Neon	EVL	0.283689629	0.032690454
USP2 / Neon	SLC6A8	0.286177797	0.039823768
USP2 / Neon	MFSD7	0.286285742	0.022960287
USP2 / Neon	SEC14L2	0.286494023	0.044223462
USP2 / Neon	BTN3A1	0.286937563	0.00704014
USP2 / Neon	CCNB1IP1	0.287701072	0.043708408
USP2 / Neon	ZSCAN18	0.288258164	0.028051239
USP2 / Neon	GGH	0.292273116	0.004870901
USP2 / Neon	DCLRE1C	0.292774235	0.045819995
USP2 / Neon	FAM189B	0.293194926	0.035033768
USP2 / Neon	BTN3A3	0.293463995	0.005389864
USP2 / Neon	ZNF783	0.295648833	0.00182702
USP2 / Neon	TPCN2	0.298075005	0.036759802
USP2 / Neon	MAPT	0.298145491	0.024944687
USP2 / Neon	GPRIN2	0.298469638	0.038037533
USP2 / Neon	PLEKHG2	0.299445544	0.040085783
USP2 / Neon	PTRF	0.302730989	0.03450653
USP2 / Neon	ZNF415	0.303475891	0.042857078
USP2 / Neon	RAB36	0.304080976	0.008579064
USP2 / Neon	FAM234B	0.304520757	0.004686958
USP2 / Neon	CEBPD	0.308320536	0.021811099
USP2 / Neon	ERO1A	0.308839133	0.033009584
USP2 / Neon	IGSF9	0.31029605	0.004111941
USP2 / Neon	SHC1	0.310575176	0.005808298
USP2 / Neon	KIF3C	0.313440801	0.010582247
USP2 / Neon	SEMA4G	0.314617193	0.025158096

USP2 / Neon	BTN2A2	0.314793196	0.01444932
USP2 / Neon	NCAM2	0.316387014	0.011763541
USP2 / Neon	FAM174A	0.316937007	0.000625263
USP2 / Neon	SAMD13	0.320959319	0.006764788
USP2 / Neon	TEAD2	0.321102655	0.039907761
USP2 / Neon	AADAT	0.322449286	0.033785249
USP2 / Neon	PKP1	0.322921677	0.039346479
USP2 / Neon	CLSTN3	0.323349173	0.006212933
USP2 / Neon	RP11-823P9.1	0.325041722	0.029463709
USP2 / Neon	PADI2	0.326273114	0.033922263
USP2 / Neon	RP11-382A20.3	0.329886986	0.018740173
USP2 / Neon	GAREM2	0.331204692	0.046372855
USP2 / Neon	RIMS3	0.331856688	0.046907831
USP2 / Neon	SEMA4C	0.333966479	0.015033192
USP2 / Neon	IRF2BP2	0.334483093	0.005279632
USP2 / Neon	CAMK2N1	0.336240265	0.041138591
USP2 / Neon	PRAME	0.336296132	0.001145991
USP2 / Neon	AC004066.1	0.336873304	0.043521352
USP2 / Neon	SLC9B2	0.337071712	0.024258346
USP2 / Neon	HMGA1	0.338272391	0.019331008
USP2 / Neon	MKNK2	0.339699828	0.025291897
USP2 / Neon	TAOK3	0.340473446	0.025582416
USP2 / Neon	INTS6L	0.341777854	0.042354394
USP2 / Neon	CISH	0.342223444	0.0461606
USP2 / Neon	KAZALD1	0.346637828	0.039807305
USP2 / Neon	PAK1	0.347490374	0.004985602
USP2 / Neon	TARBP1	0.351130427	0.004402931
USP2 / Neon	AMACR	0.351887552	0.009503283
USP2 / Neon	SPTBN5	0.352311143	0.049364723
USP2 / Neon	SORBS1	0.352353829	0.047486254
USP2 / Neon	CEP68	0.352783232	0.014753934
USP2 / Neon	CTD-3060P21.1	0.353928959	0.011084513
USP2 / Neon	GS1-358P8.4	0.354347687	0.000753677
USP2 / Neon	OTUB2	0.355618514	0.021789217
USP2 / Neon	RP11-814P23.1	0.360740728	0.045561331
USP2 / Neon	LAPTM4B	0.361088309	0.002230753
USP2 / Neon	ZNF703	0.36142615	0.031346469
USP2 / Neon	TIMP2	0.36230937	0.006579448
USP2 / Neon	RCOR2	0.362659188	0.047069301
USP2 / Neon	COL1A1	0.363003725	0.023454431
USP2 / Neon	RP11-57A19.2	0.365013373	0.023005345
USP2 / Neon	SDHAF4	0.368127605	0.001951522
USP2 / Neon	RAB6B	0.371740904	0.000484581
USP2 / Neon	L3HYPDH	0.372459913	0.031133085

USP2 / Neon	BTN3A2	0.375334675	0.015608715
USP2 / Neon	APLN	0.376447911	4.46879E-05
USP2 / Neon	RP11-21I4.1	0.377990554	0.01681389
USP2 / Neon	ANKRD29	0.380808947	0.004798356
USP2 / Neon	UBE2E1	0.38249666	0.003433699
USP2 / Neon	ZNF350	0.383443621	0.000242008
USP2 / Neon	KDM5B	0.383746369	0.017022494
USP2 / Neon	EXD3	0.388379305	0.039337114
USP2 / Neon	ESYT3	0.389913557	0.027669178
USP2 / Neon	SHANK3	0.390017091	0.000542131
USP2 / Neon	ASS1	0.390024997	0.010314642
USP2 / Neon	NRARP	0.390069431	0.006389673
USP2 / Neon	CTD-2574D22.5	0.392900299	0.047090311
USP2 / Neon	RTN4RL1	0.394293477	0.001395568
USP2 / Neon	STXBP6	0.397345332	0.02054875
USP2 / Neon	TEX22	0.398070752	0.038935719
USP2 / Neon	MAGEA10	0.399311805	0.023428896
USP2 / Neon	SMO	0.399508164	0.001764482
USP2 / Neon	TMSB15A	0.400131699	0.028560708
USP2 / Neon	RP11-14N7.2	0.401371032	0.044580907
USP2 / Neon	MYNN	0.401589534	0.010124411
USP2 / Neon	APOLD1	0.401797894	0.018562837
USP2 / Neon	RP11-412D9.4	0.402791807	0.016467665
USP2 / Neon	TRPM4	0.402842784	0.03986633
USP2 / Neon	SLC39A8	0.403885087	0.002028879
USP2 / Neon	SFXN3	0.405397627	0.010493406
USP2 / Neon	ZNF185	0.406592228	0.022927732
USP2 / Neon	ZNF827	0.409633722	0.031642485
USP2 / Neon	NLGN3	0.41194387	0.027667441
USP2 / Neon	RP11-115D19.1	0.412105921	0.033459626
USP2 / Neon	ZNF432	0.413159415	0.015322626
USP2 / Neon	EPHB4	0.414620658	9.30586E-06
USP2 / Neon	PXDN	0.415021485	0.01905759
USP2 / Neon	RP11-263K19.9	0.415096192	0.0112019
USP2 / Neon	FSCN1	0.415382239	0.031029701
USP2 / Neon	RP11-575F12.3	0.416683154	0.014892746
USP2 / Neon	NBPF26	0.416942702	0.046786441
USP2 / Neon	VWF	0.419253035	0.009800759
USP2 / Neon	PLA2G7	0.420023502	0.023515714
USP2 / Neon	LRRC26	0.420608509	0.025000704
USP2 / Neon	INSIG2	0.420904455	0.043530987
USP2 / Neon	DUSP4	0.42156824	0.006192943
USP2 / Neon	SLC34A3	0.422212883	0.020464351
USP2 / Neon	FBXW7	0.422314645	0.020099743

USP2 / Neon	MEGF6	0.422618053	0.025630906
USP2 / Neon	PLPP2	0.425022059	0.010001908
USP2 / Neon	XXbac-BPG24O18.1	0.425160562	0.026419767
USP2 / Neon	ACTRT3	0.425859587	0.016712449
USP2 / Neon	KCNQ4	0.426074006	0.001272131
USP2 / Neon	DPYSL3	0.426347797	0.007879259
USP2 / Neon	ADORA1	0.426490981	0.049053064
USP2 / Neon	RP11-395P17.3	0.427005058	0.008945043
USP2 / Neon	ELFN2	0.427037574	0.024173713
USP2 / Neon	PALMD	0.42794684	0.036110325
USP2 / Neon	WASH5P	0.428879077	0.041828785
USP2 / Neon	ZNF395	0.429626605	0.022694315
USP2 / Neon	LUZP2	0.430014074	0.019135774
USP2 / Neon	ZNF665	0.431624022	0.004423344
USP2 / Neon	GDPD1	0.431681754	0.00298103
USP2 / Neon	DLX2	0.432426872	0.005599781
USP2 / Neon	ANKRD36	0.433842844	0.020566241
USP2 / Neon	NR4A1	0.435663746	0.000242025
USP2 / Neon	ERO1B	0.437720674	0.002113932
USP2 / Neon	MYRF	0.437830854	0.015563171
USP2 / Neon	ZNF321P	0.438101428	0.049422573
USP2 / Neon	RP11-1280N14.3	0.439573204	0.039807989
USP2 / Neon	ZC3HAV1L	0.43968563	0.027391273
USP2 / Neon	ADAMTS1	0.43988462	0.02419554
USP2 / Neon	ITGA5	0.440760813	0.006271201
USP2 / Neon	ARHGEF26	0.44172407	0.002715472
USP2 / Neon	TOR4A	0.443874985	0.010547821
USP2 / Neon	OLMALINC	0.445474658	0.018823137
USP2 / Neon	TRIM46	0.44836678	0.0391512
USP2 / Neon	S1PR3	0.448891606	0.003553919
USP2 / Neon	TERT	0.449669278	0.000123298
USP2 / Neon	CADM1	0.449856522	0.001030004
USP2 / Neon	FBXL16	0.451940677	0.003306951
USP2 / Neon	CACNA1D	0.454069553	0.009392279
USP2 / Neon	GAL	0.454468311	0.001405797
USP2 / Neon	HRNR	0.455677581	0.014634536
USP2 / Neon	MARK1	0.456780651	0.005498675
USP2 / Neon	KLF3	0.456822952	0.018460854
USP2 / Neon	CBARP	0.457180102	0.01865738
USP2 / Neon	TRIM7	0.458142168	0.0247175
USP2 / Neon	KLF4	0.459018278	0.005632915
USP2 / Neon	HSPG2	0.459938962	0.03150909
USP2 / Neon	GPR160	0.461454591	0.002086326
USP2 / Neon	NAT8L	0.461725012	6.81098E-05

USP2 / Neon	RP11-21L23.2	0.463120023	0.032612756
USP2 / Neon	ASIC1	0.466106315	0.002075861
USP2 / Neon	RP11-54D18.1	0.468751108	0.02670611
USP2 / Neon	PDK1	0.469034422	0.040351627
USP2 / Neon	PGK1	0.46972282	0.008432266
USP2 / Neon	SBK1	0.470259681	0.000563425
USP2 / Neon	LRP1	0.472993118	0.001707137
USP2 / Neon	FASN	0.474577031	0.004294789
USP2 / Neon	RP11-284F21.10	0.475902494	0.000731844
USP2 / Neon	TGIF2	0.476777194	0.000324343
USP2 / Neon	RP11-174G6.5	0.479475001	0.027766229
USP2 / Neon	PRR36	0.48082513	0.014116105
USP2 / Neon	HOXA5	0.482039039	0.011798442
USP2 / Neon	TLK1	0.483514007	0.037751219
USP2 / Neon	DTNA	0.484074169	0.001794021
USP2 / Neon	PTGER4	0.484858087	0.029934419
USP2 / Neon	GPR161	0.486462442	0.000235913
USP2 / Neon	GPC2	0.488946625	0.010946728
USP2 / Neon	RP11-396C23.2	0.489096815	0.013657666
USP2 / Neon	WDR66	0.490384202	0.013776242
USP2 / Neon	LRRC75A	0.491339661	0.044627983
USP2 / Neon	ADGRD1	0.495930756	0.021152892
USP2 / Neon	ITPR3	0.496835741	0.008331953
USP2 / Neon	ZBTB12	0.497454954	4.14607E-05
USP2 / Neon	NETO1	0.499499211	0.006528335
USP2 / Neon	GFPT2	0.502129747	0.047169885
USP2 / Neon	RP11-613D13.2	0.502553908	0.043784454
USP2 / Neon	FBLN2	0.503461238	0.005439688
USP2 / Neon	RP11-713C5.1	0.504052988	0.000656332
USP2 / Neon	PRAC1	0.50658497	0.012260814
USP2 / Neon	ZNF677	0.506688905	0.030859213
USP2 / Neon	RHBG	0.507589731	0.029909832
USP2 / Neon	MAP1LC3A	0.508209564	0.049487689
USP2 / Neon	AUTS2	0.50854023	0.017809744
USP2 / Neon	PITPNM3	0.509370554	0.001467132
USP2 / Neon	NOTCH3	0.509572714	0.00074729
USP2 / Neon	VANGL2	0.511030274	0.031181709
USP2 / Neon	HLA-H	0.511143369	0.049577826
USP2 / Neon	MAPK13	0.511702212	2.12939E-06
USP2 / Neon	NUP93	0.514809544	3.86736E-06
USP2 / Neon	ZNF460	0.516292912	0.02926444
USP2 / Neon	C2orf72	0.517431038	0.014828506
USP2 / Neon	OBSCN	0.52040661	0.000245486
USP2 / Neon	TNFAIP8L1	0.521710698	0.00654043

USP2 / Neon	RP5-862P8.2	0.521766455	0.03792562
USP2 / Neon	WNK2	0.523122086	9.99714E-05
USP2 / Neon	RP11-111F16.1	0.527044529	0.045460363
USP2 / Neon	ATAD3C	0.52924017	0.005115367
USP2 / Neon	FZD2	0.529276051	0.040425717
USP2 / Neon	SLC7A2	0.530678757	0.047672339
USP2 / Neon	OLFM2	0.530981058	0.017897557
USP2 / Neon	RP11-284F21.9	0.532963627	0.023306949
USP2 / Neon	RP11-316P21.1	0.533155875	0.047727477
USP2 / Neon	ENHO	0.533679522	0.026628579
USP2 / Neon	SCARF1	0.534469618	0.019848628
USP2 / Neon	AC083843.1	0.535451521	0.034720608
USP2 / Neon	METRNL	0.535965024	0.020258867
USP2 / Neon	RP11-266A24.1	0.537296104	0.003474439
USP2 / Neon	C8orf48	0.537468818	0.020289777
USP2 / Neon	POU5F1B	0.538205673	0.035653181
USP2 / Neon	ANKRD65	0.538895471	0.03588254
USP2 / Neon	RBP5	0.539203924	0.015920012
USP2 / Neon	CD164L2	0.539395158	0.032884747
USP2 / Neon	PPM1J	0.540036344	0.014136158
USP2 / Neon	NUAK1	0.540755378	0.028568885
USP2 / Neon	UGT2B17	0.54130817	0.005203403
USP2 / Neon	KCNIP3	0.545205032	0.008466567
USP2 / Neon	CCNG2	0.54868272	0.012623686
USP2 / Neon	PAQR6	0.548698336	0.037513762
USP2 / Neon	PDZD7	0.549283541	0.031595948
USP2 / Neon	L3MBTL3	0.549476489	0.047229781
USP2 / Neon	PRKAA2	0.551415089	0.039801427
USP2 / Neon	NBPF15	0.554900651	0.000809402
USP2 / Neon	BMP8B	0.560286925	0.005341974
USP2 / Neon	ABC12-49244600F4.3	0.561280241	0.024201976
USP2 / Neon	DCHS1	0.564363978	0.000817292
USP2 / Neon	GLYATL1P2	0.568871809	0.002589433
USP2 / Neon	FUOM	0.569847049	0.01211778
USP2 / Neon	LONRF2	0.573660078	0.02479659
USP2 / Neon	RAB31	0.575197889	0.019981551
USP2 / Neon	TMEM210	0.575562706	0.001202589
USP2 / Neon	MAT1A	0.576447134	0.016547828
USP2 / Neon	P2RX5	0.577199644	0.012773392
USP2 / Neon	SLC22A3	0.577782387	0.002061068
USP2 / Neon	RNF39	0.580483468	0.026426285
USP2 / Neon	GPR27	0.58557166	0.00054667
USP2 / Neon	SIDT1	0.586278684	0.005261767
USP2 / Neon	CMTM8	0.587054623	0.003911065

USP2 / Neon	MLXIPL	0.593187316	0.010245284
USP2 / Neon	PLEKHO1	0.593217059	0.002503698
USP2 / Neon	AC144530.1	0.594961454	0.036593861
USP2 / Neon	TNFAIP2	0.595526439	0.012462952
USP2 / Neon	BHLHA15	0.595756365	7.67042E-05
USP2 / Neon	KBTBD11	0.598322188	0.003595114
USP2 / Neon	RP11-5407.16	0.600147258	0.012012913
USP2 / Neon	RP11-69L16.5	0.600405111	0.032430697
USP2 / Neon	ITGB1P1	0.601087912	0.040031588
USP2 / Neon	RNF217	0.603256549	0.023904247
USP2 / Neon	HLA-L	0.603350766	0.025182754
USP2 / Neon	ZNF697	0.606979814	0.014810028
USP2 / Neon	BNIP3P	0.612652299	0.020826118
USP2 / Neon	LINGO3	0.614894861	0.029101136
USP2 / Neon	SULT2B1	0.621434472	0.00222689
USP2 / Neon	SRCIN1	0.623559131	0.000138625
USP2 / Neon	FRMD4A	0.62392016	0.010617942
USP2 / Neon	C14orf132	0.624189862	1.52807E-05
USP2 / Neon	GLYATL2	0.62599607	1.76082E-06
USP2 / Neon	C1orf95	0.628540623	2.46767E-06
USP2 / Neon	TFF3	0.630052213	0.035810685
USP2 / Neon	ARHGEF25	0.631705676	0.002450362
USP2 / Neon	RP11-5407.1	0.634110965	0.001916672
USP2 / Neon	BOC	0.635124263	0.009585339
USP2 / Neon	RP11-520H14.6	0.636101989	0.031478071
USP2 / Neon	B4GALNT3	0.6368591	0.003890987
USP2 / Neon	PFKP	0.63703074	0.000104311
USP2 / Neon	ZNF749	0.639688878	0.044916895
USP2 / Neon	RP11-299G20.5	0.640314968	0.014780458
USP2 / Neon	KCNK5	0.642550434	0.003071353
USP2 / Neon	PTPRK	0.642838224	0.002326531
USP2 / Neon	DUSP9	0.644233015	0.004765366
USP2 / Neon	RP11-315E17.1	0.647752992	6.48515E-05
USP2 / Neon	HCN3	0.648662002	0.003466326
USP2 / Neon	ASPH	0.648866463	0.010431668
USP2 / Neon	RP11-7209.4	0.649553388	0.00013721
USP2 / Neon	H2AFJ	0.653837238	0.00292017
USP2 / Neon	SSPO	0.659220556	5.55235E-05
USP2 / Neon	TET1	0.661507461	0.045107223
USP2 / Neon	GABBR1	0.6625651	0.000247967
USP2 / Neon	UNC5A	0.662715359	0.005214255
USP2 / Neon	VPS37D	0.664466344	0.040078001
USP2 / Neon	SLC4A4	0.666845162	0.001342365
USP2 / Neon	PABPC5	0.671685415	0.019235217

USP2 / Neon	ZNF702P	0.671690567	0.013917894
USP2 / Neon	RP11-288H12.3	0.673290792	0.039510705
USP2 / Neon	CBLN2	0.682135836	6.59624E-05
USP2 / Neon	EPHA7	0.683324906	0.041783148
USP2 / Neon	RP11-598D12.3	0.687303193	0.002950272
USP2 / Neon	TUSC1	0.69267106	1.78336E-05
USP2 / Neon	ATP8B3	0.697244549	0.029140283
USP2 / Neon	ARHGEF17	0.699308995	2.79136E-09
USP2 / Neon	WAS	0.699926629	0.007112916
USP2 / Neon	KLK3	0.700594166	0.001455818
USP2 / Neon	TUBB6	0.701744417	0.000102967
USP2 / Neon	ADRB2	0.702285045	3.8334E-07
USP2 / Neon	TWIST1	0.708518287	1.045E-05
USP2 / Neon	CNNM1	0.709426007	0.00013616
USP2 / Neon	LIMD2	0.709670956	0.012690329
USP2 / Neon	TMEM45A	0.710060866	0.003891476
USP2 / Neon	ITGB2	0.711871407	0.000418238
USP2 / Neon	RGS2	0.71522769	0.001475766
USP2 / Neon	GDF15	0.715406702	0.012006458
USP2 / Neon	GLIS2	0.718403715	0.000142734
USP2 / Neon	MAB21L3	0.724634953	0.045852613
USP2 / Neon	PFKFB4	0.727221956	0.007946998
USP2 / Neon	CTD-3065B20.1	0.727458848	0.009084623
USP2 / Neon	RNF165	0.729499484	0.038451453
USP2 / Neon	CHST15	0.734087112	2.9631E-07
USP2 / Neon	FCHSD1	0.73704605	0.003964488
USP2 / Neon	ANKS1B	0.748981875	0.014459362
USP2 / Neon	MEX3A	0.750040426	8.72805E-07
USP2 / Neon	TM4SF1	0.751552498	3.83364E-05
USP2 / Neon	SMIM10L2A	0.754588502	6.16769E-06
USP2 / Neon	GPR153	0.756643422	0.000710956
USP2 / Neon	SCNN1G	0.760981863	0.027336962
USP2 / Neon	C1QL4	0.766123735	0.005811147
USP2 / Neon	EGFR	0.767594392	0.007292245
USP2 / Neon	RASSF2	0.773890639	0.000788184
USP2 / Neon	TMSB4X	0.775717884	0.001326897
USP2 / Neon	MAGEA4	0.779144926	0.000276511
USP2 / Neon	TLR5	0.780975109	0.000518118
USP2 / Neon	EF5	0.787397165	1.97669E-14
USP2 / Neon	CCDC144B	0.787854943	0.022711241
USP2 / Neon	LFNG	0.79049579	2.32067E-06
USP2 / Neon	AQP3	0.791241767	3.41696E-07
USP2 / Neon	CA14	0.79526983	0.002101787
USP2 / Neon	FOXN4	0.798339386	0.00029197

USP2 / Neon	ADAM7	0.79876956	5.33942E-06
USP2 / Neon	STAB1	0.808228479	0.014257332
USP2 / Neon	CADPS2	0.815646764	0.000211469
USP2 / Neon	RP11-342D14.1	0.824359784	0.020490528
USP2 / Neon	KIAA1324	0.836529959	1.14675E-05
USP2 / Neon	ETV1	0.856354527	8.76778E-05
USP2 / Neon	SLC7A5	0.85693863	1.62914E-06
USP2 / Neon	SLC16A7	0.857653303	0.023938623
USP2 / Neon	ANGPT2	0.858854759	0.0003988
USP2 / Neon	TRPM8	0.871203472	4.65778E-06
USP2 / Neon	FCHO1	0.873961886	0.018716186
USP2 / Neon	RASD2	0.876994811	0.003467366
USP2 / Neon	CDC42EP1	0.881665885	5.55112E-05
USP2 / Neon	NLGN4X	0.882725438	0.000101234
USP2 / Neon	NOVA1	0.891539707	3.38932E-06
USP2 / Neon	KCNQ2	0.898497009	0.000668747
USP2 / Neon	PLEKHA2	0.910551644	0.008079582
USP2 / Neon	RP11-216F19.1	0.91696843	0.002879612
USP2 / Neon	RIPOR2	0.918530489	2.49968E-07
USP2 / Neon	TNIK	0.939526145	0.005538423
USP2 / Neon	ESPN	0.950098018	0.00020259
USP2 / Neon	RP11-382M14.1	0.95263304	3.21177E-11
USP2 / Neon	SLCO2A1	0.961414539	0.000370126
USP2 / Neon	SYT4	0.971213452	7.46692E-10
USP2 / Neon	PPFIA4	0.988176343	0.013616671
USP2 / Neon	OR51E1	1.00178958	0.002509278
USP2 / Neon	DSC2	1.007390072	0.002073379
USP2 / Neon	DDX53	1.012611465	0.000484452
USP2 / Neon	PRPH	1.019076463	0.000836653
USP2 / Neon	LPCAT2	1.024125085	0.001058728
USP2 / Neon	KLHL1	1.033743891	3.03736E-23
USP2 / Neon	CACNA1H	1.043239736	2.24486E-15
USP2 / Neon	SH2D3A	1.050421772	8.86466E-06
USP2 / Neon	RP11-560I19.4	1.05455631	2.02897E-05
USP2 / Neon	ADRA2A	1.064893127	5.29822E-13
USP2 / Neon	NAP1L5	1.07852687	1.40985E-06
USP2 / Neon	RP11-945A11.1	1.090907473	0.048104426
USP2 / Neon	CDH3	1.09456759	0.002244885
USP2 / Neon	PLOD2	1.119333392	0.008876707
USP2 / Neon	DSC1	1.153818454	0.017672587
USP2 / Neon	TNNT1	1.168915832	0.000224756
USP2 / Neon	PRDM16	1.173554442	0.000109168
USP2 / Neon	AC093726.4	1.209063454	0.027519519
USP2 / Neon	PLA2G4D	1.214017692	0.005041828

USP2 / Neon	UGT8	1.267606181	2.82223E-11
USP2 / Neon	BRINP3	1.299256613	1.88426E-05
USP2 / Neon	MAGEA8	1.314289542	6.27114E-05
USP2 / Neon	TENM1	1.362690292	0.000164723
USP2 / Neon	NDUFA4L2	1.386494052	0.016911463
USP2 / Neon	SLC22A2	1.438618751	1.47864E-05
USP2 / Neon	RP1-276N6.2	1.483430598	3.46433E-25
USP2 / Neon	TNNT2	1.502647821	2.01188E-06
USP2 / Neon	PEG3	1.506393558	9.83916E-06
USP2 / Neon	ADAM2	1.774396961	3.01011E-26
USP2 / Neon	MYOD1	1.920641359	7.99292E-05
USP2 / Neon	RP11-398J5.1	2.076758787	4.19801E-07

7.4 Conference Presentations (2019 to 2022)

1. Presented at the 2022 Florey Conference (University of Adelaide, Australia)
2. Presented at the 2022 ASMR South Australian Scientific Meeting (Australia)
3. Presented at the 2022 conference held at McClaren Vale Centre (Australia)
4. Presented at the 2021 Florey Conference (University of Adelaide, Australia)
5. Presented at the 2021 Australian Society for Medical Research (ASMR) South Australian Scientific Meeting
6. Presented at the 3-Minute-Thesis in the University of Adelaide, Australia (2021)
7. Presented at the 59th ASMR National Scientific Meeting (Australia) (2020)
8. Presented at the 2020 Florey Conference (University of Adelaide, Australia) and was awarded the “Innovative and Commercial Partner” Prize.

References

R Core Team (2022). R: A language and environment for statistical computing. R Foundation for Statistical Computing, Vienna, Austria. URL <https://www.R-project.org/>.

- ABESHOU, A., AHN, J., AKBANI, R., ALLY, A., AMIN, S., ANDRY, CHRISTOPHER D., ANNALA, M., APRIKIAN, A., ARMENIA, J., ARORA, A., AUMAN, J. T., BALASUNDARAM, M., BALU, S., BARBIERI, CHRISTOPHER E., BAUER, T., BENZ, CHRISTOPHER C., BERGERON, A., BEROUKHIM, R., BERRIOS, M., BIVOL, A., BODENHEIMER, T., BOICE, L., BOOTWALLA, MOIZ S., BORGES DOS REIS, R., BOUTROS, PAUL C., BOWEN, J., BOWLBY, R., BOYD, J., BRADLEY, ROBERT K., BREGGIA, A., BRIMO, F., BRISTOW, CHRISTOPHER A., BROOKS, D., BROOM, BRADLEY M., BRYCE, ALAN H., BUBLEY, G., BURKS, E., BUTTERFIELD, YARON S. N., BUTTON, M., CANES, D., CARLOTTI, CARLOS G., CARLSEN, R., CARMEL, M., CARROLL, PETER R., CARTER, SCOTT L., CARTUN, R., CARVER, BRETT S., CHAN, JUNE M., CHANG, MATTHEW T., CHEN, Y., CHERNIACK, ANDREW D., CHEVALIER, S., CHIN, L., CHO, J., CHU, A., CHUAH, E., CHUDAMANI, S., CIBULSKIS, K., CIRIELLO, G., CLARKE, A., COOPERBERG, MATTHEW R., CORCORAN, NIAL M., COSTELLO, ANTHONY J., COWAN, J., CRAIN, D., CURLEY, E., DAVID, K., DEMCHOK, JOHN A., DEMICHELIS, F., DHALLA, N., DHIR, R., DOUEIK, A., DRAKE, B., DVINGE, H., DYAKOVA, N., FELAU, I., FERGUSON, MARTIN L., FRAZER, S., FREEDLAND, S., FU, Y., GABRIEL, STACEY B., GAO, J., GARDNER, J., GASTIER-FOSTER, JULIE M., GEHLENBORG, N., GERKEN, M., GERSTEIN, MARK B., GETZ, G., GODWIN, ANDREW K., GOPALAN, A., GRAEFEN, M., GRAIM, K., GRIBBIN, T., GUIN, R., GUPTA, M., HADJIPANAYIS, A., HAIDER, S., HAMEL, L., HAYES, D. N., HEIMAN, DAVID I., et al. 2015. The Molecular Taxonomy of Primary Prostate Cancer. *Cell*, 163, 1011-1025.
- ABIDA, W., CYRTA, J., HELLER, G., PRANDI, D., ARMENIA, J., COLEMAN, I., CIESLIK, M., BENELLI, M., ROBINSON, D., ALLEN, E. M. V., SBONER, A., FEDRIZZI, T., MOSQUERA, J. M., ROBINSON, B. D., SARKAR, N. D., KUNJU, L. P., TOMLINS, S., WU, Y. M., RODRIGUES, D. N., LODA, M., GOPALAN, A., REUTER, V. E., PRITCHARD, C. C., MATEO, J., BIANCHINI, D., MIRANDA, S., CARREIRA, S., RESCIGNO, P., FILIPENKO, J., VINSON, J., MONTGOMERY, R. B., BELTRAN, H., HEATH, E. I., SCHER, H. I., KANTOFF, P. W., TAPLIN, M.-E., SCHULTZ, N., DEBONO, J. S., DEMICHELIS, F., NELSON, P. S., RUBIN, M. A., CHINNAIYAN, A. M. & SAWYERS, C. L. 2019. Genomic correlates of clinical outcome in advanced prostate cancer. *Proceedings of the National Academy of Sciences*, 116, 11428-11436.
- ADAMS, M. S. & BRONNER-FRASER, M. 2009. Review: The Role of Neural Crest Cells in the Endocrine System. *Endocrine Pathology*, 20, 92-100.
- AGGARWAL, R., HUANG, J., ALUMKAL, J. J., ZHANG, L., FENG, F. Y., THOMAS, G. V., WEINSTEIN, A. S., FRIEDL, V., ZHANG, C., WITTE, O. N., LLOYD, P., GLEAVE, M., EVANS, C. P., YOUNGREN, J., BEER, T. M., RETTIG, M., WONG, C. K., TRUE, L., FOYE, A., PLAYDLE, D., RYAN, C. J., LARA, P., CHI, K. N., UZUNANGELOV, V., SOKOLOV, A., NEWTON, Y., BELTRAN, H., DEMICHELIS, F., RUBIN, M. A., STUART, J. M. & SMALL, E.

- J. 2018. Clinical and Genomic Characterization of Treatment-Emergent Small-Cell Neuroendocrine Prostate Cancer: A Multi-institutional Prospective Study. *Journal of Clinical Oncology*, 36, 2492-2503.
- AGORAM, B. M. 2009. Use of pharmacokinetic/ pharmacodynamic modelling for starting dose selection in first-in-human trials of high-risk biologics. *Br J Clin Pharmacol*, 67, 153-60.
- AHMAD, F., CHERUKURI, M. K. & CHOYKE, P. L. 2021. Metabolic reprogramming in prostate cancer. *British Journal of Cancer*, 125, 1185-1196.
- AHMED, E. S., ELNOUR, L. S., HASSAN, R., SIDDIG, E. E., CHACKO, M. E., ALI, E. T., MOHAMED, M. A., MUNIR, A., MUNEER, M. S., MOHAMED, N. S. & EDRIS, A. M. M. 2020. Immunohistochemical expression of Cyclin D1 among Sudanese patients diagnosed with benign and malignant prostatic lesions. *BMC Res Notes*, 13, 295.
- AHMED, H. U., EL-SHATER BOSAILY, A., BROWN, L. C., GABE, R., KAPLAN, R., PARMAR, M. K., COLLACO-MORAES, Y., WARD, K., HINDLEY, R. G., FREEMAN, A., KIRKHAM, A. P., OLDROYD, R., PARKER, C. & EMBERTON, M. 2017. Diagnostic accuracy of multi-parametric MRI and TRUS biopsy in prostate cancer (PROMIS): a paired validating confirmatory study. *The Lancet*, 389, 815-822.
- ALAVI, S., STEWART, A. J., KEFFORD, R. F., LIM, S. Y., SHKLOVSKAYA, E. & RIZOS, H. 2018. Interferon Signaling Is Frequently Downregulated in Melanoma. *Frontiers in Immunology*, 9.
- AMMANNAGARI, N. & GEORGE, S. 2015. Anti-androgen therapies for prostate cancer: A focused review. *The American Journal of Hematology/Oncology*, 11, 15-19.
- ANAND, S., PENRHYN-LOWE, S. & VENKITARAMAN, A. R. 2003. AURORA-A amplification overrides the mitotic spindle assembly checkpoint, inducing resistance to Taxol. *Cancer Cell*, 3, 51-62.
- ANDERS, S., PYL, P. T. & HUBER, W. 2015. HTSeq--a Python framework to work with high-throughput sequencing data. *Bioinformatics*, 31, 166-9.
- ANDREWS, S. 2010. FastQC: A quality control tool for high throughput sequence data. *Babraham Bioinformatics*, v0.11.3.
- ANTAO, A. M., TYAGI, A., KIM, K.-S. & RAMAKRISHNA, S. 2020. Advances in Deubiquitinating Enzyme Inhibition and Applications in Cancer Therapeutics. *Cancers*, 12, 1579.
- APARICIO, A. M., HARZSTARK, A. L., CORN, P. G., WEN, S., ARAUJO, J. C., TU, S. M., PAGLIARO, L. C., KIM, J., MILLIKAN, R. E., RYAN, C., TANNIR, N. M., ZURITA, A. J., MATHEW, P., ARAP, W., TRONCOSO, P., THALL, P. F. & LOGOTHETIS, C. J. 2013. Platinum-based chemotherapy for variant castrate-resistant prostate cancer. *Clin Cancer Res*, 19, 3621-30.
- APARICIO, A. M., SHEN, L., TAPIA, E. L., LU, J. F., CHEN, H. C., ZHANG, J., WU, G., WANG, X., TRONCOSO, P., CORN, P., THOMPSON, T. C., BROOM, B., BAGGERLY, K., MAITY, S. N. & LOGOTHETIS, C. J. 2016. Combined Tumor Suppressor Defects Characterize Clinically Defined Aggressive Variant Prostate Cancers. *Clin Cancer Res*, 22, 1520-30.
- APWEILER, R., ATTWOOD, T. K., BAIROCH, A., BATEMAN, A., BIRNEY, E., BISWAS, M., BUCHER, P., CERUTTI, L., CORPET, F., CRONING, M. D., DURBIN, R., FALQUET, L., FLEISCHMANN, W., GOUZY, J., HERMJAKOB, H., HULO, N., JONASSEN, I., KAHN, D., KANAPIN, A., KARAVIDOPOULOU, Y., LOPEZ, R., MARX, B., MULDER, N. J., OINN, T. M., PAGNI, M., SERVANT, F., SIGRIST, C. J. & ZDOBNOV, E. M. 2001. The InterPro

- database, an integrated documentation resource for protein families, domains and functional sites. *Nucleic acids research*, 29, 37-40.
- ASTERITI, I. A., DE MATTIA, F. & GUARGUAGLINI, G. 2015. Cross-Talk between AURKA and Plk1 in Mitotic Entry and Spindle Assembly. *Front Oncol*, 5, 283.
- ASTERITI, I. A., GIUBETTINI, M., LAVIA, P. & GUARGUAGLINI, G. 2011. Aurora-A inactivation causes mitotic spindle pole fragmentation by unbalancing microtubule-generated forces. *Molecular Cancer*, 10, 131.
- AUS, G., ROBINSON, D., ROSELL, J., SANDBLOM, G. & VARENHORST, E. 2005. Survival in prostate carcinoma - outcomes from a prospective population-based cohort of 8887 men with up to 15 years of follow-up. *American Cancer Society*, 103, 943-951.
- AZARENKO, O., SMIYUN, G., MAH, J., WILSON, L. & JORDAN, M. A. 2014. Antiproliferative Mechanism of Action of the Novel Taxane Cabazitaxel as Compared with the Parent Compound Docetaxel in MCF7 Breast Cancer Cells. *Molecular Cancer Therapeutics*, 13, 2092-2103.
- BALBAS, M. D., EVANS, M. J., HOSFIELD, D. J., WONGVIPAT, J., ARORA, V. K., WATSON, P. A., CHEN, Y., GREENE, G. L., SHEN, Y. & SAWYERS, C. L. 2013. Overcoming mutation-based resistance to antiandrogens with rational drug design. *Elife*, 2, e00499.
- BAOHAI, X., SHI, F. & YONGQI, F. 2019. Inhibition of ubiquitin specific protease 17 restrains prostate cancer proliferation by regulation of epithelial-to-mesenchymal transition (EMT) via ROS production. *Biomedicine & Pharmacotherapy*, 118, 108946.
- BARBIE, D. A., TAMAYO, P., BOEHM, J. S., KIM, S. Y., MOODY, S. E., DUNN, I. F., SCHINZEL, A. C., SANDY, P., MEYLAN, E., SCHOLL, C., FRÖHLING, S., CHAN, E. M., SOS, M. L., MICHEL, K., MERMEL, C., SILVER, S. J., WEIR, B. A., REILING, J. H., SHENG, Q., GUPTA, P. B., WADLOW, R. C., LE, H., HOERSCH, S., WITTNER, B. S., RAMASWAMY, S., LIVINGSTON, D. M., SABATINI, D. M., MEYERSON, M., THOMAS, R. K., LANDER, E. S., MESIROV, J. P., ROOT, D. E., GILLILAND, D. G., JACKS, T. & HAHN, W. C. 2009. Systematic RNA interference reveals that oncogenic KRAS-driven cancers require TBK1. *Nature*, 462, 108-112.
- BARBU, A., LEJONKLOU, M. H. & SKOGSEID, B. 2016. Progranulin Stimulates Proliferation of Mouse Pancreatic Islet Cells and Is Overexpressed in the Endocrine Pancreatic Tissue of an MEN1 Mouse Model. *Pancreas*, 45, 533-40.
- BARRETT, T. 2015. What is multiparametric-MRI of the prostate and why do we need it? *Imaging Medicine*, 7, 13-17.
- BELTRAN, H. & DEMICHELIS, F. 2021. Therapy considerations in neuroendocrine prostate cancer: what next? *Endocr Relat Cancer*, 28, T67-t78.
- BELTRAN, H., OROMENDIA, C., DANILA, D., MONTGOMERY, B., HOIMES, C., SZMULEWITZ, R., VAISHAMPAYAN, U., ARMSTRONG, A., STEIN, M., PINSKI, J., SAILOR, V., BAREJA, R., ROMANEL, A., GUMPENI, N., SBONER, A., DARDENNE, E., PUCA, L., PRANDI, D., MOSQUERA, J., RUBIN, M., SCHER, H., RICKMAN, D., DEMICHELIS, F., NANUS, D., BALLMAN, K. & TAGAWA, S. 2019. A phase II trial of the aurora kinase A inhibitor alisertib for patients with castration resistant and neuroendocrine prostate cancer: efficacy and biomarkers. *Clinical Cancer Research*, 25, 43-51.
- BELTRAN, H., PRANDI, D., MOSQUERA, J., BENELLI, M., PUCA, L., CYRTA, J., MAROTZ, C., GIANNOPOULOU, E., CHAKRAVARTHI, B., VARAMBALLY, S., TOMLINS, S., NANUS, D., TAGAWA, S., VAN ALLEN, E., ELEMENTO, O., SBONER, A., GARRAWAY, L., RUBIN, M.

- & DEMICHELIS, F. 2016. Divergent clonal evolution of castration-resistant neuroendocrine prostate cancer. *Nature Medicine Letters*, 22, 298-305.
- BELTRAN, H., RICKMAN, D. S., PARK, K., CHAE, S. S., SBONER, A., MACDONALD, T. Y., WANG, Y., SHEIKH, K. L., TERRY, S., TAGAWA, S. T., DHIR, R., NELSON, J. B., DE LA TAILLE, A., ALLORY, Y., GERSTEIN, M. B., PERNER, S., PIENTA, K. J., CHINNAIYAN, A. M., WANG, Y., COLLINS, C. C., GLEAVE, M. E., DEMICHELIS, F., NANUS, D. M. & RUBIN, M. A. 2011. Molecular characterization of neuroendocrine prostate cancer and identification of new drug targets. *Cancer Discov*, 1, 487-95.
- BEN-PORATH, I., THOMSON, M. W., CAREY, V. J., GE, R., BELL, G. W., REGEV, A. & WEINBERG, R. A. 2008. An embryonic stem cell-like gene expression signature in poorly differentiated aggressive human tumors. *Nat Genet*, 40, 499-507.
- BENASSI, B., FLAVIN, R., MARCHIONNI, L., ZANATA, S., PAN, Y., CHOWDHURY, D., MARANI, M., STRANO, S., MUTI, P., BLANDINO, G. & LODA, M. 2012. MYC is activated by USP2a-mediated modulation of microRNAs in prostate cancer. *Cancer Discovery*, 2, 236-247.
- BENASSI, B., MARANI, M., LODA, M. & BLANDINO, G. 2013. USP2a alters chemotherapeutic response by modulating redox. *Cell Death and Disease*, 4, 1-10.
- BERCHUCK, J. E., VISCUSE, P. V., BELTRAN, H. & APARICIO, A. 2021. Clinical considerations for the management of androgen indifferent prostate cancer. *Prostate Cancer and Prostatic Diseases*, 24, 623-637.
- BERGER, A., BRADY, N. J., BAREJA, R., ROBINSON, B., CONTEDEUCA, V., AUGELLO, M. A., PUCA, L., AHMED, A., DARDENNE, E., LU, X., HWANG, I., BAGADION, A. M., SBONER, A., ELEMENTO, O., PAIK, J., YU, J., BARBIERI, C. E., DEPHOURE, N., BELTRAN, H. & RICKMAN, D. S. 2019. N-Myc-mediated epigenetic reprogramming drives lineage plasticity in advanced prostate cancer. *J Clin Invest*, 129, 3924-3940.
- BERGER, M. F., LAWRENCE, M. S., ONOFRIO, R., CARTER, S. L., PARK, K., HABEGGER, L., AMBROGIO, L., FENNEL, T., PARKIN, M., SAKSENA, G., VOET, D., RAMOS, A. H., DEMICHELIS, F., PUGH, T. J., WILKINSON, J., FISHER, S., WINCKLER, W., MAHAN, S., ARDLIE, K., BALDWIN, J., SIMONS, J. W., KITABAYASHI, N., MACDONALD, T. Y., DRIER, Y., KANTOFF, P. W., CHIN, L., GABRIEL, S. B., GERSTEIN, M. B., GOLUB, T. R., MEYERSON, M., TEWARI, A., LANDER, E. S., GETZ, G., RUBIN, M. A., CIBULSKIS, K., GARRAWAY, L. A., SIVACHENKO, A. Y., SBONER, A., ESGUEVA, R., PFLUEGER, D. & SOUGNEZ, C. 2011. The genomic complexity of primary human prostate cancer. *Nature (London)*, 470, 214-220.
- BERTHOLD, D. R., POND, G. R., SOBAN, F., DE WIT, R., EISENBERGER, M. & TANNOCK, I. F. 2008. Docetaxel plus prednisone or mitoxantrone plus prednisone for advanced prostate cancer: updated survival in the TAX 327 study. *J Clin Oncol*, 26, 242-5.
- BINDEA, G., MLECNIK, B., HACKL, H., CHAROENTONG, P., TOSOLINI, M., KIRILOVSKY, A., FRIDMAN, W. H., PAGÈS, F., TRAJANOSKI, Z. & GALON, J. 2009. ClueGO: a Cytoscape plug-in to decipher functionally grouped gene ontology and pathway annotation networks. *Bioinformatics*, 25, 1091-3.
- BIRSA, N., NORKETT, R., WAUER, T., MEVISSSEN, T. E., WU, H. C., FOLTYNIE, T., BHATIA, K., HIRST, W. D., KOMANDER, D., PLUN-FAVREAU, H. & KITTLER, J. T. 2014. Lysine 27 ubiquitination of the mitochondrial transport protein Miro is dependent on serine 65 of the Parkin ubiquitin ligase. *J Biol Chem*, 289, 14569-82.

- BISHOP, J., THAPER, D., VAHID, S., DAVIES, A., KETOLA, K., KURUMA, H., JAMA, R., NIP, K., ANGELES, A., JOHNSON, F., WYATT, A., FAZLI, L., GLEAVE, M., LIN, D., RUBIN, M., COLLINS, C., WANG, Y., BELTRAN, H. & ZOUBEIDI, A. 2017. The master neural transcription factor BRN2 is an androgen receptor-suppressed driver of neuroendocrine differentiation in prostate cancer. *Cancer Discovery*, 7, 54-71.
- BLUEMN, E. G., COLEMAN, I. M., LUCAS, J. M., COLEMAN, R. T., HERNANDEZ-LOPEZ, S., THARAKAN, R., BIANCHI-FRIAS, D., DUMPIT, R. F., KAIPAINEN, A., CORELLA, A. N., YANG, Y. C., NYQUIST, M. D., MOSTAGHEL, E., HSIEH, A. C., ZHANG, X., COREY, E., BROWN, L. G., NGUYEN, H. M., PIENTA, K., ITTMANN, M., SCHWEIZER, M., TRUE, L. D., WISE, D., RENNIE, P. S., VESSELLA, R. L., MORRISSEY, C. & NELSON, P. S. 2017. Androgen Receptor Pathway-Independent Prostate Cancer Is Sustained through FGF Signaling. *Cancer Cell*, 32, 474-489.e6.
- BOHRER, L. R., CHEN, S., HALLSTROM, T. C. & HUANG, H. 2010. Androgens suppress EZH2 expression via retinoblastoma (RB) and p130-dependent pathways: a potential mechanism of androgen-refractory progression of prostate cancer. *Endocrinology*, 151, 5136-45.
- BORG, N. & DIXIT, V. 2017. Ubiquitin in cell-cycle regulation and dysregulation in cancer. *Annual Review of Cancer Biology*, 1, 59-77.
- BOUKHALED, G. M., HARDING, S. & BROOKS, D. G. 2021. Opposing Roles of Type I Interferons in Cancer Immunity. *Annual Review of Pathology: Mechanisms of Disease*, 16, 167-198.
- BOZZA, W. P., LIANG, Q., GONG, P. & ZHUANG, Z. 2012. Transient kinetic analysis of USP2-catalyzed deubiquitination reveals a conformational rearrangement in the K48-linked diubiquitin substrate. *Biochemistry*, 51, 10075-86.
- BRACKEN, A. P., PASINI, D., CAPRA, M., PROSPERINI, E., COLLI, E. & HELIN, K. 2003. EZH2 is downstream of the pRB-E2F pathway, essential for proliferation and amplified in cancer. *Embo j*, 22, 5323-35.
- BRAWER, M. 2004. Challenges with Luteinising Hormone-Releasing Hormone agonists: flare and surge. *Reviews in Urology*, 6, S12-S18.
- BRIGNOLE, C., MARIMPIETRI, D., DI PAOLO, D., PERRI, P., MORANDI, F., PASTORINO, F., ZORZOLI, A., PAGNAN, G., LOI, M., CAFFA, I., ERMINIO, G., HAUPT, R., GAMBINI, C., PISTOIA, V. & PONZONI, M. 2010. Therapeutic targeting of TLR9 inhibits cell growth and induces apoptosis in neuroblastoma. *Cancer Res*, 70, 9816-26.
- BROWN, C., GOSS, S., LUBAHN, D., JOSEPH, D., WILSON, E., FRENCH, F. & WILLARD, H. 1989. Androgen receptor locus on the human X chromosome: regional localisation to Xq11-12 and description of a DNA polymorphism. *American Journal of Human Genetics*, 44, 264-269.
- BUCCI, C., PARTON, R. G., MATHER, I. H., STUNNENBERG, H., SIMONS, K., HOFACK, B. & ZERIAL, M. 1992. The small GTPase rab5 functions as a regulatory factor in the early endocytic pathway. *Cell*, 70, 715-728.
- BUCHER-JOHANNESSEN, C., PAGE, C. M., HAUGEN, T. B., WOJEWODZIC, M. W., FOSSÅ, S. D., GROTMOL, T., HAUGNES, H. S. & ROUNGE, T. B. 2019. Cisplatin treatment of testicular cancer patients introduces long-term changes in the epigenome. *Clinical Epigenetics*, 11, 179.

- BUDHWANI, M., MAZZIERI, R. & DOLCETTI, R. 2018. Plasticity of Type I Interferon-Mediated Responses in Cancer Therapy: From Anti-tumor Immunity to Resistance. *Front Oncol*, 8, 322.
- BURSKA, U. L., HARLE, V. J., COFFEY, K., DARBY, S., RAMSEY, H., O'NEILL, D., LOGAN, I. R., GAUGHAN, L. & ROBSON, C. N. 2013. Deubiquitinating enzyme Usp12 is a novel co-activator of the androgen receptor. *J Biol Chem*, 288, 32641-32650.
- BUTLER, L., CENTENERA, M. M. & SWINNEN, J. 2016. Androgen control of lipid metabolism in prostate cancer: novel insights and future applications. *Endocrine-Related Cancer*, 23, R219-R227.
- BUTLER, L. M., MAH, C. Y., MACHIELS, J., VINCENT, A. D., IRANI, S., MUTUKU, S. M., SPOTBEEN, X., BAGADI, M., WALTREGNY, D., MOLDOVAN, M., DEHAIRS, J., VANDERHOYDONC, F., BLOCH, K., DAS, R., STAHL, J., KENCH, J. G., GEVAERT, T., DERUA, R., WAELKENS, E., NASSAR, Z. D., SELTH, L. A., TRIM, P. J., SNEL, M. F., LYNN, D. J., TILLEY, W. D., HORVATH, L. G., CENTENERA, M. M. & SWINNEN, J. V. 2021. Lipidomic Profiling of Clinical Prostate Cancer Reveals Targetable Alterations in Membrane Lipid Composition. *Cancer Research*, 81, 4981-4993.
- BUTLER, L. M., PERONE, Y., DEHAIRS, J., LUPIEN, L. E., DE LAAT, V., TALEBI, A., LODA, M., KINLAW, W. B. & SWINNEN, J. V. 2020. Lipids and cancer: Emerging roles in pathogenesis, diagnosis and therapeutic intervention. *Advanced Drug Delivery Reviews*, 159, 245-293.
- CAI, X., FENG, S., ZHANG, J., QIU, W., QIAN, M. & WANG, Y. 2020. USP18 deubiquitinates and stabilizes Twist1 to promote epithelial-mesenchymal transition in glioblastoma cells. *Am J Cancer Res*, 10, 1156-1169.
- CARLOS MARTÍN ZOPPINO, F., DAMIÁN MILITELLO, R., SLAVIN, I., ÁLVAREZ, C. & COLOMBO, M. I. 2010. Autophagosome Formation Depends on the Small GTPase Rab1 and Functional ER Exit Sites. *Traffic*, 11, 1246-1261.
- CARSON, C. & RITTMASER, R. 2003. The role of dihydrotestosterone in benign prostatic hyperplasia. *Elsevier Science*, 61, 1-7.
- CATALONA, W., SMITH, D., RATLIFF, T. & BASLER, J. 1993. Detection of organ-confined prostate cancer is increased through prostate-specific antigen-based screening. 270, 948-954.
- CATTRINI, C., SOLDATO, D., RUBAGOTTI, A., ZINOLI, L., ZANARDI, E., BARBORO, P., MESSINA, C., CASTRO, E., OLMOS, D. & BOCCARDO, F. 2020. Epidemiological Characteristics and Survival in Patients with De Novo Metastatic Prostate Cancer. *Cancers (Basel)*, 12.
- CENTENERA, M. M., GILLIS, J. L., HANSON, A. R., JINDAL, S., TAYLOR, R. A., RISBRIDGER, G. P., SUTHERLAND, P. D., SCHER, H. I., RAJ, G. V., KNUDSEN, K. E., YEADON, T., TILLEY, W. D. & BUTLER, L. M. 2012. Evidence for efficacy of new Hsp90 inhibitors revealed by ex vivo culture of human prostate tumors. *Clin Cancer Res*, 18, 3562-70.
- CENTENERA, M. M., HICKEY, T. E., JINDAL, S., RYAN, N. K., RAVINDRANATHAN, P., MOHAMMED, H., ROBINSON, J. L., SCHIEWER, M. J., MA, S., KAPUR, P., SUTHERLAND, P. D., HOFFMANN, C. E., ROEHRBORN, C. G., GOMELLA, L. G., CARROLL, J. S., BIRRELL, S. N., KNUDSEN, K. E., RAJ, G. V., BUTLER, L. M. & TILLEY, W. D. 2018a. A patient-derived explant (PDE) model of hormone-dependent cancer. *Mol Oncol*, 12, 1608-1622.

- CENTENERA, M. M., SELTH, L., EBRAHIMIE, E., BUTLER, L. & TILLEY, W. D. 2018b. New opportunities for targeting the androgen receptor in prostate cancer. *Cold Spring Harbor Perspectives in Medicine*, 8.
- CHANG, K. H., LI, R., KURI, B., LOTAN, Y., ROEHRBORN, C. G., LIU, J., VESSELLA, R., NELSON, P. S., KAPUR, P., GUO, X., MIRZAEI, H., AUCHUS, R. J. & SHARIFI, N. 2013. A gain-of-function mutation in DHT synthesis in castration-resistant prostate cancer. *Cell*, 154, 1074-1084.
- CHANG, P. C., WANG, T. Y., CHANG, Y. T., CHU, C. Y., LEE, C. L., HSU, H. W., ZHOU, T. A., WU, Z., KIM, R. H., DESAI, S. J., LIU, S. & KUNG, H. J. 2014. Autophagy pathway is required for IL-6 induced neuroendocrine differentiation and chemoresistance of prostate cancer LNCaP cells. *PLoS One*, 9, e88556.
- CHAVES, L. P., MELO, C. M., SAGGIORO, F. P., REIS, R. B. D. & SQUIRE, J. A. 2021. Epithelial-Mesenchymal Transition Signaling and Prostate Cancer Stem Cells: Emerging Biomarkers and Opportunities for Precision Therapeutics. *Genes (Basel)*, 12.
- CHEN, C., WELSBIE, D., TRAN, C., BAEK, S., CHEN, R., VESSELLA, R., ROSENFELD, M. & SAWYERS, C. 2004. Molecular determinants of resistance to anti-androgen therapy. *Nature Medicine*, 10, 33-39.
- CHEN, N. & ZHOU, Q. 2016. The evolving Gleason grading system. *Chinese Journal of Cancer Research*, 28, 58-64.
- CHEN, Y., WANG, D., WU, Y.-P., ZHOU, T.-Y., GAI, R.-H., FU, Y.-Y., ZHENG, L., HE, Q.-J., ZHU, H. & YANG, B. 2017a. MDM2 promotes epithelial-mesenchymal transition and metastasis of ovarian cancer SKOV3 cells. *British Journal of Cancer*, 117, 1192-1201.
- CHEN, Y., ZHOU, B. & CHEN, D. 2017b. USP21 promotes cell proliferation and metastasis through suppressing EZH2 ubiquitination in bladder carcinoma. *Oncotargets Ther*, 10, 681-689.
- CHEN, Z., WANG, H. W., WANG, S., FAN, L., FENG, S., CAI, X., PENG, C., WU, X., LU, J., CHEN, D., CHEN, Y., WU, W., LU, D., LIU, N., YOU, Y. & WANG, H. 2019. USP9X deubiquitinates ALDH1A3 and maintains mesenchymal identity in glioblastoma stem cells. *J Clin Invest*, 129, 2043-2055.
- CHOI, B. J., PARK, S. A., LEE, S. Y., CHA, Y. N. & SURH, Y. J. 2017. Hypoxia induces epithelial-mesenchymal transition in colorectal cancer cells through ubiquitin-specific protease 47-mediated stabilization of Snail: A potential role of Sox9. *Sci Rep*, 7, 15918.
- CHOI, S. Y. C., ETTINGER, S. L., LIN, D., XUE, H., CI, X., NABAVI, N., BELL, R. H., MO, F., GOUT, P. W., FLESHNER, N. E., GLEAVE, M. E., COLLINS, C. C. & WANG, Y. 2018. Targeting MCT4 to reduce lactic acid secretion and glycolysis for treatment of neuroendocrine prostate cancer. *Cancer Med*, 7, 3385-3392.
- COLEMAN, D. J., VAN HOOK, K., KING, C. J., SCHWARTZMAN, J., LISAC, R., URRUTIA, J., SEHRAWAT, A., WOODWARD, J., WANG, N. J., GULATI, R., THOMAS, G. V., BEER, T. M., GLEAVE, M., KORKOLA, J. E., GAO, L., HEISER, L. M. & ALUMKAL, J. J. 2016. Cellular androgen content influences enzalutamide agonism of F877L mutant androgen receptor. *Oncotarget*, 7, 40690-40703.
- CORNFORD, P., BELLMUNT, J., BOLLA, M., BRIERS, E., SANTIS, M. D., GROSS, T., HENRY, A. M., JONIAU, S., LAM, T. B., MASON, M. D., POEL, H. G. V. D., KWAST, T. H. V. D., ROUVIÈRE, O., WIEGEL, T. & MOTTET, N. 2017. EAU-ESTRO-SIOG Guidelines on Prostate Cancer. Part II: Treatment of Relapsing, Metastatic, and Castration-Resistant Prostate Cancer. *European Urology*, 71, 630-642.

- COULOMBE, R., GROCHULSKI, P., SIVARAMAN, J., MÉNARD, R., MORT, J. S. & CYGLER, M. 1996. Structure of human procathepsin L reveals the molecular basis of inhibition by the prosegment. *The EMBO journal*, 15, 5492-5503.
- COUTINHO, I., DAY, T., TILLEY, W. D. & SELTH, L. 2016. Androgen receptor signaling in castration-resistant prostate cancer: a lesson in persistence. *Endocrine-Related Cancer*, 23, T179-T197.
- CRAWFORD, E. D., HEIDENREICH, A., LAWRENTSCHUK, N., TOMBAL, B., POMPEO, A. C. L., MENDOZA-VALDES, A., MILLER, K., DEBRUYNE, F. M. J. & KLOTZ, L. 2019. Androgen-targeted therapy in men with prostate cancer: evolving practice and future considerations. *Prostate Cancer Prostatic Dis*, 22, 24-38.
- CROWLEY, F., STERPI, M., BUCKLEY, C., MARGETICH, L., HANDA, S. & DOVEY, Z. 2021. A Review of the Pathophysiological Mechanisms Underlying Castration-resistant Prostate Cancer. *Res Rep Urol*, 13, 457-472.
- CULIG, Z., COMUZZI, B., STEINER, H., BARTSCH, G. & HOBISCH, A. 2004. Expression and function of androgen receptor coactivators in prostate cancer. *The Journal of Steroid Biochemistry and Molecular Biology*, 92, 265-271.
- CULINE, S., EL DEMERY, M., LAMY, P. J., IBORRA, F., AVANCÈS, C. & PINGUET, F. 2007. Docetaxel and cisplatin in patients with metastatic androgen independent prostate cancer and circulating neuroendocrine markers. *J Urol*, 178, 844-8; discussion 848.
- CUNNINGHAM, C. N., BAUGHMAN, J. M., PHU, L., TEA, J. S., YU, C., COONS, M., KIRKPATRICK, D. S., BINGOL, B. & CORN, J. E. 2015. USP30 and parkin homeostatically regulate atypical ubiquitin chains on mitochondria. *Nature Cell Biology*, 17, 160-169.
- CURTIN, N. J. 2012. DNA repair dysregulation from cancer driver to therapeutic target. *Nat Rev Cancer*, 12, 801-17.
- D'ASSORO, A. B., LIU, T., QUATRARO, C., AMATO, A., OPYRCHAL, M., LEONTOVICH, A., IKEDA, Y., OHMINE, S., LINGLE, W., SUMAN, V., ECSEDY, J., IANKOV, I., DI LEONARDO, A., AYERS-INGLERS, J., DEGNIM, A., BILLADEAU, D., MCCUBREY, J., INGLE, J., SALISBURY, J. L. & GALANIS, E. 2014. The mitotic kinase Aurora-a promotes distant metastases by inducing epithelial-to-mesenchymal transition in ER α (+) breast cancer cells. *Oncogene*, 33, 599-610.
- DARDENNE, E., BELTRAN, H., BENELLI, M., GAYVERT, K., BERGER, A., PUCA, L., CYRTA, J., SBONER, A., NOORZAD, Z., MACDONALD, T., CHEUNG, C., YUEN, K. S., GAO, D., CHEN, Y., EILERS, M., MOSQUERA, J. M., ROBINSON, B. D., ELEMENTO, O., RUBIN, M. A., DEMICHELIS, F. & RICKMAN, D. S. 2016. N-Myc Induces an EZH2-Mediated Transcriptional Program Driving Neuroendocrine Prostate Cancer. *Cancer Cell*, 30, 563-577.
- DAVIES, A., NOURUZI, S., GANGULI, D., NAMEKAWA, T., THAPER, D., LINDER, S., KARAOĞLANOĞLU, F., OMUR, M. E., KIM, S., KOBELEV, M., KUMAR, S., SIVAK, O., BOSTOCK, C., BISHOP, J., HOOGSTRAAT, M., TALAL, A., STELLOO, S., VAN DER POEL, H., BERGMAN, A. M., AHMED, M., FAZLI, L., HUANG, H., TILLEY, W., GOODRICH, D., FENG, F. Y., GLEAVE, M., HE, H. H., HACH, F., ZWART, W., BELTRAN, H., SELTH, L. & ZOUBEIDI, A. 2021. An androgen receptor switch underlies lineage infidelity in treatment-resistant prostate cancer. *Nature Cell Biology*, 23, 1023-1034.
- DAVIES, A., ZOUBEIDI, A. & SELTH, L. A. 2020. The epigenetic and transcriptional landscape of neuroendocrine prostate cancer. *Endocr Relat Cancer*, 27, R35-r50.

- DAVIES, A. H., BELTRAN, H. & ZOUBEIDI, A. 2018. Cellular plasticity and the neuroendocrine phenotype in prostate cancer. *Nature Reviews Urology*, 15, 271-286.
- DAVIS, M., PRAGANI, R., FOX, J., SHEN, M., PARMAR, K., GAUDIANO, E., LIU, L., TANEGA, C., MCGEE, L., HALL, M., MCKNIGHT, C., SHINN, P., NELSON, H., CHATTOPADHYAY, D., D'ANDREA, A., AULD, D., DELUCAS, L., LI, Z., BOXER, M. & SIMEONOV, A. 2016. Small molecule inhibition of the Ubiquitin-specific protease USP2 accelerates Cyclin D1 degradation and leads to cell cycle arrest in Colorectal cancer and Mantle Cell Lymphoma models. *Journal of Biological Chemistry*, 291, 24628-24640.
- DE BONO, J., OUDARD, S., OZGUROGLU, M., HANSEN, S., MACHIELS, J., KOCAK, I., GRAVIS, G., BODROGI, I., MACKENZIE, M., SHEN, L., ROESSNER, M., GUPTA, S. & SARTOR, O. 2010. Prednisone plus cabazitaxel or mitoxantrone for metastatic castration-resistant prostate cancer progressing after docetaxel treatment: a randomised open-label trial. *The Lancet*, 376, 1147-1154.
- DE BONO, J. S., LOGOTHETIS, C. J., MOLINA, A., FIZAZI, K., NORTH, S., CHU, L., CHI, K. N., JONES, R. J., GOODMAN, O. B., SAAD, F., STAFFURTH, J. N., MAINWARING, P., HARLAND, S., FLAIG, T. W., HUTSON, T. E., CHENG, T., PATTERSON, H., HAINSWORTH, J. D., RYAN, C. J., STERNBERG, C. N., ELLARD, S. L., FLÉCHON, A., SALEH, M., SCHOLZ, M., EFSTATHIOU, E., ZIVI, A., BIANCHINI, D., LORIOT, Y., CHIEFFO, N., KHEOH, T., HAQQ, C. M. & SCHER, H. I. 2011. Abiraterone and Increased Survival in Metastatic Prostate Cancer. *New England Journal of Medicine*, 364, 1995-2005.
- DEORAH, S., RAO, M. B., RAMAN, R., GAITONDE, K. & DONOVAN, J. F. 2012. Survival of patients with small cell carcinoma of the prostate during 1973-2003: a population-based study. *BJU Int*, 109, 824-30.
- DIRAC, A. M. G. & BERNARDS, R. 2010. The Deubiquitinating Enzyme USP26 Is a Regulator of Androgen Receptor Signaling. *Molecular Cancer Research*, 8, 844-854.
- DMOCHOWSKA, N., MILANOVA, V., MUKKAMALA, R., CHOW, K. K., PHAM, N. T. H., SRINIVASARAO, M., EBERT, L. M., STAIT-GARDNER, T., LE, H., SHETTY, A., NELSON, M., LOW, P. S. & THIERRY, B. 2023. Nanoparticles Targeted to Fibroblast Activation Protein Outperform PSMA for MRI Delineation of Primary Prostate Tumors. *Small*, n/a, 2204956.
- DOAMEKPOR, S. K., PENG, P., XU, R., MA, L., TONG, Y. & TONG, L. 2023. A partially open conformation of an androgen receptor ligand-binding domain with drug-resistance mutations. *Acta Crystallographica Section F*, 79, 95-104.
- DOBIN, A., DAVIS, C. A., SCHLESINGER, F., DRENKOW, J., ZALESKI, C., JHA, S., BATUT, P., CHAISSON, M. & GINGERAS, T. R. 2013. STAR: ultrafast universal RNA-seq aligner. *Bioinformatics*, 29, 15-21.
- DORATO, M. A. & ENGELHARDT, J. A. 2005. The no-observed-adverse-effect-level in drug safety evaluations: use, issues, and definition(s). *Regul Toxicol Pharmacol*, 42, 265-74.
- DOW, M. & BAVISTER, B. 1989. Direct contact is required between serum albumin and hamster spermatozoa for capacitation in vitro. *Gamete Research*, 23, 171-180.
- DRAKER, R., SARCINELLA, E. & CHEUNG, P. 2011. USP10 deubiquitylates the histone variant H2A.Z and both are required for androgen receptor-mediated gene activation. *Nucleic acids research*, 39, 3529-3542.
- DRAULANS, C., EVERAERTS, W., ISEBAERT, S., GEVAERT, T., OYEN, R., JONIAU, S., LERUT, E., DE WEVER, L., WEYNAND, B., VANHOUTTE, E., MEERLEER, G. & HAUSTERMANS, K.

2019. Impact of magnetic resonance imaging on prostate cancer staging and European Association of Urology risk classification. *Oncology*, 130, 113-119.
- DURCAN, T. M., TANG, M. Y., PÉRUSSE, J. R., DASHTI, E. A., AGUILETA, M. A., MCLELLAND, G. L., GROS, P., SHALER, T. A., FAUBERT, D., COULOMBE, B. & FON, E. A. 2014. USP8 regulates mitophagy by removing K6-linked ubiquitin conjugates from parkin. *Embo j*, 33, 2473-91.
- DYBING, E. 1973. Microsomal drug oxidation. Function, induction, and inhibition of the cytochrome P450-system. *Acta Veterinaria Scandinavica*, 14, 11–21.
- EFSTATHIOU, E., TITUS, M., WEN, S., HOANG, A., KARLOU, M., ASHE, R., TU, S., APARICIO, A., TRONCOSO, P., MOHLER, J. & LOGOTHETIS, C. 2015. Molecular characterisation of Enzalutamide-treated bone metastatic castration-resistant prostate cancer. *European Urology*, 67, 53-60.
- EICHHORN, P., RODÓN, L., GONZÁLEZ-JUNCÀ, A., DIRAC, A., GILI, M., MARTÍNEZ-SÁEZ, E., AURA, C., BARBA, I., PEG, V., PRAT, A., CUARTAS, I., JIMENEZ, J., GARCÍA-DORADO, D., SAHUQUILLO, J., BERNARDS, R., BASELGA, J. & SEOANE, J. 2012. USP15 stabilises TGF-Beta receptor I and promotes oncogenesis through the activation of TGF-beta signaling in glioblastoma. *Nature Medicine*, 18, 429-436.
- EJTEHADIFAR, M., ZAHEDI, S., GAMEIRO, P., CABEÇADAS, J., DA SILVA, M. G., BECK, H. C., CARVALHO, A. S. & MATTHIESEN, R. 2023. Meta-Analysis of MS-Based Proteomics Studies Indicates Interferon Regulatory Factor 4 and Nucleobindin1 as Potential Prognostic and Drug Resistance Biomarkers in Diffuse Large B Cell Lymphoma. *Cells*, 12.
- EPSTEIN, J., EGEVAD, L., AMIN, M., DELAHUNT, B., SRIGLEY, J. & HUMPHREY, P. 2016. The 2014 International Society of Urological Pathology (ISUP) consensus conference on Gleason grading of prostatic carcinoma: definition of grading patterns and proposal for a new grading system. *American Journal of Surgical Pathology*, 40, 244-252.
- EPSTEIN, J. I., AMIN, M. B., BELTRAN, H., LOTAN, T. L., MOSQUERA, J. M., REUTER, V. E., ROBINSON, B. D., TRONCOSO, P. & RUBIN, M. A. 2014. Proposed morphologic classification of prostate cancer with neuroendocrine differentiation. *Am J Surg Pathol*, 38, 756-67.
- ESPOSITO, S., RUSSO, M. V., AIROLDI, I., TUPONE, M. G., SORRENTINO, C., BARBARITO, G., DI MEO, S. & DI CARLO, E. 2015. SNAI2/Slug gene is silenced in prostate cancer and regulates neuroendocrine differentiation, metastasis-suppressor and pluripotency gene expression. *Oncotarget*, 6, 17121-34.
- FAN, L., CHEN, Z., WU, X., CAI, X., FENG, S., LU, J., WANG, H. & LIU, N. 2019. Ubiquitin-Specific Protease 3 Promotes Glioblastoma Cell Invasion and Epithelial-Mesenchymal Transition via Stabilizing Snail. *Mol Cancer Res*, 17, 1975-1984.
- FANG, C. L., LIN, C. C., CHEN, H. K., HSEU, Y. C., HUNG, S. T., SUN, D. P., UEN, Y. H. & LIN, K. Y. 2018. Ubiquitin-specific protease 3 overexpression promotes gastric carcinogenesis and is predictive of poor patient prognosis. *Cancer Sci*, 109, 3438-3449.
- FAROOQ, A. U., GEMBUS, K., SANDOW, J. J., WEBB, A., MATHIVANAN, S., MANNING, J. A., SHAH, S. S., FOOT, N. J. & KUMAR, S. 2022. K-29 linked ubiquitination of Arrdc4 regulates its function in extracellular vesicle biogenesis. *Journal of Extracellular Vesicles*, 11, e12188.
- FENG, J., XU, G., LIU, J., ZHANG, N., LI, L., JI, J., ZHANG, J., ZHANG, L., WANG, G., WANG, X., TAN, J., HUANG, B., LU, J. & ZHANG, Y. 2016. Phosphorylation of LSD1 at Ser112 is

- crucial for its function in induction of EMT and metastasis in breast cancer. *Breast Cancer Research and Treatment*, 159, 443-456.
- FERNANDES, R. C., TOUBIA, J., TOWNLEY, S., HANSON, A. R., DREDGE, B. K., PILLMAN, K. A., BERT, A. G., WINTER, J. M., IGGO, R., DAS, R., OBINATA, D., SANDHU, S., RISBRIDGER, G. P., TAYLOR, R. A., LAWRENCE, M. G., BUTLER, L. M., ZOUBEIDI, A., GREGORY, P. A., TILLEY, W. D., HICKEY, T. E., GOODALL, G. J. & SELTH, L. A. 2021. Post-transcriptional Gene Regulation by MicroRNA-194 Promotes Neuroendocrine Transdifferentiation in Prostate Cancer. *Cell Rep*, 34, 108585.
- FEYERABEND, S., SAAD, F., LI, T., ITO, T., DIELS, J., VAN SANDEN, S., DE PORRE, P., ROIZ, J., ABOGUNRIN, S., KOUFOPOULOU, M. & FIZAZI, K. 2018. Survival benefit, disease progression and quality-of-life outcomes of abiraterone acetate plus prednisone versus docetaxel in metastatic hormone-sensitive prostate cancer: A network meta-analysis. *European Journal of Cancer*, 103, 78-87.
- FIZAZI, K., SCHER, H. I., MOLINA, A., LOGOTHETIS, C. J., CHI, K. N., JONES, R. J., STAFFURTH, J. N., NORTH, S., VOGELZANG, N. J., SAAD, F., MAINWARING, P., HARLAND, S., GOODMAN, O. B., JR., STERNBERG, C. N., LI, J. H., KHEOH, T., HAQQ, C. M. & DE BONO, J. S. 2012. Abiraterone acetate for treatment of metastatic castration-resistant prostate cancer: final overall survival analysis of the COU-AA-301 randomised, double-blind, placebo-controlled phase 3 study. *Lancet Oncol*, 13, 983-92.
- FOURNIER, M.-J., GAREAU, C. & MAZROUI, R. 2010. The chemotherapeutic agent bortezomib induces the formation of stress granules. *Cancer Cell International*, 10, 12.
- FUSTÉ, N. P., CASTELBLANCO, E., FELIP, I., SANTACANA, M., FERNÁNDEZ-HERNÁNDEZ, R., GATIUS, S., PEDRAZA, N., PALLARÉS, J., CEMELI, T., VALLS, J., TARRES, M., FERREZUELO, F., DOLCET, X., MATIAS-GUIU, X. & GARÍ, E. 2016. Characterization of cytoplasmic cyclin D1 as a marker of invasiveness in cancer. *Oncotarget*, 7, 26979-91.
- GAMMILL, S. L. & WEICHERT, R. 1973. Common origin for all neuroendocrine tumors. *Acta Radiol Ther Phys Biol*, 12, 321-6.
- GANSAUGE, S., GANSAUGE, F., RAMADANI, M., STOBBE, H., RAU, B., HARADA, N. & BEGER, H. G. 1997. Overexpression of cyclin D1 in human pancreatic carcinoma is associated with poor prognosis. *Cancer Res*, 57, 1634-7.
- GAO, S., CHEN, T., LI, L., LIU, X., LIU, Y., ZHAO, J., LU, Q., ZENG, Z., XU, Q., HUANG, D. & TU, K. 2020. Hypoxia-Inducible Ubiquitin Specific Peptidase 13 Contributes to Tumor Growth and Metastasis via Enhancing the Toll-Like Receptor 4/Myeloid Differentiation Primary Response Gene 88/Nuclear Factor- κ B Pathway in Hepatocellular Carcinoma. *Front Cell Dev Biol*, 8, 587389.
- GARABEDIAN, E. M., HUMPHREY, P. A. & GORDON, J. I. 1998. A transgenic mouse model of metastatic prostate cancer originating from neuroendocrine cells. *Proc Natl Acad Sci U S A*, 95, 15382-7.
- GAREAU, C., FOURNIER, M.-J., FILION, C., COUDERT, L., MARTEL, D., LABELLE, Y. & MAZROUI, R. 2011. p21WAF1/CIP1 Upregulation through the Stress Granule-Associated Protein CUGBP1 Confers Resistance to Bortezomib-Mediated Apoptosis. *PLOS ONE*, 6, e20254.
- GILLIS, J. L., HINNEH, J. A., RYAN, N. K., IRANI, S., MOLDOVAN, M., QUEK, L.-E., SHRESTHA, R. K., HANSON, A. R., XIE, J., HOY, A. J., HOLST, J., CENTENERA, M. M., MILLS, I. G.,

- LYNN, D. J., SELTH, L. A. & BUTLER, L. M. 2021. A feedback loop between the androgen receptor and 6-phosphogluconate dehydrogenase drives prostate cancer growth. *eLife*, 10.
- GILLIS, J. L., SELTH, L. A., CENTENERA, M. M., TOWNLEY, S. L., SUN, S., PLYMATE, S. R., TILLEY, W. D. & BUTLER, L. M. 2013. Constitutively-active androgen receptor variants function independently of the HSP90 chaperone but do not confer resistance to HSP90 inhibitors. *Oncotarget*, 4, 691-704.
- GONG, X., DU, J., PARSONS, S. H., MERZOUG, F. F., WEBSTER, Y., IVERSEN, P. W., CHIO, L.-C., VAN HORN, R. D., LIN, X., BLOSSER, W., HAN, B., JIN, S., YAO, S., BIAN, H., FICKLIN, C., FAN, L., KAPOOR, A., ANTONYSAMY, S., MC NULTY, A. M., FRONING, K., MANGLICMOT, D., PUSTILNIK, A., WEICHERT, K., WASSERMAN, S. R., DOWLESS, M., MARUGÁN, C., BAQUERO, C., LALLENA, M. J., EASTMAN, S. W., HUI, Y.-H., DIETER, M. Z., DOMAN, T., CHU, S., QIAN, H.-R., YE, X. S., BARDA, D. A., PLOWMAN, G. D., REINHARD, C., CAMPBELL, R. M., HENRY, J. R. & BUCHANAN, S. G. 2019. Aurora A Kinase Inhibition Is Synthetic Lethal with Loss of the RB1 Tumor Suppressor Gene. *Cancer Discovery*, 9, 248-263.
- GORDETSKY, J. & EPSTEIN, J. 2016. Grading of prostatic adenocarcinoma: current state and prognostic implications. *Diagnostic Pathology*, 11, 1-8.
- GORVEL, J.-P., CHAVRIER, P., ZERIAL, M. & GRUENBERG, J. 1991. rab5 controls early endosome fusion in vitro. *Cell*, 64, 915-925.
- GRANER, E., TANG, D., ROSSI, S., BARON, A., MIGITA, T., WEINSTEIN, L. J., LECHPAMMER, M., HUESKEN, D., ZIMMERMANN, J., SIGNORETTI, S. & LODA, M. 2004. The isopeptidase USP2a regulates the stability of fatty acid synthase in prostate cancer. *Cancer cell*, 5, 253-261.
- GRASSO, C., WU, Y., ROBINSON, D., CAO, X., DHANASEKARAN, S., KHAN, A., QUIST, M., JING, X., LONIGRO, R., BRENNER, J., ASANGANI, I., ATEEQ, B., CHUN, S., SIDDIQUI, J., SAM, L., ANSTETT, M., MEHRA, R., PRENSNER, J., PALANISAMY, N., RYSLIK, G., VANDIN, F., RAPHAEL, B., KUNJU, L., RHODES, D., PIENTA, K., CHINNAIYAN, A. & TOMLINS, S. 2012. The mutational landscape of lethal castration-resistant prostate cancer. *Nature Letter*, 487.
- GREEN, D. R. & LLAMBI, F. 2015. Cell Death Signaling. *Cold Spring Harb Perspect Biol*, 7.
- GREGORY, C., HE, B., JOHNSON, R., FORD, O., MOHLER, J., FRENCH, F. & WILSON, E. 2001. A Mechanism for Androgen Receptor-mediated Prostate Cancer Recurrence after Androgen Deprivation Therapy. *Cancer Research*, 61, 4315-4319.
- GUO, F., ZHANG, C., WANG, F., ZHANG, W., SHI, X., ZHU, Y., FANG, Z., YANG, B. & SUN, Y. 2020. Deubiquitinating enzyme USP33 restrains docetaxel-induced apoptosis via stabilising the phosphatase DUSP1 in prostate cancer. *Cell Death & Differentiation*, 27, 1938-1951.
- GUO, Z., YANG, X., SUN, F., JIANG, R., LINN, D., CHEN, H., CHEN, H., KONG, X., MELAMED, J., TEPPER, C., KUNG, H., BRODIE, A., EDWARDS, J. & QIU, Y. 2009. A novel androgen receptor splice variant is upregulated during prostate cancer progression and promotes androgen-depletion-resistant growth. *Cancer Research*, 69, 2305-2313.
- HAGLUND, K. & DIKIC, I. 2005. Ubiquitylation and cell signaling. *The EMBO Journal*, 24, 3353-3359.
- HALL, J. & GUYTON, A. 2011. *Guyton and Hall textbook of medical physiology*, Philadelphia, PA : Saunders Elsevier.

- HÄLLBERG, B. M. & LARSSON, N. G. 2014. Making proteins in the powerhouse. *Cell Metab*, 20, 226-40.
- HAN, M., LI, F., ZHANG, Y., DAI, P., HE, J., LI, Y., ZHU, Y., ZHENG, J., HUANG, H., BAI, F. & GAO, D. 2022. FOXA2 drives lineage plasticity and KIT pathway activation in neuroendocrine prostate cancer. *Cancer Cell*, 40, 1306-1323.e8.
- HARRIGAN, J., JACQ, X., MARTIN, N. & JACKSON, S. 2018. Deubiquitylating enzymes and drug discovery: emerging opportunities. *Nature Reviews Drug Discovery*, 17, 57-78.
- HAYTHORN, M. & ABLIN, R. 2011. Prostate-specific antigen testing across the spectrum of prostate cancer. *Biomarkers Medicine*, 5.
- HAZELETT, D. J., RHIE, S. K., GADDIS, M., YAN, C., LAKELAND, D. L., COETZEE, S. G., ELLIPSE, G.-O. N. C., PRACTICAL, C., HENDERSON, B. E., NOUSHMEHR, H., COZEN, W., KOTE-JARAI, Z., EELES, R. A., EASTON, D. F., HAIMAN, C. A., LU, W., FARNHAM, P. J. & COETZEE, G. A. 2014. Comprehensive Functional Annotation of 77 Prostate Cancer Risk Loci. *PLOS Genetics*, 10, e1004102.
- HE, B., KEMPPAINEN, J., VOEGEL, J., GRONEMEYER, H. & WILSON, E. 1999. Activation function 2 in the human androgen receptor ligand binding domain mediates interdomain communication with the NH2-terminal domain. *The Journal of Biological Chemistry*, 274, 37219-37225.
- HE, B., KEMPPAINEN, J. & WILSON, E. 2000. FXXLF and WXXLF sequences mediate the NH2-terminal interaction with the ligand binding domain of the androgen receptor. *The Journal of Biological Chemistry*, 275, 22986-22994.
- HE, B. & WILSON, E. 2003. Electrostatic modulation in steroid receptor recruitment of LXXLL and FXXLF motifs. *Molecular and Cellular Biology*, 23, 2135-2150.
- HE, J., LEE, H. J., SAHA, S., RUAN, D., GUO, H. & CHAN, C. H. 2019. Inhibition of USP2 eliminates cancer stem cells and enhances TNBC responsiveness to chemotherapy. *Cell Death and Disease*, 10, 285.
- HEARN, J. W. D., ABUALI, G., REICHARD, C. A., REDDY, C. A., MAGI-GALLUZZI, C., CHANG, K. H., CARLSON, R., RANGEL, L., REAGAN, K., DAVIS, B. J., KARNES, R. J., KOHLI, M., TINDALL, D., KLEIN, E. A. & SHARIFI, N. 2016. HSD3B1 and resistance to androgen-deprivation therapy in prostate cancer: a retrospective, multicohort study. *Lancet Oncol*, 17, 1435-1444.
- HEGEMANN, N. S., MORCINEK, S., BUCHNER, A., KARL, A., STIEF, C., KNÜCHEL, R., CORRADINI, S., LI, M., BELKA, C. & GANSWINDT, U. 2016. Risk of biochemical recurrence and timing of radiotherapy in pT3a N0 prostate cancer with positive surgical margin : A single center experience. *Strahlenther Onkol*, 192, 440-8.
- HEIDELBERGER, J., WAGNER, S. & BELI, P. 2016. Mass Spectrometry-Based Proteomics for Investigating DNA Damage-Associated Protein Ubiquitylation. *Frontiers in Genetics*, 7.
- HEIDENREICH, A., BASTIAN, P., BELLMUNT, J., BOLLA, M., JONIAU, S., KWAST, T. H. V. D., MASON, M. D., MATVEEV, V., WIEGEL, T., ZATTONI, F. & MOTTET, N. 2015. EAU guidelines on prostate cancer. Part II: Treatment of advanced, relapsing, and castration-resistant prostate cancer. *European Urology*, 65, 467-479.
- HETTEL, D. & SHARIFI, N. 2018. HSD3B1 status as a biomarker of androgen deprivation resistance and implications for prostate cancer. *Nat Rev Urol*, 15, 191-196.
- HIENTZ, K., MOHR, A., BHAKTA-GUHA, D. & EFFERTH, T. 2017. The role of P53 in cancer drug resistance and targeted chemotherapy. *Oncotarget*, 8, 8921-8946.

- HIRATA, A., HASHIMOTO, H., SHIBASAKI, C., NARUMI, K. & AOKI, K. 2019. Intratumoral IFN- α gene delivery reduces tumor-infiltrating regulatory T cells through the downregulation of tumor CCL17 expression. *Cancer Gene Therapy*, 26, 334-343.
- HONG, H., TAKAHASHI, K., ICHISAKA, T., AOI, T., KANAGAWA, O., NAKAGAWA, M., OKITA, K. & YAMANAKA, S. 2009. Suppression of induced pluripotent stem cell generation by the p53-p21 pathway. *Nature*, 460, 1132-5.
- HÖRNBERG, E., YLITALO, E., CRNALIC, S., ANTTI, H., STATTIN, P., WIDMARK, A., BERGH, A. & WIKSTRÖM, P. 2011. Expression of androgen receptor splice variants in prostate cancer bone metastases is associated with castration-resistance and short survival. *PLOS ONE*, 6, 1-9.
- HOY, A. J., NAGARAJAN, S. R. & BUTLER, L. M. 2021. Tumour fatty acid metabolism in the context of therapy resistance and obesity. *Nature Reviews Cancer*, 21, 753-766.
- HU, R., DUNN, T., WEI, S., ISHARWAL, S., VELTRI, R., HUMPHREYS, E., HAN, M., PARTIN, A., VESSELLA, R., ISAACS, W., BOVA, G. & LUO, J. 2009. Ligand-independent androgen receptor variants derived from splicing of cryptic exons signify hormone refractory prostate cancer. *Cancer Research*, 69, 16-22.
- HUANG, K. C., YANG, J., NG, M. C., NG, S. K., WELCH, W. R., MUTO, M. G., BERKOWITZ, R. S. & NG, S. W. 2016. Cyclin A1 expression and paclitaxel resistance in human ovarian cancer cells. *Eur J Cancer*, 67, 152-163.
- HUGGINS, C. & HODGES, C. V. 1972. Studies on prostatic cancer. I. The effect of castration, of estrogen and androgen injection on serum phosphatases in metastatic carcinoma of the prostate. *CA Cancer J Clin*, 22, 232-40.
- HUGGINS, C., STEVENS, R. & HODGES, C. 1941. Studies on prostatic cancer: the effects of castration on advanced carcinoma of the prostate gland. *Archives of Surgery*, 43, 209-223.
- HURFORD, R. K., JR., COBRINIK, D., LEE, M. H. & DYSON, N. 1997. pRB and p107/p130 are required for the regulated expression of different sets of E2F responsive genes. *Genes Dev*, 11, 1447-63.
- HUSSAIN, M., FIZAZI, K., SAAD, F., RATHENBORG, P., SHORE, N., FERREIRA, U., IVASHCHENKO, P., DEMIRHAN, E., MODELSKA, K., PHUNG, KRIVOSHIK, A. & STERNBERG, C. 2018. Enzalutamide in men with non-metastatic, castration-resistant prostate cancer. *New England Journal of Medicine*, 378, 2465-2474.
- HUUN, J., GANSMO, L., MANNSÅKER, B., IVERSEN, G., SOMMERFELT-PETTERSEN, J., ØVREBØ, J., LØNNING, P. & KNAPPSKOG, S. 2017. The Functional Roles of the MDM2 Splice Variants P2-MDM2-10 and MDM2- Δ 5 in Breast Cancer Cells. *Translational Oncology*, 10, 806-817.
- HWANG, J. H., SEO, J.-H., BESHIRI, M. L., WANKOWICZ, S., LIU, D., CHEUNG, A., LI, J., QIU, X., HONG, A. L., BOTTA, G., GOLUMB, L., RICHTER, C., SO, J., SANDOVAL, G. J., GIACOMELLI, A. O., LY, S. H., HAN, C., DAI, C., PAKULA, H., SHEAHAN, A., PICCIONI, F., GJOERUP, O., LODA, M., SOWALSKY, A. G., ELLIS, L., LONG, H., ROOT, D. E., KELLY, K., VAN ALLEN, E. M., FREEDMAN, M. L., CHOUDHURY, A. D. & HAHN, W. C. 2019. CREB5 Promotes Resistance to Androgen-Receptor Antagonists and Androgen Deprivation in Prostate Cancer. *Cell Reports*, 29, 2355-2370.e6.
- HYDBRING, P., MALUMBRES, M. & SICINSKI, P. 2016. Non-canonical functions of cell cycle cyclins and cyclin-dependent kinases. *Nature reviews. Molecular cell biology*, 17, 280-292.

- IKEDA, F. & DIKIC, I. 2008. Atypical ubiquitin chains: new molecular signals. *The EMBO Journal*, 9.
- IMRAN, M., SALEEM, S., CHAUDHURI, A., ALI, J. & BABOOTA, S. 2020. Docetaxel: An update on its molecular mechanisms, therapeutic trajectory and nanotechnology in the treatment of breast, lung and prostate cancer. *Journal of Drug Delivery Science and Technology*, 60, 101959.
- JAKOBS, B. S. & WANDERS, R. J. 1995. Fatty acid beta-oxidation in peroxisomes and mitochondria: the first, unequivocal evidence for the involvement of carnitine in shuttling propionyl-CoA from peroxisomes to mitochondria. *Biochem Biophys Res Commun*, 213, 1035-41.
- JAMES, N. D., SYDES, M. R., CLARKE, N. W., MASON, M. D., DEARNALEY, D. P., SPEARS, M. R., RITCHIE, A. W., PARKER, C. C., RUSSELL, J. M., ATTARD, G., DE BONO, J., CROSS, W., JONES, R. J., THALMANN, G., AMOS, C., MATHESON, D., MILLMAN, R., ALZOUEBI, M., BEESLEY, S., BIRTLE, A. J., BROCK, S., CATHOMAS, R., CHAKRABORTI, P., CHOWDHURY, S., COOK, A., ELLIOTT, T., GALE, J., GIBBS, S., GRAHAM, J. D., HETHERINGTON, J., HUGHES, R., LAING, R., MCKINNA, F., MCLAREN, D. B., O'SULLIVAN, J. M., PARIKH, O., PEEDELL, C., PROTHEROE, A., ROBINSON, A. J., SRIHARI, N., SRINIVASAN, R., STAFFURTH, J., SUNDAR, S., TOLAN, S., TSANG, D., WAGSTAFF, J. & PARMAR, M. K. 2016. Addition of docetaxel, zoledronic acid, or both to first-line long-term hormone therapy in prostate cancer (STAMPEDE): survival results from an adaptive, multiarm, multistage, platform randomised controlled trial. *Lancet*, 387, 1163-77.
- JAVOID, N. & CHOI, S. 2020. Toll-like Receptors from the Perspective of Cancer Treatment. *Cancers (Basel)*, 12.
- JEONG, P., HA, Y., YUN, S., YOON, H., FREEMAN, M., KIM, J. & KIM, W. 2015. Assess the expression of ubiquitin specific protease USP2a for bladder cancer diagnosis. *BMC Urology*, 15, 1-6.
- JIA, L., BERMAN, B. P., JARIWALA, U., YAN, X., COGAN, J. P., WALTERS, A., CHEN, T., BUCHANAN, G., FRENKEL, B. & COETZEE, G. A. 2008. Genomic Androgen Receptor-Occupied Regions with Different Functions, Defined by Histone Acetylation, Coregulators and Transcriptional Capacity. *PLOS ONE*, 3, e3645.
- JOSEPH, J. D., LU, N., QIAN, J., SENSINTAFFAR, J., SHAO, G., BRIGHAM, D., MOON, M., MANEVAL, E. C., CHEN, I., DARIMONT, B. & HAGER, J. H. 2013. A clinically relevant androgen receptor mutation confers resistance to second-generation antiandrogens enzalutamide and ARN-509. *Cancer Discov*, 3, 1020-9.
- JOVIC, D., LIANG, X., ZENG, H., LIN, L., XU, F. & LUO, Y. 2022. Single-cell RNA sequencing technologies and applications: A brief overview. *Clin Transl Med*, 12, e694.
- JUARRANZ, M. G., BOLAÑOS, O., GUTIÉRREZ-CAÑAS, I., LERNER, E. A., ROBBERECHT, P., CARMENA, M. J., PRIETO, J. C. & RODRÍGUEZ-HENCHE, N. 2001. Neuroendocrine differentiation of the LNCaP prostate cancer cell line maintains the expression and function of VIP and PACAP receptors. *Cell Signal*, 13, 887-94.
- KARAPETYAN, L., LUKE, J. J. & DAVAR, D. 2020. Toll-Like Receptor 9 Agonists in Cancer. *Oncotargets Ther*, 13, 10039-10060.
- KARETA, M. S., GORGES, L. L., HAFEEZ, S., BENAYOUN, B. A., MARRO, S., ZMOOS, A. F., CECCHINI, M. J., SPACEK, D., BATISTA, L. F., O'BRIEN, M., NG, Y. H., ANG, C. E., VAKA, D., ARTANDI, S. E., DICK, F. A., BRUNET, A., SAGE, J. & WERNIG, M. 2015. Inhibition of

- pluripotency networks by the Rb tumor suppressor restricts reprogramming and tumorigenesis. *Cell Stem Cell*, 16, 39-50.
- KATLINSKAYA, Y. V., KATLINSKI, K. V., YU, Q., ORTIZ, A., BEITING, D. P., BRICE, A., DAVAR, D., SANDERS, C., KIRKWOOD, J. M., RUI, H., XU, X., KOUMENIS, C., DIEHL, J. A. & FUCHS, S. Y. 2016. Suppression of Type I Interferon Signaling Overcomes Oncogene-Induced Senescence and Mediates Melanoma Development and Progression. *Cell Rep*, 15, 171-180.
- KATLINSKI, K. V., GUI, J., KATLINSKAYA, Y. V., ORTIZ, A., CHAKRABORTY, R., BHATTACHARYA, S., CARBONE, C. J., BEITING, D. P., GIRONDO, M. A., PECK, A. R., PURÉ, E., CHATTERJI, P., RUSTGI, A. K., DIEHL, J. A., KOUMENIS, C., RUI, H. & FUCHS, S. Y. 2017. Inactivation of Interferon Receptor Promotes the Establishment of Immune Privileged Tumor Microenvironment. *Cancer Cell*, 31, 194-207.
- KAWATA, H., ISHIKURA, N., WATANABE, M., NISHIMOTO, A., TSUNENARI, T. & AOKI, Y. 2010. Prolonged treatment with bicalutamide induces androgen receptor overexpression and androgen hypersensitivity. *The Prostate*, 70, 745-754.
- KE, H. L., LEE, Y. C., LI, W. M., WANG, C. S., HSU, W. C., LIN, H. H., LEE, Y. A., JHAN, J. H., LI, C. C., YE, H. C., WU, W. J. & HUANG, A. M. 2022. High Ubiquitin-Specific Protease 2a Expression Level Predicts Poor Prognosis in Upper Tract Urothelial Carcinoma. *Appl Immunohistochem Mol Morphol*, 30, 304-310.
- KHAREL, P., UPRETY, D., CHANDRA, A. B., HU, Y., BELUR, A. A. & DHAKAL, A. 2018. Bortezomib-Induced Pulmonary Toxicity: A Case Report and Review of Literature. *Case Rep Med*, 2018, 2913124.
- KIM, D., PERTEA, G., TRAPNELL, C., PIMENTEL, H., KELLEY, R. & SALZBERG, S. L. 2013. TopHat2: accurate alignment of transcriptomes in the presence of insertions, deletions and gene fusions. *Genome Biol*, 14, R36.
- KIM, E. M., JUNG, C.-H., KIM, J., HWANG, S.-G., PARK, J. K. & UM, H.-D. 2017. The P53/P21 complex regulates cancer cell invasion and apoptosis by targeting Bcl-2 family proteins. *Cancer Research*, 77, 3092-3100.
- KIM, J., KIM, W., LIU, Z., LODA, M. & FREEMAN, M. 2012. The ubiquitin-specific protease USP2a enhances tumor progression by targeting cyclin A1 in bladder cancer. *Cell Cycle*, 11, 1123-1130.
- KIM, S. J. & KIM, S. I. 2011. Current treatment strategies for castration-resistant prostate cancer. *Korean Journal of Urology*, 52, 157-165.
- KIM, Y. H., BAEK, S. H., KIM, E. K., HA, J. M., JIN, S. Y., LEE, H. S., HA, H. K., SONG, S. H., KIM, S. J., SHIN, H. K., YONG, J., KIM, D.-H., KIM, C. D. & BAE, S. S. 2016. Uncoordinated 51-like kinase 2 signaling pathway regulates epithelial-mesenchymal transition in A549 lung cancer cells. *FEBS Letters*, 590, 1365-1374.
- KISHAN, A. U., COOK, R. R., CIEZKI, J. P., ROSS, A. E., POMERANTZ, M. M., NGUYEN, P. L., SHAIKH, T., TRAN, P. T., SANDLER, K. A., STOCK, R. G., MERRICK, G. S., DEMANES, D. J., SPRATT, D. E., ABU-ISA, E. I., WEDDE, T. B., LILLEBY, W., KRAUSS, D. J., SHAW, G. K., ALAM, R., REDDY, C. A., STEPHENSON, A. J., KLEIN, E. A., SONG, D. Y., TOSOIAN, J. J., HEGDE, J. V., YOO, S. M., FIANO, R., D'AMICO, A. V., NICKOLS, N. G., ARONSON, W. J., SADEGHI, A., GRECO, S., DEVILLE, C., MCNUTT, T., DEWEESE, T. L., REITER, R. E., SAID, J. W., STEINBERG, M. L., HORWITZ, E. M., KUPELIAN, P. A. & KING, C. R. 2018. Radical prostatectomy, external beam radiotherapy, or external beam radiotherapy with brachytherapy boost and disease progression and mortality in patients with

- gleason score 9-10 prostate cancer. *JAMA - Journal of the American Medical Association*, 319, 896-905.
- KITAJIMA, K., MURPHY, R., NATHAN, M., FROEMMING, A., HAGEN, C., TAKAHASHI, N. & KAWASHIMA, A. 2014. Detection of recurrent prostate cancer after radical prostatectomy: comparison of 11C-Choline PET/CT with pelvic multiparametric MR imaging with endorectal coil. *The Journal of Nuclear Medicine*, 55, 223-232.
- KITAMURA, H. & HASHIMOTO, M. 2021. USP2-Related Cellular Signaling and Consequent Pathophysiological Outcomes. *International journal of molecular sciences*, 22, 1209.
- KITAMURA, T., QIAN, B. Z. & POLLARD, J. W. 2015. Immune cell promotion of metastasis. *Nat Rev Immunol*, 15, 73-86.
- KLUPP, F., KAHLERT, C., FRANZ, C., HALAMA, N., SCHLEUSSNER, N., WIRSIK, N. M., WARTH, A., SCHMIDT, T. & ULRICH, A. B. 2021. Granulin: An Invasive and Survival-Determining Marker in Colorectal Cancer Patients. *Int J Mol Sci*, 22.
- KOMANDER, D., CLAGUE, M. & URBÉ, S. 2009. Breaking the chains: structure and function of the deubiquitinases. *Nature Reviews*, 10, 550-563.
- KORPAL, M., KORN, J. M., GAO, X., RAKIEC, D. P., RUDDY, D. A., DOSHI, S., YUAN, J., KOVATS, S. G., KIM, S., COOKE, V. G., MONAHAN, J. E., STEGMEIER, F., ROBERTS, T. M., SELLERS, W. R., ZHOU, W. & ZHU, P. 2013. An F876L mutation in androgen receptor confers genetic and phenotypic resistance to MDV3100 (enzalutamide). *Cancer Discov*, 3, 1030-43.
- KPEMISSI, M., METOWOGO, K., MELILA, M., VEERAPUR, V. P., NEGRU, M., TAULESCU, M., POTÂRNICHE, A. V., SUHAS, D. S., PUNEETH, T. A., VIJAYAKUMAR, S., EKLUGADEGBEKU, K. & AKLIKOKOU, K. 2020. Acute and subchronic oral toxicity assessments of Combretum micranthum (Combretaceae) in Wistar rats. *Toxicol Rep*, 7, 162-168.
- KREGEL, S., KIRILUK, K. J., ROSEN, A. M., CAI, Y., REYES, E. E., OTTO, K. B., TOM, W., PANER, G. P., SZMULEWITZ, R. Z. & VANDER GRIEND, D. J. 2013. Sox2 is an androgen receptor-repressed gene that promotes castration-resistant prostate cancer. *PLoS One*, 8, e53701.
- KRIEG, A. M. 2007. Development of TLR9 agonists for cancer therapy. *J Clin Invest*, 117, 1184-94.
- KRISHNA, S. S. & GRISHIN, N. V. 2004. The Finger Domain of the Human Deubiquitinating Enzyme HAUSP is a Zinc Ribbon. *Cell Cycle*, 3, 1044-1047.
- KROHN, A., DIEDLER, T., BURKHARDT, L., MAYER, P., DE SILVA, C., MEYER-KORNBLUM, M., KÖTSCHAU, D., TENNSTEDT, P., HUANG, J., GERHÄUSER, C., MADER, M., KURTZ, S., SIRMA, H., SAAD, F., STEUBER, T., GRAEFEN, M., PLASS, C., SAUTER, G., SIMON, R., MINNER, S. & SCHLOMM, T. 2012. Genomic deletion of PTEN is associated with tumor progression and early PSA recurrence in ERG fusion-positive and fusion-negative prostate cancer. *The American Journal of Pathology*, 181, 401-412.
- KRUEGER, F. 2012. Trim galore. *Zenodo*, v0.4.4.
- KU, S.-Y., GLEAVE, M. E. & BELTRAN, H. 2019. Towards precision oncology in advanced prostate cancer. *Nature Reviews Urology*, 16, 645-654.
- KU, S., ROSARIO, S., WANG, Y., MU, P., SESHADRI, M., GOODRICH, Z., GOODRICH, M., LABBÉ, D., GOMEZ, E., WANG, J., LONG, H., XU, B., BROWN, M., LODA, M., SAWYERS, C., ELLIS, L. & GOODRICH, D. 2017. Rb1 and TRP53 cooperate to suppress prostate cancer lineage plasticity, metastasis, and antiandrogen resistance. 355.

- KUMAR, A., COLEMAN, I., MORRISSEY, C., ZHANG, X., TRUE, L., GULATI, R., ETZIONI, R., BOLOURI, H., MONTGOMERY, B., WHITE, T., LUCAS, J., BROWN, L., DUMPIT, R., DESARKAR, N., HIGANO, C., YU, E., COLEMAN, R., SCHULTZ, N., FANG, M., LANGE, P., SHENDURE, J., VASSELLA, R. & NELSON, P. S. 2016. Substantial inter-individual and limited intra-individual genomic diversity among tumors from men with metastatic prostate cancer. *Nature Medicine*, 22, 369-378.
- KUMAR, V. & MAJUMDER, P. 1995. Prostate gland: structure, functions and regulation. *International urology and nephrology*, 27, 231-243.
- KYRIAKOPOULOS, C., CHEN, Y., CARDUCCI, M., LIU, G., JARRARD, D., HAHN, N., SHEVRIN, D., DREICER, R., HUSSAIN, M., EISENBERGER, M., KOHLI, M., PLIMACK, E., VOGELZANG, N., PICUS, J., COONEY, M., GARCIA, J., DIPOLA, R. & SWEENEY, C. 2018. Chemohormonal therapy in metastatic hormone-sensitive prostate cancer: long-term survival analysis of the randomised phase III E3085 CHAARTED trial. *Journal of Clinical Oncology*, 36, 1080-1086.
- LABRECQUE, M. P., COLEMAN, I. M., BROWN, L. G., TRUE, L. D., KOLLATH, L., LAKELY, B., NGUYEN, H. M., YANG, Y. C., DA COSTA, R. M. G., KAIPAINEN, A., COLEMAN, R., HIGANO, C. S., YU, E. Y., CHENG, H. H., MOSTAGHEL, E. A., MONTGOMERY, B., SCHWEIZER, M. T., HSIEH, A. C., LIN, D. W., COREY, E., NELSON, P. S. & MORRISSEY, C. 2019. Molecular profiling stratifies diverse phenotypes of treatment-refractory metastatic castration-resistant prostate cancer. *J Clin Invest*, 129, 4492-4505.
- LALLOUS, N., VOLIK, S., AWREY, S., LEBLANC, E., TSE, R., MURILLO, J., SINGH, K., AZAD, A., WYATT, A., LEBIHAN, S., CHI, K., GLEAVE, M., RENNIE, P., COLLINS, C. & CHERKASOV, A. 2016. Functional analysis of androgen receptor mutations that confer anti-androgen resistance identified in circulating cell-free DNA from prostate cancer patients. *Genome Biology*, 17, 1-15.
- LANGLEY, E., KEMPPAINEN, J. & WILSON, E. 1998. Intermolecular NH₂-/Carboxyl-terminal interactions in androgen receptor dimerisation revealed by mutations that cause androgen insensitivity. *The Journal of Biological Chemistry*, 273, 92-101.
- LAVOIE, J.-M., ZOU, K., KHALAF, D., EIGL, B. J., KOLLMANNNSBERGER, C. K., VERGIDIS, J., NOONAN, K., ZULFIQAR, M., FINCH, D. & CHI, K. N. 2019. Clinical effectiveness of docetaxel for castration-sensitive prostate cancer in a real-world population-based analysis. *The Prostate*, 79, 281-287.
- LAWRENCE, M., OBINATA, D., SANDHU, S., SELTH, L., WONG, S., PORTER, L., LISTER, N., POOK, D., PEZARO, C., GOODE, D., REBELLO, R., CLARK, A., PAPARGIRIS, M., GRAMBERG, J., HANSON, A., BANKS, P., WANG, H., NIRANJAN, B., KEERTHIKUMAR, S., HEDWARDS, S., HUGLO, A., YANG, R., HENZLER, C., LI, Y., LOPEZ-CAMPOS, F., CASTRO, E., TOIVANEN, R., AZAD, A., BOLTON, D., GOAD, J., GRUMMET, J., HAREWOOD, L., KOURAMBAS, J., LAWRENTSCHUK, N., MOON, D., MURPHY, D., SENGUPTA, S., SNOW, R., THORNE, H., MITCHELL, C., PEDERSEN, J., CLOUSTON, D., NORDEN, S., RYAN, A., DEHM, S. M., TILLEY, W. D., PEARSON, R., HANNAN, R., FRYDENBERG, M., FURIC, L., TAYLOR, R. & RISBRIDGER, G. 2018. Patient-derived models of Abiraterone- and Enzalutamide-resistant prostate cancer reveal sensitivity to ribosome-directed therapy. *European Urology*, 74, 562-572.
- LAZAROW, P. B. & DE DUVE, C. 1976. A fatty acyl-CoA oxidizing system in rat liver peroxisomes; enhancement by clofibrate, a hypolipidemic drug. *Proc Natl Acad Sci U S A*, 73, 2043-6.

- LEE, R. J., ALBANESE, C., FU, M., D'AMICO, M., LIN, B., WATANABE, G., HAINES, G. K., SIEGEL, P. M., HUNG, M.-C., YARDEN, Y., HOROWITZ, J. M., MULLER, W. J. & PESTELL, R. G. 2000. Cyclin D1 Is Required for Transformation by Activated Neu and Is Induced through an E2F-Dependent Signaling Pathway. *Molecular and Cellular Biology*, 20, 672-683.
- LENCHINE, R. V., RAO, S. R., WANG, X., FANG, D. M. & PROUD, C. G. 2021. Elongation factor eEF2 kinase and autophagy jointly promote survival of cancer cells. *Biochemical Journal*, 478, 1547-1569.
- LI, J., CHEN, S., HU, Y. & CAI, J. 2016. Bortezomib-induced severe pulmonary complications in multiple myeloma: A case report and literature review. *Oncol Lett*, 11, 2255-2260.
- LI, J., YEN, C., LIAW, D., PODSYBANINA, K., BOSE, S., WANG, S., PUC, J., MILIARESIS, C., RODGERS, L., MCCOMBIE, R., BIGNER, S., GIOVANELLA, B., ITTMANN, M., TYCKO, B., HIBSHOOSH, H., WIGLER, M. & PARSONS, R. 1997. PTEN, a putative protein Tyrosine phosphatase gene mutated in human brain, breast and prostate cancer. *Science*, 275, 1943-1947.
- LI, Q., DONG, H., YANG, G., SONG, Y., MOU, Y. & NI, Y. 2020. Mouse Tumor-Bearing Models as Preclinical Study Platforms for Oral Squamous Cell Carcinoma. *Frontiers in Oncology*, 10.
- LI, Q., YE, C., TIAN, T., JIANG, Q., ZHAO, P., WANG, X., LIU, F., SHAN, J. & RUAN, J. 2022. The emerging role of ubiquitin-specific protease 20 in tumorigenesis and cancer therapeutics. *Cell Death & Disease*, 13, 434.
- LI, Y., ALSAGABI, M., FAN, D., BOVA, G., TEWFIK, A. & DEHM, S. 2011. Intragenic rearrangement and altered RNA splicing of the androgen receptor in a cell-based model of prostate cancer progression. *Cancer Research*, 71, 2108-2117.
- LIANG, Y., TANG, H., GUO, J., QIU, X., YANG, Z., REN, Z., SUN, Z., BIAN, Y., XU, L., XU, H., SHEN, J., HAN, Y., DONG, H., PENG, H. & FU, Y.-X. 2018. Targeting IFN α to tumor by anti-PD-L1 creates feedforward antitumor responses to overcome checkpoint blockade resistance. *Nature Communications*, 9, 4586.
- LIAO, D. J., THAKUR, A., WU, J., BILIRAN, H. & SARKAR, F. H. 2007. Perspectives on c-Myc, Cyclin D1, and their interaction in cancer formation, progression, and response to chemotherapy. *Crit Rev Oncog*, 13, 93-158.
- LIAO, Y., SMYTH, G. K. & SHI, W. 2014. featureCounts: an efficient general purpose program for assigning sequence reads to genomic features. *Bioinformatics*, 30, 923-30.
- LIBERZON, A., BIRGER, C., THORVALDSDÓTTIR, H., GHANDI, M., MESIROV, J. P. & TAMAYO, P. 2015. The Molecular Signatures Database (MSigDB) hallmark gene set collection. *Cell Syst*, 1, 417-425.
- LIEBLER, D. C. & ZIMMERMAN, L. J. 2013. Targeted Quantitation of Proteins by Mass Spectrometry. *Biochemistry*, 52, 3797-3806.
- LIGHTOWLERS, R. N., ROZANSKA, A. & CHRZANOWSKA-LIGHTOWLERS, Z. M. 2014. Mitochondrial protein synthesis: figuring the fundamentals, complexities and complications, of mammalian mitochondrial translation. *FEBS Lett*, 588, 2496-503.
- LIN, H.-M., MAK, B., YEUNG, N., HUYNH, K., MEIKLE, T. G., MELLETT, N. A., KWAN, E. M., FETTKE, H., TRAN, B., DAVIS, I. D., MAHON, K. L., ZHANG, A., STOCKLER, M. R., BRISCOE, K., MARX, G., CRUMBAKER, M., STRICKER, P. D., DU, P., YU, J., JIA, S., SCHEINBERG, T., FITZPATRICK, M., BONNITCHA, P., SULLIVAN, D. R., JOSHUA, A. M., AZAD, A. A., BUTLER, L. M., MEIKLE, P. J. & HORVATH, L. G. 2021. Overcoming

- enzalutamide resistance in metastatic prostate cancer by targeting sphingosine kinase. *eBioMedicine*, 72.
- LIN, M., ZHAO, Z., YANG, Z., MENG, Q., TAN, P., XIE, W., QIN, Y., WANG, R.-F. & CUI, J. 2016. USP38 Inhibits Type I Interferon Signaling by Editing TBK1 Ubiquitination through NLRP4 Signalosome. *Molecular Cell*, 64, 267-281.
- LIN, Y., CHEN, C., HOU, C., CHANG, P. & TSUI, K. 2011. A comparison of androgen deprivation therapy versus surgical castration for patients with advanced prostatic carcinoma. *Acta Pharmacologica Sinica*, 32, 537-542.
- LIN, Y., ZHONG, H., SUN, B., PENG, Y., LU, F., CHEN, M., ZHU, M. & HUANG, J. 2020. USP22 promotes proliferation in renal cell carcinoma by stabilizing survivin. *Oncol Lett*, 20, 246.
- LINDAHL, T. & WOOD, R. D. 1999. Quality control by DNA repair. *Science*, 286, 1897-905.
- LIU, B., JIANG, S., LI, M., XIONG, X., ZHU, M., LI, D., ZHAO, L., QIAN, L., ZHAI, L., LI, J., LU, H., SUN, S., LIN, J., LU, Y., LI, X. & TAN, M. 2018a. Proteome-wide analysis of USP14 substrates revealed its role in hepatosteatosis via stabilization of FASN. *Nature Communications*, 9, 4770.
- LIU, Q. & RUDERMAN, J. V. 2006. Aurora A, mitotic entry, and spindle bipolarity. *Proc Natl Acad Sci U S A*, 103, 5811-6.
- LIU, S., JIANG, M., WANG, W., LIU, W., SONG, X., MA, Z., ZHANG, S., LIU, L., LIU, Y. & CAO, X. 2018b. Nuclear RNF2 inhibits interferon function by promoting K33-linked STAT1 disassociation from DNA. *Nature Immunology*, 19, 41-52.
- LIU, W., XIONG, X., CHEN, W., LI, X., HUA, X., LIU, Z. & ZHANG, Z. 2020. High expression of FUSE binding protein 1 in breast cancer stimulates cell proliferation and diminishes drug sensitivity Corrigendum in /10.3892/ijo.2021.5210. *Int J Oncol*, 57, 488-499.
- LIU, X.-Q., SHAO, X.-R., LIU, Y., DONG, Z.-X., CHAN, S.-H., SHI, Y.-Y., CHEN, S.-N., QI, L., ZHONG, L., YU, Y., LV, T., YANG, P.-F., LI, L.-Y., WANG, X.-B., ZHANG, X.-D., LI, X., ZHAO, W., SEHGAL, L., LI, M. & ZHANG, X.-D. 2022. Tight junction protein 1 promotes vasculature remodeling via regulating USP2/TWIST1 in bladder cancer. *Oncogene*, 41, 502-514.
- LIU, X., LI, Z., SONG, Y., WANG, R., HAN, L., WANG, Q., JIANG, K., KANG, C. & ZHANG, Q. 2016. AURKA induces EMT by regulating histone modification through Wnt/ β -catenin and PI3K/Akt signaling pathway in gastric cancer. *Oncotarget*, 7, 33152-64.
- LIU, Z., ZANATA, S., KIM, J., PETERSON, M., VIZIO, D., CHIRIEAC, L., PYNE, S., AGOSTINI, M., FREEMAN, M. & LODA, M. 2013. The ubiquitin-specific protease USP2a prevents endocytosis-mediated EGFR degradation. *Oncogene*, 32, 1660-1669.
- LOCKE, M., TOTH, J. I. & PETROSKI, M. D. 2014. Lys11- and Lys48-linked ubiquitin chains interact with p97 during endoplasmic-reticulum-associated degradation. *Biochem J*, 459, 205-16.
- LODATO, M. A., NG, C. W., WAMSTAD, J. A., CHENG, A. W., THAI, K. K., FRAENKEL, E., JAENISCH, R. & BOYER, L. A. 2013. SOX2 co-occupies distal enhancer elements with distinct POU factors in ESCs and NPCs to specify cell state. *PLoS Genet*, 9, e1003288.
- LOVE, M. I., HUBER, W. & ANDERS, S. 2014. Moderated estimation of fold change and dispersion for RNA-seq data with DESeq2. *Genome Biology*, 15, 550.
- LU, Q., WANG, P.-S. & YANG, L. 2021. Golgi-associated Rab GTPases implicated in autophagy. *Cell & Bioscience*, 11, 35.

- LUBAHN, D., JOSEPH, D., SULLIVAN, P., WILLARD, H., FRENCH, F. & WILSON, E. 1988. Cloning of human androgen receptor complementary DNA and localisation to the X chromosome. *Science*, 240, 327-330.
- LUN, A. T., CHEN, Y. & SMYTH, G. K. 2016. It's DE-licious: A Recipe for Differential Expression Analyses of RNA-seq Experiments Using Quasi-Likelihood Methods in edgeR. *Methods Mol Biol*, 1418, 391-416.
- MAHUL-MELLIER, A.-L., DATLER, C., PAZARENTZOS, E., LIN, B., CHAISAKLERT, W., ABUALI, G. & GRIMM, S. 2012. De-ubiquitinating proteases USP2a and USP2c cause apoptosis by stabilising RIP1. *Biochimica et Biophysica Acta (BBA) - Molecular Cell Research*, 1823, 1353-1365.
- MAKKONEN, H., KAUKANEN, M., JÄÄSKELÄINEN, T. & PALVIMO, J. 2011. Androgen receptor amplification is reflected in the transcriptional responses of vertebral-cancer of the prostate cells. *Molecular and Cellular Endocrinology*, 331, 57-65.
- MARINI, F. & BINDER, H. 2019. pcaExplorer: an R/Bioconductor package for interacting with RNA-seq principal components. *BMC Bioinformatics*, 20, 331.
- MATEO, J., CARREIRA, S., SANDHU, S., MIRANDA, S., MOSSOP, H., PEREZ-LOPEZ, R., RODRIGUES, D., ROBINSON, D., OMLIN, A., TUNARIU, N., BOYSEN, G., PORTA, N., FLOHR, P., GILLMAN, A., FIGUEIREDO, I., PAULDING, C., SEED, G., JAIN, S., RALPH, C., A, P., HUSSAIN, S., JONES, R. A., ELLIOT, T., MCGOVERN, U., BIANCHINI, D., GOODALL, J., ZAFEIRIOU, Z., WILLIAMSON, C., FERRALDESCHI, R., RIISNAES, R., EBBS, B., FOWLER, G., RODA, D., YUAN, W., WU, Y., CAO, X., BROUGH, R., PEMBERTON, H., A'HERN, R., SWAIN, A., KUNJU, L., EELES, R., ATTARD, G., LORD, C., ASHWORTH, A., RUBIN, M., KNUDSEN, K., FENG, F., CHINNAIYAN, A., HALL, E. & JS, D. B. 2015. DNA-repair defects and olaparib in metastatic prostate cancer. *The New England Journal of Medicine*, 373, 1697-1708.
- MCANALLY, D., VICCHIARELLI, M., SIDDIQUEE, K. & SMITH, L. H. 2012. In Vivo Rapid Assessment of Compound Exposure (RACE) for Profiling the Pharmacokinetics of Novel Chemical Probes. *Curr Protoc Chem Biol*, 4, 299-309.
- MCCLURG, U. L., HARLE, V. J., NABBI, A., BATALHA-PEREIRA, A., WALKER, S., COFFEY, K., GAUGHAN, L., MCCRACKEN, S. R. C. & ROBSON, C. N. 2015. Ubiquitin-specific protease 12 interacting partners Uaf-1 and WDR20 are potential therapeutic targets in prostate cancer. *Oncotarget*, 6, 37724-37736.
- MCKEITHEN, D., GRAHAM, T., CHUNG, L. W. & ODERO-MARAH, V. 2010. Snail transcription factor regulates neuroendocrine differentiation in LNCaP prostate cancer cells. *Prostate*, 70, 982-92.
- MEIJERING, E., JACOB, M., SARRIA, J.-C. F., STEINER, P., HIRLING, H. & UNSER, M. 2004. Design and validation of a tool for neurite tracing and analysis in fluorescence microscopy images. *Cytometry Part A*, 58A, 167-176.
- MENG, D. & LI, D. 2022. Ubiquitin-specific protease 1 overexpression indicates poor prognosis and promotes proliferation, migration, and invasion of gastric cancer cells. *Tissue Cell*, 74, 101723.
- MEYER, T. & STOCKFLETH, E. 2008. Clinical investigations of Toll-like receptor agonists. *Expert Opin Investig Drugs*, 17, 1051-65.
- MIFTAKHOVA, R., HEDBLUM, A., SEMENAS, J., ROBINSON, B., SIMOULIS, A., MALM, J., RIZVANOV, A., HEERY, D. M., MONGAN, N. P., MAITLAND, N. J., ALLEGRUCCI, C. & PERSSON, J. L. 2016. Cyclin A1 and P450 Aromatase Promote Metastatic Homing and

- Growth of Stem-like Prostate Cancer Cells in the Bone Marrow. *Cancer Res*, 76, 2453-64.
- MIHALIK, S. J., RAINVILLE, A. M. & WATKINS, P. A. 1995. Phytanic Acid α -oxidation in Rat Liver Peroxisomes. *European Journal of Biochemistry*, 232, 545-551.
- MORADI BINABAJ, M., BAHRAMI, A., KHAZAEI, M., RYZHIKOV, M., FERNS, G. A., AVAN, A. & MAHDI HASSANIAN, S. 2020. The prognostic value of cyclin D1 expression in the survival of cancer patients: A meta-analysis. *Gene*, 728, 144283.
- MORI, D., YAMADA, M., MIMORI-KIYOSUE, Y., SHIRAI, Y., SUZUKI, A., OHNO, S., SAYA, H., WYNSHAW-BORIS, A. & HIROTSUNE, S. 2009. An essential role of the aPKC–Aurora A–NDEL1 pathway in neurite elongation by modulation of microtubule dynamics. *Nature Cell Biology*, 11, 1057-1068.
- MORITA, M. & IMANAKA, T. 2012. Peroxisomal ABC transporters: structure, function and role in disease. *Biochim Biophys Acta*, 1822, 1387-96.
- MOSQUERA, J. M., BELTRAN, H., PARK, K., MACDONALD, T. Y., ROBINSON, B. D., TAGAWA, S. T., PERNER, S., BISMAR, T. A., ERBERSDOBLER, A., DHIR, R., NELSON, J. B., NANUS, D. M. & RUBIN, M. A. 2013. Concurrent AURKA and MYCN gene amplifications are harbingers of lethal treatment-related neuroendocrine prostate cancer. *Neoplasia*, 15, 1-10.
- MOTTET, N., BELLMUNT, J., BOLLA, M., BRIERS, E., CUMBERBATCH, M., SANTIS, M., FOSSATI, N., GROSS, T., HENRY, A. M., JONIAU, S., LAM, T. B., MASON, M. D., MATVEEV, V., MOLDOVAN, P., VAN DEN BERGH, R., VAN DEN BROECK, T., VAN DER POEL, H., VAN DER KWAST, T., ROUVIÈRE, O., SCHOOTS, I., WIEGEL, T. & CORNFORD, P. 2017. EAU-ESTRO-SIOG guidelines on prostate cancer. Part 1: screening, diagnosis, and local treatment with curative intent. *European Urology*, 71, 618-629.
- MU, P., ZHANG, Z., BENELLI, M., KARTHAUS, W. R., HOOVER, E., CHEN, C. C., WONGVIPAT, J., KU, S. Y., GAO, D., CAO, Z., SHAH, N., ADAMS, E. J., ABIDA, W., WATSON, P. A., PRANDI, D., HUANG, C. H., DE STANCHINA, E., LOWE, S. W., ELLIS, L., BELTRAN, H., RUBIN, M. A., GOODRICH, D. W., DEMICHELI, F. & SAWYERS, C. L. 2017. SOX2 promotes lineage plasticity and antiandrogen resistance in TP53- and RB1-deficient prostate cancer. *Science*, 355, 84-88.
- MULLER, P. Y., MILTON, M., LLOYD, P., SIMS, J. & BRENNAN, F. R. 2009. The minimum anticipated biological effect level (MABEL) for selection of first human dose in clinical trials with monoclonal antibodies. *Current Opinion in Biotechnology*, 20, 722-729.
- MUTUKU, S. M., TRIM, P. J., PRABHALA, B. K., IRANI, S., BREMERT, K. L., LOGAN, J. M., BROOKS, D. A., STAHL, J., CENTENERA, M. M., SNEL, M. F. & BUTLER, L. M. 2019. Evaluation of Small Molecule Drug Uptake in Patient-Derived Prostate Cancer Explants by Mass Spectrometry. *Sci Rep*, 9, 15008.
- NASSAR, Z. D., MAH, C. Y., DEHAIRS, J., BURVENICH, I. J. G., IRANI, S., CENTENERA, M. M., HELM, M., SHRESTHA, R. K., MOLDOVAN, M., DON, A. S., HOLST, J., SCOTT, A. M., HORVATH, L. G., LYNN, D. J., SELTH, L. A., HOY, A. J., SWINNEN, J. V. & BUTLER, L. M. 2020. Human DECR1 is an androgen-repressed survival factor that regulates PUFA oxidation to protect prostate tumor cells from ferroptosis. *eLife*, 9, e54166.
- NCBI 2016. Database resources of the National Center for Biotechnology Information. *Nucleic Acids Res*, 44, D7-19.

- NIJMAN, S. M., LUNA-VARGAS, M. P., VELDS, A., BRUMMELKAMP, T. R., DIRAC, A. M., SIXMA, T. K. & BERNARDS, R. 2005. A genomic and functional inventory of deubiquitinating enzymes. *Cell*, 123, 773-86.
- NOGUCHI, M., NODA, S., YOSHIDA, M., UEDA, S., SHIRAIISHI, T. & ITOH, K. 2004. Chemohormonal therapy as primary treatment for metastatic prostate cancer: a randomized study of estramustine phosphate plus luteinizing hormone-releasing hormone agonist versus flutamide plus luteinizing hormone-releasing hormone agonist. *Int J Urol*, 11, 103-9.
- NOLAN, K. D., FRANCO, O. E., HANCE, M. W., HAYWARD, S. W. & ISAACS, J. S. 2015. Tumor-secreted Hsp90 Subverts Polycomb Function to Drive Prostate Tumor Growth and Invasion *. *Journal of Biological Chemistry*, 290, 8271-8282.
- NOTINI, A., DAVEY, R., MCMANUS, J., BATE, K. & ZAJAC, J. 2005. Genomic actions of the androgen receptor are required for normal male sexual differentiation in a mouse model. *Journal of Molecular Endocrinology*, 35, 547-555.
- NUHN, P., DE BONO, J., FIZAZI, K., FREEDLAND, S., GRILLI, M., KANTOFF, P., SONPAVDE, G., STERNBERG, C., YEGNASUBRAMANIAN, S. & ANTONARAKIS, E. 2019. Update on systemic prostate cancer therapies: management of metastatic castration-resistant prostate cancer in the era of precision oncology. *European Urology*, 75, 88-99.
- NYQUIST, M., LI, Y., HWANG, T. H., MANLOVE, L., VESSELLA, R., SILVERSTEIN, K. A. T., VOYTAS, D. & DEHM, S. M. 2013. TALEN-engineered AR gene arrangements reveal endocrine uncoupling of androgen receptor in prostate cancer. *Proceedings of the National Academy of Sciences*, 110, 17492-17497.
- OBACH, R. S. 1999. Prediction of human clearance of twenty-nine drugs from hepatic microsomal intrinsic clearance data: An examination of in vitro half-life approach and nonspecific binding to microsomes. *Drug Metab Dispos*, 27, 1350-9.
- OH, K., YANG, S., PARK, J., SEOL, J., LEMURA, S., NATSUME, T., MURATA, S., TANAKA, K., JEON, Y. & CHUNG, C. 2011. Control of AIF-mediated cell death by antagonistic functions of CHIP ubiquitin E3 and USP2 deubiquitinating enzyme. *Cell Death and Differentiation*, 18, 1326-1336.
- OHTAKE, F., TSUCHIYA, H., SAEKI, Y. & TANAKA, K. 2018. K63 ubiquitylation triggers proteasomal degradation by seeding branched ubiquitin chains. *Proceedings of the National Academy of Sciences*, 115, E1401-E1408.
- OHTANI, K., DEGREGORI, J. & NEVINS, J. R. 1995. Regulation of the cyclin E gene by transcription factor E2F1. *Proc Natl Acad Sci U S A*, 92, 12146-50.
- OSER, M. G., FONSECA, R., CHAKRABORTY, A. A., BROUGH, R., SPEKTOR, A., JENNINGS, R. B., FLAIFEL, A., NOVAK, J. S., GULATI, A., BUSS, E., YOUNGER, S. T., MCBRAYER, S. K., COWLEY, G. S., BONAL, D. M., NGUYEN, Q. D., BRULLE-SOUMARE, L., TAYLOR, P., CAIRO, S., RYAN, C. J., PEASE, E. J., MARATEA, K., TRAVERS, J., ROOT, D. E., SIGNORETTI, S., PELLMAN, D., ASHTON, S., LORD, C. J., BARRY, S. T. & KAELIN, W. G., JR. 2019. Cells Lacking the RB1 Tumor Suppressor Gene Are Hyperdependent on Aurora B Kinase for Survival. *Cancer Discov*, 9, 230-247.
- OTTO, T. & SICINSKI, P. 2017. Cell cycle proteins as promising targets in cancer therapy. *Nature reviews. Cancer*, 17, 93-115.
- PAK, S., PARK, S., KIM, Y., PARK, J. H., PARK, C. H., LEE, K. J., KIM, C. S. & AHN, H. 2019. The small molecule WNT/ β -catenin inhibitor CWP232291 blocks the growth of

- castration-resistant prostate cancer by activating the endoplasmic reticulum stress pathway. *J Exp Clin Cancer Res*, 38, 342.
- PAL, A., YOUNG, M. A. & DONATO, N. J. 2014. Emerging Potential of Therapeutic Targeting of Ubiquitin-Specific Proteases in the Treatment of Cancer. *Cancer Research*, 74, 4955-4966.
- PALTOGLOU, S., DAS, R., TOWNLEY, S. L., HICKEY, T. E., TARULLI, G. A., COUTINHO, I., FERNANDES, R., HANSON, A. R., DENIS, I., CARROLL, J. S., DEHM, S. M., RAJ, G. V., PLYMATE, S. R., TILLEY, W. D. & SELTH, L. A. 2017. Novel Androgen Receptor Coregulator GRHL2 Exerts Both Oncogenic and Antimetastatic Functions in Prostate Cancer. *Cancer Res*, 77, 3417-3430.
- PAPANDREOU, C. N., DALIANI, D. D., THALL, P. F., TU, S. M., WANG, X., REYES, A., TRONCOSO, P. & LOGOTHETIS, C. J. 2002. Results of a phase II study with doxorubicin, etoposide, and cisplatin in patients with fully characterized small-cell carcinoma of the prostate. *J Clin Oncol*, 20, 3072-80.
- PARANJAPE, A. N., SOUNDARARAJAN, R., WERDEN, S. J., JOSEPH, R., TAUBE, J. H., LIU, H., RODRIGUEZ-CANALES, J., SPHYRIS, N., WISTUBA, I., MIURA, N., DHILLON, J., MAHAJAN, N., MAHAJAN, K., CHANG, J. T., ITTMANN, M., MAITY, S. N., LOGOTHETIS, C., TANG, D. G. & MANI, S. A. 2016. Inhibition of FOXC2 restores epithelial phenotype and drug sensitivity in prostate cancer cells with stem-cell properties. *Oncogene*, 35, 5963-5976.
- PARASURAMAN, S. 2011. Toxicological screening. *J Pharmacol Pharmacother*, 2, 74-9.
- PARK, J. M., LEE, J. E., PARK, C. M. & KIM, J. H. 2019. USP44 Promotes the Tumorigenesis of Prostate Cancer Cells through EZH2 Protein Stabilization. *Molecules and cells*, 42, 17-27.
- PARKER, C., CASTRO, E., FIZAZI, K., HEIDENREICH, A., OST, P., PROCOPIO, G., TOMBAL, B. & GILLESSEN, S. 2020. Prostate cancer: ESMO Clinical Practice Guidelines for diagnosis, treatment and follow-up. *Ann Oncol*, 31, 1119-1134.
- PARKER, C., HEINRICH, D., JM, O. S., FOSSA, S., CHODACKI, A., LOGUE, T., SEKE, M., WIDMARK, A., JOHANNESSEN, D., NILSSON, S., HOSKIN, P., SOLBERG, A., JAMES, N., SYNDIKUS, I., CROSS, A., O'BRYAN-TEAR, C., GARCIA-VARGAS, J. & SARTOR, O. 2012. Overall survival benefit and safety profile of radium-223 chloride, a first-in-class alpha-pharmaceutical: Results from a phase III randomized trial (ALSYMPCA) in patients with castration-resistant prostate cancer (CRPC) with bone metastases. *Journal of Clinical Oncology*, 30, Abstract 8.
- PASSMORE, L. & BARFORD, D. 2004. Getting into position: the catalytic mechanisms of protein ubiquitylation. *Biochemical Journal*, 379, 513-525.
- PAULSON, K. G., VOILLET, V., MCAFEE, M. S., HUNTER, D. S., WAGENER, F. D., PERDICCHIO, M., VALENTE, W. J., KOELLE, S. J., CHURCH, C. D., VANDEVEN, N., THOMAS, H., COLUNGA, A. G., IYER, J. G., YEE, C., KULIKAUSKAS, R., KOELLE, D. M., PIERCE, R. H., BIELAS, J. H., GREENBERG, P. D., BHATIA, S., GOTTARDO, R., NGHIEM, P. & CHAPUIS, A. G. 2018. Acquired cancer resistance to combination immunotherapy from transcriptional loss of class I HLA. *Nature Communications*, 9, 3868.
- PETRYLAK, D. P., TANGEN, C. M., HUSSAIN, M. H., LARA, P. N., JR., JONES, J. A., TAPLIN, M. E., BURCH, P. A., BERRY, D., MOINPOUR, C., KOHLI, M., BENSON, M. C., SMALL, E. J., RAGHAVAN, D. & CRAWFORD, E. D. 2004. Docetaxel and estramustine compared

- with mitoxantrone and prednisone for advanced refractory prostate cancer. *N Engl J Med*, 351, 1513-20.
- POMERANTZ, M., LI, F., TAKEDA, D., LENCI, R., CHONKAR, A., CHABOT, M., CEJAS, P., VAZQUEZ, F., COOK, J., SHIVDASANI, R., BOWDEN, M., LIS, R., HAHN, W., KANTOFF, P., BROWN, M., LODA, M., LONG, H. & FREEDMAN, M. 2015. The androgen receptor cistrome is extensively reprogrammed in human prostate tumorigenesis. *Nature Genetics*, 47, 1346-1351.
- POMERANTZ, M. M., QIU, X., ZHU, Y., TAKEDA, D. Y., PAN, W., BACA, S. C., GUSEV, A., KORTHAUER, K. D., SEVERSON, T. M., HA, G., VISWANATHAN, S. R., SEO, J.-H., NGUYEN, H. M., ZHANG, B., PASANIUC, B., GIAMBARTOLOMEI, C., ALAIWI, S. A., BELL, C. A., O'CONNOR, E. P., CHABOT, M. S., STILLMAN, D. R., LIS, R., FONT-TELLO, A., LI, L., CEJAS, P., BERGMAN, A. M., SANDERS, J., VAN DER POEL, H. G., GAYTHER, S. A., LAWRENSON, K., FONSECA, M. A. S., REDDY, J., CORONA, R. I., MARTOVETSKY, G., EGAN, B., CHOUERI, T., ELLIS, L., GARRAWAY, I. P., LEE, G.-S. M., COREY, E., LONG, H. W., ZWART, W. & FREEDMAN, M. L. 2020. Prostate cancer reactivates developmental epigenomic programs during metastatic progression. *Nature Genetics*, 52, 790-799.
- POULIN, P., KENNY, J. R., HOP, C. E. C. A. & HADDAD, S. 2012. In vitro–in vivo extrapolation of clearance: Modeling hepatic metabolic clearance of highly bound drugs and comparative assessment with existing calculation methods. *Journal of Pharmaceutical Sciences*, 101, 838-851.
- PRETLOW, T., WOLMAN, S., MICALE, M., PELLEY, R., KURSH, E., RESNICK, M., BODNER, D., JACOBBERGER, J., DELMORO, C., GIACONIA, J. & PRETLOW, T. 1993. Xenografts of primary human prostatic carcinoma. *Journal of National Cancer Institute*, 85, 394-398.
- PRINCOVÁ, J., SALAT-CANELA, C., DANĚK, P., MAREŠOVÁ, A., DE CUBAS, L., BÄHLER, J., AYTÉ, J., HIDALGO, E. & PŘEVOROVSKÝ, M. 2023. Perturbed fatty-acid metabolism is linked to localized chromatin hyperacetylation, increased stress-response gene expression and resistance to oxidative stress. *PLOS Genetics*, 19, e1010582.
- PRIOLO, C., TANG, D., BRAHAMANDAN, M., BENASSI, B., SICINSKA, E., OGINO, S., FARSETTI, A., PORRELLO, A., FINN, S., ZIMMERMAN, J., FEBBO, P. & LODA, M. 2006. The isopeptidase USP2a protects human prostate cancer from apoptosis. *Cancer Research*, 66, 8625-8632.
- PU, J. Y., ZHANG, Y., WANG, L. X., WANG, J. & ZHOU, J. H. 2022. Inhibition of Ubiquitin-specific Protease 4 Attenuates Epithelial-Mesenchymal Transition of Renal Tubular Epithelial Cells via Transforming Growth Factor Beta Receptor Type I. *Curr Med Sci*, 42, 1000-1006.
- QUINTANAL-VILLALONGA, Á., CHAN, J. M., YU, H. A., PE'ER, D., SAWYERS, C. L., SEN, T. & RUDIN, C. M. 2020. Lineage plasticity in cancer: a shared pathway of therapeutic resistance. *Nat Rev Clin Oncol*, 17, 360-371.
- RAJAN, N., ELLIOTT, R., CLEWES, O., MACKAY, A., REIS-FILHO, J. S., BURN, J., LANGTRY, J., SIEBER-BLUM, M., LORD, C. J. & ASHWORTH, A. 2011. Dysregulated TRK signalling is a therapeutic target in CYLD defective tumours. *Oncogene*, 30, 4243-4260.
- RAJKUMAR, S., RICHARDSON, P., HIDESHIMA, T. & ANDERSON, K. 2005. Proteasome inhibition as a novel therapeutic target in human cancer. *Journal of Clinical Oncology*, 23, 630-639.

- RAMOS-GARCÍA, P., GIL-MONTOYA, J. A., SCULLY, C., AYÉN, A., GONZÁLEZ-RUIZ, L., NAVARRO-TRIVIÑO, F. J. & GONZÁLEZ-MOLES, M. A. 2017. An update on the implications of cyclin D1 in oral carcinogenesis. *Oral Dis*, 23, 897-912.
- REICH, M., LIEFELD, T., GOULD, J., LERNER, J., TAMAYO, P. & MESIROV, J. P. 2006. GenePattern 2.0. *Nature Genetics*, 38, 500-501.
- RENATUS, M., PARRADO, S., ARCY, A., EIDHOFF, U., GERHARTZ, B., HASSIEPEN, U., PIERRAT, B., RIEDL, R., VINZENZ, D., WORPENBERG, S. & KROEMER, M. 2006. Structural basis of ubiquitin recognition by the deubiquitinating protease USP2. *Structure*, 14, 1293-1302.
- RISBRIDGER, G., TOIVANEN, R. & TAYLOR, R. 2018. Preclinical models of prostate cancer: patient-derived xenografts, organoids, and other explant models. *Cold Spring Harbor Perspectives in Medicine*, 8, 1-13.
- RO, J. Y., TÊTU, B., AYALA, A. G. & ORDÓÑEZ, N. G. 1987. Small cell carcinoma of the prostate. II. Immunohistochemical and electron microscopic studies of 18 cases. *Cancer*, 59, 977-82.
- ROBINSON, D., ALLEN, E., WU, Y., SCHULTZ, N., LONIGRO, R., MOSQUERA, J., MONTGOMERY, B., TAPLIN, M., PRITCHARD, C., ATTARD, G., BELTRAN, H., ABIDA, W., BRADLEY, R., VINSON, J., CAO, X., VATS, P., KUNJU, L., HUSSAIN, M., FY, F., TOMLINS, S., COONEY, K., SMITH, D., BRENNAN, C., SIDDIQUI, J., MEHRA, R., CHEN, Y., RATHKOPF, D., MORRIS, M., SOLOMON, S., DURACK, J., REUTER, V., GOPALAN, A., GAO, J., LODA, M., LIS, R., BOWDEN, M., BALK, S., GAVIOLA, G., SOUGNEZ, C., GUPTA, M., YU, E., MOSTAGHEL, E., CHENG, H., MULCAHY, H., TRUE, L., PLYMATE, S., DVINGE, H., FERRALDESCHI, R., FLOHR, P., MIRANDA, S., ZAFEIRIOU, Z., TUNARIU, N., MATEO, J., PEREZ-LOPEZ, R., DEMICHELIS, F., ROBINSON, B., SCHIFFMAN, M., NANUS, D., TAGAWA, S., SIGARAS, A., ENG, K., ELEMENTO, O., SBONER, A., HEATH, E., SCHER, H., PIENTA, K., KANTOFF, P., DE BONO, J., RUBIN, M., NELSON, P., GARRAWAY, L., SAWYERS, C. & CHINNAIYAN, A. 2015. Integrative clinical genomics of advanced prostate cancer. *Cell*, 161, 1215-1228.
- ROBINSON, M. D., MCCARTHY, D. J. & SMYTH, G. K. 2010. edgeR: a Bioconductor package for differential expression analysis of digital gene expression data. *Bioinformatics*, 26, 139-40.
- RODRÍGUEZ-LARA, A., MESA, M. D., ARAGÓN-VELA, J., CASUSO, R. A., VÁZQUEZ, C. C., ZÚÑIGA, J. M. & HUERTAS, J. R. 2019. Acute/Subacute and Sub-Chronic Oral Toxicity of a Hydroxytyrosol-Rich Virgin Olive Oil Extract. *Nutrients*, 11.
- ROJAS, A., LIU, G., COLEMAN, I., NELSON, P. S., ZHANG, M., DASH, R., FISHER, P. B., PLYMATE, S. R. & WU, J. D. 2011. IL-6 promotes prostate tumorigenesis and progression through autocrine cross-activation of IGF-IR. *Oncogene*, 30, 2345-55.
- ROJAS GÓMEZ, R. & RESTREPO VALENCIA, P. 2015. In vitro-in vivo Pharmacokinetic correlation model for quality assurance of antiretroviral drugs. *Colomb Med (Cali)*, 46, 109-16.
- RONAU, J., BECKMANN, J. & HOCHSTRASSER, M. 2016. Substrate specificity of the ubiquitin and Ubl proteases. *Cell Research*, 26, 441-456.
- ROSAL, J. 2011. The origin of neuroendocrine tumors and the neural crest saga. *Modern Pathology*, 24, S53-S57.
- ROWINSKY, E. K., PANER, A., BERDEJA, J. G., PABA-PRADA, C., VENUGOPAL, P., PORKKA, K., GULLBO, J., LINDER, S., LOSKOG, A., RICHARDSON, P. G. & LANDGREN, O. 2020.

- Phase 1 study of the protein deubiquitinase inhibitor VLX1570 in patients with relapsed and/or refractory multiple myeloma. *Invest New Drugs*, 38, 1448-1453.
- RYSMAN, E., BRUSSELMANS, K., SCHEYS, K., TIMMERMANS, L., DERUA, R., MUNCK, S., VAN VELDHOVEN, P. P., WALTREGNY, D., DANIËLS, V. W., MACHIELS, J., VANDERHOYDONC, F., SMANS, K., WAELKENS, E., VERHOEVEN, G. & SWINNEN, J. V. 2010. De novo lipogenesis protects cancer cells from free radicals and chemotherapeutics by promoting membrane lipid saturation. *Cancer Res*, 70, 8117-26.
- SAAD, F. & HOTTE, S. 2010. Guidelines for the management of castrate-resistant prostate cancer. *Canadian Urological Association*, 4, 380-384.
- SAHOTA, T., DANHOF, M. & DELLA PASQUA, O. 2016. Pharmacology-based toxicity assessment: towards quantitative risk prediction in humans. *Mutagenesis*, 31, 359-374.
- SÁNCHEZ, B. G., BORT, A., VARA-CIRUELOS, D. & DÍAZ-LAVIADA, I. 2020. Androgen Deprivation Induces Reprogramming of Prostate Cancer Cells to Stem-Like Cells. *Cells*, 9.
- SCHEINBERG, T., MAK, B., BUTLER, L., SELTH, L. & HORVATH, L. G. 2023. Targeting lipid metabolism in metastatic prostate cancer. *Therapeutic Advances in Medical Oncology*, 15, 17588359231152839.
- SCHER, H. I., FIZAZI, K., SAAD, F., TAPLIN, M.-E., STERNBERG, C. N., MILLER, K., DE WIT, R., MULDER, P., CHI, K. N., SHORE, N. D., ARMSTRONG, A. J., FLAIG, T. W., FLÉCHON, A., MAINWARING, P., FLEMING, M., HAINSWORTH, J. D., HIRMAND, M., SELBY, B., SEELY, L. & DE BONO, J. S. 2012. Increased Survival with Enzalutamide in Prostate Cancer after Chemotherapy. *New England Journal of Medicine*, 367, 1187-1197.
- SCHINDELIN, J., ARGANDA-CARRERAS, I., FRISE, E., KAYNIG, V., LONGAIR, M., PIETZSCH, T., PREIBISCH, S., RUEDEN, C., SAALFELD, S., SCHMID, B., TINEVEZ, J.-Y., WHITE, D. J., HARTENSTEIN, V., ELICEIRI, K., TOMANCAK, P. & CARDONA, A. 2012. Fiji: an open-source platform for biological-image analysis. *Nature Methods*, 9, 676-682.
- SCHOOTS, I., ROOBOL, M., NIEBOER, D., BANGMA, C., STEYERBERG, E. & HUNINK, M. 2014. Magnetic resonance imaging-targeted biopsy may enhance the diagnostic accuracy of significant prostate cancer detection compared to standard transrectal ultrasound-guided biopsy: a systematic review and meta-analysis. *European Urology*, 68, 438-450.
- SCHRECEGOST, R. S., DEAN, J. L., GOODWIN, J. F., SCHIEWER, M. J., URBAN, M. W., STANEK, T. J., SUSSMAN, R. T., HICKS, J. L., BIRBE, R. C., DRAGANOVA-TACHEVA, R. A., VISAKORPI, T., DEMARZO, A. M., MCMAHON, S. B. & KNUDSEN, K. E. 2014. USP22 regulates oncogenic signaling pathways to drive lethal cancer progression. *Cancer Res*, 74, 272-86.
- SCHROEDER, A., HERRMANN, A., CHERRYHOLMES, G., KOWOLIK, C., BUETTNER, R., PAL, S., YU, H., MÜLLER-NEWEN, G. & JOVE, R. 2014. Loss of androgen receptor expression promotes a stem-like cell phenotype in prostate cancer through STAT3 signaling. *Cancer Res*, 74, 1227-37.
- SCHWED-GROSS, A., HAMIEL, H., FABER, G. P., ANGEL, M., BEN-YISHAY, R., BENICHO, J. I. C., ISHAY-RONEN, D. & SHAV-TAL, Y. 2022. Glucocorticoids enhance chemotherapy-driven stress granule assembly and impair granule dynamics, leading to cell death. *J Cell Sci*, 135.

- SEIDENFELD, J., SAMSON, D., HASSELBLAD, V., ARONSON, N., ALBERTSEN, P., BENETT, C. & WILT, T. 2000. Single-therapy androgen suppression in men with advanced prostate cancer: a systematic review and meta-analysis. *Annals of Internal Medicine*, 132, 566-577.
- SELLA, A., KONICHEZKY, M., FLEX, D., SULKES, A. & BANIEL, J. 2000. Low PSA Metastatic Androgen– Independent Prostate Cancer. *European Urology*, 38, 250-254.
- SHAMMA, A., SUZUKI, M., HAYASHI, N., KOBAYASHI, M., SASAKI, N., NISHIUCHI, T., DOKI, Y., OKAMOTO, T., KOHNO, S., MURANAKA, H., KITAJIMA, S., YAMAMOTO, K.-I. & TAKAHASHI, C. 2013. ATM Mediates pRB Function To Control DNMT1 Protein Stability and DNA Methylation. *Molecular and Cellular Biology*, 33, 3113-3124.
- SHAPIRO, D. & TAREEN, B. 2012. Current and emerging treatments in the management of castration-resistant prostate cancer. *Expert Review of Anticancer Therapy*, 12, 951-964.
- SHEN, R., DORAI, T., SZABOLES, M., KATZ, A. E., OLSSON, C. A. & BUTTYAN, R. 1997. Transdifferentiation of cultured human prostate cancer cells to a neuroendocrine cell phenotype in a hormone-depleted medium. *Urologic Oncology: Seminars and Original Investigations*, 3, 67-75.
- SHI, Y., SOLOMON, L., PEREDA-LOPEZ, A., GIRANDA, V., LUO, Y., JOHNSON, E., SHOEMAKER, A., LEVERSON, J. & LIU, X. 2011. Ubiquitin-specific Cysteine Protease 2a (USP2a) regulates the stability of Aurora-A. *The Journal of Biological Chemistry*, 286, 38960-38968.
- SHIOTA, M., BISHOP, J. L., NIP, K. M., ZARDAN, A., TAKEUCHI, A., CORDONNIER, T., BERALDI, E., BAZOV, J., FAZLI, L., CHI, K., GLEAVE, M. & ZOUBEIDI, A. 2013. Hsp27 Regulates Epithelial Mesenchymal Transition, Metastasis, and Circulating Tumor Cells in Prostate Cancer. *Cancer Research*, 73, 3109-3119.
- SHIOTA, M., YOKOMIZO, A. & NAITO, S. 2011. Increased androgen receptor transcription: a cause of castration-resistant prostate cancer and a possible therapeutic target. *Journal of Molecular Endocrinology*, 47, R25-R41.
- SIEGEL, R. L., MILLER, K. D. & JEMAL, A. 2016. Cancer statistics, 2016. *CA Cancer J Clin*, 66, 7-30.
- SIEGEL, R. L., MILLER, K. D., WAGLE, N. S. & JEMAL, A. 2023. Cancer statistics, 2023. *CA: A Cancer Journal for Clinicians*, 73, 17-48.
- SIEMENS, D., KLOTZ, L., HEIDENREICH, A., CHOWDHURY, S., VILLERS, A., BARON, B., VAN OS, S., HASABOU, N., WANG, F., LIN, P. & SHORE, N. 2018. Efficacy and safety of Enzalutamide vs Bicalutamide in younger and older patients with metastatic castration resistant prostate cancer in the TERRAIN trial. *American Urological Association Education and Research*, 199, 147-154.
- SILVA, S., CUNHA, I., NISHIMOTO, I., SOARES, F., CARRARO, D., KOWALSKI, L. & GRANER, E. 2009. Clinicopathological significance of ubiquitin-specific protease 2a (USP2a), fatty acid synthase (FASN) and ErbB2 expression in oral squamous cell carcinomas. *Oral Oncology*, 45, e134-e139.
- SILVESTRINI, V. C., THOMÉ, C. H., ALBUQUERQUE, D., DE SOUZA PALMA, C., FERREIRA, G. A., LANFREDI, G. P., MASSON, A. P., DELSIN, L. E. A., FERREIRA, F. U., DE SOUZA, F. C., DE GODOY, L. M. F., AQUINO, A., CARRILHO, E., PANEPUCCHI, R. A., COVAS, D. T. & FAÇA, V. M. 2020. Proteomics analysis reveals the role of ubiquitin specific protease

- (USP47) in Epithelial to Mesenchymal Transition (EMT) induced by TGF β 2 in breast cells. *J Proteomics*, 219, 103734.
- SINGH, D., FEBBO, P., ROSS, K., JACKSON, D., MANOLA, J., LADD, C., TAMAYO, P., RENSHAW, A., D'AMICO, A., RICHIE, J., LANDER, E., LODA, M., KANTOFF, P., GOLUB, T. & SELLERS, W. 2002. Gene expression correlates of clinical prostate cancer behavior. *Cancer Cell*, 1, 203-209.
- SINGH, H., BROGAN, M., JOHNSON, D. & POULOS, A. 1992. Peroxisomal beta-oxidation of branched chain fatty acids in human skin fibroblasts. *Journal of Lipid Research*, 33, 1597-1605.
- SMITH, B. A., BALANIS, N. G., NANJUNDIAH, A., SHEU, K. M., TSAI, B. L., ZHANG, Q., PARK, J. W., THOMPSON, M., HUANG, J., WITTE, O. N. & GRAEBER, T. G. 2018a. A Human Adult Stem Cell Signature Marks Aggressive Variants across Epithelial Cancers. *Cell Rep*, 24, 3353-3366.e5.
- SMITH, B. A., SOKOLOV, A., UZUNANGELOV, V., BAERTSCH, R., NEWTON, Y., GRAIM, K., MATHIS, C., CHENG, D., STUART, J. M. & WITTE, O. N. 2015. A basal stem cell signature identifies aggressive prostate cancer phenotypes. *Proceedings of the National Academy of Sciences*, 112, E6544-E6552.
- SMITH, M., SAAD, F., CHOWDHURY, S., OUDARD, S., HADASCHIK, B., GRAFF, J., OLMOS, D., MAINWARING, P., LEE, J., UEMURA, H., LOPEZ-GITLITZ, A., TRUDEL, G., ESPINA, B., SHU, Y., PARK, Y., RACKOFF, W., YU, M. & SMALL, E. 2018b. Apalutamide treatment and metastasis-free survival in prostate cancer. *New England Journal of Medicine*, 378, 1408-1418.
- SOHLENIUS-STERNBECK, A. K., AFZELIUS, L., PRUSIS, P., NEELISSEN, J., HOOGSTRAATE, J., JOHANSSON, J., FLOBY, E., BENGTSSON, A., GISSBERG, O., STERNBECK, J. & PETERSSON, C. 2010. Evaluation of the human prediction of clearance from hepatocyte and microsome intrinsic clearance for 52 drug compounds. *Xenobiotica*, 40, 637-649.
- SONG, C., PENG, J., WEI, Y., SHAO, J., CHEN, X., ZHANG, X. & XU, J. 2021. USP18 promotes tumor metastasis in esophageal squamous cell carcinomas via deubiquitinating ZEB1. *Exp Cell Res*, 409, 112884.
- SOWALSKY, A. G., YE, H., BHASIN, M., VAN ALLEN, E. M., LODA, M., LIS, R. T., MONTASER-KOUHSARI, L., CALAGUA, C., MA, F., RUSSO, J. W., SCHAEFER, R. J., VOZNESENSKY, O. S., ZHANG, Z., BUBLEY, G. J., MONTGOMERY, B., MOSTAGHEL, E. A., NELSON, P. S., TAPLIN, M.-E. & BALK, S. P. 2018. Neoadjuvant-Intensive Androgen Deprivation Therapy Selects for Prostate Tumor Foci with Diverse Subclonal Oncogenic Alterations. *Cancer Research*, 78, 4716-4730.
- SPANS, L., HELSEN, C., CLINCKEMALIE, L., VAN DEN BROECK, T., PREKOVIC, S., JONIAU, S., LERUT, E. & CLASSENS, F. 2014. Comparative genomic and transcriptomic analyses of LNCaP and C4-2B prostate cancer cell lines. *PLOS one*, 9, 1-8.
- SRAMKOSKI, R., PRETLOW, T., GIACONIA, J., PRETLOW, T., SCHAWARTZ, S., SY, M., MARENGO, S., RHIM, J., ZHANG, D. & JACOBBERGER, J. 1999. A new human prostate carcinoma cell line, 22rv1. *In Vitro Cellular & Developmental Biology - Animal*, 35, 403-409.
- STEELMAN, L. S., CHAPPELL, W. H., ABRAMS, S. L., KEMPF, R. C., LONG, J., LAIDLER, P., MIJATOVIC, S., MAKSIMOVIC-IVANIC, D., STIVALA, F., MAZZARINO, M. C., DONIA, M., FAGONE, P., MALAPONTE, G., NICOLETTI, F., LIBRA, M., MILELLA, M., TAFURI, A.,

- BONATI, A., BÄSECKE, J., COCCO, L., EVANGELISTI, C., MARTELLI, A. M., MONTALTO, G., CERVELLO, M. & MCCUBREY, J. A. 2011. Roles of the Raf/MEK/ERK and PI3K/PTEN/Akt/mTOR pathways in controlling growth and sensitivity to therapy-implications for cancer and aging. *Aging (Albany NY)*, 3, 192-222.
- STEPHENS, N., BHARWANI, N. & HEENAN, S. 2008. Prostate cancer staging. *Imaging*, 20, 112-121.
- STEVENSON, L., SPARKS, A., ALLENDE-VEGA, N., XIRODIMAS, D., LANE, D. & SAVILLE, M. 2007. The deubiquitinating enzyme USP2a regulates the p53 pathway by targeting MDM2. *The EMBO Journal*, 26, 976-986.
- STOTHARD, P. 2000. The sequence manipulation suite: JavaScript programs for analysing and formatting protein and DNA sequences. *BioTechniques*, 28, 1102-1104.
- STRASSER, A. & VAUX, D. L. 2020. Cell Death in the Origin and Treatment of Cancer. *Molecular Cell*, 78, 1045-1054.
- SUBRAMANIAN, A., TAMAYO, P., MOOTHA, V. K., MUKHERJEE, S., EBERT, B. L., GILLETTE, M. A., PAULOVICH, A., POMEROY, S. L., GOLUB, T. R., LANDER, E. S. & MESIROV, J. P. 2005. Gene set enrichment analysis: a knowledge-based approach for interpreting genome-wide expression profiles. *Proc Natl Acad Sci U S A*, 102, 15545-50.
- SUN, G., CHEN, X., X., GONG, U., CHEN, Y., LI, G., WEI, F., JIANG, A., NIU, Y. & SHANG, Z. 2019. Androgen deprivation therapy with chemotherapy or abiraterone for patients with metastatic hormone-naïve prostate cancer: a systematic review and meta-analysis. *Future Oncology*, 15, 1167-1179.
- SUN, H., WANG, Y., WANG, Z., MENG, J., QI, Z. & YANG, G. 2014. Aurora-A controls cancer cell radio- and chemoresistance via ATM/Chk2-mediated DNA repair networks. *Biochim Biophys Acta*, 1843, 934-44.
- SUN, Y., WANG, B. E., LEONG, K. G., YUE, P., LI, L., JHUNJHUNWALA, S., CHEN, D., SEO, K., MODRUSAN, Z., GAO, W. Q., SETTLEMAN, J. & JOHNSON, L. 2012. Androgen deprivation causes epithelial-mesenchymal transition in the prostate: implications for androgen-deprivation therapy. *Cancer Res*, 72, 527-36.
- SVENSSON, V., NATARAJAN, K. N., LY, L.-H., MIRAGAIA, R. J., LABALETTE, C., MACAULAY, I. C., CVEJIC, A. & TEICHMANN, S. A. 2017. Power analysis of single-cell rna-sequencing experiments. *Nature methods*, 14, 381-387.
- SZCZYRBA, J., NIESEN, A., WAGNER, M., WANDERNOTH, P. M., AUMÜLLER, G. & WENNEMUTH, G. 2017. Neuroendocrine Cells of the Prostate Derive from the Neural Crest. *Journal of Biological Chemistry*, 292, 2021-2031.
- TAI, S., SUN, Y., SQUIRES, J., ZHANG, H., OH, W., LIANG, C. & HUANG, J. 2011. PC3 is a cell line characteristic of prostatic small cell carcinoma. *Prostate*, 71, 1668-1679.
- TAKAYAMA, K. I., SUZUKI, T., FUJIMURA, T., TAKAHASHI, S. & INOUE, S. 2018. Association of USP10 with G3BP2 Inhibits p53 Signaling and Contributes to Poor Outcome in Prostate Cancer. *Mol Cancer Res*, 16, 846-856.
- TAKEDA, D., SPISÁK, S., SEO, J., BELL, C., O'CONNOR, E., KORTHAUER, K., RIBLI, D., CSABAI, I., SOLYMOSI, N., SZÁLLÁSI, Z., STILLMAN, D., CEJAS, P., QIU, X., LONG, H., TISZA, V., NUZZO, P., ROHANIZADEGAN, M., POMERANTZ, M., HAHN, W. & FREEDMAN, M. 2018. A somatically acquired enhancer of the androgen receptor is a non-encoding driver in advanced prostate cancer. *Cell*, 174, 422-432.
- TAN, H. L., SOOD, A., RAHIMI, H. A., WANG, W., GUPTA, N., HICKS, J., MOSIER, S., GOCKE, C. D., EPSTEIN, J. I., NETTO, G. J., LIU, W., ISAACS, W. B., DE MARZO, A. M. & LOTAN, T.

- L. 2014. Rb loss is characteristic of prostatic small cell neuroendocrine carcinoma. *Clin Cancer Res*, 20, 890-903.
- TANNOCK, I., WIT, R., BERRY, W., HORTI, J., PLUZANSKA, A., CHI, K., OUDARD, S., THÉODORE, C., JAMES, N., TURESSON, I., ROSENTHAL, M. & EISENBERGER, M. 2004. Docetaxel plus Prednisone or Mitoxantrone plus Prednisone for Advanced Prostate Cancer. *The New England Journal of Medicine*, 351, 1502-1512.
- TCGA 2015. The molecular taxonomy of primary prostate cancer. *Cell*, 163, 1011-1025.
- TENCER, A., LIANG, Q. & ZHUANG, Z. 2016. Divergence in ubiquitin interaction and catalysis among the ubiquitin-specific protease family DUBs. *Biochemistry*, 55, 4708-4719.
- TEPLY, B. & ANTONARAKIS, E. 2017. Treatment strategies for DNA repair-deficient prostate cancer. *Expert Review of Clinical Pharmacology*, 10, 889-898.
- TERLIZZI, M. & BOSSI, A. 2022. High-risk Locally Advanced Prostate Cancer: Multimodal Treatment Is the Key. *Eur Urol Open Sci*, 38, 14-16.
- TÊTU, B., RO, J. Y., AYALA, A. G., JOHNSON, D. E., LOGOTHETIS, C. J. & ORDONEZ, N. G. 1987. Small cell carcinoma of the prostate. Part I. A clinicopathologic study of 20 cases. *Cancer*, 59, 1803-9.
- THALMANN, G., SIKES, R., WU, T., DEGEORGES, A., CHANG, S., OZEN, M., PATHAK, S. & CHUNG, L. 2000. LNCaP progression model of human prostate cancer: androgen-independence and osseous metastasis. *The Prostate*, 44, 91-103.
- THOMAS, B. & NEAL, D. 2013. Androgen deprivation treatment in prostate cancer. *BMJ*, 346, 1-4.
- THOMAS, J. D., ZHANG, Y. J., WEI, Y. H., CHO, J. H., MORRIS, L. E., WANG, H. Y. & ZHENG, X. F. 2014. Rab1A is an mTORC1 activator and a colorectal oncogene. *Cancer Cell*, 26, 754-69.
- THOMSEN, F., BRASSO, K., KLOTZ, L., RØDER, M., BERG, K. & IVERSEN, P. 2014. Active surveillance for clinically localised prostate cancer - a systematic review. *2014*, 109, 830-835.
- TIEU, T., IRANI, S., BREMERT, K. L., RYAN, N. K., WOJNILOWICZ, M., HELM, M., THISSEN, H., VOELCKER, N. H., BUTLER, L. M. & CIFUENTES-RIUS, A. 2021. Patient-Derived Prostate Cancer Explants: A Clinically Relevant Model to Assess siRNA-Based Nanomedicines. *Adv Healthc Mater*, 10, e2001594.
- TOPACIO, B. R., ZATULOVSKIY, E., CRISTEA, S., XIE, S., TAMBO, C. S., RUBIN, S. M., SAGE, J., KÕIVOMÄGI, M. & SKOTHEIM, J. M. 2019. Cyclin D-Cdk4,6 Drives Cell-Cycle Progression via the Retinoblastoma Protein's C-Terminal Helix. *Molecular cell*, 74, 758-770.e4.
- TOREN, P., KIM, S., JOHNSON, F. & ZOUBEIDI, A. 2016. Combined AKT and MEK Pathway Blockade in Pre-Clinical Models of Enzalutamide-Resistant Prostate Cancer. *PLoS One*, 11, e0152861.
- TRAN, C., OUK, S., CLEGG, N., CHEN, Y., WATSON, P., ARORA, V., WONGVIPAT, J., SMITH-JONES, P., YOO, D., KWON, A., WASIELEWSKA, T., WELSBIE, D., CHEN, C., HIGANO, C., BEER, T., HUNG, D., SCHER, H., JUNG, M. & SAWYERS, C. 2009. Development of a second-generation antiandrogen for treatment of advanced prostate cancer. *Science*, 324, 787-790.
- TREMBLAY, G., TREMBLAY, A., LABRIE, F. & GIGUÈRE, V. 1999. Dominant activity of activation function 1 (AF-1) and differential stoichiometric requirements for AF-1 and

- 2 in the estrogen receptor alpha-beta heterodimeric complex. *Molecular and Cellular Biology*, 19, 1919-1927.
- TSUKUMO, Y., TOMIDA, A., KITAHARA, O., NAKAMURA, Y., ASADA, S., MORI, K. & TSURUO, T. 2007. Nucleobindin 1 controls the unfolded protein response by inhibiting ATF6 activation. *J Biol Chem*, 282, 29264-72.
- TU, Y., XU, L., XU, J., BAO, Z., TIAN, W., YE, Y., SUN, G., MIAO, Z., CHAO, H., YOU, Y., LIU, N. & JI, J. 2022. Loss of deubiquitylase USP2 triggers development of glioblastoma via TGF- β signaling. *Oncogene*, 41, 2597-2608.
- UEHARA, J., OHKURI, T., KOSAKA, A., ISHIBASHI, K., HIRATA, Y., OHARA, K., NAGATO, T., OIKAWA, K., AOKI, N., HARABUCHI, Y., ISHIDA-YAMAMOTO, A. & KOBAYASHI, H. 2017. Intratumoral injection of IFN- β induces chemokine production in melanoma and augments the therapeutic efficacy of anti-PD-L1 mAb. *Biochem Biophys Res Commun*, 490, 521-527.
- URBAN-WOJCIUK, Z., KHAN, M. M., OYLER, B. L., FÅHRAEUS, R., MAREK-TRZONKOWSKA, N., NITA-LAZAR, A., HUPP, T. R. & GOODLETT, D. R. 2019. The Role of TLRs in Anti-cancer Immunity and Tumor Rejection. *Frontiers in Immunology*, 10.
- UYSAL-ONGANER, P., KAWANO, Y., CARO, M., WALKER, M. M., DIEZ, S., DARRINGTON, R. S., WAXMAN, J. & KYPTA, R. M. 2010. Wnt-11 promotes neuroendocrine-like differentiation, survival and migration of prostate cancer cells. *Mol Cancer*, 9, 55.
- VASUDEVAMURTHY, A. K., LEDET, E., GARVEY, C., LEWIS, B. E. & SARTOR, O. 2017. Estrogen-Mediated Activation of H875Y Androgen Receptor Mutation in a Prostate Cancer Patient. *Clinical Genitourinary Cancer*, 15, e111-e113.
- VELDSCHOLTE, J., RIS-STALPERS, C., KUIPER, G., JENSTER, G., BERREVOETS, C., CLAASSEN, E., VAN ROOIJ, H., TRAPMAN, J., BRINKMANN, A. & MULDER, E. 1990. A mutation in the ligand binding domain of the androgen receptor of human LNCaP cells affects steroid binding characteristics and response to anti-androgens. *Biochemical and Biophysical Research Communications*, 173, 534-540.
- VELIKKAKATH, A. K., NISHIMURA, T., OITA, E., ISHIHARA, N. & MIZUSHIMA, N. 2012. Mammalian Atg2 proteins are essential for autophagosome formation and important for regulation of size and distribution of lipid droplets. *Mol Biol Cell*, 23, 896-909.
- VENTURUTTI, L., CORDO RUSSO, R. I., RIVAS, M. A., MERCOGLIANO, M. F., IZZO, F., OAKLEY, R. H., PEREYRA, M. G., DE MARTINO, M., PROIETTI, C. J., YANKILEVICH, P., ROA, J. C., GUZMÁN, P., CORTESE, E., ALLEMAND, D. H., HUANG, T. H., CHARREAU, E. H., CIDLOWSKI, J. A., SCHILLACI, R. & ELIZALDE, P. V. 2016. MiR-16 mediates trastuzumab and lapatinib response in ErbB-2-positive breast and gastric cancer via its novel targets CCNJ and FUBP1. *Oncogene*, 35, 6189-6202.
- VERMA, S., DIXIT, R. & PANDEY, K. C. 2016. Cysteine Proteases: Modes of Activation and Future Prospects as Pharmacological Targets. *Frontiers in pharmacology*, 7, 107-107.
- VISWANATHAN, V. S., RYAN, M. J., DHRUV, H. D., GILL, S., EICHHOFF, O. M., SEASHORE-LUDLOW, B., KAFFENBERGER, S. D., EATON, J. K., SHIMADA, K., AGUIRRE, A. J., VISWANATHAN, S. R., CHATTOPADHYAY, S., TAMAYO, P., YANG, W. S., REES, M. G., CHEN, S., BOSKOVIC, Z. V., JAVAID, S., HUANG, C., WU, X., TSENG, Y.-Y., ROIDER, E. M., GAO, D., CLEARY, J. M., WOLPIN, B. M., MESIROV, J. P., HABER, D. A., ENGELMAN, J. A., BOEHM, J. S., KOTZ, J. D., HON, C. S., CHEN, Y., HAHN, W. C., LEVESQUE, M. P., DOENCH, J. G., BERENS, M. E., SHAMJI, A. F., CLEMONS, P. A.,

- STOCKWELL, B. R. & SCHREIBER, S. L. 2017. Dependency of a therapy-resistant state of cancer cells on a lipid peroxidase pathway. *Nature*, 547, 453-457.
- WADOSKY, K. & KOOCHEKPOUR, S. 2016. Molecular mechanisms underlying resistance to androgen deprivation therapy in prostate cancer. *Oncotarget*, 7, 64447-64470.
- WAHBA, H. A. & EL-HADAAD, H. A. 2015. Current approaches in treatment of triple-negative breast cancer. *Cancer Biol Med*, 12, 106-16.
- WAN, X. B., LONG, Z. J., YAN, M., XU, J., XIA, L. P., LIU, L., ZHAO, Y., HUANG, X. F., WANG, X. R., ZHU, X. F., HONG, M. H. & LIU, Q. 2008. Inhibition of Aurora-A suppresses epithelial-mesenchymal transition and invasion by downregulating MAPK in nasopharyngeal carcinoma cells. *Carcinogenesis*, 29, 1930-7.
- WANDINGER-NESS, A. & ZERIAL, M. 2014. Rab proteins and the compartmentalization of the endosomal system. *Cold Spring Harb Perspect Biol*, 6, a022616.
- WANG, H., CUI, B., SUN, H., ZHANG, F., RAO, J., WANG, R., ZHAO, S., SHEN, S. & LIU, Y. 2021a. Aberrant GATA2 Activation in Pediatric B-Cell Acute Lymphoblastic Leukemia. *Front Pediatr*, 9, 795529.
- WANG, H. J., POCHAMPALLI, M., WANG, L. Y., ZOU, J. X., LI, P. S., HSU, S. C., WANG, B. J., HUANG, S. H., YANG, P., YANG, J. C., CHU, C. Y., HSIEH, C. L., SUNG, S. Y., LI, C. F., TEPPER, C. G., ANN, D. K., GAO, A. C., EVANS, C. P., IZUMIYA, Y., CHUU, C. P., WANG, W. C., CHEN, H. W. & KUNG, H. J. 2019. KDM8/JMJD5 as a dual coactivator of AR and PKM2 integrates AR/EZH2 network and tumor metabolism in CRPC. *Oncogene*, 38, 17-32.
- WANG, L., LU, B., HE, M., WANG, Y., WANG, Z. & DU, L. 2022. Prostate Cancer Incidence and Mortality: Global Status and Temporal Trends in 89 Countries From 2000 to 2019. *Frontiers in Public Health*, 10.
- WANG, L. & PROUD, C. G. 2002. Ras/Erk Signaling Is Essential for Activation of Protein Synthesis by Gq Protein-Coupled Receptor Agonists in Adult Cardiomyocytes. *Circulation Research*, 91, 821-829.
- WANG, W. & EPSTEIN, J. I. 2008. Small cell carcinoma of the prostate. A morphologic and immunohistochemical study of 95 cases. *Am J Surg Pathol*, 32, 65-71.
- WANG, X., MAZURKIEWICZ, M., HILLERT, E., OLOFSSON, M., PIERROU, S., HILLERTZ, P., GULBO, J., SELVARAJU, K., PAULUS, A., AKHTAR, S., BOSSLER, F., KHAN, A., LINDER, S. & D'ARCY, P. 2016. The proteasome deubiquitinase inhibitor VLX1570 shows selectivity for ubiquitin-specific protease-14 and induces apoptosis of multiple myeloma cells. *Nature Scientific Reports*, 6, 1-14.
- WANG, X., WANG, B., SORIANO, R., ZHA, J., ZHANG, Z., MODRUSAN, Z., CUNHA, G. & GAO, W. 2007. Expression profiling of the mouse prostate after castration and hormone replacement: implication of H-cadherin in prostate tumorigenesis. *Differentiation*, 75, 219-234.
- WANG, X., XIE, J. & PROUD, C. G. 2017. Eukaryotic Elongation Factor 2 Kinase (eEF2K) in Cancer. *Cancers (Basel)*, 9.
- WANG, Y., WANG, Y., CI, X., CHOI, S. Y. C., CREA, F., LIN, D. & WANG, Y. 2021b. Molecular events in neuroendocrine prostate cancer development. *Nat Rev Urol*, 18, 581-596.
- WEBSTER, C. P., SMITH, E. F., BAUER, C. S., MOLLER, A., HAUTBERGUE, G. M., FERRAIUOLO, L., MYSCZYNSKA, M. A., HIGGINBOTTOM, A., WALSH, M. J., WHITWORTH, A. J., KASPAR, B. K., MEYER, K., SHAW, P. J., GRIERSON, A. J. & DE VOS, K. J. 2016. The

- C9orf72 protein interacts with Rab1a and the ULK1 complex to regulate initiation of autophagy. *The EMBO Journal*, 35, 1656-1676.
- WEI, T., BISKUP, E., GJERDRUM, L., NIAZI, O., ODUM, N. & GNIADDECKI, R. 2016. Ubiquitin-specific protease 2 decreases P53-dependent apoptosis in cutaneous T-cell lymphoma. *Oncotarget*, 7, 48391-48400.
- WELTI, J., RODRIGUES, D., SHARP, A., SUN, S., LORENTE, D., RIISNAES, R., FIGUEIREDO, I., ZAFEIRIOU, Z., RESCIGNO, P., DE BONO, J. & PLYMATE, S. 2016. Analytical validation and clinical qualification of a new immunohistochemical assay for androgen receptor splice variant-7 protein expression in metastatic castration-resistant prostate cancer. *European Urology*, 70, 599-608.
- WHITE, R. E. 2000. High-throughput screening in drug metabolism and pharmacokinetic support of drug discovery. *Annu Rev Pharmacol Toxicol*, 40, 133-57.
- WILLEMS, E., DEBOBBELEER, M., DIGREGORIO, M., LOMBARD, A., LUMAPAT, P. N. & ROGISTER, B. 2018. The functional diversity of Aurora kinases: a comprehensive review. *Cell Div*, 13, 7.
- WILSON, B. E., ARMSTRONG, A. J., DE BONO, J., STERNBERG, C. N., RYAN, C. J., SCHER, H. I., SMITH, M. R., RATHKOPF, D., LOGOTHETIS, C. J., CHI, K. N., JONES, R. J., SAAD, F., DE PORRE, P., TRAN, N., HU, P., GILLESSEN, S., CARLES, J., FIZAZI, K. & JOSHUA, A. M. 2022. Effects of metformin and statins on outcomes in men with castration-resistant metastatic prostate cancer: Secondary analysis of COU-AA-301 and COU-AA-302. *European Journal of Cancer*, 170, 296-304.
- WONG, D. J., LIU, H., RIDKY, T. W., CASSARINO, D., SEGAL, E. & CHANG, H. Y. 2008. Module map of stem cell genes guides creation of epithelial cancer stem cells. *Cell Stem Cell*, 2, 333-44.
- WRIGHT, A., THOMAS, L., DOUGLAS, R., LAZIER, C. & RITTMASER, R. 1996. Relative potency of testosterone and dihydrotestosterone in preventing atrophy and apoptosis in the prostate of the castrated rat. *The Journal of Clinical Investigation*, 98, 2558-2563.
- XIAO, W., WANG, J., WANG, X., CAI, S., GUO, Y., YE, L., LI, D., HU, A., JIN, S., YUAN, B., ZHOU, Y., LI, Q., TONG, Q. & ZHENG, L. 2022. Therapeutic targeting of the USP2-E2F4 axis inhibits autophagic machinery essential for zinc homeostasis in cancer progression. *Autophagy*, 18, 2615-2635.
- XIONG, B., HUANG, J., LIU, Y., ZOU, M., ZHAO, Z., GONG, J., WU, X. & QIU, C. 2021. Ubiquitin-specific protease 2a promotes hepatocellular carcinoma progression via deubiquitination and stabilization of RAB1A. *Cell Oncol (Dordr)*, 44, 329-343.
- XU, K., PEI, H., ZHANG, Z., WANG, H., LI, L. & XIA, Q. 2018. Ubiquitin-specific protease 15 promotes tumor cell invasion and proliferation in glioblastoma. *Oncol Lett*, 15, 3846-3851.
- XU, X., LIU, J., SHEN, C., DING, L., ZHONG, F., OUYANG, Y., WANG, Y. & HE, S. 2015. The role of ubiquitin-specific protease 14 (USP14) in cell adhesion-mediated drug resistance (CAM-DR) of multiple myeloma cells. *European Journal of Haematology*, 98, 4-12.
- XUE, S., WU, W., WANG, Z., LU, G., SUN, J., JIN, X., XIE, L., WANG, X., TAN, C., WANG, Z., WANG, W. & DING, X. 2020. USP5 Promotes Metastasis in Non-Small Cell Lung Cancer by Inducing Epithelial-Mesenchymal Transition via Wnt/ β -Catenin Pathway. *Frontiers in Pharmacology*, 11.
- XUN, Y., YANG, H., KAMINSKA, B. & YOU, H. 2021. Toll-like receptors and toll-like receptor-targeted immunotherapy against glioma. *J Hematol Oncol*, 14, 176.

- YAMADA, Y. & BELTRAN, H. 2021. Clinical and Biological Features of Neuroendocrine Prostate Cancer. *Curr Oncol Rep*, 23, 15.
- YANG, H. & WONG, M. W. 2013. Oxyanion Hole Stabilization by C–H···O Interaction in a Transition State—A Three-Point Interaction Model for Cinchona Alkaloid-Catalyzed Asymmetric Methanolysis of meso-Cyclic Anhydrides. *Journal of the American Chemical Society*, 135, 5808-5818.
- YANG, J., ZONG, C., XIA, W., WEI, Y., ALI-SEYED, M., LI, Z., BROGLIO, K., BERRY, D. A. & HUNG, M.-C. 2006. MDM2 promotes cell motility and invasiveness by regulating E-Cadherin degradation. *Molecular and Cellular Biology*, 26, 7269-7282.
- YAO, J., LIU, Y., LIANG, X., SHAO, J., ZHANG, Y., YANG, J. & ZHENG, M. 2021. Neuroendocrine Carcinoma as an Independent Prognostic Factor for Patients With Prostate Cancer: A Population-Based Study. *Frontiers in Endocrinology*, 12.
- YAO, J. L., MADEB, R., BOURNE, P., LEI, J., YANG, X., TICKOO, S., LIU, Z., TAN, D., CHENG, L., HATEM, F., HUANG, J. & ANTHONY DI SANT'AGNESE, P. 2006. Small cell carcinoma of the prostate: an immunohistochemical study. *Am J Surg Pathol*, 30, 705-12.
- YASHI, M., TERAUCHI, F., NUKUI, A., OCHI, M., YUZAWA, M., HARA, Y. & MORITA, T. 2006. Small-cell neuroendocrine carcinoma as a variant form of prostate cancer recurrence: A case report and short literature review. *Urologic Oncology: Seminars and Original Investigations*, 24, 313-317.
- YILDIRIM, N., KOCAL, G. C., ISIK, Z., SAATLI, B., SAYGILI, U., UYSAL, T., ULUKUS, C., KOYUNCUOGLU, M., ELLIDOKUZ, H. & BASBINAR, Y. 2019. Ubiquitin-Proteasome Axis, Especially Ubiquitin-Specific Protease-17 (USP17) Gene Family, is a Potential Target for Epithelial-Mesenchymal Transition in High-Grade Serous Ovarian Cancer. *Reprod Sci*, 26, 794-805.
- YU, X., CATES, J. M., MORRISSEY, C., YOU, C., GRABOWSKA, M. M., ZHANG, J., DEGRAFF, D. J., STRAND, D. W., FRANCO, O. E., LIN-TSAI, O., HAYWARD, S. W. & MATUSIK, R. J. 2014. SOX2 expression in the developing, adult, as well as, diseased prostate. *Prostate Cancer Prostatic Dis*, 17, 301-9.
- YUAN, F., HANKEY, W., WU, D., WANG, H., SOMARELLI, J., ARMSTRONG, A. J., HUANG, J., CHEN, Z. & WANG, Q. 2019. Molecular determinants for enzalutamide-induced transcription in prostate cancer. *Nucleic Acids Research*, 47, 10104-10114.
- YUAN, T., YAN, F., YING, M., CAO, J., HE, Q., ZHU, H. & YANG, B. 2018. Inhibition of ubiquitin-specific proteases as a novel anticancer therapeutic strategy. *Frontiers in Pharmacology*, 9, 1-10.
- YUAN, T. C., VEERAMANI, S., LIN, F. F., KONDRIKOU, D., ZELIVIANSKI, S., IGAWA, T., KARAN, D., BATRA, S. K. & LIN, M. F. 2006. Androgen deprivation induces human prostate epithelial neuroendocrine differentiation of androgen-sensitive LNCaP cells. *Endocr Relat Cancer*, 13, 151-67.
- ZAFFUTO, E., POMPE, R., ZANATY, M., BONDARENKO, H. D., LEYH-BANNURAH, S.-R., MOSCHINI, M., DELL'OGGIO, P., GANDAGLIA, G., FOSSATI, N., STABILE, A., ZORN, K. C., MONTORSI, F., BRIGANTI, A. & KARAKIEWICZ, P. I. 2017. Contemporary Incidence and Cancer Control Outcomes of Primary Neuroendocrine Prostate Cancer: A Seer Database Analysis. *Clinical genitourinary cancer*, 15, e793-e800.
- ZENG, Q., LI, Z., ZHAO, X., GUO, L., YU, C., QIN, J., ZHANG, S., ZHANG, Y. & YANG, X. 2019. Ubiquitin-specific protease 7 promotes osteosarcoma cell metastasis by inducing epithelial-mesenchymal transition. *Oncol Rep*, 41, 543-551.

- ZHANG, C., SOORI, M., MILES, F. L., SIKES, R. A., CARSON, D. D., CHUNG, L. W. & FARACH-CARSON, M. C. 2011. Paracrine factors produced by bone marrow stromal cells induce apoptosis and neuroendocrine differentiation in prostate cancer cells. *Prostate*, 71, 157-67.
- ZHANG, D., JIANG, F., WANG, X. & LI, G. 2017. Downregulation of Ubiquitin-Specific Protease 22 Inhibits Proliferation, Invasion, and Epithelial-Mesenchymal Transition in Osteosarcoma Cells. *Oncol Res*, 25, 743-751.
- ZHANG, F., ZHAO, Y. & SUN, Y. 2021. USP2 is a SKP2 deubiquitylase that stabilizes both SKP2 and its substrates. *J Biol Chem*, 297, 101109.
- ZHANG, J., LIU, S., LI, Q., SHI, Y., WU, Y., LIU, F., WANG, S., ZAKY, M., YOUSUF, W., SUN, Q., GUO, D., WANG, T., ZHANG, Y., WANG, Y., LI, M. & LIU, H. 2020a. The deubiquitylase USP2 maintains ErbB2 abundance via counteracting endocytic degradation and represents a therapeutic target in ErbB2-positive breast cancer. *Cell Death & Differentiation*, 27, 2710–2725.
- ZHANG, L., ZHOU, F., DRABSCH, Y., GAO, R., SNAAR-JAGALSKA, B. E., MICKANIN, C., HUANG, H., SHEPPARD, K. A., PORTER, J. A., LU, C. X. & TEN DIJKE, P. 2012. USP4 is regulated by AKT phosphorylation and directly deubiquitylates TGF- β type I receptor. *Nat Cell Biol*, 14, 717-26.
- ZHANG, M., HUANG, L., DING, G., HUANG, H., CAO, G., SUN, X., LOU, N., WEI, Q., SHEN, T., XU, X., CAO, L. & YAN, Q. 2020b. Interferon gamma inhibits CXCL8-CXCR2 axis mediated tumor-associated macrophages tumor trafficking and enhances anti-PD1 efficacy in pancreatic cancer. *J Immunother Cancer*, 8.
- ZHANG, Q., HAN, Y., ZHANG, Y., LIU, D., MING, J., HUANG, B. & QIU, X. 2020c. Treatment-Emergent Neuroendocrine Prostate Cancer: A Clinicopathological and Immunohistochemical Analysis of 94 Cases. *Front Oncol*, 10, 571308.
- ZHANG, Y., ZHANG, G. L., SUN, X., CAO, K. X., MA, C., NAN, N., YANG, G. W., YU, M. W. & WANG, X. M. 2018a. Establishment of a murine breast tumor model by subcutaneous or orthotopic implantation. *Oncol Lett*, 15, 6233-6240.
- ZHANG, Y., ZHENG, D., ZHOU, T., SONG, H., HULSURKAR, M., SU, N., LIU, Y., WANG, Z., SHAO, L., ITTMANN, M., GLEAVE, M., HAN, H., XU, F., LIAO, W., WANG, H. & LI, W. 2018b. Androgen deprivation promotes neuroendocrine differentiation and angiogenesis through CREB-EZH2-TSP1 pathway in prostate cancers. *Nature Communications*, 9, 4080.
- ZHAO, J., ZHAO, Y., WANG, L., ZHANG, J., KARNES, R. J., KOHLI, M., WANG, G. & HUANG, H. 2016. Alterations of androgen receptor-regulated enhancer RNAs (eRNAs) contribute to enzalutamide resistance in castration-resistant prostate cancer. *Oncotarget*, 7, 38551-38565.
- ZHONG, M., ZHOU, L., FANG, Z., YAO, Y. Y., ZOU, J. P., XIONG, J. P., XIANG, X. J. & DENG, J. 2021. Ubiquitin-specific protease 15 contributes to gastric cancer progression by regulating the Wnt/ β -catenin signaling pathway. *World J Gastroenterol*, 27, 4221-4235.
- ZITO, A., LUALDI, M., GRANATA, P., COCCIADIFERRO, D., NOVELLI, A., ALBERIO, T., CASALONE, R. & FASANO, M. 2021. Gene Set Enrichment Analysis of Interaction Networks Weighted by Node Centrality. *Frontiers in Genetics*, 12.
- ZOU, M., TOIVANEN, R., MITROFANOVA, A., FLOCH, N., HAYATI, S., SUN, Y., LE MAGNEN, C., CHESTER, D., MOSTAGHEL, E. A., CALIFANO, A., RUBIN, M. A., SHEN, M. M. & ABATE-

SHEN, C. 2017. Transdifferentiation as a Mechanism of Treatment Resistance in a Mouse Model of Castration-Resistant Prostate Cancer. *Cancer Discov*, 7, 736-749.